Université catholique de Louvain

Institut de la matière condensée et des nanosciences

Faculté d'ingénierie biologique, agronomique et environnementale

Biofouling of metal surfaces: study of adsorbed biomolecules and prevention strategy based on a renewable copolymer layer

Thèse soutenue en vue de l'obtention du grade de docteur en sciences agronomiques et ingénierie biologique par

Yi YANG

Composition du jury :
Pr. Christine DUPONT-GILLAIN (UCL/IMCN) – *Promoteur*
Pr. Jacques DEVAUX (UCL/IMCN) – *Président*
Dr. Isabelle FRATEUR (Université Pierre et Marie Curie - Paris VI)
Pr. Arnaud DELCORTE (UCL/IMCN)
Pr. Jacques MAHILLON (UCL/ELI)
Pr. Karine GLINEL (UCL/IMCN)

Août 2013

Acknowledgements

First and foremost, I want to express my gratitude to my promoter Prof. Christine Dupont-Gillain. It has been an honor to be her first international Ph.D student. I appreciate her offering me this extraordinary Ph.D position and giving me the opportunity to join her group and BIOCOR project. She gave me freedom and support on my work. I appreciate her patience to read and correct my papers and the manuscript thesis repeatedly. For me, she is more like a mentor, who know how to teach and communicate with her students in a pleasant way. She is also an excellent example of young professor who manages well between her career and family.

I would like to express my deepest appreciation to Prof. Paul Rouxhet for his contribution to this thesis, excellent ideas and help in building up the method of using flow chamber to study bacterial adhesion, and guiding me to exploit a huge amount of XPS data. Dear Prof Rouxhet, I thank you for your patience in correcting my papers, even in your leisure time, and for all the things you have done for me.

For this thesis, I would like to thank Dr. Isabelle Frateur, Prof. Arnaud Delcorte, Prof. Jacques Devaux, Prof. Jacques Mahillon and Prof. Karine Glinel for being my jury members, reading the manuscript thesis and giving helpful comments for improvement. More specifically, I would like to thank Prof. Jacques Devaux to have headed, as president of my jury, organized and conducted my private defense in a very constructive and smooth way; Dr. Isabelle Frateur for her careful review of the thesis manuscript and corrections; Prof. Arnaud Delcorte for useful comments on the ToF-SIMS data.

I would like to offer my special thanks to Prof. Judit Telegdi to have welcomed me in her laboratory for one week and to have given experienced knowledge of SAM coating; Lorand Romanszki for pratical training of LB coating and discussion; Dr. Sofia Keresztes for her help on my work and introducing me to such a beautiful city, Budapest.

Special thanks also to Prof. Wolfgang Sand to have welcomed me in his laboratory for two weeks for training of bacterial culture and

fluorescence microscopy. Thanks to Agata Wikiel, Iaryna Datsenko for your organization and hands-on training during my secondment.

I am deeply grateful to Prof. José Moura to have welcomed me in his laboratory for two weeks for protein gel electrophoresis work. Thanks to Leonardo Dall'Agnol for his organization of my lab work, a lot of fun during secondments between us in Lisbon and Louvain-la-Neuve, I wish our friendship will never be ended.

I would like to thank Dr. Pierangela Cristiani and Maria Carvalho for organizing my visit to the power plant. Many thanks for your help and take care of my field samples.

I would like to thank Prof. Iwona Beech for helping me choosing the model bacteria in my work; Magdalena Sztyler for the protocol of bacteria culture.

I would particularly like to thank Regine Basseguy, Jenny Stephenson and Vincent Birrien for their effort to organize the biannual BIOCOR meeting and summer school; we have not only scientific discussion, but also a lot of friendships and joyful time across European cities: Lisbon, Bergen, Louvain-la-Neuve, Portsmouth, Stockholm, Venice, Istanbul, Essen.

My warmest thanks also go to all my BIOCOR colleagues, all senior scientists and professors. Thanks to Agata, Blanca, Claudia, Iaryna, Iulian, Jemimah, Leonardo, Loïc, Lorand, Magdalena, Maria, Marko, Marta, Omar, Rebeca, although we are from different places of the world, I wish our friendships will never be ended. A lot of joyful time during our collaboration work. That is an invaluable memory in my life.

I owe my sincere thanks to the people from SURF: Françoise, thank you for taking care of me more than my life in the lab; thanks to Rose, Yasmine for your support in my daily life in the lab; thanks to Sylvie for your support on AFM; thanks to Michel for the XPS training, it's my honor to work with you, sorry for bother you occasionally in the weekends, and I wish you start to enjoy your retired life; thanks to Claude for the ToF-SIMS training, I will definitely get stuck in ToF-SIMS spectra without your help; thanks to Kevin for your friendship, QCM training, and especially your Q-stomize, it made the data

treatment simpler for us; thanks to Dorota for her contribution to this thesis; thanks to Emilienne, Simon, Marie, Pierre de Thier, Mireya, Pierre Eloy, Guillaume Lamblin, Deepak for sharing your knowledge and experience with me; thanks to Sami, Victor Lebec, Victor Baldovino, Vincent Dupres, Prachi, Audrey, Sofia for your friendships. I also gave my best wishes to Jean-Françoise, Sara and Gilles on their way to obtain Ph.D in the near future. Thank you for all of you both in the lab and in my social life in Louvain-la-Neuve. This is the most important and unforgettable experience in my whole life. I have learned a lot in both scientific work and culture.

I gratefully acknowledge the funding source for my Ph.D work. I was funded by the Marie Curie fellowship from BIOCOR project, which is funded by the European Community's Seventh Framework (FP7) 2008 "People" Programme, under grant agreement n° 238579. Project website: www.biocor.eu

I also want to take this opportunity to express my thanks to my former supervisors and friends in Sweden: thanks to Prof. Sven Oscarsson, Dr. Emmanuelle Göthelid for leading me to surface science; thanks to Bin Pan, Jinkun Li, Yong Liu, Weiwei Liu for their encouragement.

Thanks to my friends in Louvain-la-Neuve: Ronggong Cai, Jun Yin, Wenli Peng, Yuan Li, Rachel Diao, and especially Di Zhang. My time in LLN was made enjoyable in large part due to my friends.

Thanks to my long-lasting friends in China: Lijin Zhang, Xinwen Yu, Jiang Xie, Yubin Wang, Liren Zhou, Xieshao Zhang, Chris Qiu, Ming Cheng, Haitao Liang, Lei Zhao.

Last, but most important, a great thank to my parents. Thank you for raising me, supporting me, encouraging me and loving me. This thesis is dedicated to you.

Abstract

Biofouling refers to the accumulation of organisms and their products onto surfaces immersed in a biological aqueous environment. It includes molecular-, micro- and macro-fouling. Molecular fouling is the initial step of biofouling, in which a conditioning film is formed by adsorption of organic biomolecules. Furthermore, surface-associated aggregates of microorganisms with their extracellular polymeric substances (EPS) are called biofilm, known to provoke the biocorrosion of metals.

Chlorination is still the most common treatment to control biofouling of cooling condensers fed with fresh- or seawater in power plants, provoking harmful effects to the aquatic environment. An environmental-friendly way to replace chlorination is thus highly desired.

The aim of this thesis is to design a renewable poly(ethylene oxide) (PEO)-based coating on metals (Ti, stainless steel and Al brass) used in cooling condensers, with a view to reduce biofouling. Adsorption of a PEO-poly(propylene oxide)-PEO copolymer was performed on native and hydrophobized metal surfaces. Three proteins (albumin, fibrinogen, cytochrome C) and *Pseudomonas* 2021, a marine bacterium, were used as model molecular- and micro-fouling agents, respectively. The results show that the adsorbed triblock copolymer prevents protein adsorption and significantly reduces bacterial adhesion on hydrophobized metal substrates, but not on native ones.

The copolymer conformation plays a key role in biofouling reduction; it is believed to form a brush structure on hydrophobized substrates. In addition, proteins were highlighted as an important constituent of EPS and their conditioning films, as analyzed by X-ray photoelectron spectroscopy. This confirms the relevance of preventing protein adsorption to reduce biofouling.

List of abbreviations

AFM	Atomic force microscopy
ASW	Artificial seawater
BSA	Bovine serum albumin
CMC	Critical micellization concentration
DAPI	4’,6-diamidino-2-phenylindole
EDX	Energy dispersive x-ray analysis
EPS	Extracellular polymeric substances
LB EPS	Loosely bound EPS
LPS	Lipopolysaccharides
MIC	Microbiologically influenced corrosion
OPA	Octadecylphosphonic
PEO	Poly(ethylene oxide)
PPFC	Parallel plate flow chamber
PPO	Poly(propylene oxide)
QCM	Quartz crystal microbalance
SAMs	Self-assembly monolayers
SEM	Scanning electron microscopy
SPR	Surface plasmon resonance
SRB	Sulfate-reducing bacteria
TB EPS	Tightly bound EPS
ToF-SIMS	Time-of-flight secondary ion mass spectrometry
WCA	Water contact angle
XPS	X-ray photoelectron spectroscopy

Table of contents

Chapter 1

Introduction

1.1 BIOCOR project

This thesis was performed in the frame of the BIOCOR project. BIOCOR (www.biocor.eu) is a Marie Curie Initial Training Network (ITN) project, funded by the EU 7th Framework "People" Programme. The core aim of BIOCOR ITN is to study biocorrosion issues by bringing together researchers with different scientific backgrounds in the area of biocorrosion. The research methodology, as shown in Figure 1, is based on multi-disciplinary knowledge, from chemistry, electrochemistry, material science, microbiology to molecular biology, and combined surface analytical approaches. A problem-oriented approach was chosen to tackle biocorrosion within two large industrial sectors: the oil and gas industry (water injection systems and systems for handling stabilized oil) and the power supply facilities (cooling systems in energy facilities and nuclear waste geological disposal). The field problems due to biocorrosion are raised by industry, then related applied research work was performed in the lab, and finally, useful results are expected to solve the questions as a benefit for the industry. This is a so-called "from the field through the lab to the field" approach. 12 individual projects related to the different problems raised by industrial partners are being undertaken by the project research teams with different expertise. Knowledge sharing and complementary scientific skills learning are encouraged among the early stage researchers (ESR) and senior scientists in BIOCOR ITN. The global objective of BIOCOR ITN is to train and promote qualified research project managers in biocorrosion field, capable to work in research or industry and to lead teams of experts of different disciplines and countries.

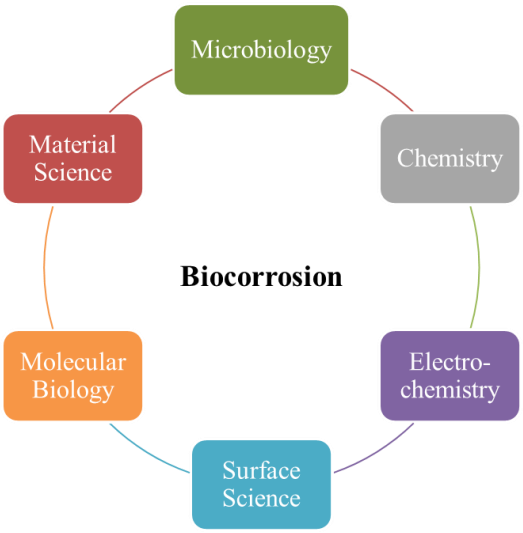

Figure 1. Main scientific disciplines involved in biocorrosion studies.

1.2 Context of the research

The aggregation of a group of surface-attached bacteria with their excreted slimy material is called **biofilm**. Biofilm formation process starts from single microbial attachment to surface, which is facilitated by production of **extracellular polymeric substances** (EPS). EPS are complex polymers secreted by bacteria, and form a major part of biofilm. The accumulation of undesirable organic matter (e.g. biofilm) on natural or man-made surfaces is generally referred to as **biofouling**. In addition, biofouling is sometimes concomitant to **biocorrosion**, which causes the deterioration of metal under the action of microorganisms from the biofilm [1].

1.2.1 Biofouling and biofilm

Biofouling refers to the undesired formation of deposits of living organisms and their products on solid substrates in contact with aqueous environment [2, 3]. Biofouling has a significantly adverse effect in different fields, e.g. loss of heat exchanger efficiency in cooling condensers, reduction in fluid flow for pipelines transporting oil and water, increasing fluid

frictional resistance and fuel consumption by a fouled ship [4-6]. As illustrated in Figure 2, the hull of ships is often fouled by marine organisms.

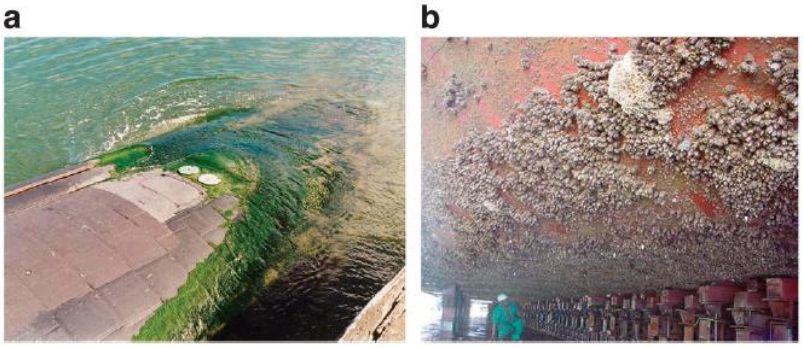

Figure 2. Vessels fouled by marine organisms. (a) fouling by the green alga (b) barnacles. Adapted from [7].

According to the size of fouling matters, they have been divided into three groups: molecular, micro- and macrofouling [8]. These foulings successively attach to the surface but in different time scale, as illustrated in Figure 3. First, from seconds to minutes, submerged surfaces are modulated by adsorption of organic and inorganic substances to form a conditioning film. Second, from minutes to hours, bacteria colonize the surface, associated with production of EPS to form biofilm. Following, from hours to days, soft foulers and hard foulers start to attach to the surface as well.

Many different organisms with different sizes are involved in fouling process in marine environment, as illustrated in Figure 4. The fouling organisms vary, depending on the season, location and other conditions (e.g. flow rate). They are found in different amount in different areas. The density of microfouling (e.g. by bacteria) is relatively higher than the density of macrofouling (e.g. by algae, larvae): e.g. the density of bacteria is in the level of million per milliliter, and algae is about thousands per milliliter, and possibly only a few larvae per liter [8]. In addition, the amount of bacteria is more constant than the amount of macroorganisms. Therefore, submerged surfaces are first colonized by bacteria, and it might affect the further approaching macroorganisms.

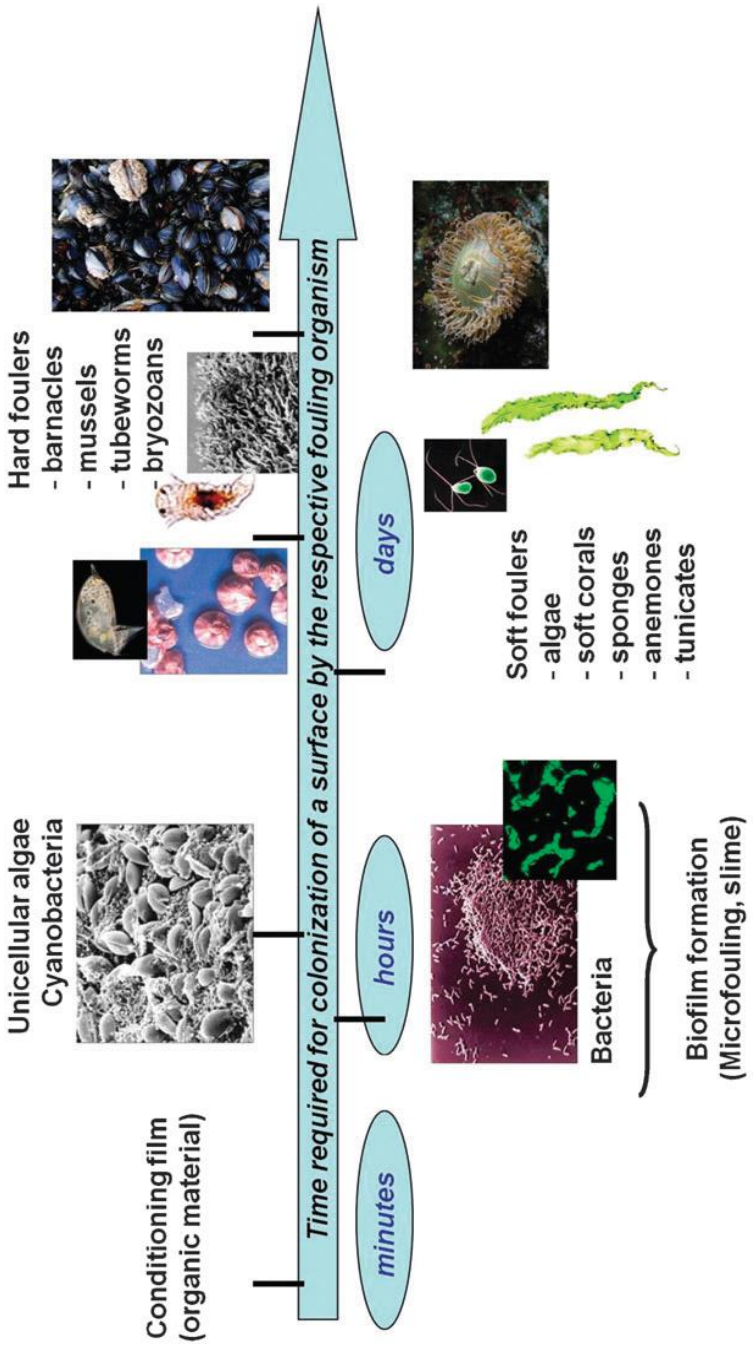

Figure 3. Time required for colonization of a surface by the respective fouling organisms. Adapted from [9].

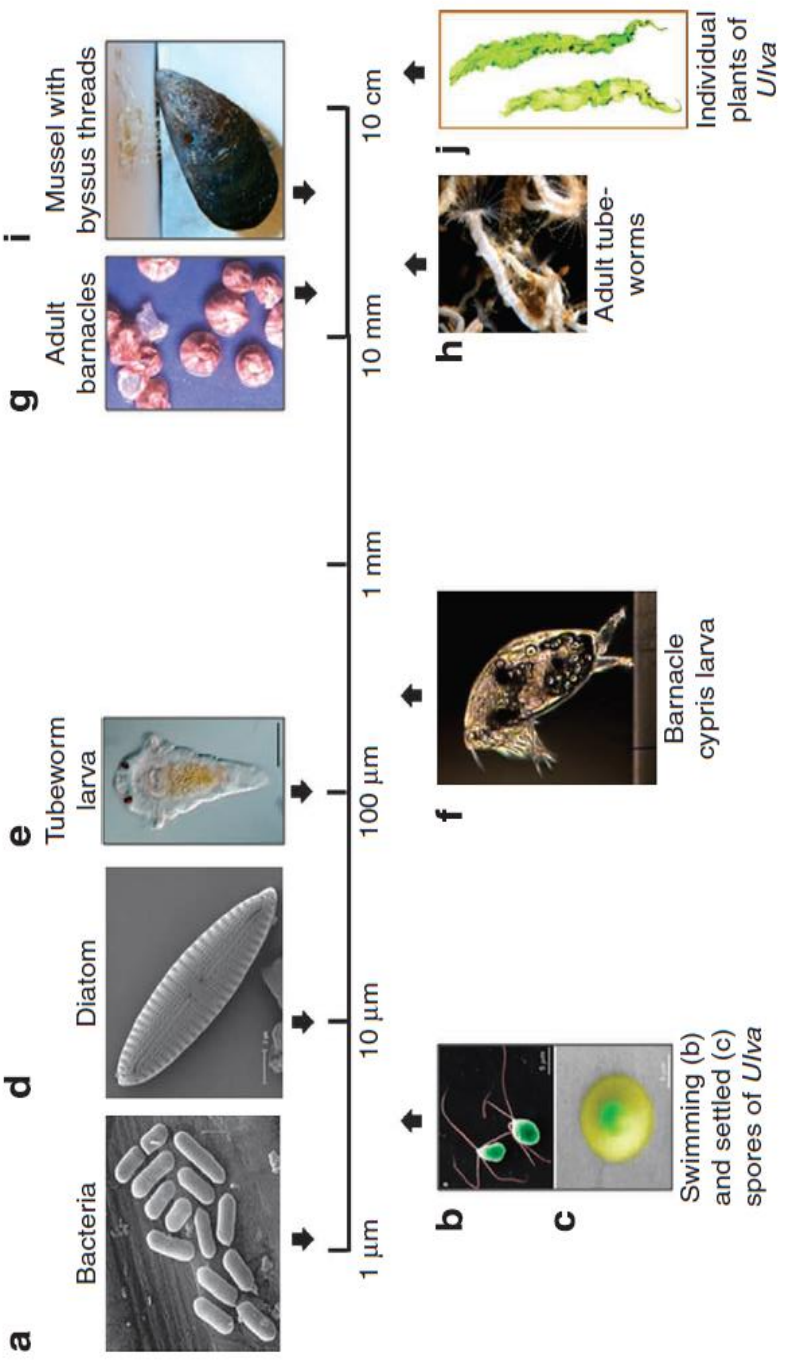

Figure 4. Diversity and size scale of a range of representative marine fouling organisms. Adapted from [7].

The accumulation of microorganisms on solid surfaces is referred to as biofilm, which consists of microbial cells and their extracellular substances. Biofilms are heterogeneous in space and changing over time [10-14]. They are mainly composed of bacteria, EPS and water, this latter constituting up to 97% of the biofilm [12]. Biofilm are found on both natural and artificial materials. Besides their adverse effect in industry, 65% of nosocomial infections occurring in hospital are due to the contamination by a biofilm, and the treatment of biofilm-associated infections costs more than 1 U.S dollar billion annually [15]. On the contrary, biofilms can be beneficial, for example to treat wastewater (e.g. remove heavy metal ions from aqueous solution) or for a variety of biotechnological applications [16].

1.2.2 Microbiologically influenced corrosion (MIC)

Microbiologically influenced corrosion (MIC) or biocorrosion, is usually referred to as accelerated deterioration process of metals owing to the participation of microorganisms, which could initiate or accelerate corrosion reaction [17-19]. Generally, the corrosion rate increases due to the presence of bacteria, which accelerate the rate of the anodic and/or cathodic corrosion reaction, while the detailed mechanism of biocorrosion process is still poorly understood and could be varied for different microorganisms [3]. However, several general features of biocorrosion have been described, mainly including the modification of the physical/chemical conditions at metal surface by biofilm formation, thereby modifying electrochemical reactions [18].

The awareness of MIC was absent in corrosion science until the late 1970s. The influence of biocorrosion has a great economic and environmental implication, and is underestimated. It covers industrial fields from shipping, oil and gas, cooling condensers (as illustrated in Figure 5), nuclear waste storage, civil engineering to implanted biomaterials. Differently from abiotic corrosion, the interaction between bacteria and

metal leads to a modification of the metal/solution interface, causing localized corrosion rate 1,000 – 100,000 times higher than in the absence of bacteria, and 20% of corrosion failure on metals is attributed to MIC [18, 19]. The direct cost of MIC is estimated about $30 − 50 billion each year [20]. In the past two decades, bacterial adhesion mechanisms and the role of bacteria in MIC have been studied to better understand biocorrosion. In some cases however, corrosion could also be slowed down or inhibited on metallic materials by the presence of a biofilm [3, 21]. Therefore, it is important to clarify the mechanisms of MIC, monitoring, preventing or taking advantage of it.

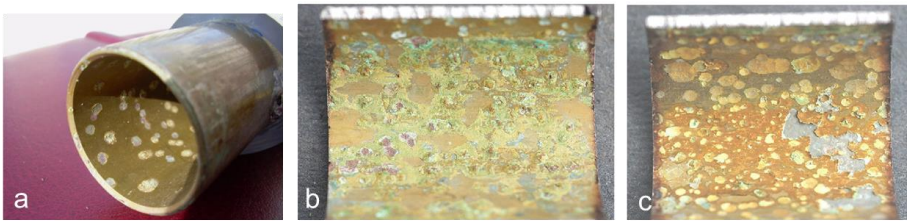

Figure 5. Examples of corroded Cu/Ni 70/30 cooling condenser tubes, (a) one month of exposure in seawater, (b) Inner surface, purplish-greenish corrosion products, (c) Exfoliation of a thin layer of corrosion products and localized attacks under the crust are clearly visible. Adapted from [22].

Biocorrosion process cannot be explained by one single mechanism, it is recognized as arising from the combined effect of metal surface, corrosion products, environmental conditions and mixture of bacteria species. It was shown by Pitonzo that the corrosion rate of carbon steel is much higher in mixed bacterial culture than in pure culture [23], which illustrates the synergetic effect between different microorganisms.

Sulfate-reducing (SRB) and acid-producing bacteria are currently the main species found in biofilm thought to cause biocorrosion on metal [3]. Up to now, SRB, a model anaerobic bacterium, is recognized as the most common and corrosive bacterial species involved in damage of iron and ferrous alloys. The biocorrosion of carbon steel by SRB is the most

investigated case. As illustrated in Figure 6, the metabolism of SRB on carbon surfaces, including consumption of oxygen and production of acid and sulfides, establishes a localized chemical gradient across metal/biofilm/liquid. The dissolution of metal from the surface is due to the existence of such gradients, which leads to the formation of electrochemical cells, enhancing anodic and/or cathodic reactions. The production of acids and sulfides are the keys to breakdown the passive layer on the steel surface, thereby enhancing corrosion [3, 24]. Besides that, Beech and colleagues investigated the role and contribution of EPS produced by bacteria to the biocorrosion process [25-28]. It is proposed that the selective binding of EPS to metal ions could promote electron transfer between biofilm and metals [19].

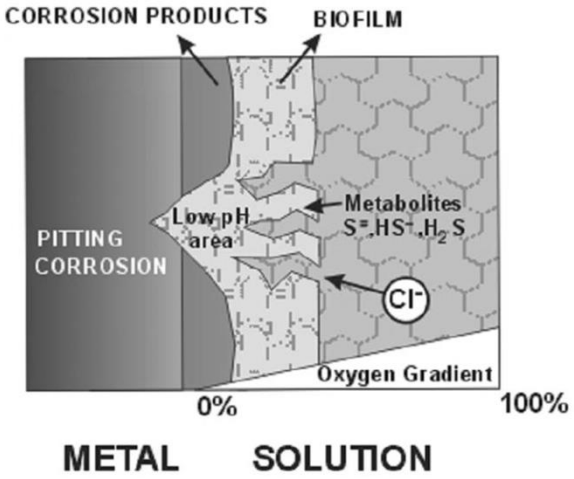

Figure 6. The bioelectrochemistry interpretation of the biocorrosion process of carbon steel in anoxic environments. Adapt from [29].

1.3 The influence of conditioning film on bacterial adhesion and biofilm formation

Biofilm formation is a complex process, which ranges from inorganic and organic molecules adsorption (conditioning film formation), initial cell attachment (bacterial adhesion) to irreversible cell adhesion

facilitated by production of EPS and cell accumulation (biofilm formation), as illustrated in Figure 7. Transportation and adsorption of organic substances from bulk liquid to underlying substrate is the initial step of biofilm formation. This process induces a new biologically conditioned interface.

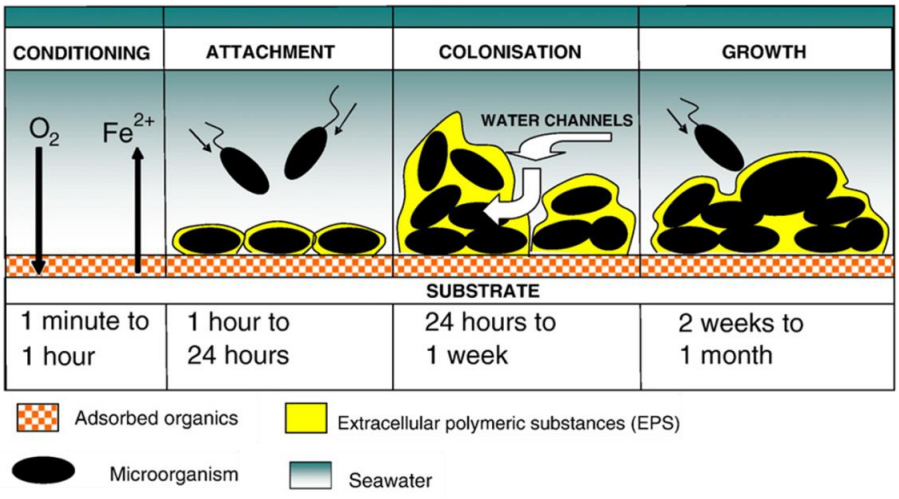

Figure 7. Schematic of critical biofilm formation stages. Adapted from [30].

1.3.1 Conditioning film

A conditioning film, consisting of ions, inorganic matters and organic biomolecules (proteins, polysaccharides, lipids and etc), is spontaneously formed from seconds to minutes after immersion of materials in natural water, as an initial stage of biofouling [31, 32]. This conditioning film strongly alters the physico-chemical properties of surfaces, such as surface free energy, electrical potential and hydrophobicity, which may affect the subsequent microbial attachment and biofilm formation process [33]. The conditioning film was reported to be about 20 – 80 nm in average thickness and adsorption rate of this layer is in the order of 0.1 nm/min [31, 34, 35]. Usually, the conditioning film becomes negatively charged in

neutral condition due to the adsorption of organic components, contributing to the charge through their carboxylic and hydroxyl groups. Besides, the conditioning film may also be considered as nutrients for microorganisms living in oligotrophic environments.

Humic substances and proteins are the major dissolved organic compounds reported in natural waters, and are expected to contribute to the conditioning film [36]. Leis showed the evidence of presence of humic substances in conditioning film from natural waters, similar results were found in seawater by Loeb previously [31, 36]. The molar mass of humic substances is ranging from 2,000 to 100,000 g/mol, and they form aggregates of 2 to 50 nm diameter in natural waters [37]. They are polyfunctional macromolecules with functional groups such as carboxylic acid, hydroxyl, ester, amides and heterocyclic nitrogen. Proteins and their hydrolysis products (small peptides, free amino acids) are mainly secreted by living organisms or originate from degradation of their dead body [38]. Although the exact nature of the organic molecules involved in conditioning film is still largely unknown due to their very diverse origin, it is expected that the functional groups and hydrophobic moieties of these organic molecules are involved in their adsorption and mediate cell attachment [37].

The composition of conditioning films formed in aqueous environments is largely unknown. It is the result of competitive adsorption between organic biomolecules present in aqueous environment. The molecular composition of the conditioning film changes with time firstly due to the replacement of adsorbed molecules by higher affinity molecules [39, 40]. It can be assumed that the conditioning film is mainly composed of organic biomolecules in addition of deposition of inorganic components. Jain showed that carbohydrate was the most abundant component in the conditioning film on glass [41]. Compère showed that the adsorption kinetics of proteins is higher than the one of carbohydrates in the first 5 h, and both are the main components observed in conditioning film on stainless steel in

marine environment. Using atomic force microscopy (AFM), they showed that the conditioning film is still heterogeneous after 24 h [42]. The composition of conditioning film varies also depending on the substrate properties [33]. Taylor *et al.* studied conditioning film formed on nine different substrates in seawater. The results suggest that the composition and structure of conditioning film vary significantly among substrates during short exposures (~3 days). It can be concluded that the conditioning film is heterogeneous, and its composition is depending on the surface properties of substrates and the location and season of natural water tested.

The physico-chemical properties of an immersed surface of materials change due to the formation of a conditioning film, like a coating layer, and it is assumed that this conditioning film gives different adhesive properties for microbes compared to the original substratum. It was shown that the conditioning film on glass formed in filtered natural seawater strongly enhanced the adhesion of *Pseudomonas sp* [41]. The influence of the conditioning film on microbial adhesion in natural water is a complex and dynamic phenomenon.

1.3.2 Bacterial adhesion and biofilm formation

Microorganisms are able to attach onto a variety of solid surfaces, from metals, polymers to human tissues, which causes problems in a wide range of fields, from medical implants to different types of industry processes. Therefore, the interaction of cells and surfaces has been a topic of study in many different fields [43]. Biofilm formation is the net result of combined physical, chemical and biological processes. As illustrated in Figure 8, bacterial adhesion and biofilm formation on solid substrates is proceeding through a succession of steps [35, 44]. First, an immersed bare substrate is conditioned instantaneously by adsorption of organic matter (e.g. proteins, polysaccharides) and deposition of inorganic substances present in

aqueous environment, which diffuse more rapidly than cells and thereby give new physico-chemical properties to the substratum (Figure 8a→b).

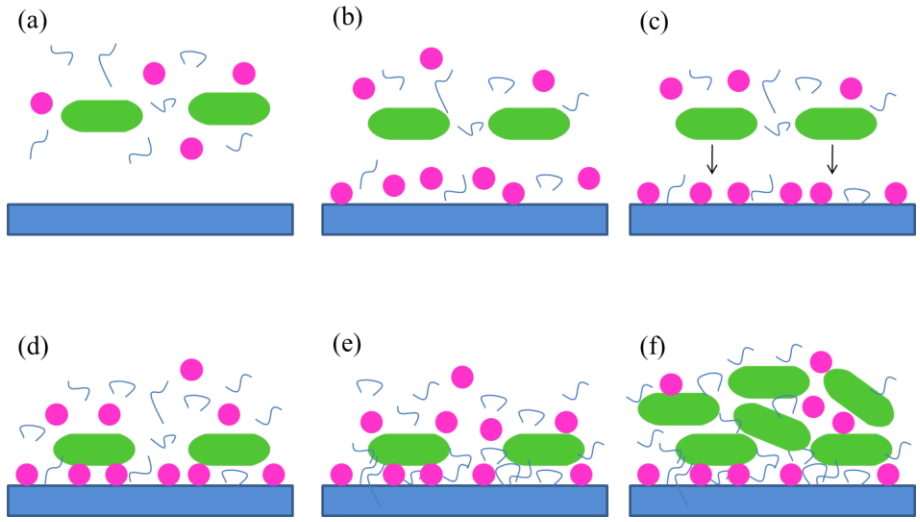

Figure 8. Schematic representation of the successive steps involved in the formation of biofilms: (a) initial situation; (b) substratum conditioning; (c) cell transport; (d) primary adhesion; (e) anchorage; (f) growth. Adapted from [44].

Subsequently, transportation of planktonic cells to the conditioned substrate occurs by diffusion, sedimentation, convection and possibly intrinsic motility and involves electrostatic, Van der Waals and hydrophobic interactions, which is referred to as reversible adhesion (Figure 8c→d). Bacteria exhibit a weak adhesion force to surfaces at this stage, and adhered bacteria may be removed by mild rinsing. Then, adhered bacteria go from reversible adhesion to irreversible adhesion on a time scale of several hours in a step which involves the specific interaction between cell surfaces and substrate. As illustrated in Figure 9, extracellular organelles, such as flagella, pili and curli, mediate the specific interaction of bacteria with surfaces for irreversible attachment. EPS are produced by attached bacteria during this stage (Figure 8e), which retain them on the substrate more firmly while the growth and reproduction of bacteria with associated EPS leads to further biofilm development (Figure 8f). Proteins play an important role for the

irreversible bacterial attachment [45]. The morphology and phenotype of bacteria change after attachment onto surfaces. As biofilms grow thicker, partial detachment of bacteria occurs due to the lack of nutrients and high fluid stress shear on the surface of biofilm.

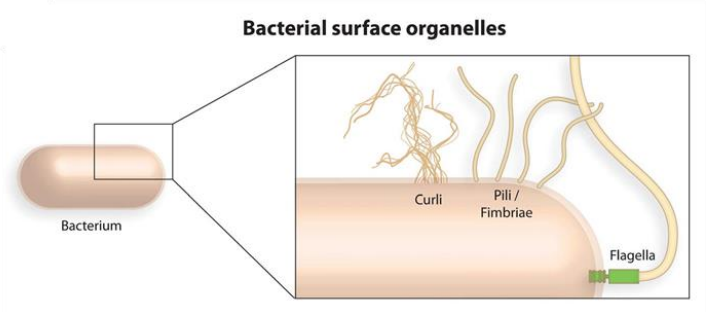

Figure 9. The bacterial surface has several organelles that facilitate interactions with substrates, including curli fibers, pili and flagella. Adapted from [43].

Almost all materials can be colonized by microorganisms sooner or later while adhesion mechanisms and kinetics might be different depending on the surface properties of materials. The preference of bacteria to associate with surfaces has its reasons [43]. As mentioned above, a conditioning film is always formed on solid substrates in aqueous media while the high organic concentration in the conditioning film could serve as nutrients to attract microorganisms. Furthermore, some metal substrates, such as iron and magnesium, can be directly useful for bacterial respiration, as terminal electron acceptor. Moreover, when forming a biofilm, bacteria exhibit 10 – 1,000 times higher resistance to the effect of biocides [15] and protect themselves from environmental stress conditions, such as protozoan grazers [46].

The composition and properties of biofilm change during biofilm development, and gradients (e.g. oxygen level) develop within the biofilm. The biofilm surface is highly adsorptive, and can continuously collect organic matter and nutrients from surrounding environment. The presence of

biofilm changes the microenvironment on the colonized surfaces, creating different conditions compared to the bulk liquid. Inorganic substances in biofilm affect the physical and biological structure of the film, e.g. metal ions, such as calcium, magnesium and iron provide intermolecular bonding in biofilm while organic matter content in the biofilm varies depending on the metabolism of bacteria species and carbon sources available. A form of cell-cell communication inside biofilms was identified and is called quorum sensing (QS), which contributes to the formation and maturation of biofilms. QS signal molecules in marine bacteria and their relationship to biofouling have been reviewed by Dobrestov *et al*. recently [47].

1.3.3 Extracellular polymeric substances (EPS)

The existence of EPS is the prerequisite to form cell aggregates and biofilm. As defined by Flemming, EPS are hydrated biopolymers (including polysaccharides, proteins, nucleic acids, lipids and other polymeric compounds) that are secreted by bacteria to encase and immobilize microbial aggregates [11]. They have been found in the intercellular space in microbial aggregates, and are responsible for keeping microbial aggregates together and attach biofilms to surfaces. The gel-like, highly hydrated EPS matrix creates a microenvironment for embedded cells, which is heterogeneous and changing over time.

Table 1. Composition of extracted EPS and concentration range of components. Adapted from [48].

Component	Content in EPS
Polysaccharides	40 – 95%
Proteins	< 1 – 60%
Nucleic acids	< 1 – 10%
Lipids	< 1 – 40%

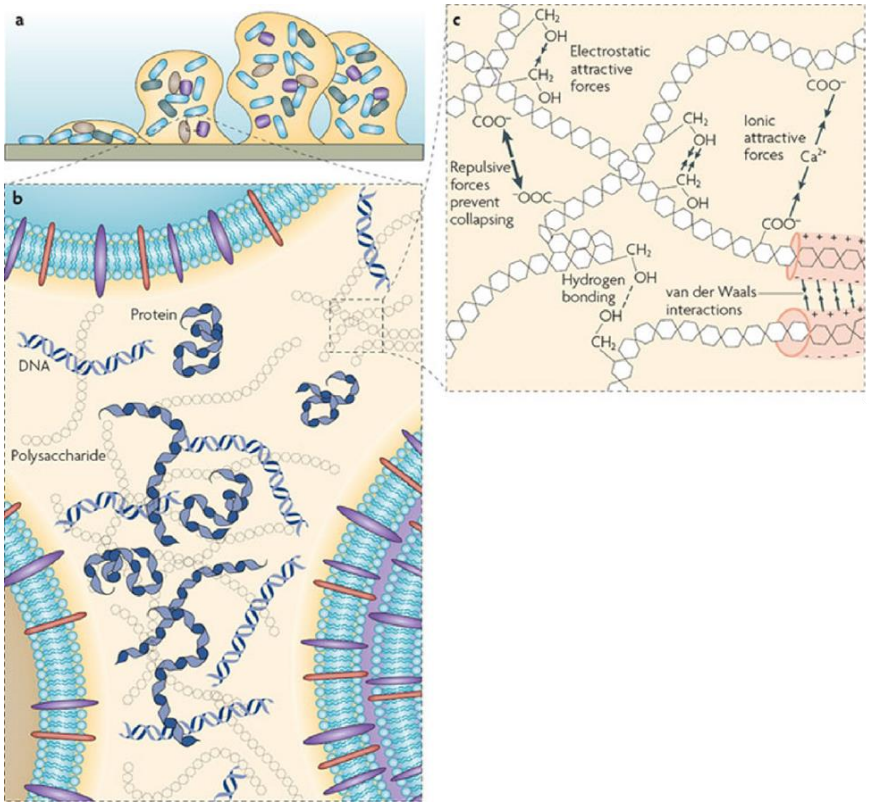

Figure 10. The extracellular polymeric substances matrix at different levels of resolution. (a) A model of a bacterial biofilm attached to a solid surface. (b) The major matrix components – polysaccharides, proteins and DNA. (c) The classes of weak physico-chemical interactions and the entanglement of biopolymers that dominate the stability of the EPS matrix. Adapted from [51].

The composition of EPS varies, not only depending on bacterial species and growth conditions, but also in function of their proximity to bacterial cells [49]. EPS released from bacteria into bulk phase of surrounding liquid are called loosely bound EPS while EPS associated with cells as a capsule are called tightly bound EPS. The component composition is different depending on the type of EPS [26, 49]. The composition of EPS, as reported in literature, also largely depends on the method used for its isolation, and contamination from cell lysis should be avoided during the extraction procedure [50]. An average component content of EPS from

various natural and engineered systems is given in Table 1 [48]. Polysaccharides and proteins are the major components of EPS. As shown in Figure 10, the weak physico-chemical interaction forces between EPS, such as electrostatic forces, hydrogen bonding, ionic bridges and Van der Waals interactions, give the mechanical stability of the biofilm.

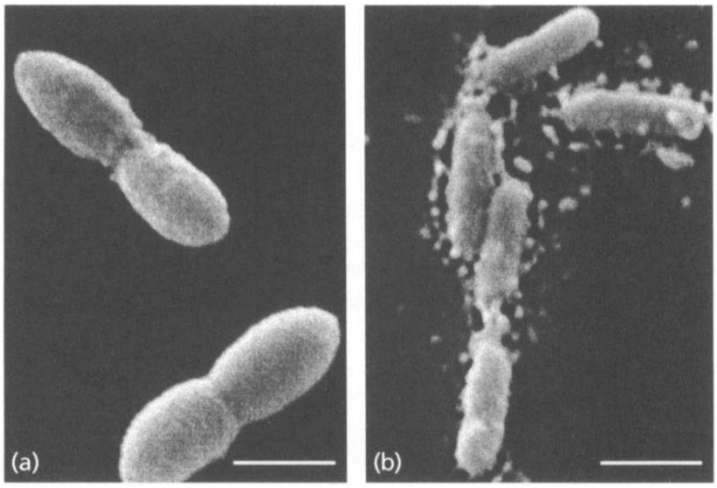

Figure 11. Scanning electron micrographs of *A. brasilense* cells adhering on glass after 2h (a) and 24h (b) contact time at 30°C; cells harvested in the exponential phase; mild rinsing. Bars, 1 μm. Adapted from [45].

The functions of EPS in bacterial biofilm were well described by Flemming [11, 51]. EPS form a three-dimensional scaffold for biofilm architecture, like a house for bacteria. As shown in Figure 11, EPS are also produced after bacterial adhesion, and can thereby promote the further attachment of bacteria. It was directly demonstrated that extracellular proteins are involved in the adhesion of *Azospirillum brasilense* onto glass [45]. EPS can not only facilitate irreversible bacterial attachment, but also provide many other ecological functions. In nature, EPS keep bacteria together with intense interactions and formation of synergistic microconsortia. One of the most important functions of EPS is to provide mechanical stability to the biofilm. The viscoelastic properties of EPS lead to increased friction resistance, which makes mechanical cleaning less efficient. The sorption ability of EPS allows pumping nutrients from

surrounding environment for utilization in biofilm community. The enzymatic activity of EPS helps to digest exogenous nutrients for bacteria. Gene transfer might also occur between different bacteria species inside biofilm.

The release of EPS to the surrounding liquid is proposed to form a conditioning film on the surface of materials. The results of Beech showed that the conditioning films formed on stainless steel by different types of EPS from *Pseudomonas* NCIMB 2021 are chemically dissimilar, and tightly bound EPS shows a higher protein content [52]. The influence of EPS conditioning film on bacterial adhesion is worth to be further investigated, it might either promote a specific bacterial adhesion or inhibit bacterial adhesion. Further results of Gubner and Beech showed that stainless steel conditioned with different types and concentrations of EPS, isolated from *Pseudomonas* NCIMB 2021, indeed affected initial attachment of *Pseudomonas* NCIMB 2021 [53]. The influence on attachment is due to the different chemical components of EPS rather than to the wettability and roughness changes of stainless steel surface after adsorption of different EPS [53]. The results of Stadlet *et al.* showed that while EPS conditioning layer is not homogeneous on steel surfaces, the adhesion of *Desulfovibrio vulgaris* is significantly decreased on EPS-coated steel in comparison to the non-coated steel in a short time scale (3 days) [54]. Recently, Hwang *et al.* also showed that EPS coating reduced bacterial adhesion (*Burkholderia cepacia* and *Pseudomonas aeruginosa*) as compared to bare glass, especially in high ionic strength conditions [55].

There are only a few reports concerning the contribution and the role of EPS on biocorrosion [25, 56]. The results of Busalmen showed the influence of catalase, produced by bacteria from genus *Pseudomonas*, on the oxygen reduction process on the surface of Al brass [56]. EPS, comprising functional groups such as hydroxyl and carboxylic acid, act as polyanions under natural conditions, which can bind to cations, thereby chelating metal

ions [57]. Beech and Cheung showed that the EPS produced by two SRB species can bind metal ions, especially Mo, and with such phenomenon, it is conceivable that EPS could directly influence the electrochemical behavior of steel, probably enhancing corrosion rate [25]. Further studies demonstrated that a protein-carbohydrate complex isolated from EPS of marine SRB of the genus *Desulfovibrio* is capable to enhance pitting corrosion on mild steel [28]. The detection of iron in the EPS isolated from SRB cultured in the presence of mild steel proved the metal chelating property of EPS [26].

1.4 Antifouling coatings

The implementation of antifouling methods strongly depends on practical applications of protected materials, e.g. coating on ship hull or localized treatment for cooling condensers. A traditional way to control biofouling in cooling condenser systems is chlorination, which must be regularly applied [6]. However, its toxic by-products including halomethanes and other organohalogens are harmful to aquatic environment.

Antifouling coatings are mainly designed according to two approaches: biocide antifouling coatings and non-biocide antifouling coatings. The former is often based on the use of tin or copper-based compounds, which however show toxic effect to marine organisms and pollute the environment. The use of tributyltin (TBT) to prevent biofouling was banned by International Maritime Organization (IMO) in 2001 due to its environmental risk. Other biocide-releasing coatings are currently the interim solution to treat biofouling in marine environment [30]. However, due to increase of concerns about their toxic effect to marine organisms, other alternatives to prevent biofouling are desired. Besides, killing bacteria might not prevent the problem of biofouling, the body of dead organisms might indeed accumulate on the surface of materials and biofouling would still remain. Therefore, non-biocide antifouling coatings constitute the actual

trend for developing methods against biofouling. Their mode of action is centered on preventing or strongly reducing the adhesion of fouling organisms, e.g. poly(ethylene oxide) (PEO) or poly(ethylene glycol) (PEG)-based antifouling coatings. Recently, approaches to design antifouling coatings have been summarized and reviewed by Banerjee *et al.* [58], as illustrated in Figure 12. Different strategies may be involved depending on the target (molecular, micro- or macrofouling).

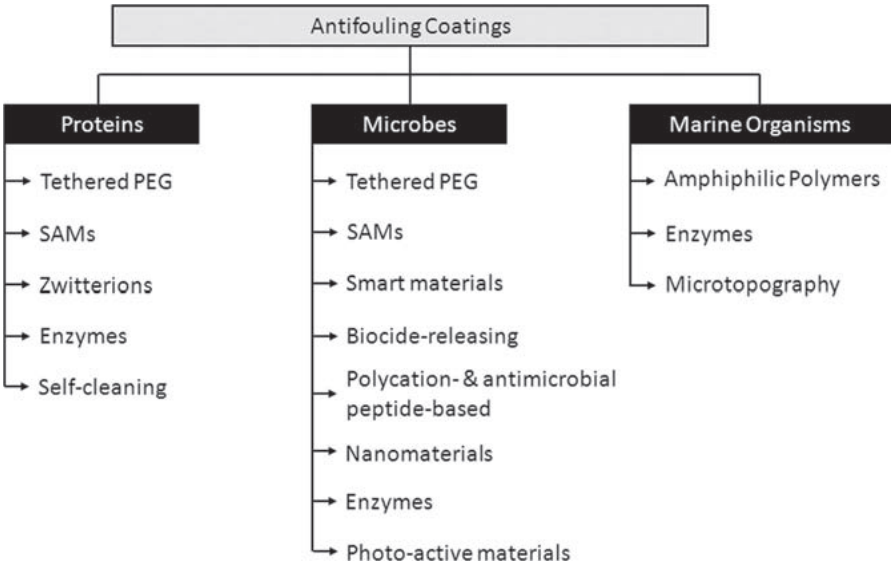

Figure 12. Various approaches to fabricate antifouling surfaces. PEG = poly(ethylene glycol). SAMs = self-assembled monolayers. Adapted from [58].

1.4.1 Self-assembled monolayers (SAMs)

Self-assembled monolayers (SAMs) are formed by the adsorption of small organic molecular constituents from the solution or gas phase onto the solid surface [59]. The SAMs formation occurs spontaneously upon immersion of the appropriate solid material into the molecular solution. The assembling time varies from minutes to hours, and the typical thickness of a SAM is 1 – 3 nm depending on the length of the chosen molecule. The

quality of SAMs depends on several factors, such as the concentration of the molecule in solution, the nature of the solvent, the duration of immersion, temperature, purity of solution, and cleanliness of substrate. As illustrated in Figure 13, in a typical SAM of alkane thiols on gold, the molecules have a thiol head group, with a high affinity for the substrate, and a terminal functional group which generates a well-defined desired functional surface for materials while keeping the bulk properties intact. Van der Waals interactions between the alkyl chains ensure the good organization of the monolayer.

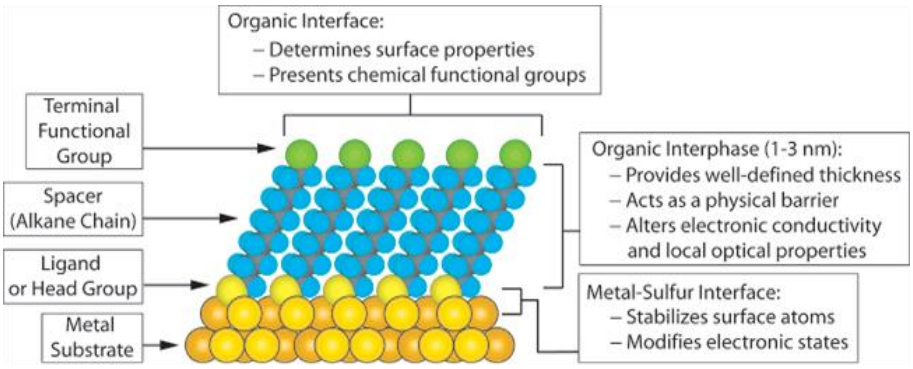

Figure 13. Schematic diagram of an ideal, single-crystalline SAM of alkanethiolates supported on a gold surface with a (111) texture. Adapted from [59].

Although the application of gold as a substrate is limited, the assembly of alkane thiols on gold is still the most studied example of SAMs, which has been reviewed by Love *et al.* and Kind *et al.* recently [59, 60]. Due to the cost and limited applications of noble metal (gold, silver, platinum), transition metals and alloys (iron, titanium, aluminium and stainless steel) have a more wide application for industry. However, the outmost surface of transition metals are in oxidized state in nature or readily oxidized, which does not allow the assembly of thiols [61]. Therefore, other substituted molecules for SAM formation on metal oxide surfaces are very necessary. Organosilane molecules are known to form SAMs on

hydroxylated surfaces, e.g. silicon oxide [62]. Their successful assembly was also reported on aluminium oxide, quartz, glass, mica, germanium oxide and titanium oxide [62, 63]. However, the quality of organosilane self-assembly is not always satisfying and poorly reproducible because it is highly affected by ambient parameters, such as humidity, temperature and presence possible contaminants. SAMs of alkane phosphonic acids have been reported to be applied on a wide range of metal oxide surfaces, including stainless steel, aluminium oxide, copper oxide, brass, tantalum oxide, niobium oxide, zirconium oxide, titanium oxide [61, 64-69].

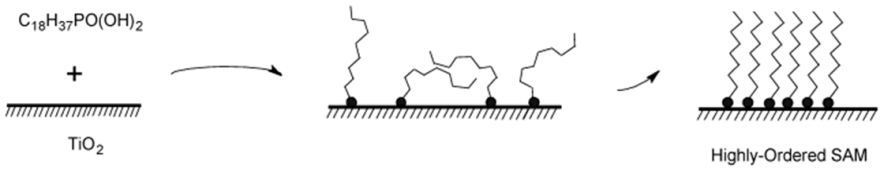

Figure 14. Schematic of formation of OPA SAM on TiO_2 surface. Adapted from [63].

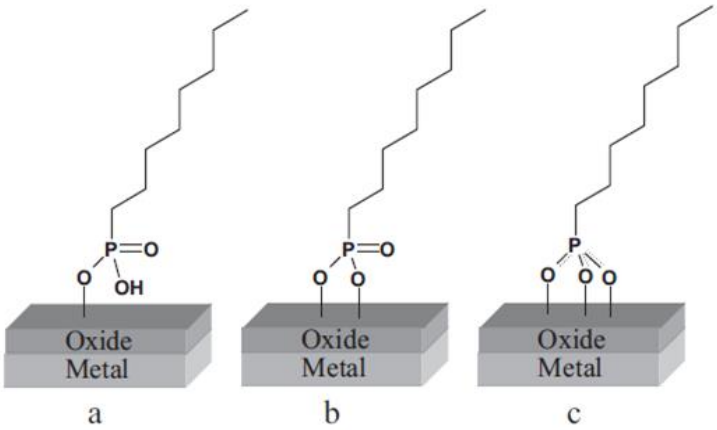

Figure 15. Schematic representation of the (a) mono-, (b) bi- and (c) tridentate grafting modes of a alkane phosphonic acid molecule onto an oxidized substrate. Adapted from [69].

The formation of octadecylphosphonic acid (OPA) SAM on TiO_2 was monitored using Fourier transform infrared spectroscopy (FTIR), as reported by Helmy [63]. As illustrated in Figure 14, individual OPA molecules are covalently bound to the surface, randomly distributed on the substrate in the early stage. As more and more OPA molecules approaches, the surface coverage and order of OPA increases to form a highly packed OPA SAM. Several possible covalent bonding modes between alkane phosphonic acids and oxide surfaces were reported (as illustrated in Figure 15), highly depending on the substrate [69-73]. The bonding strength of SAMs to different metal oxide substrate depends on the substrate nature and coating process. It was shown by Gawalt that gentle heating of titanium oxide and stainless steel after SAMs formation improves the stability of alkane phosphonic acid layers [66, 71].

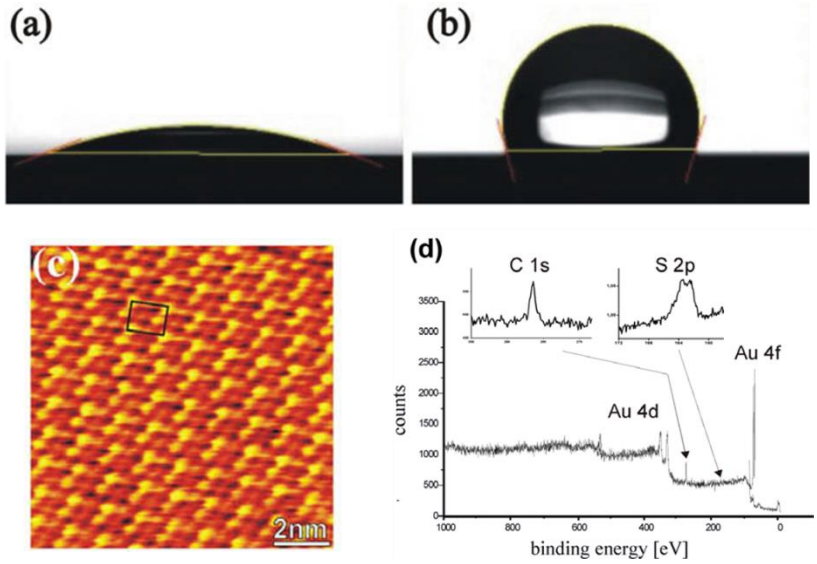

Figure 16. Representative techniques for characterization of SAMs: water contact angle measurements on (a) hydrophilic and (b) hydrophobic surfaces, (c) high resolution STM with decanethiolate molecules in the SAM, (d) XPS spectrum of a heptadecane thiolate SAM on gold. Adapted from [60].

There are a number of techniques that are available to characterize SAMs, from spectroscopic techniques to microscopic methods [60], as illustrated in Figure 16. Among them, wettability examination is the most simple and rapid method to check the SAMs formation, although the obtained information is rather limited. Depending on the functional groups of SAMs (e.g. -CH_3 and -OH groups), the surface may become hydrophobic or hydrophilic, which can be easily checked by water contact angle (WCA) measurement (Figure 16a, b). Molecular structure of SAMs can be observed by high resolution scanning tunneling microscopy (STM) with nanoscale resolution (Figure 16c). Elemental composition and chemical functionality of SAMs can be obtained from x-ray photoelectron spectroscopy (XPS) analysis (Figure 16d), which also allows the thickness of SAMs to be determined, based on attenuation of signal from the substrate. The formation of SAMs can be monitored in real time by surface plasmon resonance spectroscopy (SPR), which provides the adsorption kinetics of SAMs and quantitative information.

SAMs on metal or metal oxide surfaces have a wide range of applications. SAMs of alkanethiols on gold with different functional groups (e.g. CH_3, OH, COOH, NH_2) were used as model surfaces to study the influence of surface chemistry on protein adsorption and cell adhesion [74]. The formation of SAMs on surface of metals, as a densely packed barrier film, is capable to protect them from corrosion in aqueous environment [75]. Jennings *et al*. reported the SAMs of alkanethiols on copper to protect it from corrosion. The results pointed out that the ability of SAMs to play the role of barrier is related to the strength of intermolecular interactions within the SAMs [75]. Hydrophobic coating of SAMs on metal can reduce corrosion rate and microbial adhesion [76]. It is explained that due to the hydrophobic effect and insulating property of SAMs, aggressive ions and microorganisms cannot easily reach the underlying metal. The results of Telegdi *et al*. showed a significant reduction of microbial adhesion on iron

and copper after coating with a hydrophobic SAM of alkylhydroxamic acid or octadecylphosphonic acid [76]. Moreover, a longer alkyl chain gives better anti-adhesion efficiency.

As mentioned previously (see 1.3.1 "conditioning film"), bacterial adhesion occurs on surfaces which are already covered by a layer of organic constituents. Therefore, the ability to resist the adsorption of organic molecules, especially proteins, is believed to be a prerequisite for the ability of a surface to resist the adhesion of bacteria and biofilm formation. SAMs of alkanethiols on gold with a wide range of functional groups are also used to investigate and screen surfaces that resist the adsorption of proteins in solution [77-79]. Chapman and Ostuni reported four important features for polymers with protein-resistant property: containing a polar functional group, incorporate hydrogen bond accepting groups, absence of hydrogen bond donating groups, absence of any net charge [77, 78]. Until now, SAMs with PEG or PEO terminating groups constitute the most common approach to prepare protein-resistant surfaces.

1.4.2 PEO brushes as nonfouling surface coatings

End-tethered PEO on surfaces is still the most effective method to reduce protein adsorption from solution. However, the mechanism to explain its protein resistance properties remains elusive. The protein resistance effect of PEO is currently attributed to its large excluded volume in aqueous solutions, its surface density and thickness of PEO layer [80, 81]. The resistance of PEO to nonspecific protein adsorption is widely accepted as arising from a steric repulsion effect and to the highly hydrated PEO chains which are then very flexible in water, where the PEO layer prevents proteins from reaching the substrate surface. It was suggested by Wang that the interactions between PEO and water also exert a strong influence on protein resistance since it gives rise to the dominant steric repulsion force [82]. Additionally, the removal of water from PEO chains due to approaching

protein molecules, providing compression, creates an unfavorable osmotic and elastic stress, which generates a repulsive force as well.

Unsworth *et al*. determined an optimal PEO chain density (0.4 – 0.5 chain/nm^2) to achieve protein resistance [83]. The protein resistance property increases with increasing PEO chain density until a critical value. When PEO exceeds this critical density value, it loses its mobility and hydration state, and protein resistance is less effective. On the other hand, at low chain densities, higher length of PEO chains is more effective to resist protein adsorption due to the higher surface coverage obtained.

Recently, studies showed that the PEO chain conformation is also an important factor to determine its protein resistance ability. Harder *et al*. found that protein resistance of oligo(ethylene glycol) functional layers is influenced by its internal structure [84]. The methoxy-terminated tri(ethylene glycol) (EG3-OMe) groups of alkane thiolates are accommodated on gold substrate in helical conformation while the same molecules on silver substrate are in all-trans conformation. The former structure is found to be resistant to fibrinogen adsorption, but the latter did adsorb fibrinogen. It was speculated that the helical phase forms a stable solid-liquid interphase involving tightly bound water, which might not be displaced by proteins [85]. According to the literature, all of these factors (chain length, chain density, distal chemistry, chain conformation, state of hydration) involved in protein resistance ability of PEO are inherently correlated.

PEO-containing polymer can be immobilized onto target surfaces through several different ways, e.g. chemical adsorption using a “grafting to” or a “grafting from” approach, physical adsorption of a block copolymer or a graft copolymer [86, 87], as illustrated in Figure 17. Ma reported a method to graft oligo(ethylene glycol) methyl methacrylate (OEGMA) on gold using surface-initiated atom transfer radical polymerization (SI-ATRP) to produce a thick and robust film, which resists nonspecific protein adsorption of fibronectin, 10% fetal bovine serum (FBS) or 100% FBS, as examined by

SPR [88]. Biomimetic strategies are also developed to tether PEG layer on various surfaces. Dalsin *et al*. reported the use of 3,4-dihydroxyphenylalanine (DOPA), inspired from mussel adhesive proteins, to tether PEG on TiO_2 surface [89]. Monomethoxy-terminated PEG conjugated with DOPA is proved to attach on TiO_2 surface via the formation of charge-transfer complexes. The obtained layer shows excellent inhibition of serum adsorption, as monitored by optical waveguide lightmode spectroscopy (OWLS).

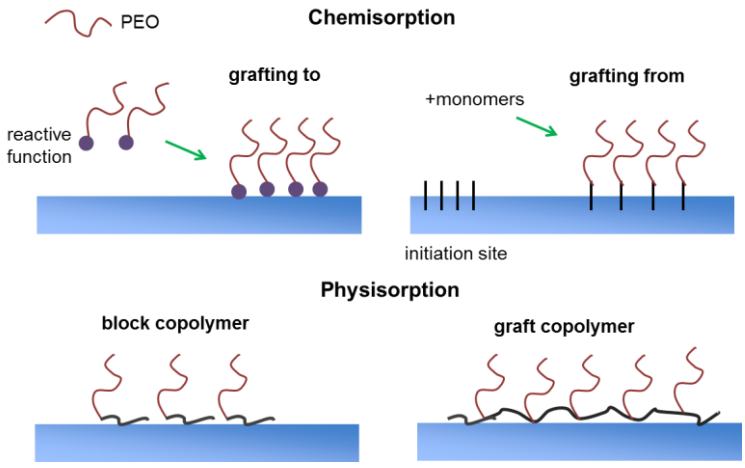

Figure 17. Classification of PEO-containing polymer adsorption methods.

PEO layers are further investigated for their potential anti-adhesion ability. Park *et al*. reported bacterial adhesion on PEG modified polyurethane surfaces [90]. They concluded that the longer PEG chain (3.4 kDa) has better bacterial resistance than short PEG chain (1 kDa) and sulfonate-terminated PEG was the most effective in reducing bacterial adhesion in comparison to hydroxyl and amino-terminated groups. The same effect of PEO chain length on microbial adhesion was also reported by Roosjen *et al.* [91]. Besides, they showed that adhering bacteria and yeast can be more easily removed from PEO-coated surface in comparison to bare glass by passing air bubbles, indicating a weak adhesion of microorganisms on the PEO brush. Poly(L-lysine) (PLL)-g-PEG has been immobilized on

titanium oxide (TiO_2) and niobium oxide (Nb_2O_5) surfaces by electrostatic attraction force between positively charged PLL and negatively charged metal oxide surfaces, and is effective to reduce serum and fibrinogen adsorption [92]. Further studies using protein-resistant PLL-g-PEG is shown to also reduce adhesion of *Staphylococcus aureus*, *Staphylococcus epidermidis*, *Streptococcus mutans* and *Pseudomonas aeruginosa* on TiO_2 [93]. Recently, poly(acrylic acid) (PAA)-g-PEG has been synthesized and used as counterpart of PLL-g-PEG, which can adsorb to positively charged surface, and thereby also reduce protein adsorption [94]. Co-grafting of lysozyme and PEG on stainless steel surface was proved to prevent albumin adsorption and *Listeria ivanovii* adhesion by a combined anti-adhesive and biocide activity [95]. PEO-PPO-PEO triblock copolymer has been shown to adsorb on hydrophobic surfaces to prevent protein adsorption and platelet adhesion [96]. The properties and applications of this triblock copolymer will be detailed hereunder.

1.4.3 PEO-PPO-PEO triblock copolymers

Water soluble triblock copolymers of poly(ethylene oxide) and poly(propylene oxide) (PEO-PPO-PEO) are non-ionic amphiphilic surfactants, commercially available under the name of Pluronics® or Poloxamers [97, 98]. A general chemical structure of PEO-PPO-PEO triblock copolymer is shown in Figure 18.

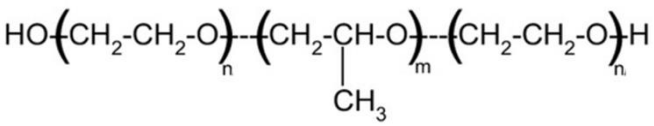

Figure 18. Chemical structure of PEO-PPO-PEO triblock copolymer. Adapted from [98].

As shown in Table 2, there are a wide range of PEO_n-PPO_m-PEO_n triblock copolymers with varying copolymer composition (PPO/PEO ratio) and molar mass (PPO and PEO block length) for different applications. Due to their surface-active properties, the applications of Pluronic range from dispersion stabilization, lubrication, foaming to drug solubilization and controlled release [99-101]. Recently, the interest has been focused on adsorbed layers of Pluronic to reduce nonspecific protein adsorption and cell adhesion on different materials, which is potentially useful to improve biocompatibility for implanted biomaterials and to design low fouling surfaces for industry [96, 102-104].

Table 2. Composition of Pluronic block copolymer surfactants. Adapted from [105].

Pluronic®*	Average mol wt	PEO/PPO/PEO (monomer units)
L31	1100	2/16/2
L35	1900	11/16/11
F38	4700	43/16/43
L61	2000	3/30/3
L62	2500	8/30/8
L63	2650	10/30/10
P65	3400	19/30/19
F68	8400	76/30/76
F88	11400	104/39/104
F98	13000	118/45/118
L101	3800	6/56/6
P103	4950	17/56/17
P105	6500	37/56/37
F108	14600	129/56/129
F127	12600	99/67/99

*F(flake), P(paste) or L(liquid)

As a surfactant, Pluronic turns into micelles in solution when it reaches a critical concentration or temperature, which is called critical

micellization concentration (CMC) or critical micellization temperature (CMT). When below CMC and/or CMT, Pluronic exists as individual unimers in solution. When above CMC and/or CMT, Pluronic aggregates, forming small micelles in solution with PPO inner core and PEO outer corona. The CMC and CMT of a wide range of Pluronics with different molar mass and PPO/PEO ratios have been determined by Alexandridis [101]. It was shown that the more apolar PPO chains are mainly responsible for the formation of micelles. With the same length of PEO groups and varying length in PPO groups, it was shown that CMC and CMT values decrease with increasing PPO length. For the same ratio of PPO/PEO, CMC and CMT decrease with increasing molar mass of Pluronic [99, 101]. On the contrary, the hydrophilic PEO groups seem to play a minor role in the formation of micelles.

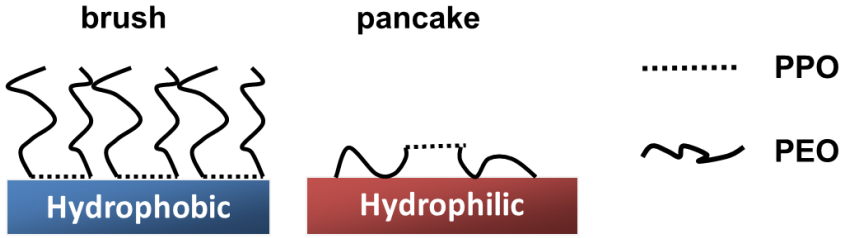

Figure 19. Schematic representation of PEO-PPO-PEO block copolymers adsorbed on a hydrophobic and a hydrophilic surface.

It was shown that the conformation of Pluronic in adsorbed layers depends on substrate hydrophobicity [106], as illustrated in Figure 19. On hydrophobic surfaces, PEO-PPO-PEO triblock copolymers are anchored on the surface through their PPO block due to hydrophobic interaction while the two water-soluble hydrophilic PEO chains protrude into the aqueous environment, forming a brush structure. The highly hydrated and flexible PEO brush layer provides the surface with a steric barrier to suppress adhesion of approaching particles, e.g. proteins or bacteria. On hydrophilic surface, PEO blocks have a relative higher affinity, forming an unstable

"pancake" structure, which is reported to be ineffective to prevent the adhesion of approaching particles.

The adsorption of Pluronic on substrates with different hydrophobicities was examined and characterized by quartz crystal microbalance with dissipation monitoring, SPR and WCA measurements [106-108]. It was shown by SPR that the quantity of adsorbed Pluronic is much larger on hydrophobic surfaces than on hydrophilic surfaces. It was shown by Nejadnik that the thickness and conformation of adsorbed Pluronic layers strongly depend on the hydrophobicity of underlying surfaces, rather than on the concentration of Pluronic in solution [106]. It was further interpreted from QCM-D results that the adsorbed Pluronic F127 (PEO_{99}-PPO_{65}-PEO_{99}) layer forms a brush-like structure on surfaces with WCA above 80° while the same polymer forms a pancake structure on surfaces with WCA below this value. The effect of varying PEO or PPO chain length of Pluronics adsorbed on hydrophobic polystyrene (PS) surface has been investigated using SPR by Green [108]. The results showed that the amount of adsorbed Pluronic increases with increasing either PPO or PEO chain length. However, the increase of PPO block size has a greater impact on mass of adsorbed Pluronic than equivalent increase of PEO block size. Although Pluronic adsorption is expected to reduce the WCA value of hydrophobic surfaces, the result of Liu showed that a limited reduction of ~10° of WCA was observed on polypropylene (PP) surface after Pluronic P105 adsorption, which might be due to a limited surface coverage [107].

AFM has been used to unravel the detailed morphology of Pluronics adsorbed on hydrophobic and hydrophilic surfaces [107, 109]. The AFM images showed smooth and flat adsorbed Pluronic P105 ($PEO_{37}PPO_{56}PEO_{37}$) molecules on both silica (hydrophilic) and graphite (hydrophobic) surfaces when its concentration was below CMC. When the concentration was higher than CMC, globular aggregates (micelles) were detected on silica surface while there was no distinguishable feature on graphite [107]. Li also studied

the adsorption of Pluronic on hydrophobic (polypropylene and polyethylene) and hydrophilic (cellulose) surfaces when polymer concentration is higher than CMC using AFM [109]. The results indicated that the micelles of polymer collapsed and turned into hemimicelle structures on the hydrophobic surfaces, which indicated the high affinity between PPO groups and hydrophobic surfaces.

As mentioned above, this PEO-containing amphiphilic copolymer is expected to adsorb on hydrophobic surfaces in a brush-like structure, which would prevent protein adsorption and cell adhesion. This effect was studied by several groups. It is shown to depend on the surface hydrophobicity, PPO/PEO ratio and molar mass of the copolymers [96, 102-104, 110-112]. The results of Schroen showed the different consequences of adsorbed Pluronics on hydrophobic and hydrophilic surfaces [104]. It was shown that Pluronic prevents lipase adsorption only if it is adsorbed onto hydrophobic surfaces, with a brush configuration, forming a layer of 10 nm thickness. As shown by Dewez, the reduction of collagen adsorption in the presence of Pluronic F68 is more pronounced when the substrate hydrophobicity is higher [111]. The study of Freij-Larsson also showed the ability of Pluronic to reduce fibrinogen and human serum albumin (HSA) adsorption on hydrophobic surfaces, even if the surface was not completely covered by Pluronic molecules as analyzed by AFM [110]. Amiji has shown the successful coating with Pluronic to prevent fibrinogen adsorption and platelet adhesion on hydrophobic surfaces [96]. Its ability to prevent protein adsorption is mainly dependent on the length of PPO, rather than the length of PEO, because longer PPO chains are more effective to anchor Pluronic to the hydrophobic surface. The work of Green showed that the increase of PPO block length appears to increase the protein resistance ability of Pluronic on hydrophobic surfaces [103]. It also confirmed that the binding strength of PPO block on hydrophobic surfaces has a stronger influence on protein resistance in comparison to the length of PEO block [103, 108].

Chang *et al.* reported the successful preadsorption of Pluronic 108 on CH_3-modified gold surface to reduce bovine serum albumin (BSA), fibrinogen and mixed plasma proteins adsorption, as monitored by SPR [102]. The Pluronic F108 treated surface is stable and still reduces protein adsorption after storage in phosphate buffered saline (PBS) for 7 days.

The protein resistant PEO-PPO-PEO triblock copolymers were also shown to reduce initial bacterial adhesion [113]. As illustrated in Figure 20, Bridgett *et al*. systematically studied *Staphlylococcus epidermidis* adhesion on model polystyrene (PS) surfaces treated with a wide range of Pluronics [105]. It was shown that the reduction of bacterial adhesion was achieved with all Pluronics tested, irrespective of the PPO or PEO block length. Further studies by Marsh *et al*. showed that adhesion of two bacteria involved in skin infection, *Staphylococcus epidermidis* and *Serratia marcescens*, was suppressed over a 24 h time period on PS surface by facile dip-coating of Pluronic [114]. The results of Dewez showed that the Pluronic F68 containing medium prevents collagen adsorption on hydrophobic PS surface, thereby preventing Hep G2 cell adhesion due to lack of specific interactions [115].

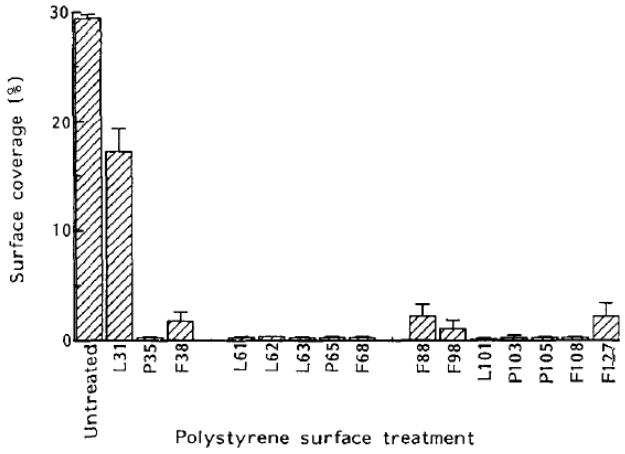

Figure 20. Effect of surface treatment of polystyrene with a range of Pluronic surfactants on the adhesion of *Staphylococcus epidermidis* expressed as a surface coverage (%) by this bacterium. Adapted from [105].

1.5 Aim and research strategy

This thesis is performed in the framework of the BIOCOR project, focusing on biofouling problems of cooling condensers in power plants. Chlorination, which has been used since 1924, is still the most widely applied and effective procedure used for biofouling control of such cooling condensers [6, 22]. However, due to the generated toxic effects for the aquatic environment, the quantity of applied chlorine must be precisely controlled. Therefore, other environmental-friendly methods are desired to replace chlorination for antifouling purpose.

The general aim of this research is to develop a PEO-based coating on metals, with a view to reduce biofouling. More particularly, our research aims at designing a renewable PEO-PPO-PEO triblock copolymer coating on metal oxide substrates to reduce molecular- and microfouling. Stainless steel (SS), titanium (Ti) and aluminum brass (Al brass) were the targeted materials in this project: Ti and Al brass are used in cooling condensers fed with seawater while SS is used with freshwater. Antifouling tests were performed using model molecular fouling agents, and adhesion of single bacterial species was investigated in laboratory assays. Treated samples were then exposed to seawater in the by-pass of a cooling circuit. Furthermore, the relevant fouling molecules from corrosive bacterial species were analyzed to highlight the biochemical composition of the conditioning layer being formed at the surface. The results of this thesis are expected to open the way to a new strategy to reduce molecular- and microfouling on metal oxide surfaces, and to disclose the main constituents of molecular fouling at interfaces.

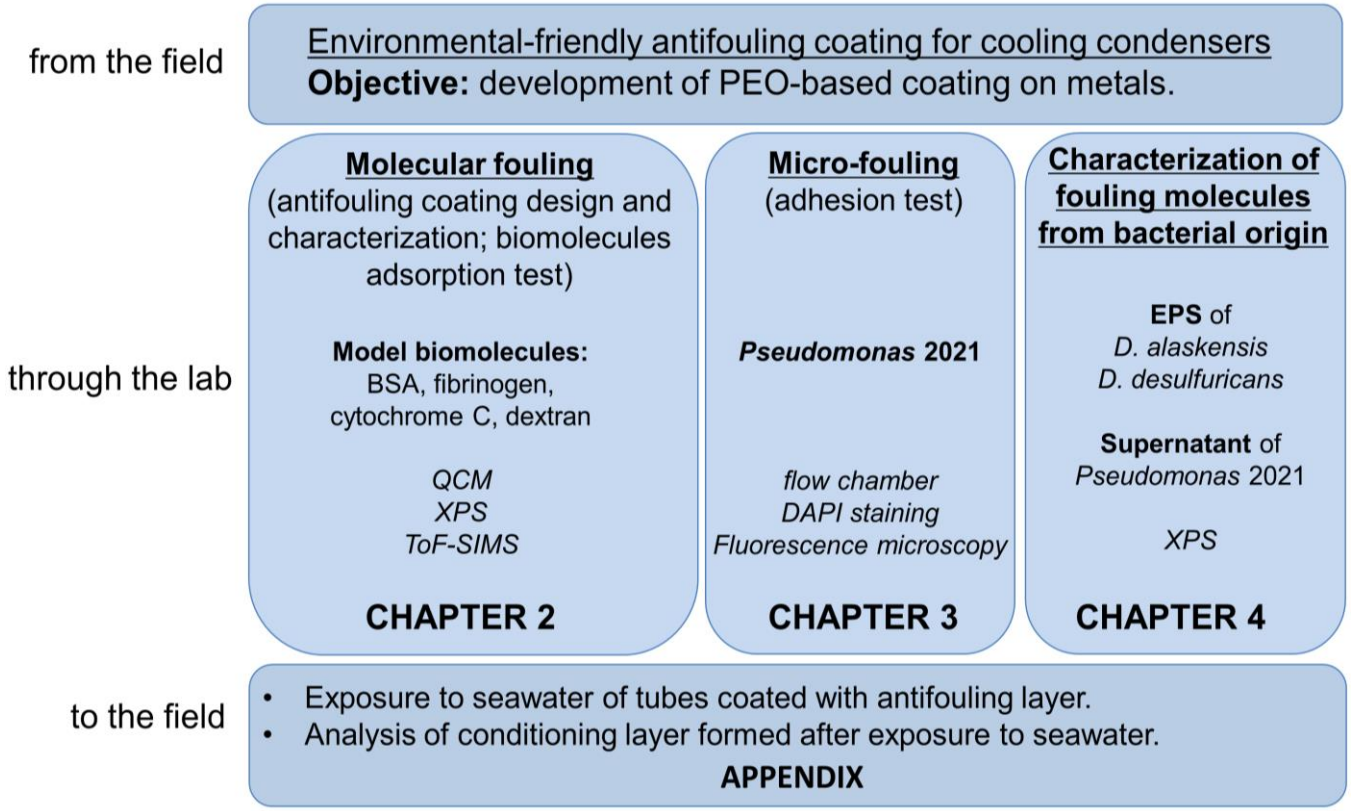

Figure 21. Outline of this thesis and objective of each chapter. This also illustrates the approach of from the field, through the lab, to the field.

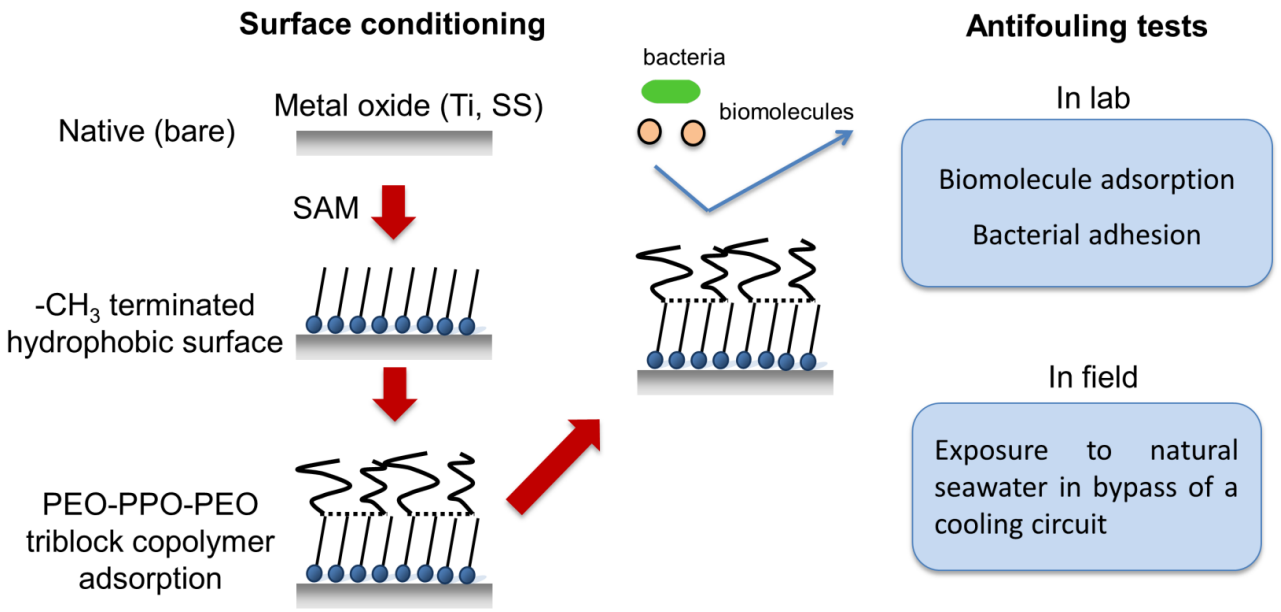

Figure 22. Schematic representation of the surface modification process used in this thesis, and performed assays. SAM: self-assembly monolayer; SS: stainless steel.

This thesis consists of four parts, as follows, and as also illustrated in Figure 21:

1. Molecular fouling – antifouling coating design and characterization; biomolecule adsorption tests (Chapter 2).
2. Microfouling – bacterial adhesion tests (Chapter 3).
3. Characterization of fouling molecules from bacterial origin (Chapter 4).
4. Field test – exposure to seawater of tubes coated with antifouling layer (Appendix).

The surface modification process selected to elaborate the antifouling coating is illustrated in Figure 22. The details are given in section 1.5.1.

1.5.1 Molecular fouling – antifouling coating and biomolecule adsorption tests

SAMs of octadecylphosphonic acid (OPA) (structure given in Figure 23) are used to create a hydrophobic coating on Ti and SS, which are hydrophilic in nature. This process confers a standardized surface state to metal oxide surfaces, allowing reproducible further modification by adsorption of an antifouling copolymer on Ti and SS. Another advantage of OPA treatment is to remove organic contaminants on Ti and SS, which could interfere with polymer coating. The thickness of obtained OPA layer is reported to be about 2.5 nm [116]. The detailed structure of OPA layer on targeted substrates was not investigated in this thesis.

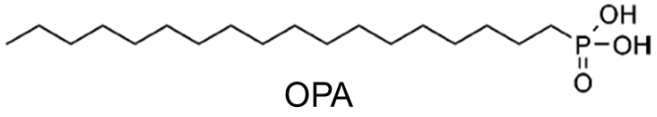

Figure 23. Structural formula of octadecylphosphonic acid (OPA). Adapted from [116].

PEO_{76}-PPO_{30}-PEO_{76} triblock copolymer (Pluronic F68, in short Plu, structure given in Figure 24) was used for adsorption on OPA-conditioned Ti and SS, and the obtained layers were further evaluated for their biomolecule-resistance ability. Native and OPA-conditioned Ti and SS are also evaluated in parallel, as references.

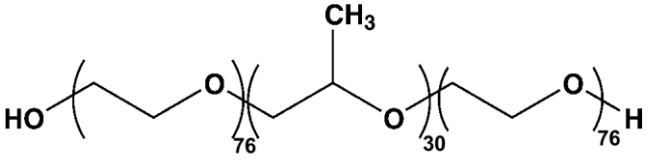

Figure 24. Structure of Pluronic F68 copolymer used in this thesis, average molar mass ~8350 g/mol. Adapted from [114].

The protein resistance tests were performed in the following two ways, according to the characterization techniques used: sequential adsorption and competitive adsorption.

Sequential adsorption was monitored using quartz crystal microbalance (QCM). The Plu adsorption on native and OPA-conditioned Ti and SS, followed by the adsorption of model molecular fouling agents (albumin, fibrinogen, cytochrome C, dextran) were monitored *in situ* and in real time by QCM. Proteins are reported as functional fouling molecules which could hinder or facilitate further microfouling (e.g. bacterial adhesion) [55]. Polysaccharides are also important compounds of biofilms, having specific interactions with bacteria. The resonant frequency difference recorded before and after biomolecule adsorption was converted into the mass adsorbed on the surfaces.

In another approach, simultaneous adsorption of albumin and Plu on native or OPA-conditioned Ti and SS was performed, in a process of competitive adsorption. The chemical composition of the outermost surface of those samples was characterized by x-ray photoelectron spectroscopy (XPS) and time-of-flight secondary ion mass spectrometry (ToF-SIMS). XPS is used to determine nitrogen elemental fraction, particularly nitrogen in amide bonds (N-C=O), as a marker for the amount of proteins. ToF-SIMS

(probed depth ~1 nm) is more surface sensitive than XPS (probed depth ~8 – 10 nm). This technique gives a semi-quantitative information on the content in fragments of amino acids, which is also related to amount of proteins.

1.5.2 Microfouling – bacterial adhesion tests

Pseudomonas NCIMB 2021 was chosen as a model marine aerobic bacterium to study its adhesion on the created antifouling surfaces. This species was reported to induce corrosion on metals [117], and was also found on fouled condensers in power plants.

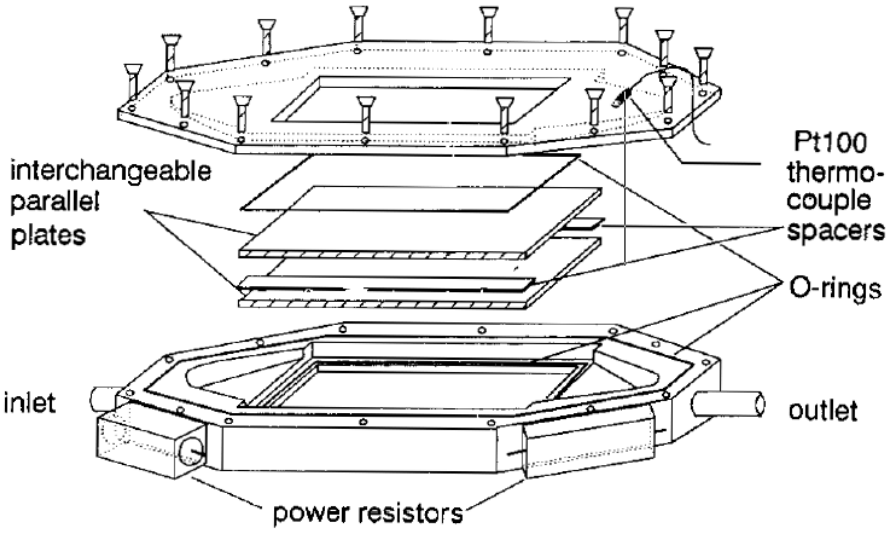

Figure 25. Schematic overview of the parallel plate flow chamber. Adapted from [118].

A parallel plate flow chamber (as illustrated in Figure 25) with minor modification was employed to study bacterial adhesion on native and OPA-conditioned SS in the presence or not of Plu. A detailed review of parallel plate flow chamber use was written by Busscher [118, 119]. The major advantage of the flow chamber used here is that the native and OPA-conditioned stainless steel coupons were placed alternately on the bottom plate (details in Chapter 3). The effect of different surface conditions of

metal coupons on bacterial adhesion could thus be compared directly in a single experiment.

The influence of Plu on bacterial adhesion was tested in two ways: pre-adsorption and post-adsorption of Plu. In pre-adsorption mode, Plu adsorption was followed by bacterial adhesion, and a rinsing step was always performed after Plu adsorption and bacterial adhesion. In post-adsorption mode, bacterial adhesion was performed first, and after that, rinsing was performed with a solution containing Plu. This latter experiment was designed to examine the possibility to renew the coating from time to time.

After that, the adherent bacteria were dyed directly in flow chamber with 4,6 diamidino-2-phenylindole (DAPI), which passes cell membrane to bind DNA and gives fluorescence. The density of adhered bacteria was measured using fluorescence microscopy.

1.5.3 Characterization of fouling molecules from bacterial origin

EPS are biopolymers which are found on the microbial cell surface or are secreted by bacteria or may be released in the medium after cell lysis. They are considered as the initial fouling matters which could attract or hinder further bacterial adhesion and biofilm formation. Beech *et al*. found that EPS could also directly induce corrosion process by coupling with metal ions [25, 26, 28]. There is however few results concerning the composition of the conditioning layers formed by EPS at interfaces.

This part of the thesis gives an overview of the composition of EPS originating from different corrosive bacterial species, and of conditioning layers formed by such EPS. The strategy used in this part of the work is illustrated in Figure 26. The chemical composition of EPS (isolated from *Desulfovibrio alaskensis*, and from *Desulfovibrio desulfuricans*), and of organic compounds present in culture media of *Pseudomonas* NCIMB 2021, dialyzed or not, were examined by combining protein gel electrophoresis,

evaluation of protein concentration by UV-visible spectrometry, surface tension measurements and surface analysis (XPS) of dried residues obtained by drying drops of solutions. The commercial lipopolysaccharides (LPS) from *Pseudomonas aeruginosa 10* were also used for comparison.

In another approach, the chemical composition of conditioning layers formed by the various solutions of bacterial origin on different materials, used as substrates, was determined by XPS. The approach was focused on information concerning chemical functions and on the expression of the chemical composition of conditioning layers in terms of model compounds (proteins, polysaccharides and lipids), which is expected to highlight the major constituents at the surface [120].

1.5.4 Field tests – exposure to seawater of tubes coated with antifouling layer

The aim of this part of the thesis is to implement the developed antifouling coating methodology on Al brass and Ti tubes, and to test its effect by exposure in a bypass of a cooling system fed with seawater, as seen in Figure 27. After exposure for a given period of time, the metal tubes were retrieved and analyzed by XPS. Data treatment was performed with a particular focus on the nature of the organic compounds found at the interface. The results, which must be considered as preliminary at this stage, are presented in the Appendix of this thesis. It must be noted that constraints related to the possibility to expose samples in the bypass did not allow a sufficient repetition of experiments, nor an adaptation of the coatings after collecting the first results.

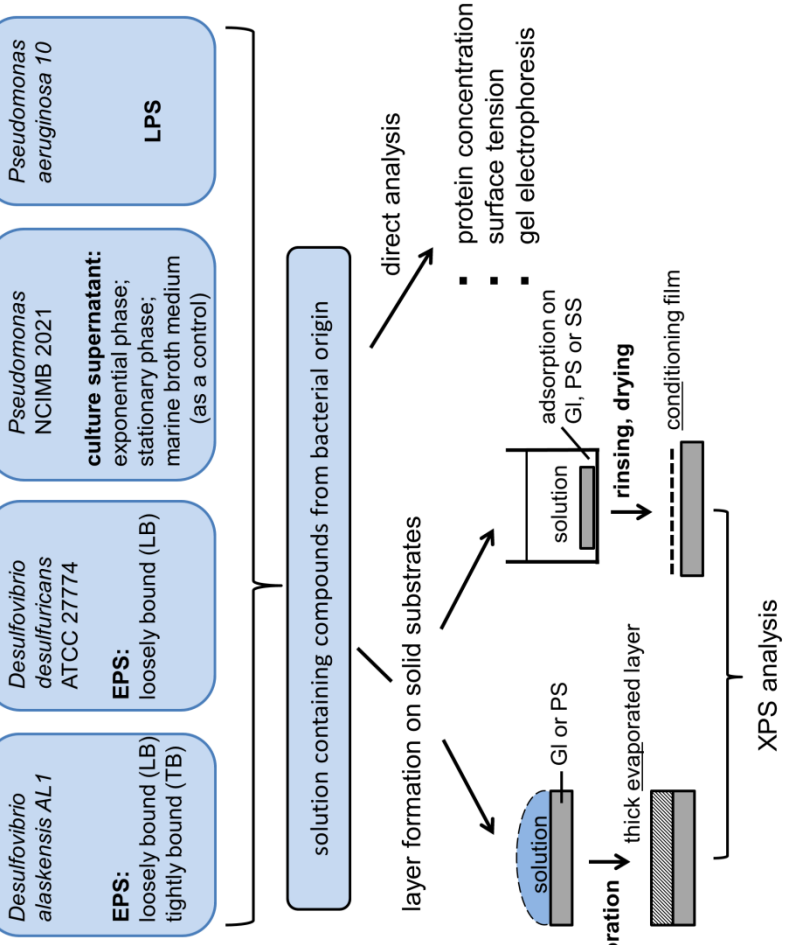

Figure 26. Illustration of the strategy used to characterize fouling molecules from bacteria origin.

Figure 27. Pictures of field experiment: (a) power plant, (b) outlet of seawater, (c) bypass setup circulated with seawater, (d) samples (indicated by arrows) exposure in seawater.

1.6 References

[1] Coetser SE and Cloete TE, 2005, Biofouling and Biocorrosion in Industrial Water Systems, Crit. Rev. Microbiol., 31, 213-232.

[2] Kumar CG and Anand SK, 1998, Significance of microbial biofilms in food industry: a review, Int. J. Food Microbiol., 42, 9-27.

[3] Mansfeld F, 2007, The interaction of bacteria and metal surfaces, Electrochim. Acta, 52, 7670-7680.

[4] Schultz MP, 2007, Effects of coating roughness and biofouling on ship resistance and powering, Biofouling, 23, 331-341.

[5] Schultz MP, Bendick JA, Holm ER and Hertel WM, 2010, Economic impact of biofouling on a naval surface ship, Biofouling, 27, 87-98.

[6] Cristiani P, 2005, Solutions to fouling in power station condensers, Appl. Therm. Eng., 25, 2630-2640.

[7] Callow JA and Callow ME, 2011, Trends in the development of environmentally friendly fouling-resistant marine coatings, Nat. Commun., 2, 244.

[8] Maki JS and Mitchell R, 2003, Biofouling in the Marine Environment, in: Bitton G (Ed.) Encyclopedia of Environmental Microbiology, Wiley, New York, Vol 2, 610-619.

[9] Rosenhahn A, Schilp S, Kreuzer HJ and Grunze M, 2010, The role of "inert" surface chemistry in marine biofouling prevention, Phys. Chem. Chem. Phys., 12, 4275-4286.

[10] Hall-Stoodley L, Costerton JW and Stoodley P, 2004, Bacterial biofilms: from the Natural environment to infectious diseases, Nat. Rev. Microbiol., 2, 95-108.

[11] Flemming H-C and Wingender J, 2010, The biofilm matrix, Nat. Rev. Microbiol., 8, 623-633.

[12] Sutherland IW, 2001, The biofilm matrix – an immobilized but dynamic microbial environment, Trends Microbiol., 9, 222-227.

[13] Costerton JW, Lewandowski Z, Caldwell DE, Korber DR and Lappin-Scott HM, 1995, Microbial Biofilms, Annu. Rev. Microbiol., 49, 711-745.

[14] Flemming H-C, 2009, Why Microorganisms Live in Biofilms and the Problem of Biofouling, in: Flemming H-C, Murthy PS, Venkatesan R, Cooksey K (Eds.) Marine and Industrial Biofouling, Springer, Berlin, Vol 4, 3-12.

[15] Mah T-FC and O'Toole GA, 2001, Mechanisms of biofilm resistance to antimicrobial agents, Trends Microbiol., 9, 34-39.

[16] Le Cloirec P, Andrè Y, Faur-Brasquet C and Gérente C, 2003, Engineered Biofilms for Metal Ion Removal, Rev. Environ. Sci. Biotechnol., 2, 177-192.

[17] Beech IB and Sunner J, 2004, Biocorrosion: towards understanding interactions between biofilms and metals, Curr. Opin. Biotechnol., 15, 181-186.

[18] Videla HA, Manual of Biocorrosion, CRC Press, Florida, 1996.

[19] Beech IB, 2003, Biocorrosion: Role of Sulfate Reducing Bacteria, in: Bitton G (Ed.) Encyclopedia of Environmental Microbiology, Wiley, New York, Vol 1, 465-475.

[20] Javaherdashti R, 1999, A review of some characteristics of MIC caused by sulfate-reducing bacteria: past, present and future, Anti-corros. Methods Mater., 46, 173-180.

[21] Nagiub A and Mansfeld F, 2002, Evaluation of microbiologically influenced corrosion inhibition (MICI) with EIS and ENA, Electrochim. Acta, 47, 2319-2333.

[22] Cristiani P, Perboni G and Debenedetti A, 2008, Effect of chlorination on the corrosion of Cu/Ni 70/30 condenser tubing, Electrochim. Acta, 54, 100-107.

[23] Pitonzo BJ, Castro P, Amy PS, Southam G, Jones DA and Ringelberg D, 2004, Microbiologically Influenced Corrosion Capability of Bacteria Isolated from Yucca Mountain, Corrosion, 60, 64-74.

[24] Little BJ, Lee JS and Ray RI, 2008, The influence of marine biofilms on corrosion: A concise review, Electrochim. Acta, 54, 2-7.

[25] Beech IB and Cheung CWS, 1995, Interactions of exopolymers produced by sulphate-reducing bacteria with metal ions, Int. Biodeterior. Biodegrad., 35, 59-72.

[26] Beech IB, Zinkevich V, Tapper R, Gubner R and Avci R, 1999, Study of the interaction of sulphate-reducing bacteria exopolymers with iron using X-ray photoelectron spectroscopy and time-of-flight secondary ionisation mass spectrometry, J. Microbiol. Methods, 36, 3-10.

[27] Beech IB, Cheung CWS, Johnson DB and Smith JR, 1996, Comparative studies of bacterial biofilms on steel surfaces using atomic force microscopy and environmental scanning electron microscopy, Biofouling, 10, 65-77.

[28] Beech IB, Zinkevich V, Tapper R and Gubner R, 1998, Direct involvement of an extracellular complex produced by a marine sulfate-reducing bacterium in deterioration of steel, Geomicrobiol. J., 15, 121-134.

[29] Videla HA and Herrera LK, 2005, Microbiologically influenced corrosion: looking to the future, Int. Microbiol., 8, 169-180.

[30] Chambers LD, Stokes KR, Walsh FC and Wood RJK, 2006, Modern approaches to marine antifouling coatings, Surf. Coat. Technol., 201, 3642-3652.

[31] Loeb GI and Neihof RA, 1975, Marine Conditioning Films, in: Baier RE (Ed.) Applied Chemistry at Protein Interfaces, Calspan Corp., Buffalo N.Y., Vol 145, 319-335.

[32] Landoulsi J, Cooksey KE and Dupres V, 2011, Review – Interactions between diatoms and stainless steel: focus on biofouling and biocorrosion, Biofouling, 27, 1105-1124.

[33] Taylor GT, Zheng D, Lee M, Troy PJ, Gyananath G and Sharma SK, 1997, Influence of surface properties on accumulation of conditioning films and marine bacteria on substrata exposed to oligotrophic waters, Biofouling, 11, 31-57.

[34] Loeb GI and Neihof RA, 1977, Adsorption of an organic film at the platinum-seawater interface, J. Mar. Res., 35, 283-291.

[35] Characklis WG, 1981, Bioengineering report: Fouling biofilm development: A process analysis, Biotechnol. Bioeng., 23, 1923-1960.

[36] Leis A, Lamb RN, Gong B and Schneider RP, 2000, Evidence for the contribution of humic substances to conditioning films from natural waters, Biofouling, 15, 207-220.

[37] Schneider RP and Leis A, 2003, Conditioning Films in Aquatic Environments, in: Bitton G (Ed.) Encyclopedia of Environmental Microbiology, Wiley, New York, Vol 2, 928-941.

[38] Ponche A, Ploux L and Anselme K, 2010, Protein/Material Interfaces: Investigation on Model Surfaces, J. Adhes. Sci. Technol., 24, 2141-2164.

[39] Schneider RP, 1997, Bacterial adhesion to solid substrata coated with conditioning films derived from chemical fractions of natural waters, J. Adhes. Sci. Technol., 11, 979-994.

[40] Cornelius RM, Wojciechowski PW and Brash JL, 1992, Measurement of protein adsorption kinetics by an in situ, “real-time,” solution depletion technique, J. Colloid Interface Sci., 150, 121-133.

[41] Jain A and Bhosle NB, 2009, Biochemical composition of the marine conditioning film: implications for bacterial adhesion, Biofouling, 25, 13-19.

[42] Compère C, Bellon-Fontaine MN, Bertrand P, Costa D, Marcus P, Poleunis C, Pradier CM, Rondot B and Walls MG, 2001, Kinetics of conditioning layer formation on stainless steel immersed in seawater, Biofouling, 17, 129-145.

[43] Tuson HH and Weibel DB, 2013, Bacteria-surface interactions, Soft Matter, 9, 4368-4380.

[44] Boonaert CJP, Dufrêne YF and Rouxhet PG, 2003, Adhesion (Primary) of Microorganisms onto Surfaces, in: Bitton G (Ed.) Encyclopedia of Environmental Microbiology, Wiley, New York, Vol 1, 113-132.

[45] Dufrêne YF, Vermeiren H, Vanderleyden J and Rouxhet PG, 1996, Direct evidence for the involvement of extracellular proteins in the adhesion of *Azospirillum brasilense*, Microbiology, 142, 855-865.

[46] Queck S-Y, Weitere M, Moreno AM, Rice SA and Kjelleberg S, 2006, The role of quorum sensing mediated developmental traits in the resistance of Serratia marcescens biofilms against protozoan grazing, Environ. Microbiol., 8, 1017-1025.

[47] Dobretsov S, Teplitski M and Paul V, 2009, Mini-review: quorum sensing in the marine environment and its relationship to biofouling, Biofouling, 25, 413-427.

[48] Flemming HC and Wingender J, 2003, Extracellular Polymeric Substances (EPS): Structural, Ecological and Technical Aspects, in: Bitton G (Ed.) Encyclopedia of Environmental Microbiology, Wiley, New York, Vol 3, 1223-1231.

[49] Beech I, Hanjagsit L, Kalaji M, Neal AL and Zinkevich V, 1999, Chemical and structural characterization of exopolymers produced by *Pseudomonas sp*. NCIMB 2021 in continuous culture, Microbiology, 145, 1491-1497.

[50] Nielsen P and Jahn A, 1999, Extraction of EPS, in: Wingender J, Neu T, Flemming H-C (Eds.) Microbial Extracellular Polymeric Substances, Springer, Berlin, 49-72.

[51] Flemming H-C, 2011, The perfect slime, Colloids Surf. B. Biointerfaces, 86, 251-259.

[52] Beech IB, Gubner R, Zinkevich V, Hanjangsit L and Avci R, 2000, Characterisation of conditioning layers formed by exopolymeric substances of *Pseudomonas* NCIMB 2021 on surfaces of AISI 316 stainless steel, Biofouling, 16, 93-104.

[53] Gubner R and Beech IB, 2000, The effect of extracellular polymeric substances on the attachment of *Pseudomonas* NCIMB 2021 to AISI 304 and 316 stainless steel, Biofouling, 15, 25-36.

[54] Stadler R, Wei L, Fürbeth W, Grooters M and Kuklinski A, 2010, Influence of bacterial exopolymers on cell adhesion of *Desulfovibrio vulgaris* on high alloyed steel: Corrosion inhibition by extracellular polymeric substances (EPS), Mater. Corros., 61, 1008-1016.

[55] Hwang G, Kang S, El-Din MG and Liu Y, 2012, Impact of an extracellular polymeric substance (EPS) precoating on the initial adhesion of *Burkholderia cepacia* and *Pseudomonas aeruginosa*, Biofouling, 28, 525-538.

[56] Busalmen JP, Vázquez M and de Sánchez SR, 2002, New evidences on the catalase mechanism of microbial corrosion, Electrochim. Acta, 47, 1857-1865.

[57] d'Abzac P, Bordas F, Joussein E, van Hullebusch ED, Lens PN and Guibaud G, 2013, Metal binding properties of extracellular polymeric substances extracted from anaerobic granular sludges, Environ. Sci. Pollut. Res., 20, 4509-4519.

[58] Banerjee I, Pangule RC and Kane RS, 2011, Antifouling Coatings: Recent Developments in the Design of Surfaces That Prevent Fouling by Proteins, Bacteria, and Marine Organisms, Adv. Mater., 23, 690-718.

[59] Love JC, Estroff LA, Kriebel JK, Nuzzo RG and Whitesides GM, 2005, Self-Assembled Monolayers of Thiolates on Metals as a Form of Nanotechnology, Chem. Rev., 105, 1103-1170.

[60] Kind M and Wöll C, 2009, Organic surfaces exposed by self-assembled organothiol monolayers: Preparation, characterization, and application, Prog. Surf. Sci., 84, 230-278.

[61] Folkers JP, Gorman CB, Laibinis PE, Buchholz S, Whitesides GM and Nuzzo RG, 1995, Self-Assembled Monolayers of Long-Chain Hydroxamic Acids on the Native Oxide of Metals, Langmuir, 11, 813-824.

[62] Ulman A, 1996, Formation and Structure of Self-Assembled Monolayers, Chem. Rev., 96, 1533-1554.

[63] Helmy R and Fadeev AY, 2002, Self-Assembled Monolayers Supported on TiO2: Comparison of C18H37SiX3 (X = H, Cl, OCH3), C18H37Si(CH3)2Cl, and C18H37PO(OH)2, Langmuir, 18, 8924-8928.

[64] Gao W, Dickinson L, Grozinger C, Morin FG and Reven L, 1996, Self-Assembled Monolayers of Alkylphosphonic Acids on Metal Oxides, Langmuir, 12, 6429-6435.

[65] Van Alsten JG, 1999, Self-Assembled Monolayers on Engineering Metals: Structure, Derivatization, and Utility, Langmuir, 15, 7605-7614.

[66] Gawalt ES, Avaltroni MJ, Koch N and Schwartz J, 2001, Self-Assembly and Bonding of Alkanephosphonic Acids on the Native Oxide Surface of Titanium, Langmuir, 17, 5736-5738.

[67] Hähner G, Hofer R and Klingenfuss I, 2001, Order and Orientation in Self-Assembled Long Chain Alkanephosphate Monolayers Adsorbed on Metal Oxide Surfaces, Langmuir, 17, 7047-7052.

[68] Hofer R, Textor M and Spencer ND, 2001, Alkyl Phosphate Monolayers, Self-Assembled from Aqueous Solution onto Metal Oxide Surfaces, Langmuir, 17, 4014-4020.

[69] Fonder G, Minet I, Volcke C, Devillers S, Delhalle J and Mekhalif Z, 2011, Anchoring of alkylphosphonic derivatives molecules on copper oxide surfaces, Appl. Surf. Sci., 257, 6300-6307.

[70] Hoque E, DeRose JA, Bhushan B and Hipps KW, 2009, Low adhesion, non-wetting phosphonate self-assembled monolayer films formed on copper oxide surfaces, Ultramicroscopy, 109, 1015-1022.

[71] Lim MS, Smiley KJ and Gawalt ES, 2010, Thermally driven stability of octadecylphosphonic acid thin films grown on SS316L, Scanning, 32, 304-311.

[72] Raman A, Quiñones R, Barriger L, Eastman R, Parsi A and Gawalt ES, 2009, Understanding Organic Film Behavior on Alloy and Metal Oxides, Langmuir, 26, 1747-1754.

[73] Raman A, Dubey M, Gouzman I and Gawalt ES, 2006, Formation of Self-Assembled Monolayers of Alkylphosphonic Acid on the Native Oxide Surface of SS316L, Langmuir, 22, 6469-6472.

[74] Arima Y and Iwata H, 2007, Effects of surface functional groups on protein adsorption and subsequent cell adhesion using self-assembled monolayers, J. Mater. Chem., 17, 4079-4087.

[75] Jennings GK, Yong T-H, Munro JC and Laibinis PE, 2003, Structural Effects on the Barrier Properties of Self-Assembled Monolayers Formed from Long-Chain ω-Alkoxy-n-alkanethiols on Copper, J. Am. Chem. Soc., 125, 2950-2957.

[76] Telegdi J, Szabó T, Al-Taher F, Pfeifer É, Kuzmann E and Vértes A, 2010, Coatings against corrosion and microbial adhesion, Mater. Corros., 61, 1000-1007.

[77] Chapman RG, Ostuni E, Takayama S, Holmlin RE, Yan L and Whitesides GM, 2000, Surveying for Surfaces that Resist the Adsorption of Proteins, J. Am. Chem. Soc., 122, 8303-8304.

[78] Ostuni E, Chapman RG, Holmlin RE, Takayama S and Whitesides GM, 2001, A Survey of Structure−Property Relationships of Surfaces that Resist the Adsorption of Protein, Langmuir, 17, 5605-5620.

[79] Ostuni E, Chapman RG, Liang MN, Meluleni G, Pier G, Ingber DE and Whitesides GM, 2001, Self-Assembled Monolayers That Resist the Adsorption of Proteins and the Adhesion of Bacterial and Mammalian Cells, Langmuir, 17, 6336-6343.

[80] Jeon SI, Lee JH, Andrade JD and De Gennes PG, 1991, Protein—surface interactions in the presence of polyethylene oxide: I. Simplified theory, J. Colloid Interface Sci., 142, 149-158.

[81] Jeon SI and Andrade JD, 1991, Protein—surface interactions in the presence of polyethylene oxide: II. Effect of protein size, J. Colloid Interface Sci., 142, 159-166.

[82] Wang RLC, Kreuzer HJ and Grunze M, 1997, Molecular Conformation and Solvation of Oligo(ethylene glycol)-Terminated Self-Assembled Monolayers and Their Resistance to Protein Adsorption, J. Phys. Chem. B, 101, 9767-9773.

[83] Unsworth LD, Sheardown H and Brash JL, 2005, Protein Resistance of Surfaces Prepared by Sorption of End-Thiolated Poly(ethylene glycol) to Gold: Effect of Surface Chain Density, Langmuir, 21, 1036-1041.

[84] Harder P, Grunze M, Dahint R, Whitesides GM and Laibinis PE, 1998, Molecular Conformation in Oligo(ethylene glycol)-Terminated Self-Assembled Monolayers on Gold and Silver Surfaces Determines Their Ability To Resist Protein Adsorption, J. Phys. Chem. B, 102, 426-436.

[85] Herrwerth S, Eck W, Reinhardt S and Grunze M, 2003, Factors that Determine the Protein Resistance of Oligoether Self-Assembled Monolayers − Internal Hydrophilicity, Terminal Hydrophilicity, and Lateral Packing Density, J. Am. Chem. Soc., 125, 9359-9366.

[86] Llanos GR and Sefton MV, 1993, Review Does polyethylene oxide possess a low thrombogenicity?, J. Biomater. Sci. Polym. Ed., 4, 381-400.

[87] Zhao B and Brittain WJ, 2000, Polymer brushes: surface-immobilized macromolecules, Prog. Polym. Sci., 25, 677-710.

[88] Ma H, Hyun J, Stiller P and Chilkoti A, 2004, "Non-Fouling" Oligo(ethylene glycol)- Functionalized Polymer Brushes Synthesized by Surface-Initiated Atom Transfer Radical Polymerization, Adv. Mater., 16, 338-341.

[89] Dalsin JL, Lin L, Tosatti S, Vörös J, Textor M and Messersmith PB, 2004, Protein Resistance of Titanium Oxide Surfaces Modified by Biologically Inspired mPEG−DOPA, Langmuir, 21, 640-646.

[90] Park KD, Kim YS, Han DK, Kim YH, Lee EHB, Suh H and Choi KS, 1998, Bacterial adhesion on PEG modified polyurethane surfaces, Biomaterials, 19, 851-859.

[91] Roosjen A, van der Mei HC, Busscher HJ and Norde W, 2004, Microbial Adhesion to Poly(ethylene oxide) Brushes: Influence of Polymer Chain Length and Temperature, Langmuir, 20, 10949-10955.

[92] Kenausis GL, Vörös J, Elbert DL, Huang N, Hofer R, Ruiz-Taylor L, Textor M, Hubbell JA and Spencer ND, 2000, Poly(l-lysine)-g-Poly(ethylene glycol) Layers on Metal Oxide Surfaces: Attachment Mechanism and Effects of Polymer Architecture on Resistance to Protein Adsorption, J. Phys. Chem. B, 104, 3298-3309.

[93] Maddikeri RR, Tosatti S, Schuler M, Chessari S, Textor M, Richards RG and Harris LG, 2008, Reduced medical infection related bacterial strains adhesion on bioactive RGD modified titanium surfaces: A first step toward cell selective surfaces, J. Biomed. Mater. Res. A, 84A, 425-435.

[94] Seehuber A, Schmidt D and Dahint R, 2012, Poly(acrylic acid)–Poly(ethylene glycol) Layers on Positively Charged Surface Coatings: Molecular Structure, Protein Resistance, and Application to Single Protein Deposition, Langmuir, 28, 8700-8710.

[95] Caro A, Humblot V, Méthivier C, Minier M, Salmain Ml and Pradier C-M, 2009, Grafting of Lysozyme and/or Poly(ethylene glycol) to Prevent Biofilm Growth on Stainless Steel Surfaces, J. Phys. Chem. B, 113, 2101-2109.

[96] Amiji M and Park K, 1992, Prevention of protein adsorption and platelet adhesion on surfaces by PEO/PPO/PEO triblock copolymers, Biomaterials, 13, 682-692.

[97] Caldwell KD, 1997, Surface Modifications with Adsorbed Poly(ethylene oxide)-Based Block Coploymers, in: Harris JM, Zalipsky S (Eds.) Poly(ethylene glycol), ACS, Vol 680, 400-419.

[98] Werle M, 2008, Natural and Synthetic Polymers as Inhibitors of Drug Efflux Pumps, Pharm. Res., 25, 500-511.

[99] Alexandridis P and Alan Hatton T, 1995, Poly(ethylene oxide)-poly(propylene oxide)-poly(ethylene oxide) block copolymer surfactants in aqueous solutions and at interfaces: thermodynamics, structure, dynamics, and modeling, Colloids Surf. Physicochem. Eng. Aspects, 96, 1-46.

[100] Alexandridis P, Athanassiou V, Fukuda S and Hatton TA, 1994, Surface Activity of Poly(ethylene oxide)-block-Poly(propylene oxide)-block-Poly(ethylene oxide) Copolymers, Langmuir, 10, 2604-2612.

[101] Alexandridis P, Holzwarth JF and Hatton TA, 1994, Micellization of Poly(ethylene oxide)-Poly(propylene oxide)-Poly(ethylene oxide) Triblock Copolymers in Aqueous Solutions: Thermodynamics of Copolymer Association, Macromolecules, 27, 2414-2425.

[102] Chang Y, Chu W-L, Chen W-Y, Zheng J, Liu L, Ruaan R-C and Higuchi A, 2010, A systematic SPR study of human plasma protein adsorption behavior on the controlled surface packing of self-assembled poly(ethylene oxide) triblock copolymer surfaces, J. Biomed. Mater. Res. A, 93A, 400-408.

[103] Green RJ, Davies MC, Roberts CJ and Tendler SJB, 1998, A surface plasmon resonance study of albumin adsorption to PEO–PPO–PEO triblock copolymers, J. Biomed. Mater. Res., 42, 165-171.

[104] Schroen CGPH, Stuart MAC, van der Voort Maarschalk K, van der Padt A and van't Riet K, 1995, Influence of Preadsorbed Block Copolymers on Protein Adsorption: Surface Properties, Layer Thickness, and Surface Coverage, Langmuir, 11, 3068-3074.

[105] Bridgett MJ, Davies MC and Denyer SP, 1992, Control of staphylococcal adhesion to polystyrene surfaces by polymer surface modification with surfactants, Biomaterials, 13, 411-416.

[106] Nejadnik MR, Olsson ALJ, Sharma PK, van der Mei HC, Norde W and Busscher HJ, 2009, Adsorption of Pluronic F-127 on Surfaces with Different Hydrophobicities Probed by Quartz Crystal Microbalance with Dissipation, Langmuir, 25, 6245-6249.

[107] Liu X, Wu D, Turgman-Cohen S, Genzer J, Theyson TW and Rojas OJ, 2010, Adsorption of a Nonionic Symmetric Triblock Copolymer on Surfaces with Different Hydrophobicity, Langmuir, 26, 9565-9574.

[108] Green RJ, Tasker S, Davies J, Davies MC, Roberts CJ and Tendler SJB, 1997, Adsorption of PEO−PPO−PEO Triblock Copolymers at the Solid/Liquid Interface: A Surface Plasmon Resonance Study, Langmuir, 13, 6510-6515.

[109] Li Y, Liu H, Song J, Rojas OJ and Hinestroza JP, 2011, Adsorption and Association of a Symmetric PEO-PPO-PEO Triblock Copolymer on Polypropylene, Polyethylene, and Cellulose Surfaces, ACS Appl. Mater. Interfaces, 3, 2349-2357.

[110] Freij-Larsson C, Nylander T, Jannasch P and Wesslén B, 1996, Adsorption behaviour of amphiphilic polymers at hydrophobic surfaces: effects on protein adsorption, Biomaterials, 17, 2199-2207.

[111] Dewez J-L, Berger V, Schneider Y-J and Rouxhet PG, 1997, Influence of Substrate Hydrophobicity on the Adsorption of Collagen in the Presence of Pluronic F68, Albumin, or Calf Serum, J. Colloid Interface Sci., 191, 1-10.

[112] Nonckreman CJ, Fleith S, Rouxhet PG and Dupont-Gillain CC, 2010, Competitive adsorption of fibrinogen and albumin and blood platelet adhesion on surfaces modified with nanoparticles and/or PEO, Colloids Surf. B. Biointerfaces, 77, 139-149.

[113] Blainey BL and Marshall KC, 1991, The use of block copolymers to inhibit bacterial adhesion and biofilm formation on hydrophobic surfaces in marine habitats, Biofouling, 4, 309-318.

[114] Marsh LH, Coke M, Dettmar PW, Ewen RJ, Havler M, Nevell TG, Smart JD, Smith JR, Timmins B, Tsibouklis J and Alexander C, 2002, Adsorbed poly(ethyleneoxide)–poly(propyleneoxide) copolymers on synthetic surfaces: Spectroscopy and microscopy of polymer structures and effects on adhesion of skin-borne bacteria, J. Biomed. Mater. Res., 61, 641-652.

[115] Dewez J-L, Schneider Y-J and Rouxhet PG, 1996, Coupled influence of substratum hydrophilicity and surfactant on epithelial cell adhesion, J. Biomed. Mater. Res., 30, 373-383.

[116] Keszthelyi T, Pászti Z, Rigó T, Hakkel O, Telegdi J and Guczi L, 2006, Investigation of Solid Surfaces Modified by Langmuir−Blodgett Monolayers Using Sum-Frequency Vibrational Spectroscopy and X-ray Photoelectron Spectroscopy, J. Phys. Chem. B, 110, 8701-8714.

[117] Yuan SJ and Pehkonen SO, 2007, Microbiologically influenced corrosion of 304 stainless steel by aerobic *Pseudomonas* NCIMB 2021 bacteria: AFM and XPS study, Colloids Surf. B. Biointerfaces, 59, 87-99.

[118] Busscher HJ and van Der Mei HC, 1995, [37] Use of flow chamber devices and image analysis methods to study microbial adhesion, Methods Enzymol., 253, 455-477.

[119] Busscher HJ and van der Mei HC, 2006, Microbial Adhesion in Flow Displacement Systems, Clin. Microbiol. Rev., 19, 127-141.

[120] Rouxhet PG and Genet MJ, 2011, XPS analysis of bio-organic systems, Surf. Interface Anal., 43, 1453-1470.

Chapter 2

Adsorption of a PEO-PPO-PEO triblock copolymer on metal oxide surfaces with a view to reduce biomolecule adsorption and further biofouling

The presentation of Chapter 2 is derived from the paper "Adsorption of a PEO-PPO-PEO triblock copolymer on metal oxide surfaces with a view to reduce protein adsorption and further biofouling", Y. Yang, C. Poleunis, L. Romanszki, J. Telegdi, C.C Dupont-Gillain, Biofouling, in press.

Summary

Biomolecule adsorption is the first stage of biofouling. The aim of this work is to reduce biomolecule adsorption on stainless steel and titanium surfaces by modifying them with a poly(ethylene oxide) (PEO)-poly(propylene oxide) (PPO)-PEO triblock copolymer. Anchoring of the central PPO block of the copolymer is known to be favored by hydrophobic interaction with the substrate. Therefore, the metal oxide surfaces were first modified by self-assembly of octadecylphosphonic acid (OPA). PEO-PPO-PEO preadsorbed on the hydrophobized titanium or stainless steel was shown to prevent bovine serum albumin (BSA), fibrinogen, cytochrome C and dextran adsorption, as was monitored by quartz crystal microbalance (QCM). Moreover, x-ray photoelectron spectroscopy (XPS) and time-of-flight secondary ion mass spectrometry (ToF-SIMS) were used to characterize stainless steel and titanium surfaces after competitive adsorption of PEO-PPO-PEO and BSA. The results show that BSA adsorption is well prevented on hydrophobized surfaces, in contrast to native metal oxide surfaces.

2.1 Introduction

Biofouling or bioadhesion refer to uncontrolled and irreversible accumulation of biological material on synthetic surfaces, leading to the formation of a biofilm [1]. The accumulation of biofilm on metallic materials can bring adverse effects, as illustrated in Table 1.

Table 1. Examples of fouling issues in various industries, and involved metals. (SS = stainless steel).

Fouling issue	**Industry**	**Metal involved**	**References**
Biocorrosion in Pipelines	Oil industry	carbon steel	[2]
Reduced efficiency of heat exchange	Power plant	Ti, SS, copper alloy	[3]
Food spoilage	Food process	SS	[4]
Implant infection	Biomaterials	Ti and its alloys	[5]
Increased frictional drag and fuel consumption	Marine Vessels	Steel	[6]

The initial step of biofouling of materials consists in the spontaneous adsorption of biomolecules present in the aqueous environment [7, 8]. It is indeed recognized that bacteria adhere onto material surfaces through a conditioning film composed of proteins and polysaccharides [9]. The formation of a protein layer on the material surface is actually thought to be a requisite for microorganism adhesion which might be attributed to specific recognitions. Adsorbed proteins could moreover serve as concentrated nutrients to attract microorganisms. Adsorption of proteins on metal surfaces is therefore particularly important with respect to biofouling problems. Proteins are known to be the major constituent of fouling substances due to their high activity and affinity toward metal surfaces. Therefore, an efficient surface modification strategy to prevent protein adsorption on metallic surfaces is highly desired.

Immobilization of poly(ethylene oxide) (PEO) on surfaces [10] is currently the most common method to reduce protein adsorption on metallic materials, through chemical adsorption using a "grafting to" or a "grafting from" approach [11], or through physical adsorption of block or graft copolymers [12]. The protein resistance properties of hydrophilic PEO-based surfaces are mainly attributed to steric repulsion between proteins and the highly hydrated and flexible PEO chains [13, 14]. Poly(L-lysine)-g-PEG (PLL-g-PEG, where PEG stands for poly(ethylene glycol), a synonym of PEO) is well-known to anchor to negatively charged metal oxide surfaces through the positively charged PLL backbone [15], and is efficient to reduce protein adsorption. However, the amount of adsorbed PLL-g-PEG on metal oxide surfaces is pH- and ionic strength-dependent.

PEO-PPO-PEO (where PPO stands for poly(propylene oxide)) triblock copolymers, commercially available under the name of Pluronic®, can also be used to form PEO-based polymer coatings through adsorption on hydrophobic surfaces [16], thereby reducing protein adsorption [17]. Pluronic® is commonly used as a non-ionic polymeric surfactant in chemical and pharmaceutical industries [13, 18]. The more apolar PPO block of the triblock copolymer is expected to interact with hydrophobic surfaces, leaving free PEO chains extending into the bulk aqueous medium [19]. There are a wide range of PEO-PPO-PEO triblock copolymers with varying PEO and PPO chain lengths. The conformation and density of adsorbed PEO-PPO-PEO on hydrophobic surfaces vary depending on chain length of PEO and PPO blocks. It has been reported [19] that collagen adsorption and epithelial cell adhesion were prevented on hydrophobic substrates in the presence of Pluronic® F68. It is expected that, more generally, PEO-PPO-PEO can reduce biomolecule adsorption [20], bacterial adhesion [21] and thus biofilm formation. However, until now, to the best of our knowledge, a PEO-PPO-PEO triblock copolymer has not been immobilized on metal oxide surfaces to reduce protein adsorption, due to the hydrophilic nature of such

surfaces. The results of Nejadnik show that the adsorbed layer of Pluronic F127 is less than 2 nm thick on titanium oxide, suggesting a pancake rather than brush conformation, but these authors did not further investigate the protein resistance of the layer [22].

Several methods have been reported to hydrophobize the surface of metal oxides by modifying surface chemistry and possibly also surface topography, e.g. by means of self-assembled monolayers (SAM) or by introducing nano- or microstructures [23, 24]. Self-assembly of small molecules on metal surfaces is widely used to modify their properties. Alkylthiols and more generally organosulfur compounds are commonly assembled on gold or silver [25, 26]. Such strategy can however not be used on metal oxide surfaces. The self-assembly of alkylsilanes is another possible approach, but the control of assembly and the stability of the obtained layers raise many issues [27, 28]. Recently, self-assembly of alkane phosphonic acid has been applied on a wide range of metal oxide surfaces, including stainless steel [29], aluminium oxide [30], copper oxide [31], copper-nickel alloy [32] and titanium oxide [33]. It was reported that alkane phosphonic acid molecules bind covalently to the oxide surface [34]. The bonding mode (e.g. monodentate, bidentate or tridentate) however highly depends on the substrate [35]. It was shown that the water contact angle of copper oxide modified with a self-assembled monolayer of octadecylphosphonic acid is higher than 140° [31].

The aim of this study is to design a protein-resistant layer on metal oxide surfaces (titanium and stainless steel) by a two-step approach (Figure 1). First, self-assembly of octadecylphosphonic acid (OPA) was performed on titanium or stainless steel to obtain a hydrophobic surface, which is expected to favor PEO-PPO-PEO adsorption. The ability of PEO-PPO-PEO to prevent protein adsorption was then tested in two ways. On the one hand, PEO-PPO-PEO was preadsorbed on OPA-conditioned titanium or stainless steel, and the subsequent adsorption of three different model proteins

(bovine serum albumin, fibrinogen, cytochrome C) and of dextran, used as a model polysaccharides, was monitored by quartz crystal microbalance (QCM), a well-suited tool to monitor the successive deposition of the copolymer and the biomolecules. On the other hand, the competitive adsorption of PEO-PPO-PEO and BSA was examined using x-ray photoelectron spectroscopy (XPS) and time-of-flight secondary ion mass spectrometry (ToF-SIMS). These surface-sensitive techniques allow the respective presence of the copolymer and the protein in the adsorbed layer to be established. All experiments were performed in artificial seawater to mimic the conditions encountered in the case of marine biofouling.

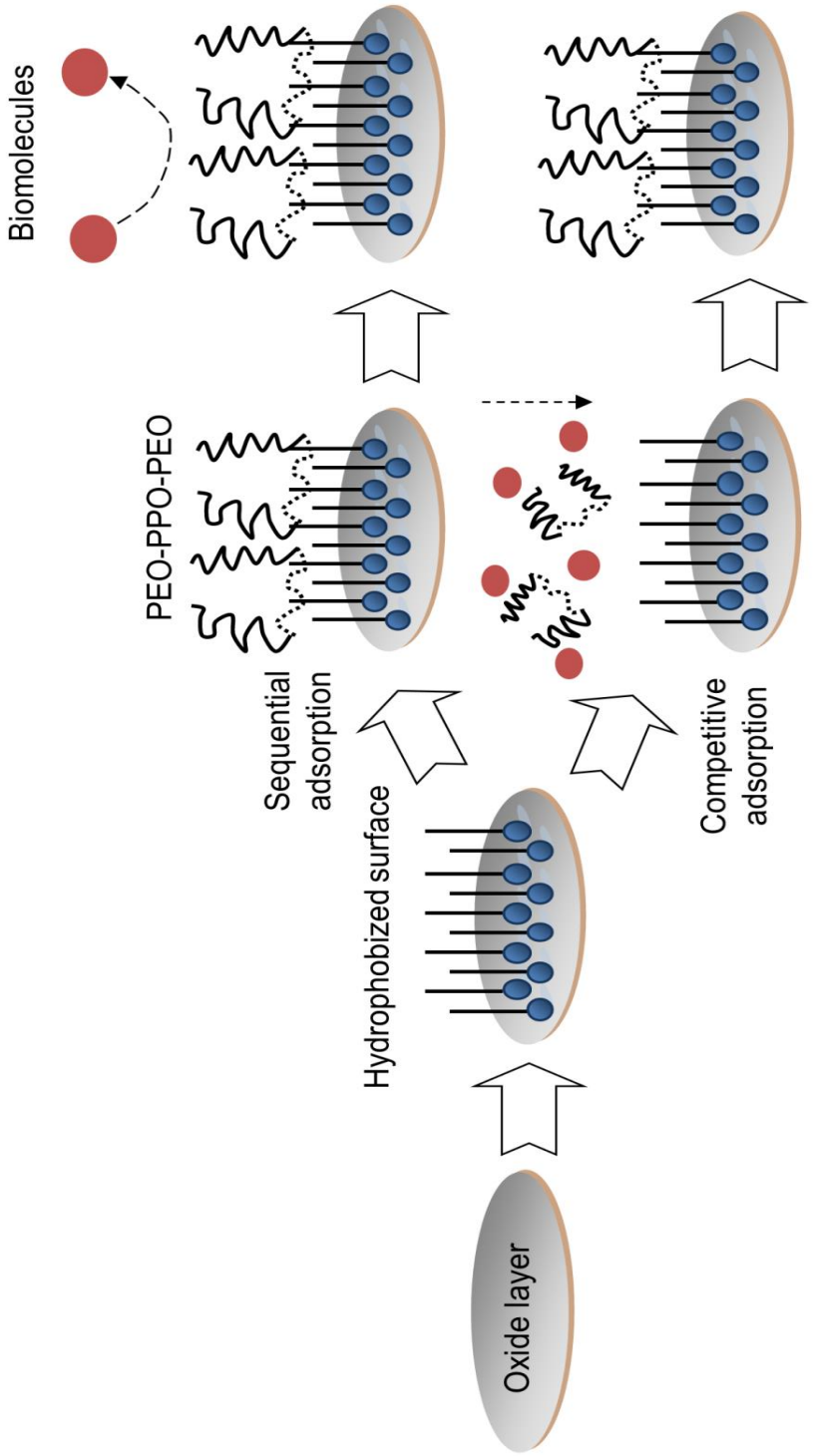

Figure 1. Surface modification strategy used in this work, and expected outcome.

2.2 Experimental

2.2.1 Materials

Albumin (BSA, from bovine serum, A4919), fibrinogen (Fb, fraction I, type I, from human plasma), cytochrome C (CytC, from horse heart, 99.7 wt% purity), dextran (from *Leuconostoc mesenteroides*, average mol. wt. 60,000 – 75,000, D8821), Pluronic® F68 (polyethylene oxide (PEO)-polypropylene oxide (PPO)-polyethylene oxide block copolymer with a degree of polymerization of 76 for the PEO blocks and 30 for the central PPO block ($PEO_{76}PPO_{30}PEO_{76}$) and a molar mass of 8350 Da, P1300), in short Plu in the following text, and octadecylphosphonic acid (97 wt%, OPA, 715166) were purchased from Sigma-Aldrich, and used without further purification.

Table 2. Composition of artificial seawater used in this work.

	mmol L^{-1}	g L^{-1}
NaCl	421.2	24.62
KCl	10.5	0.78
Na_2SO_4	28.9	4.11
$MgCl_2{\cdot}(H_2O)_6$	54.4	11.06
$CaCl_2{\cdot}(H_2O)_2$	10.6	1.56

Artificial seawater (ASW) [36] (see composition in Table 2) was sterilized after preparation, and then stored at 4°C. Filtered (0.2 μm) ASW was used to prepare protein and Plu solutions. BSA (65 kDa, isoelectric point (IEP) = 4.6) [37], Fb (340 kDa, IEP = 5.4) [38], CytC (11.7 kDa, IEP = 10) [39], dextran and Plu were dissolved in ASW at a concentration of 0.2, 0.1, 0.5, 0.5 and 2 mg mL^{-1}, respectively. It was checked that at these concentrations, these proteins and dextran reach their adsorption plateau over a short period of time. Regarding Plu, in a preliminary experiment, adsorption was performed on hydrophobic polystyrene with sequential increase of concentration, and monitored by QCM. It was concluded that the

adsorbed Plu amount reaches a plateau after a short period of time using 2 mg mL^{-1}. The plateau value did not increase anymore upon further increase of the concentration (results now shown).

Stainless steel 304 (SS) plates were 1 × 1 cm^2 squares (mass%, 18.10 Cr, 9.10 Ni, 1.11 Mn, 0.24 Mo, 0.36 Si, 0.051 C, 0.024 P, 0.001 S, balance Fe), in short SS, with 1 mm thickness and mirror-like surfaces received from Arcelor Mittal (Belgium). Titanium (Ti) samples (mass%, 0.10 C, 0.30 Fe, 0.03 N, 0.25 O, 0.015 H, balance Ti, diameter of 1.2 cm) were cut from cooling condenser tubes purchased from Ricerca sul Sistema Energetico (RSE) S.p.A (Italy), squeezed into relatively flat surfaces, and hand-polished using emery paper with grain size 600, then 1200. SS and Ti samples were cleaned three times with acetone in an ultrasonic bath for 15 min, and then submitted to UV-ozone cleaning for 15 min just before any further experiment.

2.2.2 Self-assembled monolayer preparation

Octadecylphosphonic acid (OPA) was dissolved in tetrahydrofuran (THF) at a concentration of 0.01 M. The cleaned metallic samples were immersed in OPA solution for 24 h. After removal from solution, the samples were rinsed 3 times with fresh THF in order to remove physisorbed molecules from the substrate surface, and dried in room conditions. The OPA-modified samples are referred to as Ti/OPA or SS/OPA.

2.2.3 Water contact angle (WCA) measurements

The wettability of metal surfaces before and after coating with OPA was investigated by measuring the contact angle using the sessile water drop method. A water drop of 1 μl was used for measurement at room temperature, and the contact angle was recorded 5 s after the water drop was deposited on the sample. For each type of sample, the reported value is the average of measurements made on triplicate samples (4 drops each).

2.2.4 Quartz crystal microbalance with dissipation monoitoring (QCM-D)

The AT-cut quartz crystals, coated with either titanium (QSX310) or stainless steel 2343 (QSX304, similar to US standard 316), with a fundamental resonant frequency of 5 MHz and a diameter of 14 mm, were purchased from LOT-ORIEL Europe. The experiments were performed using a Q-Sense E4 instrument (Q-Sense, Gothenburg, Sweden). The crystals were cleaned according to the protocol provided by Q-Sense. All experiments were carried out at 20°C and the flow, driven by a peristaltic pump, was set at 50 µl min^{-1}. The resonance frequency and dissipation were monitored simultaneously, and the results were recorded for different overtones (overtone number n = 1, 3, 5, 7, 9, 11, 13).

The principle and applications of QCM have been reviewed elsewhere [40]. In summary, the recorded shifts of frequency (Δf) are proportional to the mass loaded on the surface of the crystal while the changes of dissipation (ΔD) are related to the viscoelastic properties of the adsorbed layer. If the adsorbed layer is assumed to be rigid and evenly distributed, the changes of adsorbed mass (Δm) can be calculated from Δf, based on Sauerbrey equation (1) as follows:

$$\Delta m = -\frac{c \times \Delta f}{n} \quad (1)$$

Where c =17.7 ng Hz^{-1} cm^{-2} for a 5 MHz quartz crystal and n is the overtone number. Note that all observed ΔD/Δf ratios recorded here were lower than 0.4×10^{-6} (data not shown). Therefore, Δf may be considered proportional to the mass of the adsorbed layer [41] as described by Sauerbrey equation. Adsorbed Plu or protein mass was determined using all overtones except n = 1.

Artificial seawater was used as the background solution in all the experiments and was flowed into QCM cells for at least 1 h before

performing adsorption steps, to ensure a flat baseline. To avoid bubbles, all solutions were degassed before use.

2.2.5 X-ray photoelectron spectroscopy

XPS measurements were carried out with a Kratos Axis Ultra spectrometer (Kratos Analytical, UK), using monochromated Al Kα radiation (powered at 10 mA and 15 kV) and an eight-channeltrons detector. The analyzed area was 700 × 300 μm^2. The vacuum in the analysis chamber was about 10^{-6} Pa. The direction of photoelectron collection was perpendicular to the sample surface. Charging stabilization was achieved by using the Kratos Axis device. Survey spectra were recorded with 160 eV pass energy and 40 eV pass energy was used for narrow scans. In the latter conditions, the full width at half maximum (FWHM) of the Ag $3d_{5/2}$ peak of a standard silver sample was about 0.9 eV. The C-(C,H) component of the C 1s peak of carbon has been fixed to 284.8 eV to set the binding energy scale. The following sequence of spectra was recorded: survey spectrum, C 1s, O 1s, N 1s, Si 2p, P 2p, Cl 2p, S 2p, Ca 2p, Na 1s, Mg 2p, (Cr 2p, Mn 2p, Fe 2p, Zn 2p, Sn 3d for SS, Ti 2p, Zn 2p, Fe 2p for Ti) and C 1s again to check for charge stability and absence of degradation as a function of time. Molar fractions were calculated after a linear background subtraction using peak areas normalized on the basis of acquisition parameters, experimental sensitivity factors and transmission factors provided by the manufacturer. Elemental mole fractions are provided, excluding hydrogen which is not detected by XPS. The C 1s spectra were decomposed with the CasaXPS program (Casa Software Ltd., U.K.) using a Gaussian/Lorentzian (70/30) product function. The FWHM of the four carbon components was kept identical.

2.2.6 Time-of-flight secondary ion mass spectroscopy

ToF-SIMS measurements were performed with an ION-TOF V (ION-TOF, GmbH, Münster, Germany) spectrometer, using a Bi_3^+ primary ion source. The analyzed area was 500 × 500 μm^2 and the acquisition time for each spectrum was 1 min. Three positive spectra were acquired on each sample with a pulsed 30 keV, 0.67 pA primary ion beam in the high current bunched mode. The total ion dose density was 1.1×10^{11} Bi_3^+ cm^{-2}, below the static SIMS limit. The mass resolution (m/Δm) of the positive secondary ion spectra was 9700 for $C_4H_7^+$. ToF-SIMS imaging from negative spectra was obtained in 10 min using a Bi_3^{++} primary ion source, with a pulsed 60 keV, I_{ac} = 0.003 pA ion beam. Each image (surface area of 500 μm×500 μm) was composed of 256 × 256 pixels. The total ion dose density of acquired images was 2.3×10^9 Bi_3^{++} cm^{-2} in burst-sine 1 pulse mode. Positive ion mass spectra were calibrated using the CH_3^+, $C_2H_3^+$, $C_3H_5^+$ and $C_4H_7^+$ peaks. Negative ion mass spectra were calibrated using the CH_2^-, C_2H^-, C_3^- and C_4H^- peaks.

99 peaks were selected, from the positive spectra, including mainly signal from amino acids, salts, metal oxides and contaminations, and the sum of their intensities was defined as the total intensity I_{tot}. The relative intensity attributed to the signal from amino acids ($I_{rel,\ AA}$) was obtained using the following equation:

$$I_{rel,\ AA} = \frac{\sum I_{AA}}{I_{tot} - \sum I_{salt}} \qquad (2)$$

Where I_{AA} is the intensity of peaks attributed to amino acids, and I_{salt} is the intensity of peaks attributed to salts. $I_{rel,\ AA}$ measured on reference native and OPA-conditioned samples was systematically subtracted from $I_{rel,\ AA}$ of corresponding treated samples. All reported values are the average of three different positions on each sample.

2.2.7 Sample preparation and characterization

The process of Ti or SS surface modification using OPA self-assembly, then Plu and protein or dextran adsorption is shown schematically in Figure 1. Ti and SS were first coated by OPA as described above to obtain hydrophobic surfaces. Hydrophobized Ti and SS crystals were mounted in QCM cells, where Plu then protein or dextran adsorption was successively performed (sequential adsorption). In another set of experiments, hydrophobic Ti and SS coupons were incubated in a mixed Plu (2 mg mL^{-1}) and protein (BSA at 0.2 mg mL^{-1}) solution in artificial seawater for 2 h (competitive adsorption), then rinsed 10 times in ultrapure water, dried under a nitrogen flow and analyzed by ToF-SIMS and XPS.

2.3 Results

2.3.1 OPA coating on Ti and SS

Ti/OPA and SS/OPA QCM crystals were characterized by WCA measurements, XPS and ToF-SIMS imaging. The WCA values are reported in Table 3 for Ti, and Table 4 for SS. The wettability of the native Ti and SS crystals was measured just after cleaning. While the WCA of native Ti and SS was < 10º, the hydrophobicity of metal oxide surfaces increased after OPA coating up to 105.5° and 99.3° for Ti and SS, respectively. The stability of OPA coating was also tested. After 90 min of ultrasonication in ultrapure water, the value of the WCA was still 100.0° ± 1.1° and 100.9° ± 1.2° for Ti/OPA and SS/OPA, respectively, showing the good stability of the coatings. After the same treatment, the value of WCA was still below 10° for native Ti and SS.

Table 3. Elemental surface composition (at. %) and C/P elemental ratio determined by XPS, and water contact angle (θ_w) value for Ti before and after OPA self-assembly, bdl = below detection limit (<0.1%). Standard deviation of θ_w was about 1°.

	O	Ti	N	C	P	Si	C/P	θ_w (°)
Ti	47.3	21.0	0.9	29.9	0.7	0.2	42.7	<10
Ti/OPA	33.0	15.9	1.0	48.0	2.1	bdl	22.9	105.5

Table 4. Elemental surface composition (at. %) and C/P elemental ratio determined by XPS, and water contact angle (θ_w) value for SS before and after OPA self-assembly. Standard deviation of θ_w was about 1°. Ni was below detection limit, < 0.5%.

	Fe	Mn	Cr	O	N	C	S	P	Si	C/P	θ_w(°)
SS	13.2	0.1	3.7	44.7	0.5	34.1	0.2	1.1	2.4	31.0	<10
SS/OPA	8.6	0.1	2.3	34.2	0.8	48.4	0.5	2.6	2.4	18.6	99.3

The surface chemical composition obtained by XPS on Ti and SS crystals before and after OPA assembly is presented in Table 3 (Ti) and 4 (SS). Elements typical of these materials (Ti/O in a ratio close to 0.5 for Ti; Fe, Cr, Mn and O for SS) were found as expected. A high level of carbon-based contamination was always observed [15] on native Ti and SS surface due to adventitious hydrocarbon from air or XPS chamber, and low concentrations of nitrogen, phosphorus, silicon and sulfur were detected as well. After OPA assembly, an increase in carbon and phosphorus content is observed as was expected from OPA composition. The ratio of C/P was close to 18, which is the expected value of C/P in OPA molecules. Moreover, the atomic fraction of elements from the substrate (Ti, Fe, Cr) was significantly attenuated after OPA coating.

The C 1s spectra of Ti and SS before and after OPA coating are shown in Figure 2. The C 1s spectra of native Ti and SS (Figure 2a, 2c) are mainly composed of two peaks at 284.8 eV, due to carbon only bound to carbon and hydrogen C-(C,H), and at 286.2 eV, due to carbon bound to

oxygen or nitrogen C-(N,O). These carbon species are considered as originating from organic contaminants present in the atmosphere, which are adsorbing on the native Ti and SS because of the high surface energy of these materials. After OPA coating, the C 1s peaks were narrower (Figure 2b, 2d). One single and symmetric peak component (Figure 2b) is found on Ti/OPA, with a binding energy of 284.8 eV, in agreement with the presence of C-(C,H) bonds from aliphatic chains in OPA. The C-O compound has disappeared, which indicates that contamination was removed and replaced by OPA molecules. The C 1s spectrum of SS/OPA is similar to the one of Ti/OPA, except for a small residual component at about 286 eV. It might be attributed to defects of the OPA coating on SS, allowing the detection of some residual contamination.

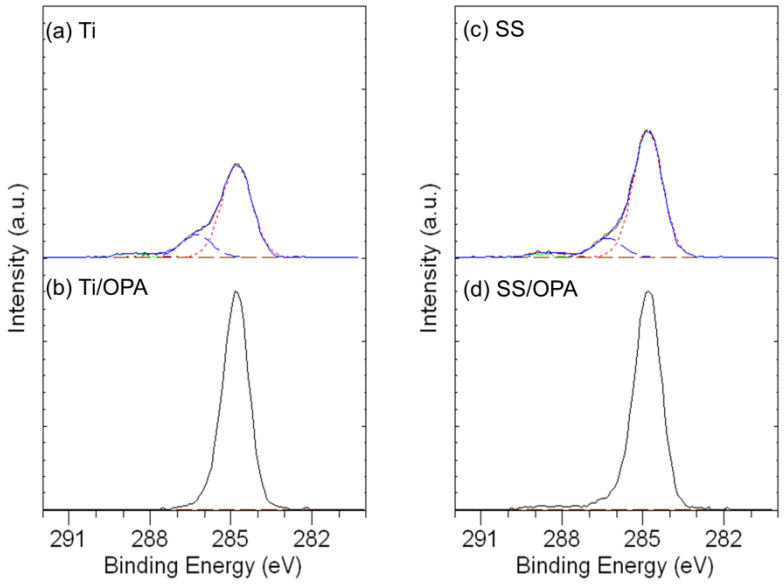

Figure 2. C 1s XPS spectra of (a) Ti, (b) Ti/OPA, (c) SS, (d) SS/OPA.

ToF-SIMS spectra (data not shown) show high intensities of typical OPA molecular peaks on Ti/OPA and SS/OPA. ToF-SIMS imaging was used to check the homogeneity of OPA coating on Ti and SS. Images of total intensity from selected fragments typical of OPA ($C_2H_4PO_3^-$, $C_2H_8PO_3^-$,

$C_8H_{18}PO_3^-$, $C_{18}H_{38}PO_2^-$, $C_{18}H_{38}PO_3^-$) recorded before and after OPA coating are presented in Figure 3. The images clearly highlight the presence of OPA at the surface after treatment (Figure 3b, 3d). On the contrary, only noise is detected on native Ti and SS (Figure 3a, 3c). The signal of OPA coating also more intense on Ti/OPA compared to SS/OPA.

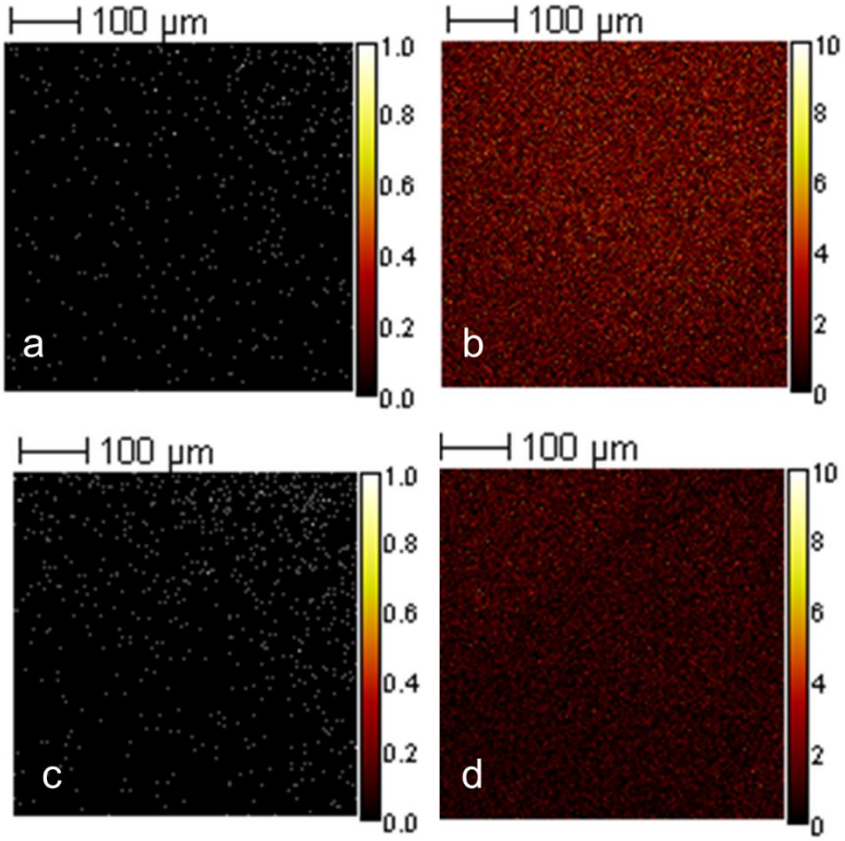

Figure 3. Field of view of 500 µm×500 µm negative ToF-SIMS images, showing the sum of $C_2H_4PO_3^-$, $C_2H_8PO_3^-$, $C_8H_{16}PO_3^-$, $C_{18}H_{38}PO_2^-$, $C_{18}H_{38}PO_3^-$ peak intensities on (a) native Ti, (b) Ti/OPA, (c) native SS, (d) SS/OPA.

2.3.2 Monitoring Plu and protein or dextran sequential adsorption using QCM

QCM has first been used to study Plu adsorption on SS, Ti, SS/OPA and Ti/OPA. Graphs showing the evolution of Δf and ΔD with time are presented in Figure 4. Both Δf and ΔD are markedly larger on Ti/OPA and SS/OPA compared to Ti and SS. On treated metal oxides, Δf decreased rapidly in the first 10 min and was associated to a clear ΔD increase. After that, Δf still decreased slightly up to –40 Hz in the next hour without any further dissipation shift. After rinsing with ASW to remove loosely adsorbed Plu, only a small increase of Δf was observed, associated with a more pronounced decrease of ΔD. The values of Δf and ΔD at this stage reveal the adsorption of a significant amount of Plu on Ti/OPA and SS/OPA. In contrast, both Δf and ΔD went back to baseline after rinsing on native Ti and SS, which means that no significant amount of Plu remained adsorbed on these substrates.

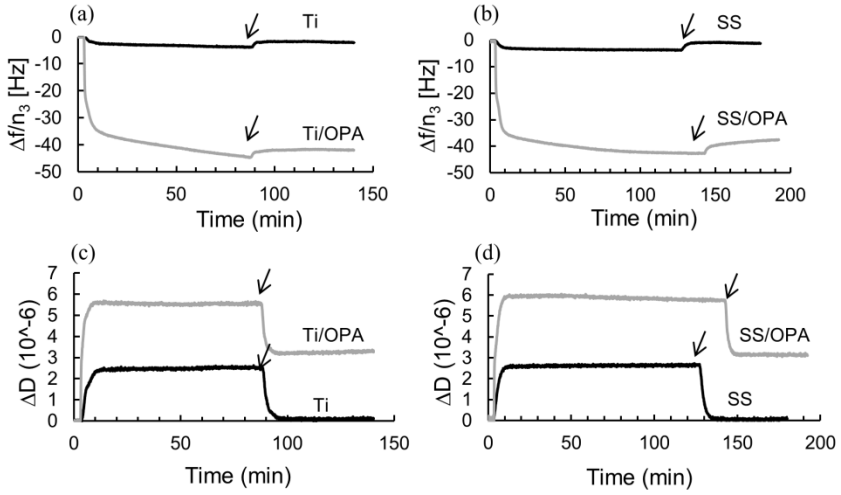

Figure 4. Δf vs time (a, b) and ΔD vs time (c, d) for Plu (2 mg ml^{-1}) adsorption on (a, c) Ti or Ti/OPA; (b, d) SS or SS/OPA. Arrows indicate rinsing using ASW. The results shown here were recorded from the 3rd overtone.

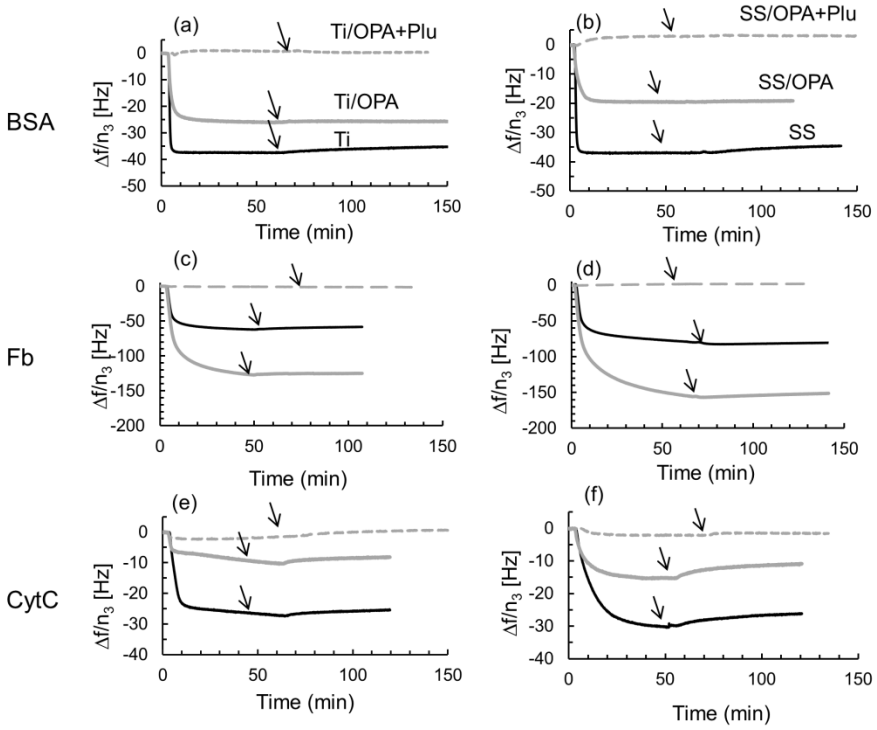

Figure 5. Δf vs time for the adsorption of different proteins (a, b: BSA), (c, d: Fb), (e, f: CytC) on Ti (a, c, e) and SS (b, d, f) with different surface conditions (black: native; grey: +OPA; dashed line: +OPA+Plu). OPA coating was prepared before QCM experiment, and Plu adsorption was performed within the same QCM experiment. All graphs were however set to $\Delta f = 0$ at $t = 0$ min when protein adsorption started, to allow comparisons to be made. Arrows indicate ASW rinsing after protein adsorption.

The protein resistance ability of Plu on Ti and SS surfaces was examined in presence or absence of OPA coating. Figure 5 shows the results obtained by QCM. Protein adsorption was first monitored in absence of Plu adsorption step (solid lines). For a given type of surface, Δf was more negative and therefore the amount of adsorbed protein increased with increasing molecular mass of the protein (CytC < BSA < Fb). For a given protein, the level of adsorption was however different on native and OPA-conditioned surfaces: BSA and CytC adsorption was favored on the native compared to the OPA-conditioned surfaces, while the contrary was observed

for Fb.

Plu preadsorption was carried out as follows: first, Plu was adsorbed for 2 h until saturation was reached. Then the surface was rinsed with ASW to get a flat baseline again. For the sake of clarity, the baseline was set to zero at that stage. After that, protein adsorption was performed (see dashed lines in Figure 5). The changes of Δf were negligible after protein adsorption when Plu was preadsorbed on Ti/OPA and SS/OPA (Figure 5, dashed lines). This demonstrates the protein resistance of Plu coatings on Ti/OPA and SS/OPA. The control experiments presented in Figure 6 (dashed lines) prove that preadsorption of Plu on native Ti and SS does not allow protein adsorption to be prevented. The observed adsorption is indeed very similar to the one observed in the absence of Plu precoating on Ti or SS (Figure 6, solid lines).

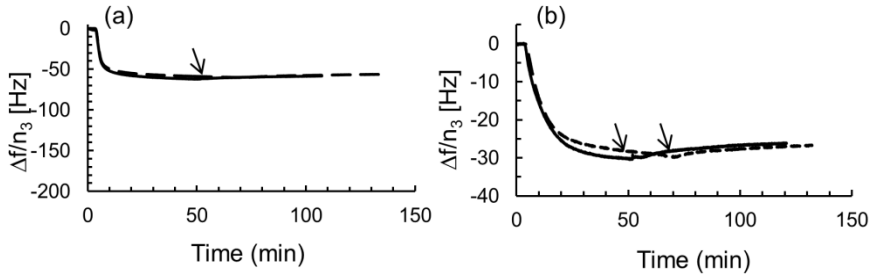

Figure 6. Δf vs time for the adsorption of Fb on Ti (a) and of CytC on SS (b) with (dashed line) or without (solid line) preadsorption of Plu. Plu adsorption was performed within the same QCM experiment. All graphs were however set to $\Delta f = 0$ at $t = 0$ min when protein adsorption started, to allow comparisons to be made. Arrows indicate ASW rinsing after protein adsorption.

The biomolecule resistance property of Plu was further tested using dextran, chosen as a model polysaccharide. The results are shown in Figure 7. The changes of Δf during dextran adsorption (before rinsing) may be attributed to adsorbed dextran or to the properties (viscosity, density) of the dextran solution, which differ from those of ASW used to establish the

baseline (t = 0). Δf went back to zero after rinsing on Ti/OPA+Plu, which demonstrates resistance to dextran adsorption achieved when Plu is previously adsorbed on Ti/OPA. On the contrary, preadsorption of Plu on Ti did not prevent dextran adsorption. A significant Δf is indeed measured between baselines established in ASW before and after dextran adsorption on Ti+Plu, showing the presence of adsorbed dextran.

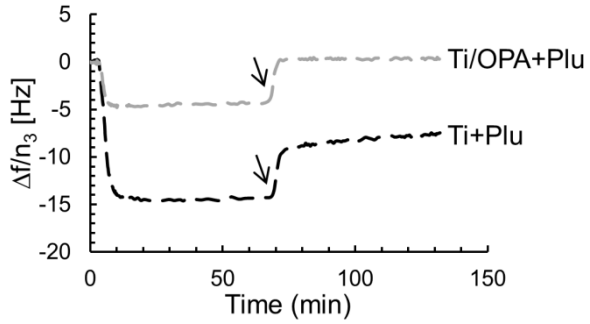

Figure 7. Δf vs time for the adsorption of dextran on Ti and Ti/OPA with preadsorption of Plu. Plu adsorption was performed within the same QCM experiment. The graph was however set to Δf = 0 at t = 0 min when dextran adsorption strated, to allow comparison to be made. Arrows indicate ASW rinsing after dextran adsorption.

2.3.3 Competitive Plu and protein adsorption examined by XPS and ToF-SIMS

Competitive adsorption from a mixed Plu and BSA solution was carried for 2 h on native and OPA-conditioned Ti and SS. Single adsorption experiments (BSA or Plu alone) were performed as control. It is shown by previous QCM results (Figures 4 for Plu and 5a, 5b for BSA) that 2 h is sufficient to reach the plateau of Plu and BSA adsorption. The extent of BSA adsorption on Ti or SS was examined by ToF-SIMS and XPS. The C 1s spectra obtained after BSA and/or Plu adsorption are shown in Figure 8. A small SiC component appeared at about 281.5 eV on the native Ti surface, probably due to the polishing process. Except for that, very similar results

were obtained for Ti and SS. Therefore, only the results for Ti will be described in the text.

The C 1s peaks recorded on Ti and Ti/OPA after BSA and/or Plu adsorption were decomposed in four components (SiC was excluded): at 284.8 eV, due to carbon bound to carbon or hydrogen C-(C,H); at 286.2 eV, due to carbon bound to nitrogen or oxygen C-(N,O); at 288.0 eV, due to carbon from the peptidic link (N-C=O) which indicated the presence of protein; and at 289 eV, due to carbon from carboxylic acid or ester groups (O-C=O). The shape of C 1s peaks recorded after BSA adsorption on native Ti surface in the absence and presence of Plu was similar (Figure 8(I)b, c), and the shape of the C 1s peaks recorded after single Plu adsorption was very close to the one obtained on native Ti (Figure 8(I)a, d). The adsorption of Plu on Ti/OPA surface led to a clear increase of the C-O component in the C 1s peak (Figure 8(II)a, d), in line with the composition of Plu. Finally, the C 1s peak obtained after competitive adsorption was very similar to the one obtained after single Plu adsorption (Figure 8(II)c, d). The XPS O 1s spectra (not shown) were less useful in this work because of the high intensity of oxygen coming from metal oxide surfaces.

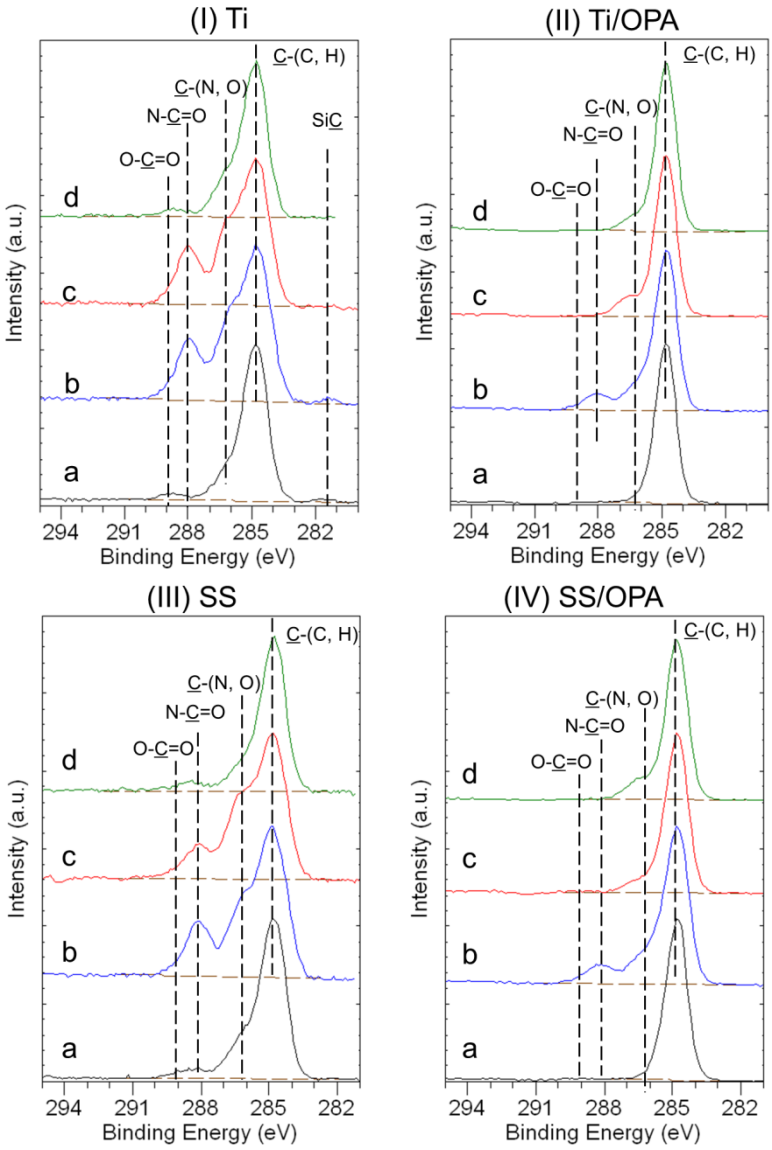

Figure 8. C 1s spectra of Ti (I), Ti/OPA (II), SS (III), SS/OPA (IV) conditioned with: (a) ASW, (b) single BSA adsorption, (c) BSA adsorption in the presence of Plu, (d) single Plu adsorption. The C 1s peaks were normalized in such a way that their maxima have the same height. Peak intensities can thus not be directly compared here. Attribution of the components of the C 1s peak is reported.

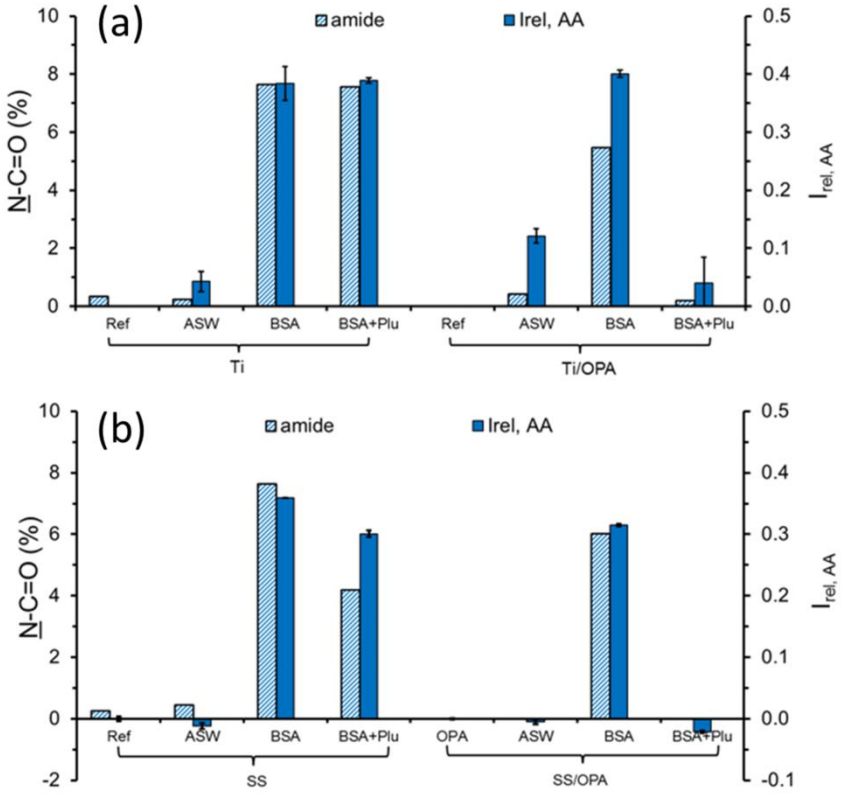

Figure 9. Amide (N-C=O) mole fraction (in %) determined by XPS and relative amino acid intensities ($I_{rel,\ AA}$) measured by ToF-SIMS on Ti (a) and SS (b) with or without OPA coating for BSA adsorption in the presence or absence of Plu. $I_{rel,\ AA}$ measured on reference native and OPA-conditioned samples was systematically subtracted from $I_{rel,\ AA}$ of corresponding treated samples.

After decomposition of the N 1s peak (not shown here), amide (400.0 eV, N-C=O) molar fraction (in %) was used as an indicator for the relative amount of BSA adsorbed on native Ti and Ti/OPA surface (Figure 9a). The amide content is close to zero when BSA is adsorbed together with Plu on Ti/OPA or SS/OPA, while it is similar to the one recorded in absence of Plu on Ti and SS. The intensities of fragments of amino acids from BSA measured on ToF-SIMS mass spectra ($I_{rel,\ AA}$) is plotted in Figure 9 together

with the amide fraction measured by XPS, for the different experimental conditions. BSA is almost not detected after competitive adsorption with Plu on Ti/OPA and SS/OPA, while its signal is again similar to the one recorded in absence of Plu on Ti and SS.

2.4 Discussion

OPA assembly on Ti and SS was assessed by WCA, ToF-SIMS and XPS measurements. These complementary results indicate that a CH_3-terminated hydrophobic layer was successfully formed on Ti/OPA and SS/OPA samples. Second, the biomolecule resistance properties of Plu on Ti/OPA and SS/OPA were examined by sequential adsorption and competitive adsorption of Plu and model proteins or dextran. QCM results showed that the adsorption of these proteins (BSA, Fb and CytC) and dextran, taken as model fouling biomacromolecules, can be prevented on Ti/OPA and SS/OPA with preadsorption of Plu. The control experiments showed a significant amount of protein adsorbed on both native and OPA-conditioned Ti and SS in absence of Plu. Adsorption of Plu on native Ti and SS surfaces did not prevent protein and dextran adsorption due to the lack of adsorption of Plu on these hydrophilic surfaces. Competitive adsorption of Plu and BSA on OPA-conditioned Ti and SS surfaces showed that BSA adsorption could be prevented or adsorbed BSA could be displaced on Ti/OPA and SS/OPA in the presence of Plu.

Self-assembly of small molecules, such as alkanethiols on gold [26] and alkylsilanes on silica [25], produce well-ordered coatings which may be used to control wettability, biocompatibility and functional groups on the surface [29]. Here, octadecylphosphonic acid (OPA) was self-assembled on Ti and SS surfaces because this strategy is well-suited for metal oxide surfaces. The thickness and structure of OPA layer was studied in detail elsewhere [42]. Briefly, the mechanism of assembly is based on the reaction of phosphonic acid head group of OPA molecule with metal oxide on the

surface, leaving alkyl chains pointing outwards, which interact through Van der Waals forces. The presence of metal oxide at the extreme surface is necessary for the success of OPA self-assembly. This was the case here for Ti and SS (see elemental composition in Table 3 and 4, and shape of O 1s peaks, not shown here). The WCA measured after OPA assembly (see Table 3 and 4) are attributed to the terminal methyl groups of alkyl chains, pointing outward from the metal surface after treatment. Well-organized hydrophobic layers are thus obtained. XPS and ToF-SIMS results (see Figures 2 and 3) also point to the formation of a relatively homogeneous coating, and to the displacement of carbon-based contaminants upon assembly. The obtained OPA layer was somewhat less homogeneous on SS/OPA compared to Ti/OPA, maybe due to the fact that SS is an alloy.

It is shown in Figure 5 that surface hydrophobicity influences protein adsorption. The adsorbed amount of BSA and CytC on Ti/OPA and SS/OPA was less than on native Ti and SS surfaces (Figure 5a, 5b, 5e, 5f). As calculated by Sauerbrey equation, the respective adsorbed mass of BSA and CytC are ~630 ng cm^{-2} and ~370 ng cm^{-2} on Ti, and 420 ng cm^{-2} and 130 ng cm^{-2} on Ti/OPA. Similar values are found on SS. Hydrophobic interaction is identified as the main driving force for BSA and CytC adsorption onto hydrophobic surfaces [43]. It was shown by Roach *et al.* that BSA, a so-called soft protein, undergoes a structural rearrangement (deformation) when adsorbed on hydrophobic surfaces [44]. Flattening of the protein molecules on the surface leads to a lower adsorbed amount because the area occupied per molecule increases and a monolayer is thus formed which contains fewer molecules. In contrast, fibrinogen is known to be a hard protein, with a rod shape [39]. Here, we show that it adsorbs more onto Ti/OPA and SS/OPA, compared to native Ti and SS (Figure 5c, 5d). The adsorbed mass of Fb was ~950 ng cm^{-2} on Ti and ~1940 ng cm^{-2} on Ti/OPA, respectively. This could be explained by orientation difference of Fb on these two different surfaces. On OPA-conditioned surfaces (Figure 5c, 5d), Fb adsorption may undergo a

two-stage process, in which adsorbed fibrinogen may reorient to the "end-on" configuration, with the long axis of Fb perpendicular to the hydrophobic surface. A similar explanation was given by Roach *et al.*, and was attributed to attractive forces between fibrinogen molecules, which would be dominant on hydrophobic surfaces [44]. On the native Ti and SS surfaces, most of Fb molecules may be in the "side-on" configuration, with the long axis parallel to the surface, which gives more contact area per Fb molecule. It is expected that electrostatic attraction force governs protein adsorption on native Ti and SS surfaces. Here, we observe that the adsorbed mass increases with the molecular mass of the proteins. This is not surprising since proteins tend to form monolayers, whose thickness increases with the size of the molecules. Such a trend may however not always be found, depending on the anisotropy of the molecules, their orientation once adsorbed, and their denaturation at the interface.

The PEO-PPO-PEO triblock copolymer adsorption mechanism is thought to be based on the hydrophobic interaction between PPO blocks and alkyl groups of OPA on Ti/OPA or SS/OPA surfaces. As shown in Figure 4, Plu adsorbs very fast (~10 min) onto the OPA-conditioned surfaces. This fast adsorption rate may be attributed to the abundant free sites for adsorption on hydrophobic surfaces in the beginning of the process. As more and more sites were occupied, the changes in frequency shift related to adsorption slowed down, and a plateau was reached. At this stage, it is assumed that Plu forms a brush structure with relatively high density on Ti/OPA and SS/OPA, which prevents further Plu molecules to approach [22]. It has been reported that PEO-PPO-PEO can form a brush structure on hydrophobic surfaces with WCA above 80° [22], which is then effective to reduce protein adsorption [45]. In contrast, PEO-PPO-PEO can form a pancake structure on hydrophilic surfaces [45], which is insufficient to prevent protein adsorption. However, QCM results obtained here indicate that Plu does not even remain in significant amount on the native Ti and SS

after rinsing (Figure 4). This explains the similar results found for protein adsorption on Ti and SS in absence or presence of Plu adsorption step (see Figure 6). The extent of Pluronic adsorption on metallic surfaces might be related to their cleanness. It is known that, due to their high surface energy, metal substrates get contaminated by adsorption of adventitious hydrocarbon after exposure to ambient environment, resulting in increased WCA after cleaning. It is worth to point out here that the native Ti and SS crystals were used for QCM-D experiments just after the cleaning procedure, and were very hydrophilic (WCA < 10°).

The adsorbed Plu mass calculated based on Sauerbrey equation is equal to 460 ng cm^{-2} and 480 ng cm^{-2} on Ti/OPA and SS/OPA, respectively. Due to the similar values obtained on Ti/OPA and SS/OPA, the average value of 470 ng cm^{-2} is used for further computation. It is assumed here that the hydrated Plu layer contained 20% to 50% of water based on previous literature results [46]. Based on this range of water content, we estimated the number of adsorbed Plu molecules and PEO chains per unit area. The results give an estimated range of 0.17 – 0.27 Plu molecules nm^{-2}, 0.34 – 0.54 PEO chains nm^{-2} and 26 – 41 EO monomers nm^{-2}. The Plu density obtained here is in the same range as the one reported for Pluronic P105 (PEO_{37}-PPO_{56}-PEO_{37}) adsorption on hydrophobic polypropylene surface (0.19 – 0.21 molecules nm^{-2}) [46]. The PEO chain density or EO monomer density is a more critical value to evaluate the protein resistance ability of adsorbed Plu. It was indeed shown that the smaller proteins can penetrate and adsorb between PEO chains [12] if the PEO chain density is not high enough. The PEO density and EO monomer density obtained here are comparable with those achieved by adsorption of PLL(20)-g-PEG(2) (g < 5) on Nb_2O_5 surface [47], which showed a good protein resistance ability in serum solution. The PEO chain density could still be improved using Pluronic with different PPO and/or PEO chain lengths [20].

The biomolecule resistance ability of PEO-PPO-PEO triblock copolymer was tested by adsorption of proteins and dextran, and monitored by QCM. It was shown (Figure 5) that protein or dextran adsorption was negligible on Ti/OPA and SS/OPA with preadsorbed Plu. These results show that the adsorption of all tested proteins (BSA, Fb and CytC, with different molecular masses and shapes) and dextran can be prevented by pre-adsorption of Plu on Ti/OPA and SS/OPA, showing the versatility of the approach. Other studies also reported that adsorption of Plu on CH_3-terminated self-assembled monolayer on gold prevents albumin and fibrinogen adsorption, as demonstrated by surface plasmon resonance (SPR) [48]. The mechanism of protein resistance ability of PEO-PPO-PEO is attributed to the high hydration of PEO chains extending into the bulk solution, resulting in a steric barrier [16, 17].

By comparing the QCM results for BSA (Figure 5a, 5b) and Plu (Figure 4a, 4b) adsorption on Ti/OPA and SS/OPA surfaces, it can be seen that BSA adsorption reaches saturation faster than Plu (in the conditions used here). Therefore, we may wonder if bringing Plu together with BSA in solution may still be relevant to prevent protein adsorption, or if it is necessary to pre-adsorb Plu to prevent BSA adsorption. Competitive adsorption was thus performed. The XPS (Figures 8 and 9) and ToF-SIMS (Figure 9) results show, in excellent agreement with each other, that prevention of protein adsorption is as well obtained when Plu is brought in solution together with the protein instead of being preadsorbed. This suggests that Plu might have a higher affinity toward hydrophobic surfaces compared to BSA and that adsorbed BSA could be replaced by Plu molecules. A similar result was reported by Dewez [49]. The presence of Pluronic F68 was shown to reduce collagen adsorption, and the effect was more pronounced as the substrate hydrophobicity was higher [49]. Other results of the same author showed that pre-adsorbed extracellular matrix (ECM) proteins are not displaced by Pluronic F68, whatever the substratum

hydrophobicity [50]. The displacement kinetics of BSA or other fouling compounds by Plu might be related to the hydrophobicity of underlying substrate and the nature of these compounds. Furthermore, Detrait *et al.* showed that Pluronic F68 reduces the adsorption of adhesive proteins (fibronectin or collagen) on hydrophobic polystyrene surface by competitive adsorption, thereby reducing cell adhesion [51]. The possibility to desorb an already formed conditioning film would open the way to an interesting strategy of decontamination of fouled surfaces. In Chapter 3, we have actually shown that *Pseudomonas* adhesion on SS/OPA is strongly reduced by preadsorption of Plu, or by addition of Plu after the bacterial adhesion step.

2.5 Conclusions

The present work provides a two-step approach to create PEO-modified surfaces on metallic oxide surfaces (here, SS and Ti). First, the surfaces are modified by an OPA self-assembled coating which makes them hydrophobic. Then, a PEO-PPO-PEO copolymer (Plu) is adsorbed. Anchoring of the copolymer through its central PPO block is thought to occur, leaving free PEO chains in solution. The adsorption of three proteins (BSA, Fb and CytC) and dextran, used as model fouling biomolecules, was shown to be prevented on Ti and SS surfaces, previously hydrophobized and treated with Plu. The obtained PEO chain density on OPA-conditioned Ti and SS is in the range of 0.3 – 0.5 chains nm^{-2}, which is comparable to the density measured on PLL-g-PEG adsorbed on metal oxide surfaces. A one-step approach was then investigated, in which the metal oxide surfaces are only modified by OPA self-assembly. Plu is then simply added to the fouling solution. The results show that in these conditions, prevention of protein adsorption is also successful. These approaches could be used to reduce bacterial adhesion and biofilm formation, and are applicable on other metal oxide surfaces as well. The adhesion properties of marine microorganisms

on this anti-protein layer will be investigated further.

2.6 References

[1] Kingshott P and Griesser HJ, 1999, Surfaces that resist bioadhesion, Curr. Opin. Solid State Mater. Sci., 4, 403-412.

[2] Coetser SE and Cloete TE, 2005, Biofouling and biocorrosion in industrial water systems, Crit. Rev. Microbiol., 31, 213-232.

[3] Cristiani P, 2005, Solutions to fouling in power station condensers, Appl. Therm. Eng., 25, 2630-2640.

[4] Chmielewski RAN and Frank JF, 2003, Biofilm Formation and Control in Food Processing Facilities, Compr. Rev. Food. Sci. F., 2, 22-32.

[5] Page K, Wilson M and Parkin IP, 2009, Antimicrobial surfaces and their potential in reducing the role of the inanimate environment in the incidence of hospital-acquired infections, J. Mater. Chem., 19, 3819-3831.

[6] Callow JA and Callow ME, 2011, Trends in the development of environmentally friendly fouling-resistant marine coatings, Nat. Commun., 2, 244.

[7] Boonaert CJP, Dufrêne YF and Rouxhet PG, 2003, Adhesion (Primary) of Microorganisms onto Surfaces, in: Bitton G (Ed.) Encyclopedia of Environmental Microbiology, Wiley, New York, Vol 1, 113-132.

[8] Schneider RP and Leis A, 2003, Conditioning Films in Aquatic Environments, in: Bitton G (Ed.) Encyclopedia of Environmental Microbiology, Wiley, New York, Vol 2, 928-941.

[9] Compère C, Bellon-Fontaine MN, Bertrand P, Costa D, Marcus P, Poleunis C, Pradier CM, Rondot B and Walls MG, 2001, Kinetics of conditioning layer formation on stainless steel immersed in seawater, Biofouling, 17, 129-145.

[10] Leckband D, Sheth S and Halperin A, 1999, Grafted poly(ethylene oxide) brushes as nonfouling surface coatings, J. Biomater. Sci. Polym. Ed., 10, 1125-1147.
[11] Zhao B and Brittain WJ, 2000, Polymer brushes: surface-immobilized macromolecules, Prog. Polym. Sci., 25, 677-710.

[12] Michel R, Pasche S, Textor M and Castner DG, 2005, Influence of PEG architecture on protein adsorption and conformation, Langmuir, 21, 12327-12332.

[13] Amiji M and Park K, 1992, Prevention of protein adsorption and platelet adhesion on surfaces by PEO/PPO/PEO triblock copolymers, Biomaterials, 13, 682-692.

[14] Rosenhahn A, Schilp S, Kreuzer HJ and Grunze M, 2010, The role of "inert" surface chemistry in marine biofouling prevention, Phys. Chem. Chem. Phys., 12, 4275-4286.

[15] Kenausis GL, Vörös J, Elbert DL, Huang N, Hofer R, Ruiz-Taylor L, Textor M, Hubbell JA and Spencer ND, 2000, Poly(l-lysine)-g-Poly(ethylene glycol) Layers on Metal Oxide Surfaces: Attachment Mechanism and Effects of Polymer Architecture on Resistance to Protein Adsorption, J. Phys. Chem. B, 104, 3298-3309.

[16] Freij-Larsson C, Nylander T, Jannasch P and Wesslen B, 1996, Adsorption behaviour of amphiphilic polymers at hydrophobic surfaces: effects on protein adsorption, Biomaterials, 17, 2199-2207.

[17] Green RJ, Davies MC, Roberts CJ and Tendler SJ, 1998, A surface plasmon resonance study of albumin adsorption to PEO-PPO-PEO triblock copolymers, J. Biomed. Mater. Res., 42, 165-171.

[18] Green RJ, Tasker S, Davies J, Davies MC, Roberts CJ and Tendler SJB, 1997, Adsorption of PEO−PPO−PEO Triblock Copolymers at the Solid/Liquid Interface: A Surface Plasmon Resonance Study, Langmuir, 13, 6510-6515.

[19] Dewez JL, Schneider YJ and Rouxhet PG, 1996, Coupled influence of substratum hydrophilicity and surfactant on epithelial cell adhesion, J. Biomed. Mater. Res., 30, 373-383.

[20] Caldwell KD, 1997, Surface Modifications with Adsorbed Poly(ethylene oxide)-Based Block Coploymers, in: Harris JM, Zalipsky S (Eds.) Poly(ethylene glycol), ACS, Vol 680, 400-419.

[21] Nejadnik MR, van der Mei HC, Norde W and Busscher HJ, 2008, Bacterial adhesion and growth on a polymer brush-coating, Biomaterials, 29, 4117-4121.

[22] Nejadnik MR, Olsson AL, Sharma PK, van der Mei HC, Norde W and Busscher HJ, 2009, Adsorption of pluronic F-127 on surfaces with different hydrophobicities probed by quartz crystal microbalance with dissipation, Langmuir, 25, 6245-6249.

[23] Chen LJ, Chen M, Zhou HD and Chen JM, 2008, Preparation of super-hydrophobic surface on stainless steel, Appl. Surf. Sci., 255, 3459-3462.

[24] Li L, Breedveld V and Hess DW, 2012, Creation of superhydrophobic stainless steel surfaces by acid treatments and hydrophobic film deposition, ACS Appl. Mater. Interfaces., 4, 4549-4556.

[25] Ulman A, 1996, Formation and Structure of Self-Assembled Monolayers, Chem. Rev., 96, 1533-1554.

[26] Love JC, Estroff LA, Kriebel JK, Nuzzo RG and Whitesides GM, 2005, Self-assembled monolayers of thiolates on metals as a form of nanotechnology, Chem. Rev., 105, 1103-1169.

[27] Dekeyser CM, Buron CC, Mc Evoy K, Dupont-Gillain CC, Marchand-Brynaert J, Jonas AM and Rouxhet PG, 2008, Oligo(ethylene glycol) monolayers by silanization of silicon wafers: Real nature and stability, J. Colloid Interface Sci., 324, 118-126.

[28] Dekeyser CM, Buron CC, Derclaye SR, Jonas AM, Marchand-Brynaert J and Rouxhet PG, 2012, Degradation of bare and silanized silicon wafer surfaces by constituents of biological fluids, J. Colloid Interface Sci., 378, 77-82.

[29] Van Alsten JG, 1999, Self-Assembled Monolayers on Engineering Metals: Structure, Derivatization, and Utility, Langmuir, 15, 7605-7614.

[30] Nie HY, 2010, Revealing different bonding modes of self-assembled octadecylphosphonic acid monolayers on oxides by time-of-flight secondary ion mass spectrometry: silicon vs aluminum, Anal. Chem., 82, 3371-3376.

[31] Hoque E, DeRose JA, Bhushan B and Hipps KW, 2009, Low adhesion, non-wetting phosphonate self-assembled monolayer films formed on copper oxide surfaces, Ultramicroscopy, 109, 1015-1022.

[32] Kruszewski KM, Renk ER and Gawalt ES, 2012, Self-assembly of organic acid molecules on the metal oxide surface of a cupronickel alloy, Thin Solid Films, 520, 4326-4331.

[33] Gawalt ES, Avaltroni MJ, Koch N and Schwartz J, 2001, Self-Assembly and Bonding of Alkanephosphonic Acids on the Native Oxide Surface of Titanium, Langmuir, 17, 5736-5738.

[34] Helmy R and Fadeev AY, 2002, Self-Assembled Monolayers Supported on TiO2: Comparison of C18H37SiX3(X = H, Cl, OCH3), C18H37Si(CH3)2Cl, and C18H37PO(OH)2, Langmuir, 18, 8924-8928.

[35] Fonder G, Minet I, Volcke C, Devillers S, Delhalle J and Mekhalif Z, 2011, Anchoring of alkylphosphonic derivatives molecules on copper oxide surfaces, Appl. Surf. Sci., 257, 6300-6307.

[36] Berglin M and Elwing H, 2008, Erosion of a model rosin-based marine antifouling paint binder as studied with quartz crystal microbalance with dissipation monitoring (QCM-D) and ellipsometry, Prog. Org. Coat., 61, 83-88.

[37] Carter DC and Ho JX, 1994, Structure of Serum Albumin, Adv. Protein Chem., 45, 153-203.

[38] Haynes CA and Norde W, 1994, Globular proteins at solid/liquid interfaces, Colloids Surf. B. Biointerfaces, 2, 517-566.

[39] Nakanishi K, Sakiyama T and Imamura K, 2001, On the adsorption of proteins on solid surfaces, a common but very complicated phenomenon, J. Biosci. Bioeng., 91, 233-244.

[40] Marx KA, 2003, Quartz crystal microbalance: a useful tool for studying thin polymer films and complex biomolecular systems at the solution-surface interface, Biomacromolecules, 4, 1099-1120.

[41] Reviakine I, Johannsmann D and Richter RP, 2011, Hearing what you cannot see and visualizing what you hear: interpreting quartz crystal microbalance data from solvated interfaces, Anal. Chem., 83, 8838-8848.

[42] Keszthelyi T, Paszti Z, Rigo T, Hakkel O, Telegdi J and Guczi L, 2006, Investigation of solid surfaces modified by Langmuir-Blodgett monolayers using sum-frequency vibrational spectroscopy and X-ray photoelectron spectroscopy, J. Phys. Chem. B, 110, 8701-8714.

[43] van der Veen M, Stuart MC and Norde W, 2007, Spreading of proteins and its effect on adsorption and desorption kinetics, Colloids Surf. B. Biointerfaces, 54, 136-142.

[44] Roach P, Farrar D and Perry CC, 2005, Interpretation of protein adsorption: surface-induced conformational changes, J. Am. Chem. Soc., 127, 8168-8173.

[45] Schroen CGPH, Stuart MAC, van der Voort Maarschalk K, van der Padt A and van't Riet K, 1995, Influence of Preadsorbed Block Copolymers on Protein Adsorption: Surface Properties, Layer Thickness, and Surface Coverage, Langmuir, 11, 3068-3074.

[46] Liu X, Wu D, Turgman-Cohen S, Genzer J, Theyson TW and Rojas OJ, 2010, Adsorption of a nonionic symmetric triblock copolymer on surfaces with different hydrophobicity, Langmuir, 26, 9565-9574.

[47] Pasche S, De Paul SM, Vörös J, Spencer ND and Textor M, 2003, Poly(l-lysine)-graft-poly(ethylene glycol) Assembled Monolayers on Niobium Oxide Surfaces: A Quantitative Study of the Influence of Polymer Interfacial Architecture on Resistance to Protein Adsorption by ToF-SIMS and in Situ OWLS, Langmuir, 19, 9216-9225.

[48] Chang Y, Chu WL, Chen WY, Zheng J, Liu L, Ruaan RC and Higuchi A, 2010, A systematic SPR study of human plasma protein adsorption behavior on the controlled surface packing of self-assembled poly(ethylene oxide) triblock copolymer surfaces, J. Biomed. Mater. Res. A, 93, 400-408.

[49] Dewez JL, Berger VV, Schneider YJ and Rouxhet PG, 1997, Influence of Substrate Hydrophobicity on the Adsorption of Collagen in the Presence of Pluronic F68, Albumin, or Calf Serum, J. Colloid Interface Sci., 191, 1-10.

[50] Dewez J-L, Doren A, Schneider Y-J and Rouxhet PG, 1999, Competitive adsorption of proteins: Key of the relationship between substratum surface properties and adhesion of epithelial cells, Biomaterials, 20, 547-559.

[51] Detrait E, Lhoest JB, Knoops B, Bertrand P and van den Bosch de Aguilar P, 1998, Orientation of cell adhesion and growth on patterned heterogeneous polystyrene surface, J. Neurosci. Methods, 84, 193-204.

Chapter 3

Influence of poly(ethylene oxide)-based copolymer on protein adsorption and bacterial adhesion on stainless steel: modulation by surface hydrophobicity

The presentation of Chapter 3 is derived from the paper submitted to Bioelectrochemistry (Special issue on biocorrosion) with the same title, Y. Yang, P. G. Rouxhet, D. Chudziak, J. Telegdi, C.C. Dupont-Gillain.

Summary

The aim of the present work is to study the adhesion of *Pseudomonas* NCIMB 2021, a typical aerobic marine microorganism, on stainless steel (SS) substrate. More particularly, the potential effect on adhesion of adsorbed poly(ethylene oxide)-poly(propylene oxide)-poly(ethylene oxide) (PEO-PPO-PEO) triblock copolymer is investigated. In addition, already adhered bacteria were submitted to a PEO-PPO-PEO solution and their detachment was examined. Bacterial attachment experiments were carried out using a modified parallel plate flow chamber, allowing different surface treatments to be compared in a single experiment. The amount of adhering bacteria was determined via DAPI staining and fluorescence microscopy. x-ray photoelectron spectroscopy (XPS) was used to characterize the surface chemical composition of SS and hydrophobized SS before and after PEO-PPO-PEO adsorption. The adsorption of bovine serum albumin (BSA), a model protein, was investigated to test the resistance of PEO-PPO-PEO layers to protein adsorption. The results show that BSA adsorption and *Pseudomonas* 2021 adhesion are significantly reduced on hydrophobized SS conditioned with PEO-PPO-PEO. Although PEO-PPO-PEO is also found to adsorb on SS, it does not prevent BSA adsorption nor bacterial adhesion, which is attributed to different PEO-PPO-PEO adlayer structures on hydrophobic and hydrophilic surfaces. Moreover, rinsing with a PEO-PPO-PEO solution is also an efficient strategy to remove already adhered bacteria on hydrophobized SS. The obtained results open the way to a new strategy to reduce biofouling on metal oxide surfaces using PEO-PPO-PEO triblock copolymer.

3.1 Introduction

Biofilm formation on solid substrates starts with single bacterial adhesion, followed by their proliferation and encapsulation in extracellular polymeric substances (EPS), which leads to a worldwide problem called biofouling [1]. The growth of biofilms on metallic materials can cause the so-called microbially influenced corrosion (MIC) [2]. The adhering bacteria and their associated EPS alter the metal/solution interface (e.g. lower pH, lower oxygen level, change in ionic strength), which might disrupt the passive layer, thereby causing corrosion. These phenomena have a negative effect on economy, e.g. biofouling reduces the efficiency of heat exchangers [3], and biocorrosion reduces the life time of cooling condensers and related equipments. Until now, chlorination [4] is still the most effective method to control biofilm growth on cooling condensers in offshore power plants. However, due to the environmental issues related to chlorine discharge [5], a more eco-friendly way to control biofouling in cooling condensers is highly demanded.

Bacterial adhesion is influenced by the surface properties of materials (chemical composition, roughness) [6, 7] and environmental conditions (pH, ionic strength) [8, 9]. The contact between bacteria and substrates occurs through a layer of organic compounds (biomolecules) which is formed by adsorption rapidly after immersion of substrates into the biological aqueous environment [10]. This spontaneously formed organic layer is called conditioning layer [11], which is made of organic matter or EPS secreted by microorganisms in aqueous environment. The conditioning layer may further facilitate bacterial colonization [12] owing to modification of the surface properties (surface charge and wettability) as well as to specific interactions, promoting irreversible bacterial attachment [13]. The conditioning layer formation occurs prior to bacterial adhesion, and therefore plays an important role in microorganism attachment. The development of anti-fouling coatings may be focused on the prevention of

biomacromolecules adsorption which would in turn reduce bacterial adhesion. The initial bacterial adhesion is indeed a critical step for further biofilm formation.

Pseudomonas species are recognized as primary colonizers [14] involved in biocorrosion, and they are prevalent in marine and industrial environments [15]. Therefore, *Pseudomonas* NCIMB 2021, which was originally isolated by Fletcher and Floodgate in 1973 [16], was chosen as a typical aerobic marine bacteria for the study of initial bacterial adhesion in this work. *Pseudomonas* 2021 was reported to cause micro-pitting corrosion on stainless steel [17, 18]. The same authors also showed that selective elemental depletion on stainless steel (e.g. enrichment of Cr and depletion of Fe) was due to the colonization by this bacterium. The colonization by *Pseudomonas* could remove oxygen by respiration, thus creating an anaerobic environment to harbor anaerobic bacteria, such as sulfate reducing bacteria (SRB) [14]. Due to the above reasons, we are particularly interested to test *Pseudomonas* 2021 adhesion on poly(ethylene oxide) (PEO)-based anti-fouling coatings. The antifouling properties of hydrophilic PEO-based surfaces are mainly attributed to steric repulsion [19] between proteins and the highly hydrated and flexible PEO chains [20]. PEO-PPO-PEO (where PPO stands for poly(propylene oxide)) triblock copolymers are commercially available under the name of Pluronic®, and can be used to form PEO-based polymer coatings on hydrophobic surfaces [21]. The more apolar PPO segments are thought to be in close contact with the surface, allowing the PEO segments to protrude into the aqueous phase, thereby reducing protein adsorption [22]. It has been reported [23] that collagen adsorption and epithelial cell adhesion were prevented on hydrophobic substrates in the presence of PEO-PPO-PEO. Recently, we have also shown that the adsorption of PEO-PPO-PEO on hydrophobized stainless steel and titanium prevents protein adsorption [24]. In the present work, we extend the use of PEO-modified surfaces to the prevention of bacterial adhesion on

metallic surfaces. It was reported [25] that PEO grafted on stainless steel surfaces prevents protein adsorption but is ineffective at reducing bacterial adhesion. Bacterial adhesion was examined in this work to investigate the anti-fouling ability of PEO-PPO-PEO adsorbed on hydrophobized stainless steel. It is expected that PEO-PPO-PEO-based coating can not only prevent biomacromolecule adsorption, but also reduce bacterial adhesion [26] and biofilm formation.

The aim of the present work is to investigate the efficiency of adsorbed PEO-PPO-PEO to reduce *Pseudomonas* 2021 adhesion on stainless steel. The obtained results are compared to the behavior of a model biomacromolecule (bovine serum albumin, BSA). Stainless steel was hydrophobized through self-assembly of octadecylphosphonic acid (OPA) [27] to ensure PEO-PPO-PEO adsorption. Adsorption and adhesion steps were performed using a modified parallel plate flow chamber. x-ray photoelectron spectroscopy (XPS) and water contact angle (WCA) measurements were used to characterize the obtained surfaces, with a view to better understand the anti-fouling properties of PEO-PPO-PEO on hydrophobized stainless steel. *Pseudomonas* 2021 adhesion was examined and bacteria were enumerated using fluorescence microscopy. In another approach, the effect of PEO-PPO-PEO brought in contact with already adhering bacteria was also studied, to check whether bacteria could be removed from the interface using a treatment that could be repeated with time.

3.2 Materials and methods

3.2.1 Preparation of stainless steel coupons

Stainless steel 304-2R plates (bulk composition in mass / mass: C(Cr) = 18.10%, C(Ni) = 9.10%, C(Mn) = 1.11%, C(Mo) = 0.24%, C(Si) = 0.36%, C(C) = 0.051%, C(P) = 0.024%, C(S) = 0.001%, balance Fe), in short SS, with a mirror-like surface (bright anneal obtained by annealing in a

N_2 + H_2 atmosphere followed by skin-passing) were received from Arcelor Mittal (Belgium). The coupons, 1 cm × 1 cm squares, 0.1 cm thickness, were cleaned 3 times with acetone in ultrasonic bath for 15 min, and then submitted to UV/ozone cleaning for 15 min just before use. Hydrophobized SS was prepared by self-assembly of octadecylphosphonic acid (OPA, Sigma 715166), which was dissolved in tetrahydrofuran (THF) at [OPA] = 0.01 M. The cleaned samples were immersed in OPA solution for 24 h. After removal from solution, the samples were thermally treated in an oven at 120°C for 1 h [28], then rinsed with THF 3 times and dried in room conditions. Hereafter, cleaned samples are named SS while the OPA-coated samples are named SS/OPA.

3.2.2 Water contact angle measurement

The wettability of SS and SS/OPA was investigated by measuring the water contact angle (WCA) using the sessile drop method. A water droplet of 1 µl was used for measurement at room temperature, and the contact angle was recorded 5 s after the water droplet was deposited on the sample. For each condition, the reported value is the average of three different samples with three drops each.

3.2.3 Bacterial strain, growth conditions and harvesting

A marine aerobic *Pseudomonas* sp. 2021 bacterium strain was obtained from the National Collection of Industrial and Marine Bacteria (NCIMB, U.K.). A new culture was reactivated from a freeze-dried ampoule, and sub-cultured twice in a marine broth 2216 medium, then mixed with 20% (volume/volume) glycerol and stored at -80 °C. The composition of marine broth 2216 medium is: C(peptone) = 5.0 g/L; C(yeast extract) = 1.0 g/L; C(ferric citrate) = 0.1 g/L; C(NaCl) = 19.45 g/L; C($MgSO_4$) = 5.9 g/L; C(Na_2SO_4) = 3.24 g/L; C($CaCl_2$) = 1.8 g/L; C(KCl) = 0.55 g/L; C($NaHCO_3$) = 0.16 g/L; C(KBr) = 0.08 g/L; C($SrCl_2$) = 0.034 g/L; C(H_3BO_3) = 0.022

g/L; C(Na_2SiO_4) = 0.004 g/L; C(NaF) = 0.0024 g/L; C(NH_4NO_3) = 0.0016 g/L and C(Na_2HPO_4) = 0.008 g/L. The final pH is 7.6 ± 0.2.

For each experiment, stored bacteria were inoculated on a marine agar 2216 plate at room temperature. A single bacterial colony was selected and cultured in 5 mL marine broth 2216 for 24 h (room temperature, agitation on a rotary shaker set at 120 rpm), and then sub-cultured in 200 mL Erlenmeyer flask (room temperature, agitation on a rotary shaker at 120 rpm). Bacteria were harvested at the middle of exponential phase of growth when the optical density (OD) measured at λ = 600 nm (OD_{600}) ~1 or at the stationary phase of growth when OD_{600} ~ 1.8 (3 days batch culture) by centrifugation for 5 min at 5000× g (Multifuge X1R centrifuge, Thermo Scientific). According to calibration performed using bacteria counting (Neubauer improved chamber, Marienfeld, Germany) vs. OD_{600} measurement, OD_{600} = 1 corresponds to about 2.5 × 10^8 cells/mL. The bacterial pellets were washed, resuspended in C(NaCl) = 35 g/L solution, and centrifuged again twice. Finally, bacteria were suspended in C(NaCl) = 35 g/L solution at a concentration of 1 × 10^8 cell/mL for all adhesion experiments, whatever the growth phase.

3.2.4 Modified parallel plate flow chamber system

All bacterial adhesion experiments were performed using a modified parallel plate flow chamber, as presented in Figure 1. The top and bottom plates are separated by silicone rubber spacer (0.2 cm thickness), and they are made of glass and polypropylene, respectively. The effective chamber dimensions are 7.6 cm × 1 cm × 0.2 cm in the absence of stainless steel coupons (0.1 cm thickness). The design of the parallel plate flow chamber allows a laminar flow to pass through the chamber (see Figure 1a), which produces a well-controlled shear stress on the substrates. The presented picture shows the passage of inked water into the flow chamber in the absence of stainless steel coupons. The shape of the interface between pure

water and inked water indicates the laminar character of the flow passing through the chamber. The same behavior of inked water was observed in the presence of stainless steel coupons in the chamber.

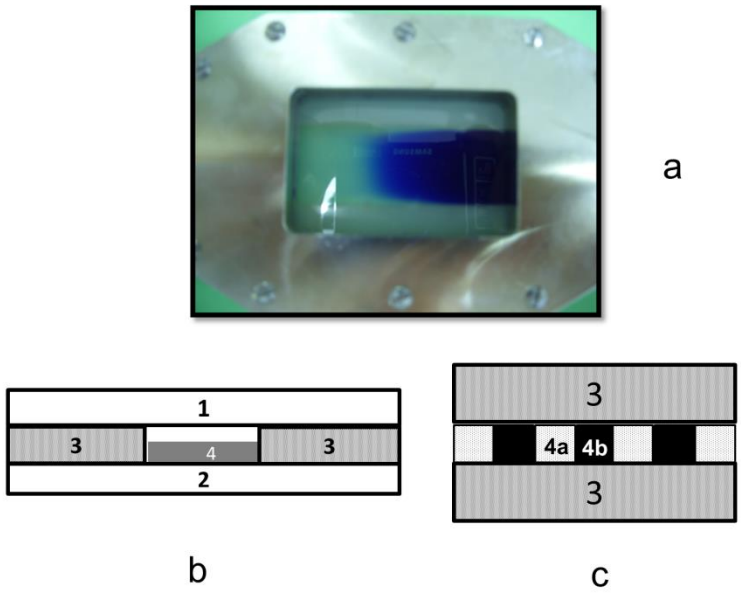

Figure 1. Picture and schemes of the flow chamber used for bacterial adhesion test: (a) general view of the device; (b) scheme of a vertical cross-section through the chamber; (c) scheme of a horizontal cross-section at mid-height; 1: top glass plate; 2: bottom polypropylene plate; 3: silicone rubber spacer; 4: coupons; 4a: SS and 4b: SS/OPA. In (a), ink was introduced in the chamber to show the laminar character of the flow.

Usually, the bottom plate itself is used as a substrate for bacterial adhesion tests in a parallel plate flow chamber [29]. In the present study, however, the flow chamber was mounted with stainless steel coupons placed on the bottom plate (Figure 1b and 1c). The advantage of this system is that seven coupons can be placed on the bottom plate in each experiment, and stainless steel coupons with two different surface treatments (SS and SS/OPA) were placed alternately (Figure 1c).

The effective chamber volume was 7 cm × 1 cm × 0.1 cm in the presence of seven stainless steel coupons during the experiment. The

bacterial adhesion test parameters (e.g. flow rate, shear stress, rinse force) applied on samples were controlled by using a peristaltic pump. Prior to bacterial adhesion, the flow chamber was used to condition the surface with PEO-PPO-PEO as well, and cell staining was also performed in situ after the rinsing process. In each experiment, at least three stainless steel coupons with the same surface treatment can be enumerated after bacterial adhesion, using fluorescent microscopy. A direct comparison between SS and SS/OPA coupons is possible because the coupons were processed under the same and controlled hydrodynamic conditions during the experiment.

3.2.5 Surface conditioning and bacterial adhesion experiments

Bacterial suspensions (exponential or stationary phase of growth) were prepared at the same concentration of 1×10^8 cell/mL in C(NaCl) = 35 g/L (as described above). A total volume of 400 mL of bacterial suspension was prepared for a given experiment. The flask from which the bacterial suspension was sent to the flow chamber was shaken on a rotary shaker at 80 rpm during adhesion process to avoid bacterial sedimentation. PEO-PPO-PEO triblock copolymer was purchased from Sigma (P1300) under the name of Pluronic® F68, in short Plu in the following text. The numbers of repeating units were 76 for each PEO block and 30 for PPO. Plu solution was prepared at C(Plu) = 2 g/L in C(NaCl) = 35 g/L solution, which is higher than its critical micellar concentration (CMC), or C(Plu) = 0.1 g/L in C(NaCl) = 35 g/L solution, which is lower than its CMC. The Plu solution was degassed before use to avoid the presence of air bubbles.

Constant flow (6.5 mL/min) was used for Plu adsorption, bacterial adhesion and rinsing steps, and all the experiments were performed at room temperature. A closed loop was used for Plu adsorption and bacterial adhesion while an open loop was used for rinsing. Stainless steel coupons were exposed to Plu solution for 50 min, and loosely bound polymer was removed from the flow chamber by 10 min rinsing (unless otherwise stated)

with C(NaCl) = 35 g/L solution. Then the flow was switched from C(NaCl) = 35 g/L solution to bacterial suspension. The bacterial suspension was circulated for 3 h, followed by rinsing for 30 min using C(NaCl) = 35 g/L solution. After rinsing, 4',6–diamidino–2–phenylindole (DAPI) solution (purchased from Merck; C(DAPI) = 0.1 mg/mL in filtered ultrapure water) was introduced into the chamber for staining and left for 20 min (i.e the flow was stopped after filling the chamber), and rinsing was performed for 20 min using sterile ultrapure water. To avoid bubbles passing through the chamber, the flow direction was reversed for 3 s at each change of the flowing liquid. After draining away ultrapure water from the chamber, stainless steel coupons were removed, placed in Petri dishes, and stored in a desiccator overnight for drying. Table 1 gives an overview of the experimental procedure used for adhesion tests.

Table 1. Steps used in a typical bacterial adhesion experiment carried in the flow chamber. Steps 1 and 2 were omitted to prepare control samples.

Step	**Solution or suspension used**	**duration**[a]
1. Plu adsorption	C(Plu) = 2 g/L dissolved in C(NaCl) = 35 g/L	50 min
2. rinsing	C(NaCl) = 35 g/L	10 min
3. bacterial adhesion	*Pseudomonas* 2021 at 1×10^8 cell/mL in C(NaCl) = 35 g/L	3 h
4. rinsing	C(NaCl) = 35 g/L	30 min
5. staining	C(DAPI) = 0.1 g/L in ultrapure water	20 min
6. rinsing	ultrapure water	20 min

a: All steps were performed under flow at 6.5 mL/min, except for step 5 which was performed in static conditions

A control bacterial adhesion experiment was carried out without adsorption of Plu on SS and SS/OPA coupons. The experiment was directly started by flowing the bacterial suspension, and the rest of the protocol was the same as described above.

Table 2. Steps used in a bacterial adhesion experiment, followed by rinsing with Plu-containing solution.

Step	Solution or suspension used	duration[a]
1. bacterial adhesion	*Pseudomonas* 2021 at 1×10^8 cell/mL in C(NaCl) = 35 g/L	3 h
2. rinsing	C(Plu) = 2 g/L dissolved in C(NaCl) = 35 g/L	30 min
3. staining	C(DAPI) = 0.1 g/L in ultrapure water	20 min
4. rinsing	ultrapure water	20 min

a: All steps were performed under a flow at 6.5 mL/min, except for step 3 which was performed in static conditions

In another experimental approach, bacterial adhesion step was followed by rinsing using Plu solution, as described in Table 2. All the rest of the protocol was the same as in the control experiment, as described in Table 1, which made the results comparable.

3.2.6 Fluorescence microscopy (FM)

Stainless steel coupons with adhering bacteria stained with DAPI were analyzed using fluorescence microscopy (Leica DMRA2, excitation wavelength 372 nm and emission wavelength 456 nm). A 40× objective was used in air. Bacterial counting was facilitated by mounting a grid on the eyepiece of the microscope. The amount of adhering bacteria was counted on 10 different areas (0.25 mm × 0.25 mm) on each coupon. The calculated density of adhering bacteria was based on at least three samples for each experiment and each surface treatment.

3.2.7 Plu and BSA adsorption using flow chamber

To better understand the results obtained from bacterial adhesion tests, the adsorption of Plu and of bovine serum albumin (BSA, Sigma A4919), a typical protein, were investigated further. After adsorption of Plu (C(Plu) = 2 g/L or 0.1 g/L) for 50 min in the flow chamber, SS and SS/OPA coupons were rinsed using sterile ultrapure water for 10, 40 or 80 min, and water was then drained off from the chamber. In another experiment, BSA adsorption (C(BSA) = 0.02 g/L, C(NaCl) = 35 g/L) was carried for 30 min after Plu (C(Plu) = 2 g/L) adsorption to check the ability of Plu to prevent

protein adsorption. Rinsing was then performed with ultrapure water for 20 min. After Plu or BSA adsorption, all stainless steel coupons were removed, placed in Petri dishes, and stored in a desiccator overnight for drying. SS and SS/OPA with and without adsorption of Plu and/or BSA in flow chamber were subjected to surface chemical analysis, using x-ray photoelectron spectroscopy (XPS). Hereafter, +Plu and +Plu+BSA designate samples after Plu adsorption and after Plu adsorption followed by BSA adsorption, respectively.

3.2.8 X-ray photoelectron spectroscopy (XPS) measurements

XPS measurements were carried out with a Kratos Axis Ultra spectrometer (Kratos Analytical, UK), using monochromated Al Kα radiation (powered at 10 mA and 15 kV) and an eight-channeltrons detector. The analyzed area was 700 μm × 300 μm. The vacuum in the analysis chamber was about 10^{-6} Pa. The direction of photoelectron collection was perpendicular to the sample surface. Charge stabilization was achieved by using the Kratos Axis device. Survey spectra were recorded with 160 eV pass energy and 40 eV pass energy was used for narrow scans. In the latter conditions, the full width at half maximum (FWHM) of the Ag $3d_{5/2}$ peak of a standard silver sample was about 0.9 eV. The C-(C, H) component of the C 1s peak of carbon has been fixed to 284.8 eV to set the binding energy scale. The following sequence of spectra was recorded: survey spectrum, C 1s, O 1s, N 1s, Si 2p, P 2p, Cl 2p, S 2p, Ca 2p, Na 1s, Cr 2p, Mn 2p, Fe 2p, Zn 2p and C 1s again to check for charge stability and absence of degradation as a function of time. Mole fractions x were calculated after a linear background subtraction using peak areas normalized on the basis of acquisition parameters, experimental sensitivity factors and transmission factors provided by the manufacturer. Elemental mole fractions are provided, excluding hydrogen which is not detected by XPS. The C 1s and O 1s peaks were decomposed with the CasaXPS program (Casa Software Ltd., U.K.)

using a Gaussian/Lorentzian (70/30) product function. Details regarding FWHM will be given with the results.

3.3 Results

3.3.1 Characterization of SS and SS/OPA conditioned or not with Plu

The WCA values of SS and SS/OPA were 26.5° ± 0.7° and 108° ± 0.7°, respectively. The increase of WCA is attributed to the terminal methyl group of alkyl chains pointing outward from the surface after OPA coating. Adsorption of Plu on SS and SS/OPA surfaces was performed using the flow chamber. Table 3 summarizes the surface chemical composition determined by XPS and Figure 2 (a, b, d, e) presents XPS C 1s peaks for the different stainless steel surfaces: SS and SS/OPA, before and after Plu adsorption. The C 1s peak was decomposed in 4 components as illustrated in Figure 2c, with the constraint of the same FWHM. Table 3 gives the concentration of carbon only bound to carbon and hydrogen, $x(C_{284.8})$, responsible for the component at 284.8 eV, and the sum of all the forms of oxidized carbon C_{ox} (C-O, C-N, N-C=O, O-C=O), i.e $x(C_{tot}) - x(C_{284.8})$. The O 1s peaks were decomposed in three components, as described elsewhere [30]. One, near 530.0 eV, attributed to inorganic oxygen in metal oxides, was fitted according to the low binding energy edge of the peak, without imposing constraint on the FWHM. The FWHM of the other two components were imposed to be equal. The component near 531.4 eV may be due both to metal hydroxide, to phosphonate and to oxygen making a double bond with carbon, as in amide (N-C=O). The component near 533.0 eV is attributed to oxygen making single bonds with carbon (O-C), as in alcohol and ether. The presence of Si is attributed to contaminants, either silica dust or adsorbed silane. Traces of different elements (Zn, Na, Ca, Cl, S, Pb) may be due to different sources (substrate, contaminants, solutions) and will not be considered here.

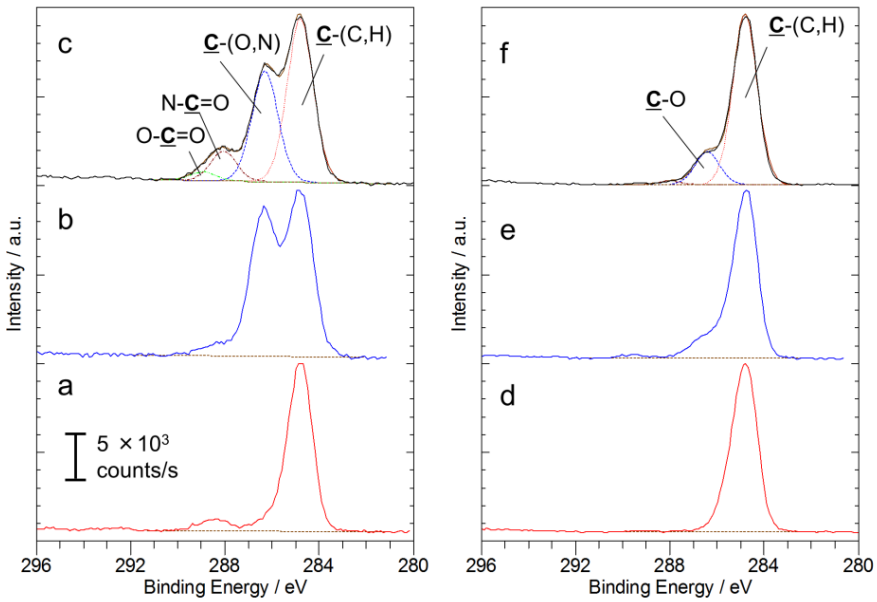

Figure 2. XPS C 1s peaks of SS (a, b, c) and SS/OPA (d, e, f) as such (a, d) or +Plu (b, e) or +Plu+BSA (c, f). The intensity scale of spectra b to f does not differ much (factor less than 2) from that shown for spectrum a. Quantitative data cannot be extracted directly from the Figure and are reported in Table 3.

Elements typical of stainless steel (Fe, Cr, Mn and O) were found as expected. A high level of organic contamination was observed on SS surface, attributed to material processing, or to adsorption from air and from the spectrometer chambers [30, 31]. The C 1s peak recorded on SS (Figure 2a) had a main component at 284.8 eV and smaller contributions at higher binding energies, attributed to more oxidized carbon (C_{ox}). Low concentrations of nitrogen, phosphorus, silicon and sulfur were detected as well. After OPA assembly, an increase in carbon and phosphorus concentration was observed as expected from OPA composition. The C 1s peak (Figure 2d) consisted in a single component at 284.8 eV, in agreement with the presence of the long hydrocarbon chain of OPA. The ratio of C/P was close to 18, which is the value expected for C/P in OPA. Moreover, the concentration of elements from the substrate (Fe, Cr, Mn and $O_{530.0}$) was significantly attenuated after OPA coating.

Table 3. Elemental surface composition (mole fraction x over all elements except hydrogen) determined by XPS on stainless steel after different surface treatments. Reported values are based on three different samples for each condition, standard deviations are given between brackets. bdl = below detection limit.

Sample	x(Fe) ×100	x(Mn) ×100	x(Cr) ×100	O				x(N) ×100	C			x(P) ×100	x(Si) ×100	x(Zn+Na+Ca+Cl+S+Pb) ×100
				$x(O_{tot})$ ×100	x(O-C) ×100	$x(O_{531.4})$ ×100	$x(O_{530.0})$ ×100		$x(C_{tot})$ ×100	$x(C_{ox})$ ×100	$x(C_{284.8})$ ×100			
SS	9.75 [0.75]	1.07 [0.13]	2.30 [0.21]	43.55 [1.82]	2.79 [0.27]	19.53 [1.11]	21.22 [2.38]	0.52 [0.2]	36.74 [2.18]	6.06 [0.07]	30.68 [2.23]	0.60 [0.04]	2.35 [1.25]	3.23 [1.79]
SS+Plu	6.66 [1.01]	0.32 [0.1]	1.44 [0.2]	38.65 [2.05]	**13.73** [2.08]	9.34 [2.18]	15.58 [1.79]	0.40 [0.09]	47.95 [3.92]	**28.24** [5.67]	19.70 [2.95]	0.95 [0.2]	1.40 [0.59]	2.28 [1.18]
SS+Plu+BSA	2.73 [0.51]	0.19 [0.07]	0.85 [0.15]	27.95 [1.35]	10.10 [0.83]	10.50 [0.72]	7.35 [1.21]	**5.16** [0.15]	53.84 [2.00]	25.47 [1.39]	28.37 [0.73]	0.57 [0.08]	3.26 [0.39]	5.46 [0.96]
SS/OPA	5.58 [0.47]	0.40 [0.16]	1.56 [0.21]	26.58 [3.85]	1.84 [0.78]	15.00 [3.74]	9.74 [1.07]	bdl [bdl]	59.96 [4.97]	2.03 [1.76]	57.92 [5.83]	3.10 [0.26]	1.23 [0.4]	1.58 [1.79]
SS/OPA+Plu	6.11 [0.73]	0.48 [0.10]	1.43 [0.13]	29.09 [1.64]	**3.46** [1.28]	14.25 [0.45]	11.38 [2.48]	0.07 [0.12]	57.16 [2.12]	**6.69** [3.2]	50.47 [1.33]	2.60 [0.14]	1.45 [0.81]	1.62 [1.31]
SS/OPA+Plu+BSA	5.00 [0.25]	0.19 [0.03]	1.56 [0.27]	25.32 [0.72]	5.05 [1.32]	10.98 [1.49]	9.29 [0.54]	**0.49** [0.10]	61.66 [0.94]	9.65 [2.23]	52.01 [1.44]	2.64 [0.20]	2.01 [0.28]	1.15 [0.15]

On both SS+Plu and SS/OPA+Plu surfaces, the component attributed to carbon involved in a single bond with oxygen (C-O at 286.3 eV) is a marker for the presence of Plu (Figure 2b, 2e). After 10 min of rinsing, a low concentration of this C-O component was detected on SS/OPA after Plu adsorption, while a high concentration was observed after adsorption of the same compound on SS. The efficiency of rinsing after Plu adsorption was further examined by increasing the duration of the rinsing step (40 min and 80 min). Similar results (not shown) were obtained, showing that the adsorbed layer did not change after 10 min of rinsing in the flow conditions used. These observations were confirmed by analyzing the O 1s component near 533.0 eV (O-C) which may also be considered as a marker for Plu.

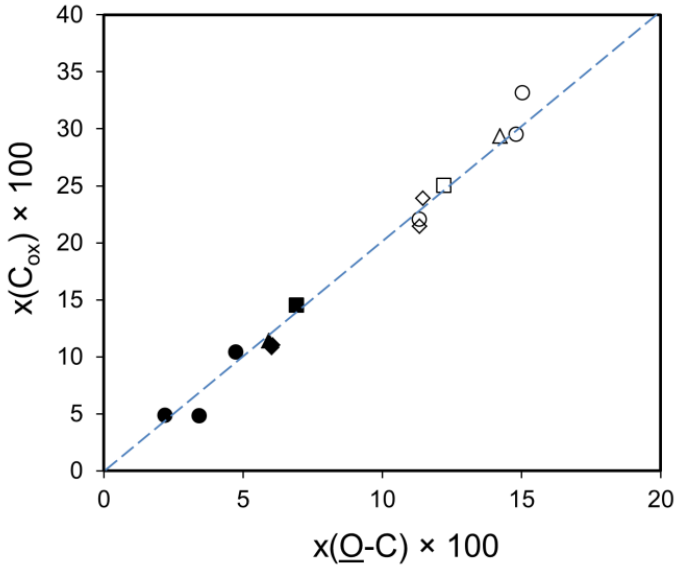

Figure 3. Relationship between the mole fractions of C_{ox} [oxidized carbon] and O-C, for samples submitted to Plu adsorption at different concentrations, and rinsed for different times. SS: Plu adsorption at 2 g/L, rinsed for 10 min (○), 40 min (□) and 80 min (△); Plu adsorption at 0.1 g/L, rinsed for 10 min (◇). SS/OPA: Plu adsorption at 2 g/L, rinsed for 10 min (●), 40 min (■) and 80 min (▲); Plu adsorption at 0.1 g/L, rinsed for 10 min (◆). The dashed line represents a y:x ratio of 2.

Correlations between spectral data were examined in order to establish more firmly the reliability of spectral markers for specific compounds. Figure 3 shows the relationship between the x(O-C) and x(C_{ox}) concentrations determined by XPS, for SS and SS/OPA samples conditioned with Plu. Results obtained with different rinsing times and C(Plu) = 0.1 g/L were added to the set of results presented in Table 3. x(C_{ox}) should in this case mainly be due to carbon singly bound to oxygen x(C-O). The slope is close to the ratio x(C-O)/x(O-C) of 2 expected for Plu, in which oxygen is in the form of ether group C-O-C. It is also evidenced that the detected amount of Plu is higher on SS compared to SS/OPA. Prolongation of rinsing and use of a lower concentration (C(Plu) = 0.1 g/L) did not change much the amount of Plu on both SS and SS/OPA samples. Based on these results, Plu solution at C(Plu) = 2 g/L and a rinsing step of 10 min were used hereafter for the study of BSA adsorption and bacterial adhesion.

3.3.2 BSA adsorption on stainless steel conditioned with Plu

BSA adsorption was performed *in situ* after Plu adsorption on SS and SS/OPA, using the flow chamber. Table 3 reports the corresponding XPS data and Figure 2 (c, f) presents the XPS C 1s peaks of SS and SS/OPA after Plu and BSA adsorption. Nitrogen is a marker for adsorbed BSA. It is equal to x(N) ≈ 5.2% on SS and x(N) ≈ 0.5% on SS/OPA after Plu and BSA adsorption, showing that protein adsorption is significantly reduced when Plu is adsorbed on SS/OPA. This is confirmed by the shape of the C 1s peaks (Figure 2c, 2f): after BSA adsorption, the component attributed to the peptidic link of proteins (N-C=O at 288 eV) is indeed much higher on SS+Plu+BSA compared to SS/OPA+Plu+BSA.

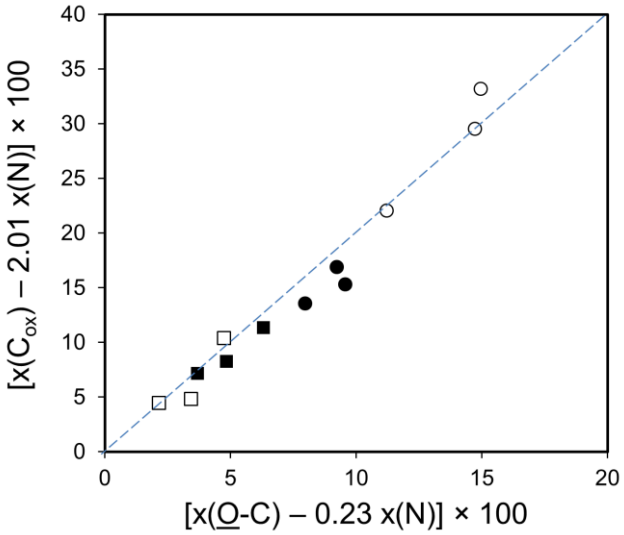

Figure 4. Relationship between the mole fraction [x(C_{ox}) – 2.01 x(N)] (oxidized carbon, excluding the one from BSA) and [x(O-C) – 0.23 x(N)] (O-C, excluding the one from BSA), for Plu-conditioned samples before and after BSA adsorption. SS+Plu (○); SS+Plu+BSA (●); SS/OPA+Plu (□); SS/OPA+Plu+BSA (■). The dashed line represents a y:x ratio of 2.

To go one step further in the quantification of the adlayer composition, [x(C_{ox}) – 2.01 x(N)] is plotted against [x(O-C) – 0.23 x(N)] in Figure 4, for SS and SS/OPA conditioned with Plu, before or after BSA adsorption. [x(O-C) – 0.23 x(N)] is attributed to oxygen making single bonds with carbon (O-C), excluding the one coming from BSA, while [x(C_{ox}) – 2.01 x(N)] is attributed to oxidized carbon, excluding the one coming from BSA. The coefficients used to subtract BSA contribution were calculated from the amino acid composition of BSA [32], as detailed by Toure *et al.* [to be published]. Briefly, for each amino acid, functional groups were listed, and the respective contribution of these groups to the albumin spectra was calculated on the basis of the frequency of presence of the different amino acids. Therefore, the relationship between [x(C_{ox}) – 2.01 x(N)] and [x(O-C) – 0.23 x(N)] should only be related to Plu or to contaminants. Again, a slope of ~2 is found, in agreement with the stoichiometry of Plu. In Figure 4, high values for x(C_{ox}) – 2.01 x(N) and x(O-C) – 0.23 x(N) may then be linked to a

higher Plu detected amount. The distribution of data points in Figure 4 (○ vs ●) shows that, in case of SS, the apparent concentration of Plu was reduced after BSA adsorption, which confirms that Plu did not prevent BSA adsorption when pre-adsorbed on SS, as already shown by the shape of the C 1s peak (Figure 2c) and by the observed nitrogen concentration (Table 3). Part of Plu molecules might be replaced by adsorbed BSA, or BSA might be adsorbed on top of Plu, thereby screening the signal of Plu molecules in XPS analysis. On SS/OPA (Figure 4, □ vs ■), the concentration of Plu, which was lower than on SS, was in the same range before and after BSA adsorption.

3.3.3 Pseudomonas 2021 adhesion on stainless steel with different surface treatments

SS and SS/OPA coupons were placed in alternating position in the flow chamber, and the adhesion test was thus carried out in exactly the same conditions for SS and SS/OPA samples. Therefore, the influence of hydrophobization of SS on bacterial adhesion could be directly examined. The tests were performed after Plu adsorption or not. Representative images of *Pseudomonas* 2021 cells (harvested in the exponential phase) adhering on SS and SS/OPA are presented in Figure 5. Table 4 gives the density of adhering *Pseudomonas* 2021 cells on coupons characterized by different surface treatments after a 3 h adhesion test in flow conditions. As illustrated by Figure 5, the amount of adhering bacteria was higher on SS, SS/OPA and SS+Plu than on SS/OPA+Plu. The amounts of adhering bacteria (exponential phase) on SS and SS/OPA were $(17.0 \pm 5.6) \times 10^4$ and $(13.0 \pm 3.5) \times 10^4$ cell/cm^2, respectively (Table 4); the difference was not significant considering the values of standard deviations (SD). It may be concluded that the surface hydrophobicity did not influence significantly *Pseudomonas* 2021 adhesion. When adsorption of Plu was performed before the adhesion step (Figure 5b, d), only a few cells were observed on SS/OPA+Plu [(1.8 ±

0.9) × 10^4 cell/cm^2] while there were still many cells on SS+Plu [(23.0 ± 7.6) × 10^4 cell/cm^2]. These results show that the adsorption of Plu on SS/OPA significantly reduced subsequent bacterial adhesion. In contrast, adsorption of Plu on SS did not reduce *Pseudomonas* 2021 adhesion. Compared to the bacteria harvested in exponential phase, less adhering bacteria were found on SS and SS/OPA (Table 4) when harvested in stationary phase, but the results again show that adsorption of Plu on SS/OPA significantly reduced bacterial adhesion.

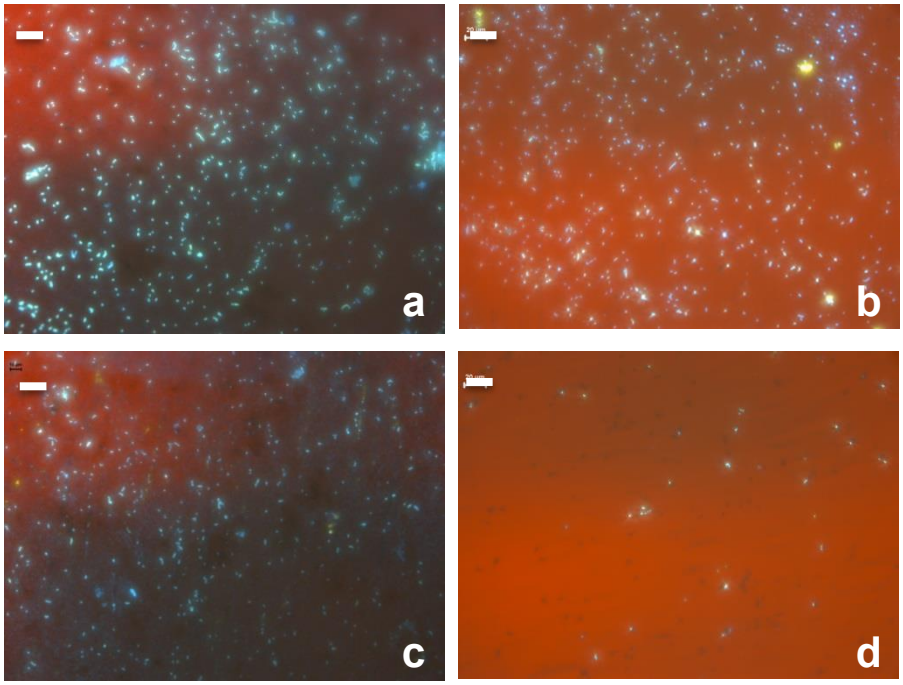

Figure 5. Representative fluorescence images of *Pseudomonas* 2021 (exponential phase) cells stained with DAPI, after adhesion for 3 h in flow condition on: (a) SS; (b) SS+Plu; (c) SS/OPA; (d) SS/OPA+Plu. Scale bar is 20 µm.

Table 4. Density of adhering *Pseudomonas* 2021 cells on stainless steel after different surface treatments. The bacteria were harvested during exponential or stationary phase. The mean and standard deviation (SD) are based on at least three samples per condition.

Substrate	SS	SS+Plu	SS/OPA	SS/OPA+Plu
	density of cell / 10^4 cell/cm^2			
exponential phase	17.0 ± 5.6	23.0 ± 7.6	13.0 ± 3.5	1.8 ± 0.9
stationary phase	8.9 ± 3.1	15.0 ± 2.7	6.5 ± 2.1	1.8 ± 0.6

3.3.4 Rinsing with Plu solution after Pseudomonas 2021 adhesion

In contrast with previous experiments, Plu solution was here used for rinsing after 3 h of *Pseudomonas* 2021 adhesion in flow condition. This experimental approach was only tested for bacteria harvested in exponential phase. The results are shown in Figure 6 and Table 5. It appears that the amount of adhering bacteria is lower on SS/OPA ((6.4 ± 1.8) ×10^4 cell/cm^2) compared to SS ((16.0 ± 4.5) ×10^4 cell/cm^2). When these results are compared to the previous experiment using NaCl for rinsing step (Table 4), it can be deduced that rinsing with Plu does not provoke bacterial detachment on SS, while about 50% of bacteria are detached on SS/OPA.

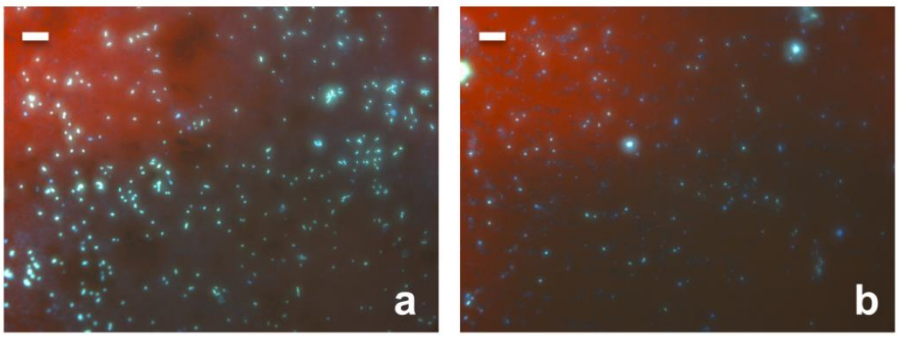

Figure 6. Representative fluorescence images of *Pseudomonas* 2021 (exponential phase) cells stained with DAPI, after adhesion for 3 h followed by rinsing with Plu solution in flow condition on: (a) SS; (b) SS/OPA. Scale bar is 20 µm.

Table 5. Density of adhering *Pseudomonas* 2021 cells on SS and SS/OPA after rinsing with Plu solution. The bacteria were harvested during exponential phase. The mean and standard deviation (SD) are based on at least three samples per condition.

Substrate	SS	SS/OPA
	density of cell / 10^4 cell/cm^2	
exponential phase	16.0 ± 4.5	6.4 ± 1.8

3.4 Discussion

3.4.1 Advantages of flow chamber

There is no standardized method to study bacterial adhesion. The methodologies reported in the literature vary between laboratories: they are mainly dependent on the purpose of the experiment and on constraints brought by studied materials (e.g. size and nature). A rinsing step is required at the end of most experimental procedures used to study bacterial adhesion. Rinsing is a critical step which may certainly influence the reproducibility of the results and it is poorly controlled when improper methods are used [33]. Rinsing is necessary to remove unattached or loosely adhering bacteria which are simply lying on the surface after their sedimentation. "Slight rinse under flow" and "dipping in suspension fluid to remove loosely adhering bacteria" are improper methods because the removal force involved in these methods is not controlled, and may vary from one experiment to another.

The parallel plate flow chamber system was developed and used for bacterial adhesion with the major advantage of controlled shear and mass transport. A detailed report, highlighting advantages of this system, was written by Busscher and Van der Mei [34]. The disadvantage of the system is that only one field of view per experiment can be examined when *in situ* observations are made, which requires a lot of work and time to repeat the experiments.

The system used in this work is based on a parallel plate flow chamber, with minor modifications, e.g. small coupons are placed inside the chamber rather than using the bottom plate as a substrate. Moreover, coupons were stained *in situ* for *ex situ* enumeration, instead of direct *in situ* observation. The major advantage of this procedure is that several coupons with different surface treatments can be placed alternately inside the chamber in one experiment. Coupons do not move during the experiment under flow condition, and they are under the same hydrodynamic conditions (shear force) for adhesion and rinsing. Coupons are not exposed to air-liquid interface during experiment until the last step when all the liquid is drained off from the chamber. However, all the coupons are assumed to go through the same air-liquid interface at the last step. In this way, the influence of different surface treatments on bacterial adhesion can be directly compared.

3.4.2 Composition of the organic adlayer

A description of the organic adlayer present on stainless steel can go beyond a qualitative discussion of the concentrations of elements and moieties associated to peak components. Therefore, certain XPS data are taken as markers for organic compounds. For BSA, the suitable marker is N, with 1 marker unit for the formula $C_{3.76}O_{1.15}N_1S_{0.05}H_{5.92}$ (formula mass 85.19 g) deduced from the amino-acid composition of BSA [32], as detailed by Toure *et al.* [to be published]. Figure 4 shows that, when Plu is involved in surface conditioning, its concentration may be estimated from $x(C_{ox})$ after deduction of the contribution of BSA. Accordingly, a concentration marker for Plu is $[x(C_{ox}) - 2.01\ x(N)]$. If the structural formula of Plu is considered to be $HO\text{-}[CH_2\text{-}CH_2\text{-}O]_{0.5}\text{-}[CH(CH_3)\text{-}CH_2\text{-}O]_{0.197}\text{-}[CH_2\text{-}CH_2\text{-}O]_{0.5}\text{-}H$, in accordance with the PEO/PPO proportions, there are 2.394 marker units per structural formula (formula mass 55.43 g). OPA is considered as an octadecyl chain (formula mass 253 g), thereby neglecting the phosphonate head expected to be closely linked to the surface. If the $C_{284.8}$ component is

only due to contribution of octadecyl chains (hydrocarbon, HC), Plu and BSA, a concentration marker for HC may be [x($C_{284.8}$) – 0.082 (x(C_{ox}) – 2.01 x(N)) – 1.75 x(N)], with 18 marker units per formula. The factor 0.082 comes from 0.197/2.394 computed for Plu, and 1.75 is the molar ratio x($C_{284.8}$) / x(N) computed from BSA amino-acid composition.

Assuming that the organic adlayer has a random organization, one may compute relative amounts of HC, Plu and BSA from the marker concentration x_i, the number k_i of markers units per formula and the mass M_i of formula, either in number of formula units $U_i = X_i / k_i$ or in mass units $W_i = U_i \times M_i$. This provides the mass % of each constituent in the adlayer, given in Table 6 as average with standard deviation. The set of samples obtained with the substrates conditioned with C(Plu) = 0.1 g/L and rinsing times of 40 and 80 min (details not shown) is in agreement with the set of samples obtained with C(Plu) = 2 g/L and rinsing time of 10 min. This way of modeling the composition of the organic adlayer in terms of mass % of BSA, Plu and HC is purely formal for certain results marked by a star in Table 6, in which case, the constituent was not involved in the sample preparation. The concentration indicated has no physical meaning and is just a way to express the relative amount of organic contaminants. Alternative approaches considering the expected nature of contaminants (not shown) did not bring any additional information.

Another possible marker for HC, independent from the first one, is the phosphorous concentration x(P), with 1 marker unit per formula of HC. Table 6 provides a comparison with the results obtained with a marker based on x($C_{284.8}$). The differences for samples not treated with OPA are due to the presence of traces of phosphorous in the substrate.

In the case of samples conditioned with OPA (Table 6), an excellent agreement was found between the results obtained with the two markers selected for HC. The concentration of HC was above 90 % for SS/OPA, which supports the data treatment performed. Conditioning with Plu brought

Table 6. Surface concentration determined by XPS on stainless steel samples treated in different ways: SS or SS/OPA and the same submitted to Plu adsorption (SS+Plu or SS/OPA+Plu), and to subsequent BSA adsorption (SS+Plu+BSA or SS/OPA+Plu+BSA). Mass % of compounds (BSA, Plu, HC) in the organic adlayer and mole % of elements ($x(O_{org})$, $\sum x(M_{sub}) = x(Fe) + x(Cr) + x(Mn)$, $\sum x(ad) = x(C) + x(N) + x(O_{org})$).

Sample	Compound concentration						Element concentration		
	HC marker from $C_{284.8}$			HC marker from P			$x(O_{org})$ ×100	$\sum x(M_{sub})$ ×100	$\sum x(ad_i)$ ×100
	C(BSA) / %	C(Plu) / %	C(HC) / %	C(BSA) / %	C(Plu) / %	C(HC) / %			
SS	*5.0**	*22.0**	*73.0**	*9.6**	*40.8**	*49.6**	3.1	13.1	**40.2**
	[4.7]	*[4.3]*	*[0.4]*	*[9.2]*	*[5.8]*	*[3.4]*	[0.0]	[0.7]	[2.5]
SS+Plu	*3.9**	**69.7**	*26.4**	*3.9**	**69.2**	*26.9**	14.2	8.4	**62.5**
	[1.3]	[8.6]	*[7.4]*	*[1.3]*	[8.8]	*[7.6]*	[2.8]	[1.3]	[6.4]
SS+Plu+BSA	**42.2**	33.4	*24.4**	**47.1**	37.4	*15.5**	13.5	3.8	**72.5**
	[2.6]	[2.5]	*[0.7]*	[1.8]	[3.8]	*[2.4]*	[0.7]	[0.7]	[2.5]
SS/OPA	*0.0**	*5.6**	94.4	*0.0**	*5.6**	94.4	1.0	7.5	**61.0**
	[0.0]	*[4.9]*	[4.9]	*[0.0]*	*[4.9]*	[4.9]	[0.9]	[0.7]	[4.7]
SS/OPA+Plu	*0.7**	**17.4**	81.9	*0.7**	**18.2**	81.1	3.4	8.0	**60.6**
	[1.2]	[7.6]	[7.0]	*[1.2]*	[7.4]	[6.7]	[1.6]	[0.9]	[3.6]
SS/OPA+Plu+BSA	**4.4**	21.0	74.6	**4.6**	22.1	73.3	4.9	6.8	**67.0**
	[0.9]	[4.6]	[4.7]	[1.0]	[5.5]	[5.7]	[1.1]	[0.4]	[2.1]

* formal result from composition modeling, actually due to organic contaminants

a: $C(i) = 100 \times m(i) / (m(BSA) + m(Plu) + m(HC))$

b: $x(i) = n(i) / \sum n$ (all elements)

a Plu concentration which did not exceed about 20%. Further conditioning with BSA had no significant influence on the composition of the adlayer. For SS+Plu, the Plu concentration is about 70%. As a result of further conditioning with BSA, the BSA concentration reached about 45%, while Plu decreased to about 35%.

A description of the organic adlayer present on stainless steel should ideally involve the vertical and lateral distribution of its constituents. This is however not reliable owing to the multiplicity of compounds and the lack of discrimination between different models used for data simulation. Nevertheless, rough information was gathered by computing the relative amounts, in mole fractions, of the metal elements typical of the substrate $\Sigma x(M_{sub}) = x(Fe) + x(Cr) + x(Mn)$, and of the elements belonging to the organic adlayer $\Sigma x(ad_i) = x(C) + x(N) + x(O_{org})$. According to the above explanations, the concentration of the organic form of oxygen (O_{org}) was computed as the sum of the contributions due to BSA and to Plu for all samples:

$$x(O_{org}) = 1.15\ x(N) + (x(C_{ox}) - 2.01\ x(N))\ 0.5 = 0.5\ x(C_{ox}) + 0.15\ x(N) \quad (1)$$

where 1.15 is the O/N molar ratio of BSA, and 0.5 is the O/C_{ox} molar ratio of Plu. Note that O_{org} could not directly be computed from the O 1s peak decomposition, because contributions due to organic matter and metallic hydroxide overlap in the component near 531.4 eV. Table 6 presents the concentration of O_{org}, ΣM_{sub} and Σad, in mole % of the elements detected by XPS, i.e all elements except hydrogen. The difference with respect to 100% represents the elements which were neglected because of their unclear or complex assignment (Zn, P, Si, Na, Ca, Cl, S, Pb and inorganic O).

3.4.3 Influence of surface hydrophobicity on Plu and BSA adsorption

Table 6 ($\sum ad_i$) shows that the organic adlayer represents an apparent amount of organic compounds which is about the same for all samples treated with OPA, Plu or BSA, and is about 1.5 higher than for SS. Thus conditioning SS with Plu or self-assembling OPA on its surface increased only slightly the importance of the organic adlayer, compared to that of contaminants present on SS as analyzed. However, the nature of the compounds was quite different. SS/OPA showed a high surface concentration of hydrocarbon chains, which may safely be attributed to OPA. Conditioning SS/OPA (WCA = 108°) with Plu had a noticeable effect on the adlayer composition, with a decrease of the apparent OPA concentration (C(HC) decreased). Subsequent conditioning with BSA did not lead to any significant BSA adsorption, which is in agreement with literature data [35]. It is indeed commonly considered that PEO-PPO-PEO triblock copolymer can anchor on hydrophobic surfaces through its PPO segment, while polar PEO chains are protruding into the aqueous solution, forming a brush structure [36]. These hydrated chains may act as a steric barrier and prevent protein adsorption. It was shown that PEO-PPO-PEO adsorbed on a CH_3-modified gold surface prevented adsorption of single protein solutions and of proteins from mixed human plasma solutions [35]. It was also reported that adsorbed PEO-PPO-PEO prevents collagen adsorption on polystyrene, which further reduced mammalian cell adhesion [23].

Table 6 shows that conditioning SS (WCA = 26.5°) with Plu was effective and reduced significantly the amount of hydrocarbons attributed to contaminants. Subsequent conditioning with BSA led to a marked adsorption with a large displacement of Plu. Our results thus show that Plu conditioning prevents BSA adsorption on SS/OPA+Plu and does not on SS+Plu. This is in agreement with previous observations. It was reported that adsorption in competition between Plu and proteins promoting mammalian cell adhesion

was in favor of Plu on hydrophobic surfaces but not on hydrophilic surfaces [23, 37]. Human serum albumin in competition with adhesive proteins showed a behavior analogous to Plu, but was a weaker competitor [37].

It is striking that the apparent amount of Plu present on SS+Plu was higher than on SS/OPA+Plu and remained higher after BSA conditioning, despite the fact that BSA adsorption was higher in SS+Plu+BSA than in SS/OPA+Plu+BSA. It is suggested that the conformation of adsorbed Plu molecules was different on SS (WCA = 26.5°) compared to SS/OPA (WCA = 108°). The Plu adsorption mechanism on SS/OPA is thought to be based on the hydrophobic interaction between PPO blocks and alkyl groups of OPA coating. On the contrary, when Plu enters in contact with hydrophilic surfaces, the PEO chains have a higher affinity toward this surface compared to PPO segments, and pancake structures are obtained [38]. Accordingly it may be concluded that Plu adsorption did not prevent subsequent BSA adsorption on SS+Plu in reason of the adlayer structure. It might even incorporate BSA. It was indeed reported that proteins may penetrate a thick PEO brush grafted with a low density on polystyrene, and adsorb in greater amount than on non-grafted polystyrene [39]. Until now, much less work was focused on the adsorption of Plu on hydrophilic surface compared to hydrophobic ones, because Plu is mainly used to prevent irreversible non-specific protein adsorption, which is observed on hydrophobic substrates [22, 23, 36, 38, 40].

3.4.4 Influence of conditioning layer on adhesion of Pseudomonas 2021

It is known that initial single bacteria adhesion is a complicated process, which is the first step of biofilm formation. It is generally understood that the adhesion of bacteria strongly depends on bacterial properties (strain, physiological conditions), environmental factors (presence of biomolecules, ions, pH, oxygen level and flow velocity) and surface

characteristics of materials (chemical composition and roughness) [13, 41]. It was reported that OPA coating effectively reduced adhesion of mixed population microorganisms of cooling water as well as of *Desulfovibrio* on iron and copper [27], but, in our case, the adhesion of *Pseudomonas* was not reduced by the same coating. This might be due to the different bacterial strain and experimental conditions used in these studies. The comparison between SS and SS/OPA (Table 4) shows that the surface hydrophobicity does not influence significantly the amount of adhering *Pseudomonas* 2021 bacteria.

The present work also considered the influence of hydrated conditioning layers on *Pseudomonas* 2021 adhesion. It is shown that the presence of Plu significantly reduced *Pseudomonas* 2021 adhesion on SS/OPA+Plu. PEO-based coatings are among the popular treatments used to reduce biomacromolecule adsorption. This may in turn reduce bacterial adhesion since the adsorbed biomacromolecules may provide specific recognition sites. Thereby, adsorbed proteins may promote or inhibit specific bacterial adhesion [41]. For example, the presence of fibronectin (Fn) increased *Staphylococcus aureus* adhesion on substratum surface, and adsorbed albumin inhibited *S. aureus* adhesion on polyurethane. The mechanism of reduction of bacterial adhesion on SS/OPA+Plu may also be explained by non-specific interactions. The bacteria approaching the substrate surface may be seen as a colloidal particle, and is repelled by the hydrated PEO layer acting as a steric barrier, similarly to the principle of action reported for the prevention of protein adsorption.

Table 4 demonstrates that SS+Plu did not reduce *Pseudomonas* 2021 adhesion, while the XPS results indicate the presence of adsorbed Plu (Table 6). In contrast, the results obtained at the same time on SS/OPA+Plu show a significantly reduced adhesion of bacteria (Table 4), which is in line with the prevention of BSA (taken as a model biomacromolecule) adsorption on the same surface (Table 6). It turns out that the presence of a large amount of

Plu adsorbed on SS+Plu did not prevent neither BSA adsorption nor bacterial adhesion. In contrast, the presence of a smaller amount of adsorbed Plu on SS/OPA+Plu did prevent BSA adsorption (Table 6) and significantly reduced bacterial adhesion (Table 4). This may be explained as follows. The SS/OPA+Plu surface exposes a dense and uniform layer of hydrated PEO chains which is repellent for both BSA and bacteria owing to steric interactions. The SS+Plu surface is characterized by a higher amount of adsorbed Plu as compared with SS/OPA+Plu (see C(Plu) and $\sum x(ad_i)$ in Table 6). However, the Plu layer of SS+Plu is not well organized and is able to incorporate BSA molecules. On the other hand, it does not show particular adhesive or repulsive properties with respect to the bacteria, compared to hydrophobic or hydrophilic surfaces unable to exert steric repulsions. It appears thus that the organization of the PEO-PPO-PEO layer at the surface, which depends on the hydrophobicity of the substrate, is a key to allow a differential control of the retention of biomacromolecules and bacteria. In order to decipher this organization, the combination of other methods, among which quartz crystal microbalance (QCM) and atomic force microscopy (AFM) are particularly attractive, is required to make a distinction between the adsorbed amount and the structure of the adsorbed layer.

3.4.5 The effect of rinsing with Plu after Pseudomonas 2021 adhesion

The introduction of a post rinsing step with a Plu solution on already adhered bacteria was inspired from the results of competitive adsorption in Chapter 2. These previous results showed the potential of Plu to replace adsorbed BSA on OPA-conditioned surface, and we expected to generate the same effect on adhered bacteria. After comparison of Table 4 and Table 5, it is shown that rinsing with Plu solution has no effect on bacteria adhered on SS. In contrast, rinsing with Plu solution reduces partially the amount of

adhered *Pseudomonas* 2021 on SS/OPA. However, the amount of adhered bacteria on SS/OPA was higher after rinsing with Plu compared to pre-adsorption of Plu. These results show that Plu can remove adhered bacteria, in a way which also strongly depends on the hydrophobicity of the underlying substrates.

3.4.6 Discrepancy observed for Plu adsorption in Chapters 2 and 3

Table 7. Summary of experimental conditions used for Plu adsorption on native stainless steel (SS) in Chapters 2 and 3, and observed results. QCM = quartz crystal microbalance. SS crystal means SS coating on a QCM crystal.

Chapter	Substrate	Adsorption	Flow	Analysis	Adsorbed Plu
2	SS crystal	QCM	50 µL/min	*in-situ*	No
2	SS plate	24-well plate	static	XPS	No
3	SS plate	flow chamber	6.5 mL/min	XPS	Yes

The results of Plu adsorption obtained here (Chapter 3, Figure 2b) show a significant amount of adsorbed Plu on native SS, which is inconsistent with the results presented in Chapter 2 (QCM results in Figure 4b and XPS results in Figure 8 IIId) showing the absence of Plu on native SS. The conditions used for Plu adsorption in these different experiments are summarized in Table 7. It may also be noted that the Plu concentration used in all cases was higher than its critical micelle concentration (CMC). Lower concentration of Plu (< CMC) was also tested by the same approaches, and similar results were obtained (results not shown). We suspected that rinsing may not be performed adequately in the flow chamber. Extensive rinsing procedures were then tested without however leading to a reduced Plu adsorbed amount. Despite our efforts to understand the observed difference, we have not been able to explain it rationally. We suppose that it is related to the different experimental conditions, as presented in Table 7. Since the

results of Chapter 2 were also collected on year before those obtained in Chapter 3, aging of SS substrates or Plu may also be involved.

3.5 Conclusions

The present work demonstrates the possibility to study the influence of different surface treatments of the same material on bacterial adhesion in a single experiment, using a modified parallel plate flow chamber. The adhesion of *Pseudomonas* 2021 was performed during 3 h in a laminar flow chamber in order to evaluate anti-fouling ability of different coatings on stainless steel. Preadsorption of Plu on SS hydrophobized using OPA significantly reduced adhesion of marine bacteria *Pseudomonas* 2021. The same treatment was not effective on SS, although XPS data indicate that the adsorbed Plu amount was higher on SS compared to SS/OPA. The SS surface hydrophobization by OPA had a similar effect on the efficiency of Plu conditioning to reduce BSA adsorption. This confirms the parallelism between the effect of surface modification on bacterial adhesion and protein adsorption. Furthermore, the results show that the influence of Plu is not just a matter of adsorbed amount but is determined by the structure of the adsorbed PEO-PPO-PEO layers. In another approach, it is shown that the amount of adhered bacteria was also reduced on SS/OPA when rinsing with Plu solution after the adhesion step, which gives the perspective to eliminate already adhered bacteria and renew the Plu coating from time to time. These results open the way to a new strategy for optimizing the use of PEO-PPO-PEO triblock copolymers to reduce biofouling (molecular fouling, microfouling) on inorganic substrates, which is of particular interest for corrosion-sensitive materials.

3.6 References

[1] Videla HA and Characklis WG, 1992, Biofouling and microbially influenced corrosion, Int. Biodeterior. Biodegrad., 29, 195-212.

[2] Videla HA and Herrera LK, 2005, Microbiologically influenced corrosion: looking to the future, Int. Microbiol., 8, 169-180.

[3] Müller-Steinhagen H, Malayeri MR and Watkinson AP, 2011, Heat Exchanger Fouling: Mitigation and Cleaning Strategies, Heat Transfer Eng., 32, 189-196.

[4] Cristiani P, Perboni G and Debenedetti A, 2008, Effect of chlorination on the corrosion of Cu/Ni 70/30 condenser tubing, Electrochim. Acta, 54, 100-107.

[5] Cristiani P, 2005, Solutions to fouling in power station condensers, Appl. Therm. Eng., 25, 2630-2640.

[6] Busalmen JP and de Sánchez SR, 2003, Influence of surface oxides on the adhesion of a wild strain of *Pseudomonas sp.* to aluminium brass, Int. Biodeterior. Biodegrad., 52, 13-19.

[7] Li B and Logan BE, 2004, Bacterial adhesion to glass and metal-oxide surfaces, Colloids Surf. B. Biointerfaces, 36, 81-90.

[8] Busalmen JP and de Sanchez SR, 2001, Influence of pH and ionic strength on adhesion of a wild strain of *Pseudomonas sp.* to titanium, J. Ind. Microbiol. Biotechnol., 26, 303-308.

[9] Sheng X, Ting YP and Pehkonen SO, 2008, The influence of ionic strength, nutrients and pH on bacterial adhesion to metals, J. Colloid Interface Sci., 321, 256-264.

[10] Boonaert CJP, Dufrêne YF and Rouxhet PG, 2003, Adhesion (Primary) of Microorganisms onto Surfaces, in: Bitton G (Ed.) Encyclopedia of Environmental Microbiology, Wiley, New York, Vol 1, 113-132.

[11] Jain A and Bhosle NB, 2009, Biochemical composition of the marine conditioning film: implications for bacterial adhesion, Biofouling, 25, 13-19.

[12] Beech IB, Sunner JA and Hiraoka K, 2005, Microbe-surface interactions in biofouling and biocorrosion processes, Int. Microbiol., 8, 157-168.

[13] Hwang G, Kang S, El-Din MG and Liu Y, 2012, Impact of conditioning films on the initial adhesion of *Burkholderia cepacia*, Colloids Surf. B. Biointerfaces, 91, 181-188.

[14] Coetser SE and Cloete TE, 2005, Biofouling and biocorrosion in industrial water systems, Crit. Rev. Microbiol., 31, 213-232.

[15] Yuan SJ, Choong AMF and Pehkonen SO, 2007, The influence of the marine aerobic *Pseudomonas* strain on the corrosion of 70/30 Cu–Ni alloy, Corros. Sci., 49, 4352-4385.

[16] Gubner R and Beech IB, 2000, The effect of extracellular polymeric substances on the attachment of *Pseudomonas* NCIMB 2021 to AISI 304 and 316 stainless steel, Biofouling, 15, 25-36.

[17] Yuan SJ and Pehkonen SO, 2007, Microbiologically influenced corrosion of 304 stainless steel by aerobic *Pseudomonas* NCIMB 2021 bacteria: AFM and XPS study, Colloids Surf. B. Biointerfaces, 59, 87-99.

[18] Yuan SJ, Pehkonen SO, Ting YP, Kang ET and Neoh KG, 2008, Corrosion Behavior of Type 304 Stainless Steel in a Simulated Seawater-Based Medium in the Presence and Absence of Aerobic Pseudomonas NCIMB 2021 Bacteria, Ind. Eng. Chem. Res., 47, 3008-3020.

[19] Rosenhahn A, Schilp S, Kreuzer HJ and Grunze M, 2010, The role of "inert" surface chemistry in marine biofouling prevention, Phys. Chem. Chem. Phys., 12, 4275-4286.

[20] Amiji M and Park K, 1992, Prevention of protein adsorption and platelet adhesion on surfaces by PEO/PPO/PEO triblock copolymers, Biomaterials, 13, 682-692.

[21] Freij-Larsson C, Nylander T, Jannasch P and Wesslen B, 1996, Adsorption behaviour of amphiphilic polymers at hydrophobic surfaces: effects on protein adsorption, Biomaterials, 17, 2199-2207.

[22] Green RJ, Davies MC, Roberts CJ and Tendler SJ, 1998, A surface plasmon resonance study of albumin adsorption to PEO-PPO-PEO triblock copolymers, J. Biomed. Mater. Res., 42, 165-171.

[23] Dewez JL, Schneider YJ and Rouxhet PG, 1996, Coupled influence of substratum hydrophilicity and surfactant on epithelial cell adhesion, J. Biomed. Mater. Res., 30, 373-383.

[24] Yang Y, Poleunis C, Romanszki L, Telegdi J and Dupont-Gillain CC, 2013, Adsorption of a PEO-PPO-PEO triblock copolymer on metal oxide surfaces with a view to reduce protein adsorption and further biofouling, Biofouling, in press.

[25] Wei J, Ravn DB, Gram L and Kingshott P, 2003, Stainless steel modified with poly(ethylene glycol) can prevent protein adsorption but not bacterial adhesion, Colloids Surf. B. Biointerfaces, 32, 275-291.

[26] Nejadnik MR, van der Mei HC, Norde W and Busscher HJ, 2008, Bacterial adhesion and growth on a polymer brush-coating, Biomaterials, 29, 4117-4121.

[27] Telegdi J, Rigó T, Pfeifer É, Keszthelyi T and Kálmán E, 2008, Nanolayer Coatings, in: Hórvölgyi Z, Kiss É (Eds.) Colloids for Nano- and Biotechnology, Springer, Berlin, Vol 135, 77-86.

[28] Lim MS, Smiley KJ and Gawalt ES, 2010, Thermally driven stability of octadecylphosphonic acid thin films grown on SS316L, Scanning, 32, 304-311.

[29] Roosjen A, Kaper HJ, van der Mei HC, Norde W and Busscher HJ, 2003, Inhibition of adhesion of yeasts and bacteria by poly(ethylene oxide)-brushes on glass in a parallel plate flow chamber, Microbiology, 149, 3239-3246.

[30] Landoulsi J, Genet MJ, Richard C, El Kirat K, Pulvin S and Rouxhet PG, 2008, Evolution of the passive film and organic constituents at the surface of stainless steel immersed in fresh water, J. Colloid Interface Sci., 318, 278-289.

[31] Genet M, Dupont-Gillain CC and Rouxhet PG, 2008, XPS analysis of biosystems and biomaterials, in: Matijevic E (Ed.) Medical Applications of Colloids, Springer, New York, 177-307.

[32] Hirayama K, Akashi S, Furuya M and Fukuhara K, 1990, Rapid confirmation and revision of the primary structure of bovine serum albumin by ESIMS and Frit-FAB LC/MS, Biochem. Biophys. Res. Commun., 173, 639-646.

[33] Busscher HJ and van der Mei HC, 1995, Use of flow chamber devices and image analysis methods to study microbial adhesion, Methods Enzymol., 253, 455-477.

[34] Busscher HJ and van der Mei HC, 2006, Microbial adhesion in flow displacement systems, Clin. Microbiol. Rev., 19, 127-141.

[35] Chang Y, Chu WL, Chen WY, Zheng J, Liu L, Ruaan RC and Higuchi A, 2010, A systematic SPR study of human plasma protein adsorption behavior on the controlled surface packing of self-assembled poly(ethylene oxide) triblock copolymer surfaces, J. Biomed. Mater. Res. A, 93, 400-408.

[36] Green RJ, Tasker S, Davies J, Davies MC, Roberts CJ and Tendler SJB, 1997, Adsorption of PEO−PPO−PEO Triblock Copolymers at the Solid/Liquid Interface: A Surface Plasmon Resonance Study, Langmuir, 13, 6510-6515.

[37] Dewez JL, Berger VV, Schneider YJ and Rouxhet PG, 1997, Influence of Substrate Hydrophobicity on the Adsorption of Collagen in the Presence of Pluronic F68, Albumin, or Calf Serum, J. Colloid Interface Sci., 191, 1-10.

[38] Schroen CGPH, Stuart MAC, van der Voort Maarschalk K, van der Padt A and van't Riet K, 1995, Influence of Preadsorbed Block Copolymers on Protein Adsorption: Surface Properties, Layer Thickness, and Surface Coverage, Langmuir, 11, 3068-3074.

[39] Norde W and Gage D, 2004, Interaction of Bovine Serum Albumin and Human Blood Plasma with PEO-Tethered Surfaces: Influence of PEO Chain Length, Grafting Density, and Temperature, Langmuir, 20, 4162-4167.

[40] Dewez JL, Lhoest JB, Detrait E, Berger V, Dupont-Gillain CC, Vincent LM, Schneider YJ, Bertrand P and Rouxhet PG, 1998, Adhesion of mammalian cells to polymer surfaces: from physical chemistry of surfaces to selective adhesion on defined patterns, Biomaterials, 19, 1441-1445.

[41] Katsikogianni M and Missirlis YF, 2004, Concise review of mechanisms of bacterial adhesion to biomaterials and of techniques used in estimating bacteria-material interactions, Eur. Cell Mater., 8, 37-57.

Chapter 4

Proteins dominate in surface layers formed on materials exposed to extracellular polymeric substances from bacterial cultures

The presentation of Chapter 4 is derived from the paper submitted to Colloids and surfaces B: Biointerfaces with the same title, Y. Yang, A. J. Wikiel, L. T. Dall'Agnol, P. Eloy, M. J. Genet, J. J. G. Moura, W. Sand, C. C. Dupont-Gillain, P. G. Rouxhet.

Summary

Extracellular polymeric substances (EPS) are produced by or associated with bacteria in the formation of microbial aggregrates and biofilms. In this paper, the chemical composition of EPS (isolated from *Desulfovibrio alaskensis*, and from *Desulfovibrio desulfuricans* cultured in different conditions) and of organic compounds present in the supernatants of *Pseudomonas* NCIMB 2021 culture was examined by x-ray photoelectron spectroscopy (XPS) of residues obtained by drying drops of solutions. In parallel, conditioning layers formed on model substrates (glass, polystyrene and stainless steel) by adsorption were also investigated. The relevance of peak decomposition was demonstrated by correlations between spectral data. The concentration of elements and chemical functions were exploited to evaluate the weight fraction of three model constituents in the adlayers: amide and CH_2 groups, related mainly to the presence of proteins or acetylated amino-sugars and lipids, respectively, and the sum of additional carbon and organic oxygen, which includes polysaccharides. Proteins were found to be a major component in all conditioning layers. No significant difference was found between adlayers formed by adsorption from solutions covering a broad range of protein concentrations and molar masses, except for glass conditioned by tightly bound EPS from *D. alaskensis*, which showed a higher protein concentration.

4.1 Introduction

Biomolecules may adsorb in a very short period of time (minutes) onto materials when these are placed in natural aqueous environments (e.g. biological fluid, freshwater or seawater) [1]. This adlayer, also called conditioning layer, may influence bacterial attachment by affecting the physico-chemical properties of substrate surface or by its involvement in specific interactions with the cells [2]. It may affect further biofilm formation and even be directly related to biocorrosion process [3].

Biofilms are composed of microbial cells in a matrix containing dead cells, cell fragments and macromolecules, often called extracellular polymeric substances (EPS), which may represent about 90% of the biofilm in dry mass [4]. The constituting biomolecules may be secreted by the microorganisms or originate from cell lysis [5]. EPS play a major role in the mechanical stability of the biofilm through physico-chemical interactions, such as ionic interactions, complex formation, hydrogen bonds and Van der Waals forces [6]. It was reported that surface conditioning by EPS reduces the initial bacterial adhesion in comparison to non-conditioned substrates [7-9]. The use of EPS as a coating layer could be developed as an environmental-friendly way to reduce bacterial adhesion and biofilm formation. However, due to their complexity and variability, the influence of EPS at interfaces is still not clear.

EPS was initially used to refer to extracellular polysaccharides. Nowadays, it designates extracellular polymeric substances because it was found that EPS not only contain polysaccharides but also proteins, DNA, lipids and humic substances [10]. In some cases, it was found that the EPS could contain more proteins than polysaccharides, on a mass basis [11]. Their composition highly depends on the microbial species present and environmental conditions, such as temperature, shear force and nutrients; they are a dynamic system, heterogeneous in composition and changing over time [4]. The work of Zinkevich *et al*. showed that the chemical composition

of EPS produced by the same sulphate-reducing bacteria (SRB) is different in the presence and absence of carbon steel, which highlights the role of EPS in biocorrosion [12]. Further work of Beech *et al*. showed that the EPS isolated from SRB directly induce pitting corrosion on mild steel [13].

Loosely bound (LB) EPS can be obtained by collecting the bacteria supernatant by centrifugation. Tightly bound (TB) EPS, which are more strongly associated to cells, can be extracted in different ways: a mild way involves cation-exchange resins; aggressive ways may cause cell lysis and lead to contamination with intracellular components. The results of Beech *et al*. showed difference of molecular composition between LB and TB EPS [14]. However, there is little work concerning the chemical composition of EPS conditioning layer on surfaces [15].

The aim of this work is to determine the chemical nature of interfaces involving EPS related to bacteria of interest in the field of biocorrosion. It is mainly based on x-ray photoelectron spectroscopy (XPS) analysis of air-dried specimens and of conditioning layers formed on materials exposed to EPS. A large set of solutions of biomolecules were examined, with a focus on the comparison between tightly and loosely bound EPS, and an extension to simple supernatants of bacteria cultures and to a commercial lipopolysaccharide, taken as a possible point of comparison. Model materials (glass, polystyrene and stainless steel) were selected as substrates, considering the interest to vary surface hydrophobicity and the technical relevance. Complementary analysis of the solutions of biological origin were performed, including UV-visible absorbance, surface tension determination, and protein gel electrophoresis.

4.2 Material and methods

4.2.1 Solutions

Experimental details regarding the bacterial cultures and separation of related compounds are given in Supplementary Information (Section 1). EPS were prepared from cultures of the marine bacterium *Desulfovibrio alaskensis AL1* (DA_) in VMN medium containing 0.6% or 0.06% (g/100mL) lactate (noted _0.6_ and _0.06_) [16]. Loosely bound (_LB_) EPS were obtained by centrifugation and supernatant microfiltration followed by dialysis against deionized water (_D). Tightly bound (_TB_) EPS were extracted from the cell pellets by use of a cation exchange resin and finally dialyzed. This provided a set of four samples with names of the type DA_LB_0.06_D. EPS of *Desulfovibrio desulfuricans* ATCC 27774 (DD_) were obtained by centrifugation of a culture in sulfate-(_SO_4_) or nitrate-(_NO_3_) VMN base medium, followed by microfiltration and dialysis. This provided the samples named DD_LB_SO_4_D and DD_LB_NO_3_D.

The supernatants of cultures of *Pseudomonas* NCIMB 2021 in a marine broth medium were collected by centrifugation at the middle of exponential (Sup_expo_) or in the stationary (Sup_stat_) growth phase. The sterilized marine broth (MB) was also used for comparison. Depending on the experiments, these were dialyzed (_D) or not (_ND).

Lipopolysaccharides (LPS) from *Pseudomonas aeruginosa 10* were purchased from Sigma-Aldrich (L7018) and used without any further purification. Single-strand DNA was customer made by Sigma-Aldrich: reference number SY110400604-032 (TCATGATTTGTCACTGAACCG, in short DNA-032) and SY120431805-028 (GAGAGAAACCTTTACACCTTTAGGTTTACGACCT, in short DNA-028). Bovine serum albumin (BSA) was purchased from Sigma-Aldrich (A4919). Ultrapure water was obtained with the PURELAB Ultra device, purchased from ELGA (U.K.).

4.2.2 Substrates

Glass disks (Gl) with diameter of 1.2 cm (Menzel-Gläser, Germany) were cleaned using a piranha solution (7:3 V/V mixture of 97% sulfuric acid (VWR BDH Prolabo, Leuven, Belgium) and 30% peroxide water (VWR BDH Prolabo, Leuven, Belgium)) for 30 s, followed by rinsing with ultrapure water and drying under nitrogen flow. They were used immediately after cleaning.

Polystyrene (PS) substrates were prepared by spin coating (3000 rpm for 30 s) a polystyrene solution (4.3 g/L in toluene; PS from Sigma-Aldrich, CAS number 9003-53-6) on glass. They were prepared 1 day before use, and characterized by water contact angle measurements which provided values of 90° ± 0.4°.

Stainless steel 304-2R (Arcelor, Belgium) plates (mass %, 18.10 Cr, 9.10 Ni, 1.11 Mn, 0.24 Mo, 0.36 Si, 0.051 C, 0.024 P, 0.001 S, balance Fe), in short SS, were 1 cm × 1 cm squares, 1 mm thick, with mirror-like surfaces. After removal of the protective plastic film, the coupons were cleaned 3 times with acetone in ultrasonic bath for 15 min (SS-cl). Certain coupons were submitted to UV/ozone treatment (UVO cleaner, Model No.42-220, Jelight Company Inc. U.S.A) for 15 min just before use (SS-UVO).

4.2.3 XPS analysis

Two kinds of samples were analyzed by XPS: (i) substrates Gl, PS or SS conditioned by adsorption from the solution; (ii) residues of evaporation of the same solutions, noted EVAP. Adsorption was performed on the substrates by immersion in 0.6 mL of the solution in 24-well plates for 2 h, and rinsing. Rinsing was carried out by performing 3 times the following operations, which provided in principle a dilution by a factor of 43 while avoiding repeated removal from the liquid: adding 1.5 mL of ultrapure water, homogeneous stirring, and removing 1.5 mL of liquid. The coupon

was then removed and quickly dried under a nitrogen flow. To prepare EVAP samples, an aliquot of 100 µL of the liquid was deposited onto Gl substrates and left drying in ambient conditions. This process was repeated another 2 times to form a layer of residue which was visible to the naked eyes. For most EVAP samples, the substrate did not contribute significantly to the obtained signals (Si < 0.6 %).

XPS measurements were carried out with a Kratos Axis Ultra spectrometer (Kratos Analytical, U.K.), using monochromated Al Kα radiation. The C 1s peak component due to carbon exclusively bound to carbon and hydrogen [**C**-(C,H)] was fixed at 284.8 eV to set the binding energy scale. Quantification was made after linear background subtraction and peak area normalization on the basis of acquisition parameters, using experimental sensitivity factors and transmission factors given by the manufacturer. This provided elemental mole fractions, excluding hydrogen which is not detected by XPS. The C 1s, O 1s and N 1s peaks were decomposed with the CasaXPS program (Casa Software Ltd., U.K.) using a Gaussian/Lorentzian (70/30) product function. Further details are given in Supplementary Information (Section 3.1).

4.2.4 Characterization of the solutions

The UV-visible spectra of the solutions were recorded between 190 and 800 nm (Beckman Coulter DU800) after a dilution allowing measurements to be made in the range of 0.1 to 2 of absorbance.

The surface tension of the solutions was measured at room temperature, using the du Nouy's ring method [17], by means of a Kruss K100 tensiometer (Kruss GmbH, Hamburg, Germany). The solutions were examined at increasing dilution with ultrapure water, until the surface tension was closed to that of ultrapure water (72.8 mN/m)

One-dimensional polyacrylamide gel electrophoresis was performed on 10% SDS-PAGE using BioRad Mini-Protean 1-D cell according to the method of Laemmli [18]. The protein gels were stained for visualization with Coomassie blue protocol described by Dyballa *et al.* [19].

4.3 Results and discussion

4.3.1 Characterization of the solutions

Representative UV-visible absorption spectra of solutions of interest are presented in Supplementary Information (Figure S1a). They are compatible with a mixture of proteins and nucleotides, as illustrated by spectra of BSA and DNA-028 (Figure S1b). In addition, the spectra of DA_TB samples show a band near 410 nm which may be due to the Soret band of heme structures [20]. The absorbance at 280 nm, A_{280}, multiplied by the dilution factor, and the ratio of absorbances A_{280}/A_{260} are given in Table 1. The ratio measured for solutions of interest is closer to that of nucleotides (not higher than 0.6 [21]) than that of proteins (1.6 for BSA). However the absorption coefficients are much higher for DNA than for proteins, as shown by values presented in Supplementary Information (Table S1). Considering these absorption coefficents and the absorbance values showed (details not presented) that the concentration of proteins is at least 10 times larger than that of nucleotides for DA_LB, DA_TB and Sup. Note that most polysaccharides do not absorb in the UV-visible range.

Table 1. Characteristics of solutions used for substrate conditioning and of reference solutions: UV absorption data (absorbance at 280 nm and ratio of absorbance at 280 nm and 260 nm) and surface tension data (value at the indicated dilution and dilution leading to a surface tension equal or above 70 mN/m).

Solutions	UV absorption		Surface tension γ (mN/m)	
	A280 × dilution	A_{280}/A_{260}	Value [Dilution]	Dilution (γ >70)
DA_LB_0.06_D	0.21	0.76	62.3 [1]	≈ 10
DA_LB_0.6_D	0.15	0.73	71.0 [3]	< 3
DA_TB_0.06_D	0.38	0.89	66.2 [3]	≈ 10
DA_TB_0.6_D	2.0	0.85	61.0 [3]	≈ 20
MB_ND	4.3	0.60	54.9 [1]	≈ 20
Sup_expo_ND	2.2	0.71	59.4 [1]	≈ 16
Sup_stat_ND	2.7	0.79	59.3 [1]	≈ 16
BSA (200 µg/mL)	0.10	1.6	58.4 [1]	≥ 100
DNA-028 (50 µg/mL)	0.88	0.60	–	–

The surface tension data are presented in two ways (Table 1): the value measured at an indicated dilution, and the dilution required to reach a surface tension higher than 70 mN/m, keeping in mind that the surface tension of water is close to 72.8 mN/m. The data show a rough correlation between A_{280} corrected for dilution and the lowering of surface tension with respect to that of water for the EPS solutions and bacterial cultures, in agreement with the expected surface-active character of proteins.

Polyacrylamide gel electrophoresis (not shown) confirmed the presence of proteins in the range of 20 to 200 kDa in DD_LB_SO_4_D and DD_LB_NO_3_D. For MB, no coloration appeared above 20 kDa. Protein bands were visible between 20 kDa and 120 kDa for Sup_expo_D, and were more numerous and intense for Sup_stat_D.

These results show that the solutions used cover a broad range of protein concentrations and protein molar masses.

4.3.2 XPS data

The samples analyzed by XPS are presented in Table 2 in a matrix showing the combination between the solutions and the sample nature: residue of evaporation (EVAP) and conditioned Gl, PS and SS. The elemental compositions determined by XPS are listed in Supplementary Information (Tables S2 to S5). The non-conditioned Gl and SS-UVO samples showed carbon concentrations of 12% and 39%, respectively. This is attributed to organic contaminants which may originate from material processing, from artefacts due to sample preparation, or from contamination by adsorption from the surroundings, either the ambient atmosphere or the spectrometer vacuum chamber. The higher carbon concentration on bare stainless steel compared to glass is a frequent observation [22].

Table 2. Overview of samples analyzed by XPS: residues of evaporation of solutions and substrates conditioned with solutions.

Solution	EVAP	Substrates			
		PS	Gl	SS-cl	SS-UVO
None		x	x		x
DA_LB_0.06_D	x	x	x		
DA_LB_0.6_D	x	x	x		
DA_TB_0.06_D	x	x	x		
DA_TB_0.6_D	x	x	x		
DD_LB_SO_4_D		x	x	x	x
DD_LB_NO_3_D		x	x	x	x
Sup_expo_ND		x	x	x	x
Sup_expo_D	x	x	x	x	x
Sup_stat_ND		x	x	x	x
Sup_stat_D	x	x	x	x	x
MB_ND		x	x	x	x
MB_D	x	x	x	x	x
LPS	x	x	x		x
DNA-032	x				

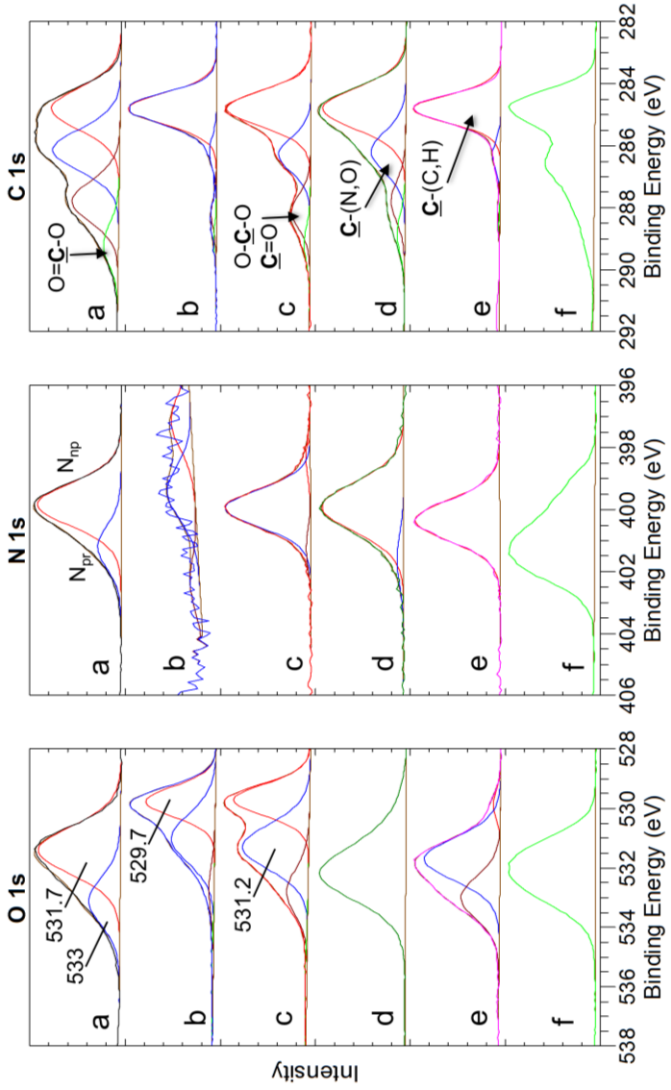

Figure 1. Representative XPS peaks recorded on: (a) EVAP_DA_TB_0.06_D; (b) SS-UVO; (c) SS-UVO_Sup_stat_D; (d) Gl_Sup_stat_D; (e) PS_Sup_stat_D, and (f) EVAP_DNA-032, with peak decomposition and component position or assignment when reliable. N_{np} = non protonated nitrogen; N_{pr} = protonated nitrogen.

Figure 1 presents the range of observed shapes for O 1s, N 1s and C 1s peaks, which were decomposed with constraints insuring the consistency required to make quantitative comparison between samples [23, 24]. Owing to the overlap of inorganic oxides or hydroxides and organic compounds, no reliable decomposition could be performed for the O 1s peak of Gl samples. Illustrations of peak decompositions are shown with the assignment of C 1s and N 1s components and typical binding energies of O 1s components. Details on peak decomposition and attribution are given in Supplementary Information (Section 3.2). The results of peak decomposition, expressed in mole fraction of the corresponding elements and functions, are presented in Supplementary Information (Tables S2 to S5).

The N 1s peak of the samples of interest is quite different from that of nucleotides, as shown in Figure 1f for a single-stranded DNA-032. This peak presents a maximum near 401.5 eV, in agreement with published spectra of nucleotides [25, 26], which is due to the abundance, in DNA, of nitrogen atoms either protonated or making both a double and a single bond with carbon. This information allows excluding a significant contribution of nucleic acids to the conditioning layers.

The XPS analysis of the evaporation residues of the LPS solution (7 replicates) gave unexpected results: sulfur concentration 3.9%, S 2p binding energy of 168.5 eV typical of sulfate or sulfonate, sodium concentration 3.6 %, 79 % of carbon bound only to carbon and hydrogen, S/C molar ratio about 5 times higher than measured by elemental analysis of the bulk. These were attributed to surface accumulation of sodium dodecylsulfate used in the preparation of the LPS (Sigma Product Information). This limits the relevance of commercial LPS as a possible model for EPS; however the data for substrates conditioned with LPS were kept for comparison.

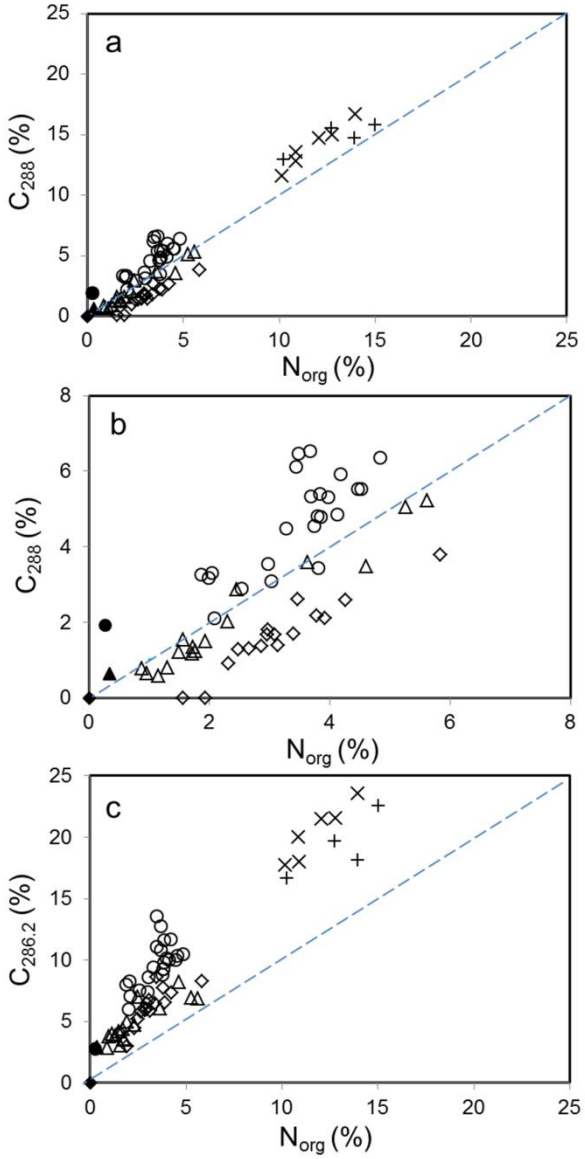

Figure 2. Plot of the molar concentrations associated to C 1s peak components (C_{288} in a and b; $C_{286.2}$ in c), versus the organic nitrogen concentration (N_{org}) determined by XPS: EVAP of DA (+), of MB and Sup (×); non-conditioned Gl (▲), PS (◆) and SS (●); Gl (△), PS (◇) and SS (○) conditioned with the various solutions. Note that (b) is a zoom of (a). The broken lines show the 1:1 relations expected if all the involved C 1s components and N_{org} were in the form of amide. For all samples in (a), $y = (1.18 \pm 0.04)x - (0.49 \pm 0.24)$, $R^2 = 0.92$; for all samples in (b), $y = (1.06 \pm 0.13)x - (0.18 \pm 0.41)$, $R^2 = 0.55$.

Correlations between spectral data were used to evaluate the significance (relevance and limitation) of peak decomposition and to generate information from peak components [24, 27-29]. Figure 2a presents the plot of the concentration of carbon responsible for the component close to 288.0 eV, C_{288}, due to carbon making two single bonds with oxygen in acetal [C-O-**C**-O-C, one per hexose unit in polysaccharides] or making one double bond with oxygen in amide [N-**C**=O], as a function of the concentration of organic nitrogen, N_{org}. The latter differs from total nitrogen only for SS samples which showed a weak component at low binding energy (<398 eV) attributed to a reduced form of nitrogen present on the substrate. The correlation coefficients and linear regression parameters, including error ranges, are given in the caption of Figure 2. The data are close to a 1:1 relation, which is expected for the amide function [HC-NH-(C=O)], forming the backbone of proteins (peptidic link). However, the zoom in Figure 2b shows a systematic difference between PS samples, on the one hand, and Gl and SS samples, on the other hand, owing to the contribution of oxidized carbon of contaminants for Gl and SS. Figure 2c presents the plot of the concentration of carbon responsible for the C 1s component at 286.1 to 286.3 eV (noted $C_{286.2}$), which is due to carbon making a single bond with oxygen or nitrogen [**C**-(O,N)] in alcohol, ester, ether, amine or amide, as a function of N_{org}. The deviation with respect to the 1:1 relation may be attributed to the presence of polysaccharides or oxygen-containing organic contaminants.

The major O 1s component in the range from 531.2 to 531.8 eV, noted $O_{531.5}$, for EVAP and PS samples is due to oxygen doubly bound to carbon [**O**=C] in amide, carboxyl or ester functions. Figure 3a shows that concentration of $O_{531.5}$ is very close to that of N_{org} for PS samples. It is slightly higher for EVAP samples owing to a contribution of inorganic compounds (presence of phosphate, sulfate, Si, B, Al; see Table S2) due to residual salts or to the glass substrate. In contrast, the concentration of $O_{531.5}$

is much higher than that of N_{org} for SS samples, owing to the overlapping contribution of metal hydroxide [30].

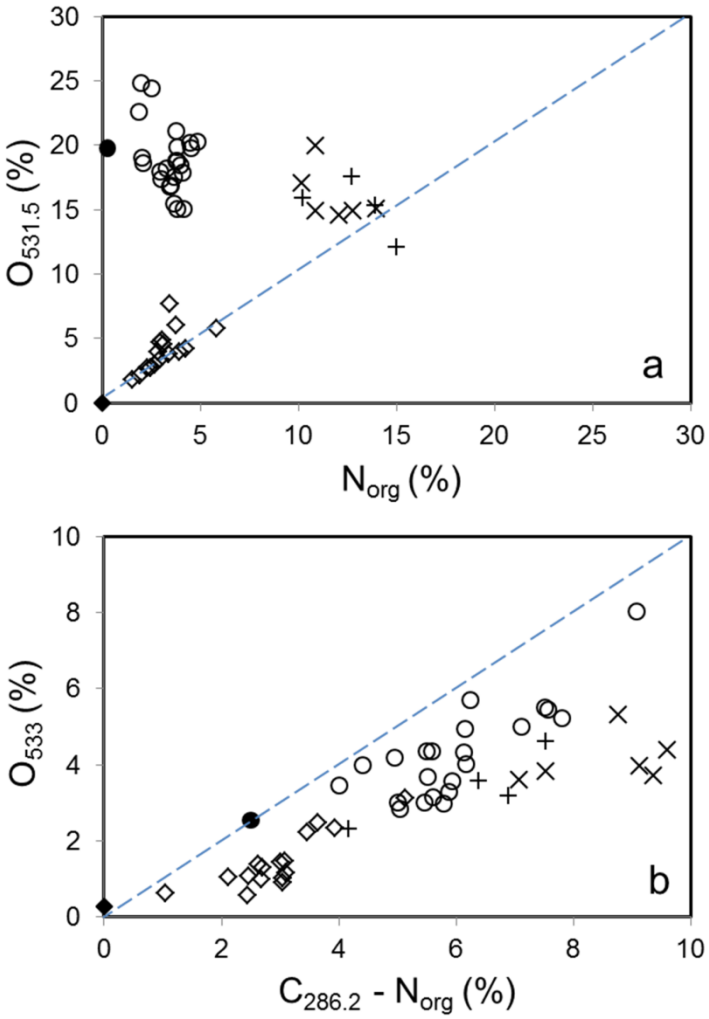

Figure 3. Plot of molar concentrations determined by XPS: (a) $O_{531.5}$ vs N_{org} and (b) O_{533} vs ($C_{286.2}$ - N_{org}). EVAP of DA (+), of MB and Sup (×); non-conditioned PS (◆) and SS (●); PS (◇) and SS (○) conditioned with the various solutions. (a) Broken line, 1:1 relation expected for amide; for PS samples, $y = (1.13 \pm 0.23)x + (0.47 \pm 0.75)$, $R^2 = 0.61$; for PS+EVAP samples, $y = (1.19 \pm 0.1)x + (0.63 \pm 0.79)$, $R^2 = 0.85$. (b) Broken line, 1:1 relation expected for alcohol, ester and polysaccharide; for PS+SS samples, $y = (0.89 \pm 0.05)x - (1.02 \pm 0.28)$, $R^2 = 0.88$; for PS+SS+EVAP samples, $y = (0.68 \pm 0.06)x - (0.28 \pm 0.34)$, $R^2 = 0.73$.

The O 1s component near 533 eV, noted O_{533}, is due to oxygen making one (alcohol, carboxyl, ester) or two (ether) single bonds with carbon, while $C_{286.2}$ is due to carbon singly bound to O or N. Figure 3b presents the plot of the concentration of O_{533} vs ($C_{286.2} - N_{org}$). Here, N_{org} is subtracted from $C_{286.2}$ to remove the contribution of amide functions, according to the correlation established in Figure 2a. The correlation coefficients and linear regression parameters are given in the caption of Figure 3. A 1:1 relation is expected for alcohol (**C**-**O**H), ester (**C**-**O**-C=O) and polysaccharide (C-**O**-H, C-**O**-C vs C-**C**-O). The experimental data roughly follow this trend, but are rather scattered and shifted regarding both the intercept and slope, which may be due to the uncertainties inherent to the weak O_{533} concentration and to the result of the ($C_{286.2} - N_{org}$) subtraction.

The correlations presented in Figures 2a and 3a clearly show the importance of amide functions at the surface of evaporation residues and of conditioned substrates. In previous reports on the surface analysis of microbial cells, nitrogen was attributed to amide and was considered as a marker for proteins [5, 23, 24, 29]. Accordingly, the surface composition was modeled in terms of proteins, polysaccharides and hydrocarbons. However, polysaccharides frequently contain N-acetylated aminosugars in which nitrogen is also in the form of amide. In N-acetylated aminosugars and in proteins, the amide function has the structural formula [HC-NH-(C=O)] and ($C_{tot} - 2*N_{org}$) represents carbon which is not in the form of amide (if all N_{org} is attributed to amide). On the other hand, the C 1s component at 284.8 eV, $C_{284.8}$, is due to carbon only bound to carbon and hydrogen (hydrocarbon function, typical of lipids).

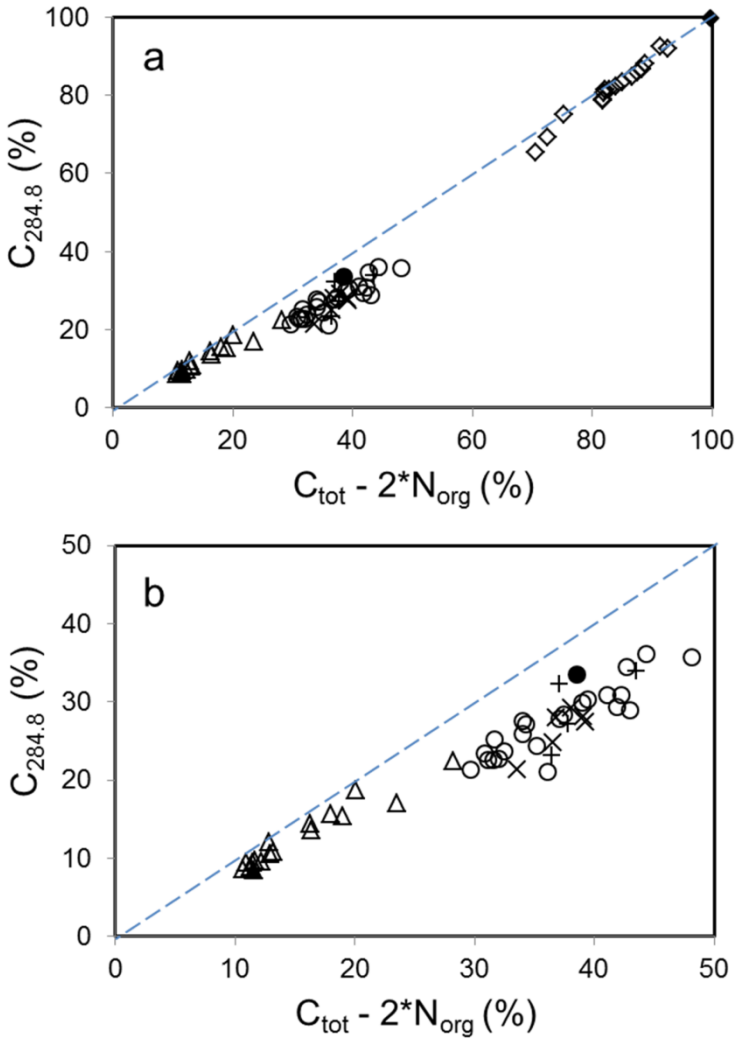

Figure 4. Plot of the molar concentrations of $C_{284.8}$ vs (C_{tot} – 2*N_{org}) determined by XPS: EVAP of DA (+), of MB and Sup (×); non-conditioned glass (▲), PS (◆) and SS (●); glass (△), PS (◇) and SS (○) conditioned with the various solutions. Broken line: unit slope; for Gl samples, y = (0.79 ± 0.05)x + (0.61 ± 0.82), R^2 = 0.94; for SS+EVAP samples, y = (0.82 ± 0.09)x – (2.8 ± 3.4), R^2 = 0.72; for Gl+SS+EVAP samples, y = (0.70 ± 0.03)x + (1.58 ± 0.79), R^2 = 0.94. (b) All data except for PS samples. Note that (b) is a zoom of (a).

Figure 4 presents the plot of $C_{284.8}$ vs (C_{tot} – 2*N_{org}). All the data are distributed along a bow shape, the ends of which are close to the 1:1

relationship. The data for PS samples are located at the high end but are not informative owing to the strong contribution of the substrate. The correlation coefficients and linear regression parameters for different subsets of samples are given in the caption of Figure 4. The deviations with respect to the 1:1 relation along the x axis reflect the concentration of carbon which is neither in the form of hydrocarbon function, nor in the form of amide. Figure 4b shows that this type of carbon is more abundant on SS than on Gl, while Figure 2b shows that SS and Gl samples cover the same range of nitrogen and thus amide concentration. The difference is found for bare samples, in which organic compounds are contaminants, and for samples which have adsorbed organic compounds as a result of conditioning. The EVAP samples fall in the same range as SS samples.

4.3.3 Nature of the adlayer

Expressing the composition of the organic adlayers in terms of compounds of interest is made difficult by the complexity of the biochemical compounds and the presence of organic contaminants at the surface of simply "cleaned" substrates. The correlations presented in Figures 2 and 3 show that amide moieties are important constituents and can reliably be quantified by using nitrogen as a marker. Figure 4 shows that carbon which is not in the form of amide ($C_{tot} - 2*N_{org}$) may be separated in two categories: carbon only bound to carbon and hydrogen ($C_{284.8}$), and oxidized carbon in addition to the one present in the form of amide: $C_{add} = C_{tot} - C_{284.8} - 2*N_{org} = C_{ox} - 2*N_{org}$ where $C_{ox} = C_{tot} - C_{284.8} = C_{286.2} + C_{288.0} + C_{289.0}$. For many organic functions (alcohol, primary amide or amine, ester, aldehyde, ketone), and mostly for those which are relevant in biosystems, $C_{ox} = O_{org} + N_{org}$. An exception is the case of ether functions ($C_{ox}/O_{org} = 2$), which is responsible for a ratio $C_{ox}/O_{org} = 1.2$ for non-chemically modified polysaccharides, the link between sugar units being an ether function. Another exception is the case of carboxylic acid or carboxylate functions, for which $C_{ox}/O = 0.5$. As

mentioned before, the oxygen due to the organic layer adsorbed on an inorganic oxide substrate cannot often be distinguished from the oxygen of the substrate. However the concentration of organic oxygen may then be approximated by $O_{org} = C_{ox} – N_{org}$ [30, 31].

The composition of the adlayers and evaporation residues examined here was expressed in terms of 4 chemical entities: amide [HC-NH-(C=O)], CH_2, additional carbon quantified by $C_{add} = C_{ox} – 2*N_{org}$ and additional organic oxygen quantified by $O_{add} = O_{org} – N_{org} = C_{ox} – 2*N_{org}$. The elemental molar concentrations were converted into weight percentage of these chemical entities in the organic adlayer (g / 100 g of adlayer), as explained in Supplementary Information (Section 4 and Table S6). The results are given in Tables S7 and S8. The discussion below is based on the composition of the adlayer expessed as weight % of amide [HC-NH-(C=O)], CH_2 and sum of $C_{add} + O_{add}$. If the sum of C_{add} and O_{add} is due to non-chemically modified polysaccharide, the molar concentration of O_{add} should be $C_{add}/1.2 = [C_{ox} – 2*N_{org}]/1.2$, instead of $[C_{ox} – 2*N_{org}]$. In practice, neglecting the 1.2 ratio leads to a satisfactory evaluation of the weight of polysaccharides, as a moiety made of 6 C atom and 6 O atoms weights 168 g, which is close to the weight of 1 repeat unit of polysaccharides $C_6H_{10}O_5$ equal to 162 g.

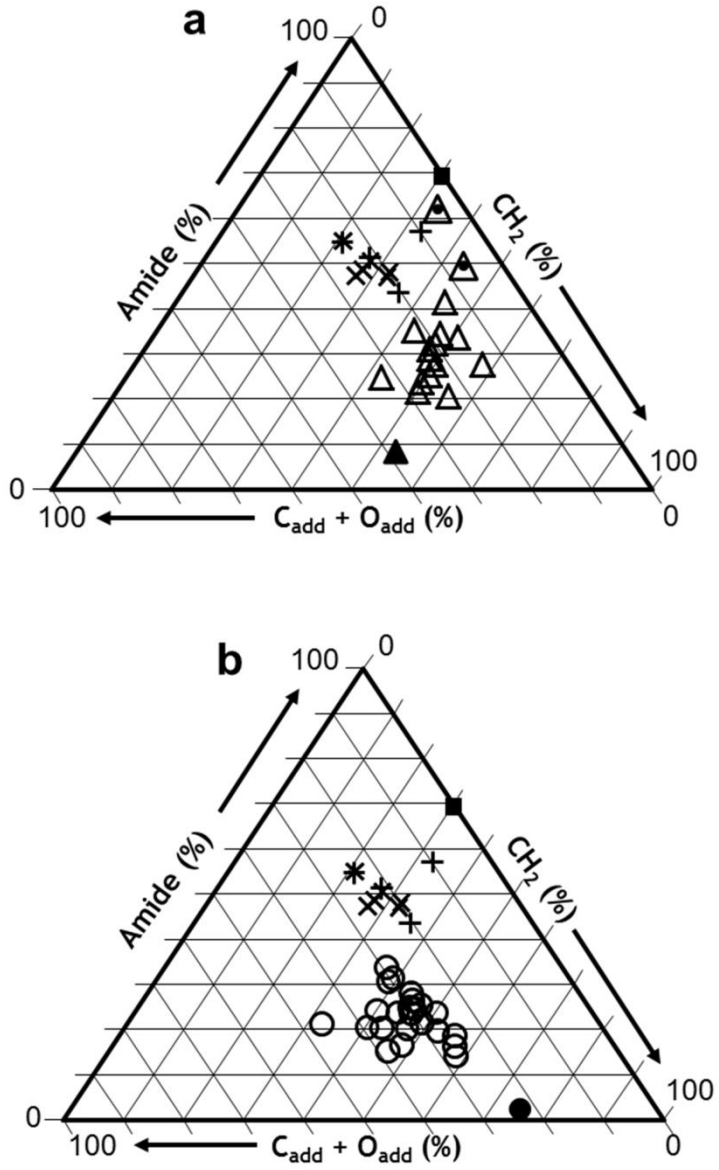

Figure 5. Mass concentration of amide (HC-NH-C=O), hydrocarbon CH_2 and additional carbon and oxygen (C_{add} + O_{add}) determined by XPS on EVAP of DA (+), and of MB and Sup (×), on (a) Gl non-conditioned (▲) and conditioned (△) with the various solutions, DA_TB being identified by including a black dot, and on (b) non-conditioned SS-UVO (●) and SS-cl or SS-UVO conditioned (○) with the various solutions. Computed value for BSA (■).

The weight percentages of the 3 moeities considered are presented in Figure 5 in the form of ternary composition diagrams [32], the corners of which represent 100 wt % of amide, 100 wt % CH_2 and 100 wt % C_{add} + O_{add}. The use of these diagrams avoids attributing a priori the amide functions to proteins and using nitrogen as an exclusive marker for proteins. On the other hand, the figure is convenient to represent the composition of surfaces and adlayers with respect to an amide pole, shared by proteins and N-acetylated functions of polysaccharides, the hydrocarbon pole, typical of lipids, and a pole representative of oxidized organic compounds, including polysaccharide moieties. The data for PS samples are not taken in consideration due to the dominant contribution of CH_2, attributed to the substrate (Table S8). Figure 5 presents also the data computed for BSA, according to the amino-acid composition of BSA [33], as detailed by Toure *et al.* [to be published].

Figure 5 shows that all evaporation residues fall close together, and differ from BSA by a proportion of about 20% (C_{add} + O_{add}). They were mainly composed of proteins, either because these are the major bulk constituent, as shown by biochemical analysis of DA and DD samples (results not shown), or because they are accumulated at the liquid-air interface, as revealed by the lower surface tension of the solutions, compared to water, and at the resulting solid-air interface. Non-conditoned Gl (Figure 5a) shows 40% (C_{add} + O_{add}) and 50% CH_2, due to organic contaminants. Conditioning Gl with the solution brings proteins and decreases the relative concentration of oxidized carbon which is not in the form of amide. The influence of the nature of the conditioning solution is not significant except for tightly bound EPS solutions (DA_TB), which bring the adlayer composition closer to that of pure protein. The higher protein concentration of surface conditioned with tightly compared to loosely bound EPS is in agreement with the results reported by Beech *et al.* [15]. It may be noted

from Table 1 that DA_TB solutions were more concentrated in proteins, compared to DA_LB.

Non-conditioned SS-UVO (Figure 5b) shows about 25% of (C_{add} + O_{add}) and 75% CH_2, which are due to organic contaminants. The SS samples conditioned with all solutions, dialyzed or not, are clustered in a narrow domain of composition, without any significant difference between samples cleaned with acetone and samples treated with UV-Ozone. With respect to non-conditioned SS, the concentration of proteins increases essentially at the expense of hydrocarbons. It may be pointed out that each substrate conditioned with LPS (details in Tables S7 and S8) falls in the cluster. It does not show a higher concentration of polysaccharides, indicating that the adsorbed molecules are mainly proteins, the commercial LPS sample containing about 10% denatured proteins (Sigma Product Information). While substrate conditioning shifts the adlayer composition to a higher concentration of amide functions, it does not shift it to higher value of C_{add} + O_{add}, which indicates that adsorbed compounds are protein rather than polysaccharides, amino-acetylated or not.

The description of the nature of the organic adlayer present on substrates should ideally be completed by the evaluation of its thickness [31]. This would require modelling with approximations and is not justified in this paper. However, an interesting information may be obtained by comparing the mole fraction of C + C_{ox} provided by the XPS analysis, as it is an evaluation of the sum of concentrations C + O_{org} + N_{org}, and thus reflects the contribution of the adlayer to the XPS spectrum, with respect to elements from the substrate. The data are presented in Supplementary Information (Tables S7 and S8). Obviously, only samples involving the same substrate may be compared with each other and data for samples with PS substrates are not informative, due to the domination of the substrate in the hydrocarbon contribution. Substrate conditioning with the solutions increased only moderately (factor 1 to 2 on Gl, about 1.5 on SS) the

contribution of the adlayer to the XPS spectrum (Tables S7 and S8), and thus its thickness, while it changed its composition, essentially by bringing proteins to the surface. It is noteworthy that no significant difference was found between loosely bound EPS, culture supernatants and marine broth medium, and commercial LPS despite the difference of protein concentration and molar mass. However, tightly bound EPS provide an adlayer slightly richer in proteins.

In Figure 5, the position of data points for adlayers formed by substrate conditioning, between non-conditioned substrates and evaporation residues (more C_{add} + O_{add} on SS and less on Gl), indicates that the fate of organic contaminants as a result of conditioning differs between glass and stainless steel. However it leaves open questions. Are the organic contaminants displaced or not by the proteins of the conditioning solutions? Does protein adsorption protect the surface from subsequent contamination either in the ambient atmosphere, in the spectrometer vacuum chamber or during analysis?

4.4 Conclusions

This paper addresses the composition of interfaces involving EPS and related compounds: surfaces of residues left by evaporation and adlayers formed by conditioning different substrates (glass, polystyrene and stainless steel). The XPS analysis was focused not only on the elemental composition but also on chemical functions identified by components of C 1s, N 1s and O 1s peaks. Correlations between spectral data revealed that most of nitrogen was in the form of amide. The contribution of proteins and acetylated amino-sugars could be determined by assessing the respective contributions of other forms of oxidized carbon and of hydrocarbon functions, and comparing the results with computations based on the structural formula of BSA. A convenient way of comparing different systems was to use ternary diagrams

presenting the weight fraction of 3 model moieties: amide [HC-NH-(C=O)], CH_2, and the sum of C_{add} and O_{add}.

Proteins were found to be a major biochemical constituent in both the evaporation residues and the adlayers formed by conditioning the substrates with EPS of *D. alaskensis* and *D. desulfuricans*, and with marine broth and supernatants of culture medium. There was no significant difference between the adlayer formed from solutions covering a broad range of protein concentrations and molar masses, except for glass conditioned with the tightly bound EPS extracted from *D. alaskensis*, which showed a protein concentration higher than that of other systems. Conditioning the substrates increased only moderately the amount of organic matter present at the surface with respect to that found on non-conditioned substrates, which was due to adventitious contaminants.

4.5 References

[1] Schneider RP and Leis A, 2003, Conditioning Films in Aquatic Environments, in: Bitton G (Ed.) Encyclopedia of Environmental Microbiology, Wiley, New York, Vol 2, 928-941.

[2] Boonaert CJP, Dufrêne YF and Rouxhet PG, 2003, Adhesion (Primary) of Microorganisms onto Surfaces, in: Bitton G (Ed.) Encyclopedia of Environmental Microbiology, Wiley, New York, Vol 1, 113-132.

[3] Beech IB, Zinkevich V, Tapper R, Gubner R and Avci R, 1999, Study of the interaction of sulphate-reducing bacteria exopolymers with iron using X-ray photoelectron spectroscopy and time-of-flight secondary ionisation mass spectrometry, J. Microbiol. Methods, 36, 3-10.

[4] Flemming HC and Wingender J, 2003, Extracellular Polymeric Substances (EPS): Structural, Ecological and Technical Aspects, in: Bitton G (Ed.) Encyclopedia of Environmental Microbiology, Wiley, New York, Vol 3, 1223-1231.

[5] Dufrêne YF, Vermeiren H, Vanderleyden J and Rouxhet PG, 1996, Direct evidence for the involvement of extracellular proteins in the adhesion of *Azospirillum brasilense*, Microbiology, 142, 855-865.

[6] Flemming H-C, 2011, The perfect slime, Colloids Surf. B. Biointerfaces, 86, 251-259.

[7] Hwang G, Kang S, El-Din MG and Liu Y, 2012, Impact of an extracellular polymeric substance (EPS) precoating on the initial adhesion of *Burkholderia cepacia* and *Pseudomonas aeruginosa*, Biofouling, 28, 525-538.

[8] Gómez-Suárez C, Pasma J, van der Borden AJ, Wingender J, Flemming H-C, Busscher HJ and van der Mei HC, 2002, Influence of extracellular polymeric substances on deposition and redeposition of *Pseudomonas aeruginosa* to surfaces, Microbiology, 148, 1161-1169.

[9] Stadler R, Wei L, Fürbeth W, Grooters M and Kuklinski A, 2010, Influence of bacterial exopolymers on cell adhesion of *Desulfovibrio vulgaris* on high alloyed steel: Corrosion inhibition by extracellular polymeric substances (EPS), Mater. Corros., 61, 1008-1016.

[10] Wingender J, Strathmann M, Rode A, Leis A and Flemming H-C, 2001, Isolation and biochemical characterization of extracellular polymeric substances from *Pseudomonas aeruginosa*, Methods Enzymol., 336, 302-314.

[11] Conrad A, Kontro M, Keinänen M, Cadoret A, Faure P, Mansuy-Huault L and Block J-C, 2003, Fatty acids of lipid fractions in extracellular polymeric substances of activated sludge flocs, Lipids, 38, 1093-1105.

[12] Zinkevich V, Bogdarina I, Kang H, Hill MAW, Tapper R and Beech IB, 1996, Characterisation of exopolymers produced by different isolates of marine sulphate-reducing bacteria, Int. Biodeterior. Biodegrad., 37, 163-172.

[13] Beech IB, Zinkevich V, Tapper R and Gubner R, 1998, Direct involvement of an extracellular complex produced by a marine sulfate-reducing bacterium in deterioration of steel, Geomicrobiol. J., 15, 121-134.

[14] Beech I, Hanjagsit L, Kalaji M, Neal AL and Zinkevich V, 1999, Chemical and structural characterization of exopolymers produced by *Pseudomonas* sp. NCIMB 2021 in continuous culture, Microbiology, 145, 1491-1497.

[15] Beech IB, Gubner R, Zinkevich V, Hanjangsit L and Avci R, 2000, Characterisation of conditioning layers formed by exopolymeric substances of *Pseudomonas* NCIMB 2021 on surfaces of AISI 316 stainless steel, Biofouling, 16, 93-104.

[16] Zinkevich V and Beech IB, 2000, Screening of sulfate-reducing bacteria in colonoscopy samples from healthy and colitic human gut mucosa, FEMS Microbiol. Ecol., 34, 147-155.

[17] Huh C and Mason SG, 1975, A rigorous theory of ring tensiometry, Colloid. Polym. Sci., 253, 566-580.

[18] Laemmli UK, 1970, Cleavage of structural proteins during the assembly of the head of bacteriophage T4, Nature, 227, 680-685.

[19] Dyballa N and Metzger S, 2009, Fast and Sensitive Colloidal Coomassie G-250 Staining for Proteins in Polyacrylamide Gels, J. Vis. Exp., e1431.

[20] Collinson M and Bowden EF, 1992, UV-visible spectroscopy of adsorbed cytochrome c on tin oxide electrodes, Anal. Chem., 64, 1470-1476.

[21] Olson N and Morrow J, 2012, DNA extract characterization process for microbial detection methods development and validation, BMC Res. Notes, 5, 668.

[22] Rouxhet PG, 2013, Contact angles and surface energy of solids: Relevance and limitations, in: Mittal KL (Ed.) Advances in Contact Angle, Wettability and Adhesion, Schrivener Publishing, Vol 1, in press.

[23] Genet MJ, Dupont-Gillain CC and Rouxhet PG, 2008, XPS Analysis of Biosystems and Biomaterials, in: Matijevic E (Ed.) Medical Applications of Colloids, Springer, New York, 177-307.

[24] Rouxhet PG and Genet MJ, 2011, XPS analysis of bio-organic systems, Surf. Interface Anal., 43, 1453-1470.

[25] Petrovykh DY, Kimura-Suda H, Whitman LJ and Tarlov MJ, 2003, Quantitative Analysis and Characterization of DNA Immobilized on Gold, J. Am. Chem. Soc., 125, 5219-5226.

[26] May CJ, Canavan HE and Castner DG, 2004, Quantitative X-ray Photoelectron Spectroscopy and Time-of-Flight Secondary Ion Mass Spectrometry Characterization of the Components in DNA, Anal. Chem., 76, 1114-1122.

[27] Aguié-Béghin V, Adriaensen Y, Péron N, Valade M, Rouxhet P and Douillard R, 2009, Structure and Chemical Composition of Layers Adsorbed at Interfaces with Champagne, J. Agric. Food. Chem., 57, 10399-10407.

[28] Rouxhet PG, Misselyn-Bauduin AM, Ahimou F, Genet MJ, Adriaensen Y, Desille T, Bodson P and Deroanne C, 2008, XPS analysis of food products: toward chemical functions and molecular compounds, Surf. Interface Anal., 40, 718-724.

[29] Ahimou F, Boonaert CJP, Adriaensen Y, Jacques P, Thonart P, Paquot M and Rouxhet PG, 2007, XPS analysis of chemical functions at the surface of *Bacillus subtilis*, J. Colloid Interface Sci., 309, 49-55.

[30] Landoulsi J, Genet MJ, Richard C, El Kirat K, Pulvin S and Rouxhet PG, 2008, Evolution of the passive film and organic constituents at the surface of stainless steel immersed in fresh water, J. Colloid Interface Sci., 318, 278-289.

[31] Landoulsi J, Genet MJ, El Kirat K, Richard C, Pulvin S and Rouxhet PG, 2011, Silanization with APTES for controlling the interactions between stainless steel and biocomponents: reality vs expectation, in: Pignatello R (Ed.) Biomaterials - Physics and Chemistry, InTech Open Access, 99-126.

[32] Graham DJ and Midgley NG, 2000, Graphical representation of particle shape using triangular diagrams: an Excel spreadsheet method, Earth Surf. Process. Landf., 25, 1473-1477.

[33] Hirayama K, Akashi S, Furuya M and Fukuhara K-i, 1990, Rapid confirmation and revision of the primary structure of bovine serum albumin by ESIMS and frit-FAB LC/MS, Biochem. Biophys. Res. Commun., 173, 639-646.

4.6 Supplementary Information

4.6.1 Culture conditions and biological solutions

Loosely bound (LB) and tightly bound (TB) EPS were extracted from cultures of the marine bacterium *Desulfovibrio alaskensis AL1,* isolated from a soured oil well in Purdu Bay, Alaska [1]. Detailed information on the cultivation conditions can be found elsewhere (Wikieł *et al.*, to be published). Briefly, *D. alaskensis* were grown anaerobically under stirring of 100 rpm at 30°C in a VMN sulfate growth medium (composition in g/L: KH_2PO_4 0.5; NH_4Cl 1.0; $CaCl_2 \cdot 2H_2O$ 0.04; sodium citrate 0.3; casamino acids 2.0; Tryptone 2.0; Na_2SO_4 4.5; $MgSO_4 \cdot 7H_2O$ 0.06; $FeSO_4 \cdot 7H_2O$ 0.004; 1 mL/L modified Wolfes mineral elixir and 2 mL/L vitamin solution) supplemented with 2% NaCl (g/100mL) [2] and containing either 0.6% or 0.06% (g/100mL) lactate. After 72 h of growth, the suspension was centrifuged (9,400 g, 12 min, 4°C). One liter of supernatant was collected and immediately double filtered with 0.22 µm pore size cellulose acetate membrane, providing the solution of EPS_LB. Tightly bound EPS were extracted from the cell pellet as detailed elsewhere [Wikieł *et al.*, to be published]. The extraction was performed by use of Dowex® Marathon™C cation exchange resin, Na^+ form, 20–50 mesh size at 4°C [3]. It is advised to use an extraction buffer with an ionic strength/conductivity similar to that of the sample collected [3]. For that reason phosphate buffer saline (PBS) used as an extraction buffer was modified as follows: 2 mM $Na_2PO_4 \cdot 12H_2O$, 4 mM $NaH_2PO_4 \cdot H_2O$, 0.34 M NaCl, 1 mM KCl, pH=7.4 (adjusted with NaOH). The proportions between Dowex cation exchange resin and the PBS extraction buffer were equal to 1:2 (mass/vol). The EPS_LB and EPS_TB solutions were dialyzed overnight against running deionized water, using Spectra/Por 3.5 kDa membrane. The dialysis was continued for additional 48 h at 4°C under stirring at 100 rpm, with deionized water, which was changed 3 times a day. The volume of water used was at least 25 times greater than the volume of the EPS solution. Aliquots of the solutions were frozen, stored

at –20°C and thawed prior to use. The absence of cell lysis was controlled by an assay with 2–keto–3–deoxyoctonate (KDO) [4], a marker for the damage of the outer membrane and with intracellular material occurred. The assay indicated that cell lysis did not exceed 0.3%.

Loosely bound (LB) EPS were extracted from cultures of *Desulfovibrio desulfuricans* ATCC 27774. In brief, besides the VMN sulfate growth medium described above, a nitrate growth medium was used, in which 4.5 g/L Na_2SO_4, 0.06 g/L $MgSO_4 \cdot 7H_2O$, 0.004 g/L $FeSO_7 \cdot 7H_2O$ were replaced by 2.4 g/L $NaNO_3$, 0.05 g/L $MgCl_2 \cdot 6H_2O$, 0.003 g/L $FeCl_2 \cdot H_2O$, adjusted pH at 7.45 – 7.55 with concentrated KOH. The culture media were deaerated by bubbling with nitrogen gas (20 minutes for 100 mL of solution) and autoclaved (20 minutes, 121°C) on preparation day. A preculture of 24 h was used as inoculum (10% V/V) for 100 mL anaerobic bottles, which were incubated at 30°C for 6 days, with no agitation. The cultures were centrifuged (10,000 g; 15 min). The supernatants were collected and filtered close to a Bunsen burner with a 0.22 μm pore cellulose membrane. They were dialyzed with a 3.5 kDa membrane against distilled water for 16 h at room temperature and then three times for 2 h changing the water at 4°C. Aliquots were frozen, stored at –20°C and thawed prior to use.

Pseudomonas NCIMB 2021 was cultured in Difco™ marine broth 2216 medium (Becton, Dickinson and Company, 279110). The marine broth 2216 medium consists of (g/L): peptone 5.0; yeast extract 1.0; ferric citrate 0.1; NaCl 19.45; $MgSO_4$ 5.9; Na_2SO_4 3.24; $CaCl_2$ 1.8; KCl 0.55; $NaHCO_3$ 0.16; KBr 0.08; $SrCl_2$ 0.034; H_3BO_3 0.022; Na_2SiO_4 0.004; NaF 0.0024; NH_4NO_3 0.0016 and Na_2HPO_4 0.008. The final pH is 7.6 ± 0.2. Stored bacteria were inoculated on a marine agar 2216 plate at room temperature. A single bacterial colony was selected and cultured in 5 mL marine broth 2216 for 24 h (room temperature, agitation on a rotary shaker set at 120 rpm), and then sub-cultured in 200 ml Erlenmeyer flask (room temperature, agitation on a rotary shaker at 120 rpm). Bacteria supernatants (Sup) were collected at

the middle of exponential growth phase (optical density at 600 nm, OD_{600}, ≅ 1.0) or in the stationary phase (OD_{600} ≅ 1.8; 3 days culture), by 2 successive centrifugations (5,000 g, 5 min; Multifuge X1R centrifuge, Thermo Scientific). Sterilized marine broth (MB) medium was also used as a reference liquid. For certain experiments, the supernatants and the culture medium were dialyzed by centrifugation at 4,000 g using cellulose membrane 3,000 MWCO (Millipore UFC900308) to remove salts and small peptides.

4.6.2 UV-visible spectra

Representative UV-visible absorption spectra of solutions of interest, and spectra of BSA and DNA-028 are presented in Figure S1.

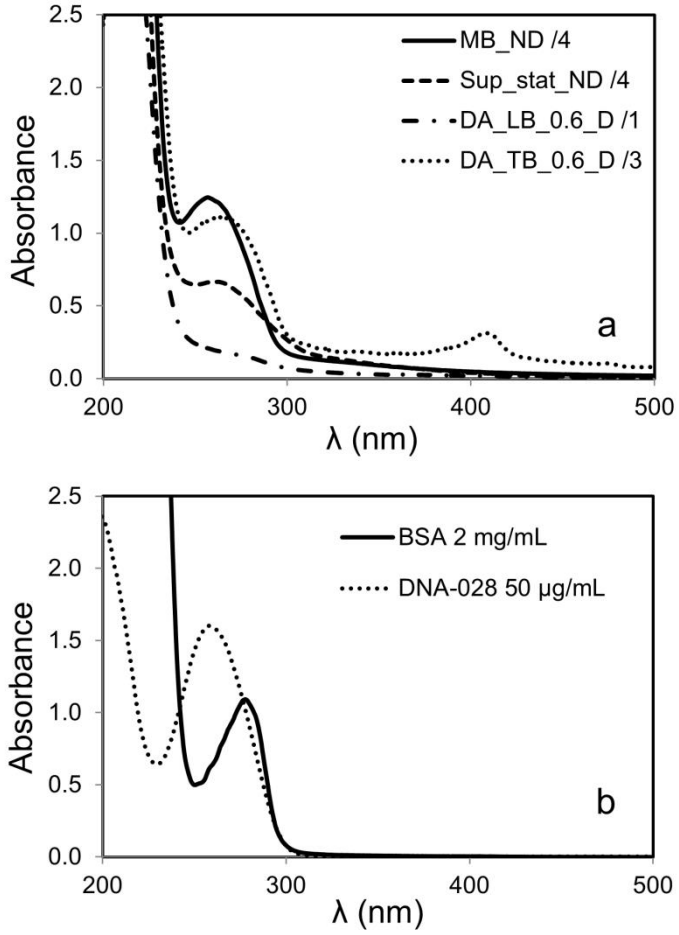

Figure S1. Representative UV-visible absorption spectra: (a) conditioning solutions: MB_ND, Sup_stat_ND, DA_LB_0.6_D and DA_TB_0.6_D (/dilution factor); (b) reference solutions: BSA 2 mg/mL, DNA-028 50 µg/mL.

Absorption coefficients of solutions of BSA and DNA-028 were determined at 280 and 260 nm from regression equations between the absorbance and the concentration. The values are given in Table S1.

Table S1. Absorption coefficients of BSA and DNA-028 at λ=280 nm and 260 nm.

	K_{280} (L·(g·cm)$^{-1}$)	K_{260} (L·(g·cm)$^{-1}$)
BSA	0.52	0.32
DNA-028	16.9	29.7

4.6.3 XPS measurements

4.6.3.1 Experimental

XPS measurements were carried out with a Kratos Axis Ultra spectrometer (Kratos Analytical, UK), using monochromated Al Kα radiation (powered at 10 mA and 15 kV) and an eight-channeltrons detector. The analyzed area was 700 μm × 300 μm. The vacuum in the analysis chamber was about 10^{-6} Pa. The direction of photoelectron collection was perpendicular to the sample surface. Charge stabilization was insured by using the Kratos Axis device. Survey spectra were recorded with 160 eV pass energy and the narrow scans with a 40 eV pass energy. In the latter conditions, the full width at half maximum (FWHM) of the Ag $3d_{5/2}$ peak of a standard silver sample was about 0.9 eV. The C 1s peak component due to carbon exclusively bound to carbon and hydrogen [**C**-(C,H)] was fixed at 284.8 eV to set the binding energy scale. The survey spectrum was recorded on each sample and the individual peaks were recorded at the high resolution when the element was detected on the survey spectrum. The C 1s peak was always recorded twice, at the beginning and at the end, to check for charge stability and absence of sample evolution as a function of time.

Quantification was made after linear background subtraction and peak area normalization on the basis of acquisition parameters, using experimental sensitivity factors and transmission factors given by the manufacturer. This provided elemental mole fractions, excluding hydrogen which is not detected by XPS. The C 1s, O 1s and N 1s peaks were decomposed with the CasaXPS program (Casa Software Ltd., U.K.) using a

Gaussian/Lorentzian (70/30) product function. Further details on peak decomposition are given below.

4.6.3.2 Results

The elemental compositions determined by XPS are given in Tables S2, S3, S4 and S5 for residues of liquid evaporation (EVAP), glass (Gl) substrates, polystyrene (PS) substrates and stainless steel (SS) substrates, respectively. They are expressed in mole fraction of the corresponding species, with respect to the sum of all elements except hydrogen, which is not detected by XPS. Some measurements were duplicated with independent samples. For one sample of Gl conditioned with the supernatant collected in exponential phase (Table S3, Sup_expo_ND) the concentration of salts indicated ineffective rinsing. Depending on the sample, the position of the S 2p peak was near 169 ev, which is typical of sulfate, or near 162 – 163 eV, which is typical of a reduced form, typically sulfide in protein [5]. Fe in SS samples was quantified with the Fe $2p_{3/2}$ component, using a linear baseline as shown before [6]. The assignment of the small Si 2p peak found on samples other than SS and Gl (silica dust contamination, adsorption of silicone compounds) will not be considered here.

Figure 1 presents the range of shapes observed for O 1s, N 1s and C 1s peaks. These were decomposed with constraints insuring the consistency required to make quantitative comparison between samples [7, 8], and the results of peak decompositions are presented in Table S2 to S5. For the C 1s peak, the possibility of 4 components was allowed, with the addition, for PS samples, of a shake-up due to $\pi \rightarrow \pi^*$ transition of the aromatic ring [9], found near 291.5 eV. The 4 components of the same peak were imposed to have the same FWHM; fitting gave FWHM between 1.2 and 1.5 eV for Gl and SS samples, close to 1.2 eV for PS samples and between 1.3 and 1.6 eV for EVAP samples. The C 1s component typical of carbon bound only to carbon and hydrogen [**C**-(C,H)] was fixed at 284.8 eV. A second component

was found at 286.1 – 286.3 eV (noted 286.2 eV below), which is due to carbon making a single bond with oxygen or nitrogen [**C**-(O,N)] in alcohol, amine or amide. A third component was close to 288.0 eV, due to carbon making two single bonds with oxygen in acetal [C-O-**C**-O-C, one per hexose unit in polysaccharides] or making one double bond with oxygen in amide [N-**C**=O]. Some samples showed a weak fourth component at 288.8 – 289.2 eV (noted 289.0 eV below), due to carbon making one double bond and one single bond with oxygen [O=**C**-O] in carboxyl or ester functions [7, 8, 10].

The O 1s peak of EVAP and PS samples was decomposed into two components (Tables S2 and S4), with the constraints of the same FWHM for both of them [10, 11]. The major component in the range 531.2 to 531.8 eV is mainly due to oxygen doubly bound to carbon [**O**=C] in amide, carboxyl or ester; another component near 533.0 eV is mainly due to oxygen singly bound to carbon [**O**-C] in alcohol, carboxyl or ester, or to oxygen of ether [C-**O**-C]. Their FWHM was in the range of 1.6 – 2 eV. Note that inorganic compounds which are present in small but significant amounts may bring additional contributions, particularly near 531.5 eV. SS samples showed (Figure 1) the presence of a third component at lower binding energy, due to metal oxides [6]. In peak fitting, the following constraints were imposed: intensity of this peak governed by the low binding energy edge of the peak without constraint regarding the FWHM; two other components with equal FWHM. Accordingly, the 3 components were found near 529.7, 531.2 and 532.8 eV, respectively. The component near 531.2 eV is attributed to the overlap of oxygen doubly bound to carbon and hydroxide of SS substrate [6]. The Gl samples showed a broad O 1s peak near 532.3 eV, with a tail on the low binding energy side. It is due to the overlap of inorganic oxides or hydroxides and organic compounds and no reliable decomposition could be performed.

The N 1s peak was decomposed with the following constraints: possibility of 3 components for SS samples and 2 components for other

samples, same FWHM of all components of the same peak. Fitting gave FWHM values between 1.5 and 2.0 eV depending on the sample. The main N 1s component was found at 399.8 – 400.2 eV, typical of non-protonated amine and of amide (N_{np}); a weak component was often observed at a higher binding energy (>401 eV) and attributed to protonated amine (N_{pr}). The sum of these components is the total organic nitrogen, N_{org}. SS samples showed a third component at lower binding energy (<398 eV) which was attributed to a reduced form of nitrogen due to the substrate.

Table S2. XPS analysis of residues of evaporation (EVAP) of EPS from *D. alaskensis* (DA), and culture medium (MB) and culture supernatants (Sup) of *Pseudomonas* NCIMB 2021: surface concentration (mole fraction with respect to all elements except hydrogen, %) of elements and functions defined by the indicated binding energy (E_b, eV) of peak components.

EVAP	C 1s					O 1s			N 1s			P 2p	S 2p	Na 1s	Na 2s	K 2p3/2	Ca 2p	Cl 2p	Si 2p	B 1s	Al 2p	Fe $2p_{3/2}$
E_b (eV)	289.0	288.0	286.2	284.8	total	532.7	531.5	total	401.2	399.8	total	133.2		1071.1	63.4	292.7		197.8	d	192.5	74.1	≈710
DA_LB_0.06_D	1.0	15.5	19.6	27.2	63.3	3.2	17.6	20.7	bdl	12.7	12.7	0.6	0.43 a	1.2	NM	NM	0.38	NM	0.58	NM	NM	NM
DA_LB_0.6_D	0.7	12.9	16.6	33.9	64.1	3.6	15.9	19.4	bdl	10.2	10.2	1.1	0.55 c	2.7	NM	NM	0.23	0.48	1.17	NM	NM	NM
DA_TB_0.06_D	5.1	15.8	22.5	23.2	66.5	4.6	12.1	16.7	3.3	11.7	15.0	0.3	0.62 a	NM	0.2	NM	0.12	NM	0.50	NM	NM	NM
DA_TB_0.6_D	bdl	14.6	18.1	32.2	65.0	2.3	15.3	17.6	bdl	13.9	13.9	0.8	0.52 a	NM	1.5	NM	0.51	NM	0.15	NM	NM	NM
MB_D	bdl	11.5	17.7	28.0	57.2	3.8	17.0	20.8	0.5	9.7	10.2	0.2	0.64 b	NM	3.4	0.21	0.37	1.33	4.08	0.98	0.38	0.14
MB_D	bdl	12.7	18.0	29.2	59.9	3.6	14.9	18.5	0.5	10.4	10.9	0.2	0.43 b	NM	3.2	bdl	0.34	1.62	3.54	0.70	0.33	0.29
Sup_expo_D	bdl	14.6	21.5	27.4	63.5	3.7	14.6	18.3	0.8	11.3	12.1	bdl	0.48 b	NM	2.4	bdl	0.19	2.33	0.22	bdl	bdl	0.57
Sup_expo_D	bdl	16.6	23.6	21.4	61.5	4.4	15.1	19.5	1.0	13.0	14.0	bdl	0.40 b	NM	2.9	bdl	0.16	1.28	0.35	bdl	bdl	bdl
Sup_stat_D	bdl	14.9	21.5	28.1	64.6	5.3	14.9	20.2	bdl	12.8	12.8	0.1	0.33 b	NM	1.3	bdl	0.28	0.13	0.15	bdl	bdl	0.20
Sup_stat_D	bdl	13.5	20.0	24.8	58.3	4.0	20.0	23.9	0.5	10.4	10.9	0.0	0.29 b	NM	2.0	bdl	0.23	0.46	2.89	0.39	0.22	0.17

bdl, below detection limit; NM, not measured

a, S 2p near 163.5 eV

b, S 2p near 168.5 eV

c, S 2p near 168.5 and 163.5 eV

d, Si 2p in range of 102 to 103 eV

Table S3. XPS analysis of glass (Gl) substrates cleaned, conditioned by LPS, by EPS from *D. alaskensis* (DA) and *D. desulfuricans* (DD), and by culture medium (MB) and culture supernatants (Sup) of *Pseudomonas* NCIMB 2021: surface concentration (mole fraction with respect to all elements except hydrogen, %) of elements and functions defined by the indicated binding energy (E_b, eV) of peak components.

Gl	C 1s					O 1s	N 1s			Si 2p	B 1s	Al 2p	Ti 2p	Zn $2p_{3/2}$	Fe $2p_{3/2}$	Na 2s	K 2p	Ca 2p	Cl 2p
E_b (eV)	288.8	288.0	286.2	284.8	Total	Total	402.0	400.0	Total	103	192.7	74.2		1022	~710	63.7	293.5		198.5
Cleaned	0.2	0.6	2.9	8.5	12.3	50.9	0.08	0.25	0.34	28.3	3.1	1.6	0.47	0.17	NM	2.1	0.74	NM	NM
LPS	0.2	0.8	2.8	9.5	13.2	48.9	0.17	0.71	0.87	26.8	3.5	1.7	0.60	0.35	NM	2.8	1.23	0.02	NM
DA_LB_0.06_D	0.3	1.3	3.6	14.5	19.7	44.5	0.25	1.48	1.72	25.2	3.0	1.6	0.47	NM	NM	2.3	0.99	0.05	NM
DA_LB_0.6_D		1.5	3.0	9.5	14.0	47.7	0.10	1.47	1.57	26.2	3.3	1.7	0.57	0.35	NM	3.1	1.38	0.12	NM
DA_TB_0.06_D		5.1	6.9	18.6	30.6	37.0	0.32	4.94	5.26	20.2	2.3	1.4	0.35	NM	NM	2.0	0.78	0.05	NM
DA_TB_0.6_D		5.2	6.8	12.0	24.1	40.9	0.27	5.34	5.61	21.9	2.6	1.3	0.40	0.21	NM	2.1	0.91	0.03	NM
DD_LB_SO_4_D		0.7	3.7	8.8	13.2	47.5	0.22	0.73	0.95	28.4	3.3	1.8	0.54	0.23	NM	2.8	1.30	NM	NM
DD_LB_NO_3_D		0.8	3.8	8.7	13.3	43.5	0.30	1.01	1.30	26.9	3.1	1.8	0.47	0.21	NM	2.9	6.40	NM	NM
MB_ND	0.6	1.2	3.5	9.8	15.2	49.0	0.22	1.55	1.77	24.5	2.8	1.5	0.45	0.26	NM	3.3	1.10	NM	0.12
MB_ND		3.6	6.1	15.6	25.3	40.7	0.20	3.43	3.63	26.8	0.3	0.9	0.15	0.05	0.16	2.0	bdl	0.07	bdl
MB_D		1.2	4.2	10.8	16.2	46.6	0.23	1.26	1.50	27.2	3.0	1.6	0.45	0.18	0.06	2.4	0.82	bdl	bdl
Sup_expo_ND	0.7	2.0	4.7	13.5	21.0	44.5	0.16	2.14	2.30	22.0	2.6	1.3	0.41	0.20	1.31	3.2	0.99	NM	0.27
Sup_expo_ND	3.3	3.5	8.2	22.5	37.4	20.0	0.43	4.17	4.60	7.1		NM	0.06	0.03	0.17	15.3	0.31	0.48	13.4
Sup_expo_D	0.3	1.2	4.3	10.5	16.4	46.7	0.36	1.36	1.71	27.1	2.7	1.5	0.44	0.18	0.09	2.4	0.79	bdl	bdl
Sup_stat_ND	1.6	2.9	7.0	17.0	28.4	38.2		2.46	2.46	19.8	2.2	1.2	0.34	0.10	1.87	3.8	0.74	0.13	0.64
Sup_stat_ND	1.1	1.5	5.0	15.3	22.9	40.8	0.23	1.70	1.93	23.8	2.5	1.5	0.40	0.15	0.60	3.4	0.93	0.16	0.83
Sup_stat_D	0.3	0.6	4.0	9.6	14.5	47.2	0.34	0.81	1.14	27.8	3.0	1.8	0.47	0.19	bdl	3.0	0.92	0.03	bdl
Phosphorous and sulfur concentrations below 0.2 %																			

Table S4. XPS analysis of polystyrene (PS) substrates cleaned, conditioned by LPS, by EPS from *D. alaskensis* (DA) and *D. desulfuricans* (DD), and by culture medium (MB) and culture supernatants (Sup) of *Pseudomonas* NCIMB 2021: surface concentration (mole fraction with respect to all elements except hydrogen, %) of elements and functions defined by the indicated binding energy (E_b, eV) of peak components.

PS	C 1s						O 1s				N 1s			S 2p	Na 1s	Fe $2p_{3/2}$	Cl 2p	Si 2p
E_b (eV)	291.5	288.7	288.0	286.2	284.8	Total	533	531.7	529.9	Total	401.8	400.2	Total		1071	710.6	198.7	c
Cleaned	9.2				90.6	99.7	0.3	bdl		0.27			bdl	NM	NM	NM	NM	NM
LPS	4.9			3.0	87.5	95.3	0.6	2.1		2.8	0.1	1.8	1.9	NM	NM	NM	NM	NM
DA_LB_0.06_D	4.9		1.8	6.0	79.9	92.6	0.9	3.4		4.3		3.0	3.0	NM	0.18	NM	NM	NM
DA_LB_0.6_D	5.3		1.3	5.2	81.4	93.2	1.0	2.7		3.7		2.5	2.5	b 0.06	NM	NM	NM	0.54
DA_TB_0.06_D	3.2		2.6	7.3	77.4	90.5	1.0	4.2		5.2	0.2	4.1	4.3	NM	NM	NM	NM	NM
DA_TB_0.6_D	2.6		3.8	8.3	72.3	87.0	1.1	5.8		6.9	0.2	5.6	5.8	b 0.22	NM	NM	NM	0.07
DD_LB_SO_4_D	4.9		bdl	4.01	86.9	95.8	0.6	1.8		2.4		1.6	1.6	NM	NM	NM	NM	0.29
DD_LB_NO_3_D	3.6		1.30	5.75	82.2	92.8	1.1	2.9		4.1	0.1	2.6	2.7	NM	NM	NM	NM	0.43
MB_ND	2.8		2.1	6.5	78.6	90.0	1.4	3.9		5.3		3.9	3.9	NM	0.52	NM	0.29	NM
MB_ND	1.8	1.1	2.2	7.7	67.3	80.1	2.3	6.0		8.3	0.1	3.7	3.8	a 0.44	3.15	bdl	3.81	0.35
MB_D	3.1	0.5	1.7	6.5	79.0	90.7	1.5	3.8		5.2	0.2	3.2	3.4	b 0.15	bdl	bdl	bdl	0.50
Sup_expo_ND	3.6	0.7	1.4	5.8	77.7	89.2	1.3	4.5	0.3	6.1		3.1	3.1	a 0.11	0.56	0.45	0.42	NM
Sup_expo_ND	1.4	1.0	2.6	8.6	63.9	77.6	3.1	7.7	1.1	12	0.2	3.3	3.5	a 0.33	2.04	0.98	2.77	0.82
Sup_expo_D	3.2	0.3	1.4	5.9	80.0	90.7	1.4	4.0		5.4	0.2	2.6	2.9	b 0.10	bdl	0.10	bdl	0.79
Sup_stat_ND	2.9	0.9	1.7	6.7	75.8	88.0	2.5	4.8	0.3	7.6		3.1	3.1	NM	0.42	0.35	0.47	0.11
Sup_stat_ND	3.1	0.7	1.7	6.4	75.8	87.7	2.2	4.7		6.9	0.1	2.9	3.0	a 0.22	0.52	bdl	1.05	0.67
Sup_stat_D	4.3	0.2	0.9	4.4	83.6	93.5	1.0	2.7		3.7	0.1	2.2	2.3	bdl	bdl	bdl	bdl	0.51
bdl, below detection limit; NM, not measured																		
a, S 2p near 169.0 eV																		
b, S 2p near 163.5 eV																		
c, Si 2p in range of 102 to 103 eV																		
Phosphorous concentration below 0.1 %																		

Table S5. XPS analysis of stainless steel (SS) substrates UVO treated and acetone cleaned (cl), conditioned by LPS, by EPS from *D. alaskensis* and *D. desulfuricans* (DA), and by culture medium (MB) and culture supernatants (Sup) of *Pseudomonas* NCIMB 2021: surface concentration (mole fraction with respect to all elements except hydrogen, %) of elements and functions defined by the indicated binding energy (E_b, eV) of peak components.

SS	C 1s					O 1s				N 1s				P 2p	S 2p	Fe $2p_{3/2}$	Cr $2p_{3/2}$	Mn $2p_{1/2}$	Zn $2p_{3/2}$	Na 1s	Ca 2p	Cl 2p	Si 2p
E_b (eV)	289.0	288.0	286.2	284.8	Total	532.8	531.2	529.7	Total	401.8	400.0	c	Total	~133		710.5	576.5	~653	1021.5	1071.5		198.4	101.5
UVO	0.9	1.9	2.8	33.4	39.1	2.5	19.8	19.3	41.7	0.1	0.2	0.1	0.4	0.52	b 0.52	9.3	2.1	1.01	0.41	1.42	0.27	0.16	3.1
UVO\LPS	1.5	3.6	7.4	25.2	37.6	4.0	18.0	20.7	42.7		3.0	0.2	3.1	1.25	NM	9.9	2.1	0.33	NM	NM	bdl	NM	3.0
UVO\DD_LB_SO_4_D	1.3	3.2	6.0	27.6	38.0	3.5	24.8	16.7	44.9	0.2	1.8	0.1	2.1	2.88	NM	8.9	2.4	0.44	NM	NM	0.26	NM	NM
UVO\DD_LB_NO_3_D	1.8	2.9	7.5	27.1	39.4	3.0	24.4	16.0	43.5	0.4	2.2	0.1	2.7	2.55	NM	9.0	2.3	0.42	NM	NM	0.25	NM	NM
cl\DD_LB_SO_4_D	3.2	2.1	7.0	34.5	46.9	4.2	18.6	13.9	36.7	0.2	1.9	0.3	2.3	0.94	NM	9.1	3.8	0.17	NM	NM	0.16	NM	NM
cl\DD_LB_NO_3_D	2.6	3.1	8.6	36.1	50.4	4.3	17.3	12.7	34.4	0.3	2.7	0.2	3.2	1.01	NM	7.6	3.1	0.19	NM	NM	0.16	NM	NM
UVO\MB_ND	1.2	3.3	8.3	23.7	36.5	5.7	19.0	19.2	43.9	0.1	2.0	0.2	2.2	1.39	NM	9.8	2.1	0.26	NM	0.36	0.11	0.30	3.2
UVO\MB_ND	1.8	3.3	8.0	22.6	35.7	4.9	22.6	13.9	41.4	0.1	1.8	0.0	1.9	2.20	a 0.73	7.2	1.7	0.25	0.06	1.74	0.78	3.47	2.8
UVO\MB_D	1.6	4.6	8.8	23.4	38.3	2.8	21.1	18.0	41.9	0.1	3.6	0.2	3.9	1.34	b 0.43	8.6	2.1	0.45	0.04	bdl	bdl	bdl	2.9
UVO\Sup_expo_ND	2.3	5.5	10.0	22.6	40.5	3.7	20.2	14.9	38.8	0.2	4.3	0.1	4.6	bdl	a 0.56	7.5	1.3	0.31	0.12	0.85	0.42	2.39	2.6
UVO\Sup_expo_ND	2.0	5.3	10.8	24.4	42.5	5.0	17.5	12.8	35.3	0.2	3.5		3.7	0.38	a 0.66	5.9	1.2	0.19	bdl	2.68	0.48	4.84	2.2
UVO\Sup_expo_D	1.3	6.4	10.5	21.3	39.4	3.1	20.3	17.6	41.1	0.2	4.6	0.1	5.0	0.56	b 0.43	8.1	2.0	0.20	0.09	bdl	bdl	bdl	3.1
UVO\Sup_stat_ND	2.0	6.5	11.1	29.3	48.8	5.4	16.9	13.3	35.6	0.2	3.3	0.2	3.7	0.43	NM	6.5	1.0	0.19	NM	0.36	0.31	0.76	2.4
UVO\Sup_stat_ND	2.2	6.1	13.6	21.1	43.0	9.7	16.8	12.7	39.1	0.1	3.4	0.1	3.5	0.56	b 0.54	5.5	1.2	0.18	0.03	1.20	0.54	2.12	2.4
UVO\Sup_stat_D	1.7	5.5	10.3	22.6	40.2	3.0	19.8	17.6	40.3	0.1	4.4	0.2	4.7	0.52	b 0.62	8.0	1.9	0.54	0.08	bdl	bdl	bdl	3.1
cl\MB_ND	2.5	4.8	9.3	28.4	45.0	4.3	18.8	11.9	35.0	0.2	3.6	0.2	4.0	1.02	NM	7.8	2.8	0.15	NM	1.01	0.30	1.00	1.9
cl\MB_ND	1.7	4.5	9.4	29.9	45.5	4.3	18.2	10.1	32.6	0.2	3.1	0.2	3.4	0.97	b 0.98	6.3	2.4	0.14	bdl	1.67	0.51	3.40	2.1
cl\MB_D	2.4	4.8	9.8	27.8	44.7	3.6	18.8	13.6	35.9	0.2	3.7	0.2	4.1	0.59	b 0.75	8.3	3.1	0.16	bdl	bdl	bdl	bdl	2.3
cl\Sup_expo_ND	2.6	5.3	10.1	30.9	49.0	4.0	18.5	10.8	33.3	0.1	3.8	0.1	4.1	NM	a 0.10	6.9	2.2	0.08	bdl	1.01	0.36	1.08	1.8
cl\Sup_expo_ND	2.2	5.9	11.7	30.8	50.6	5.5	15.0	7.7	28.2	0.2	4.0	0.2	4.3	0.28	b 0.80	4.3	1.4	bdl	bdl	2.91	0.42	4.90	1.8
cl\Sup_expo_D	2.4	4.9	10.0	30.4	47.6	3.3	17.9	12.7	33.9	0.3	3.8	0.2	4.3	0.43	b 0.77	7.5	3.0	0.18	bdl	bdl	bdl	bdl	2.3
cl\Sup_stat_ND	3.0	5.4	11.6	35.8	55.8	5.2	15.1	9.6	29.9	0.1	3.7	0.2	4.0	0.33	NM	5.5	1.5	0.14	NM	0.38	0.26	0.51	1.6
cl\Sup_stat_ND	2.1	6.5	12.8	29.0	50.3	8.0	15.4	9.0	32.4	0.1	3.6	0.2	3.8	0.49	b 0.81	4.6	1.5	0.15	bdl	1.23	0.57	2.21	1.8
cl\Sup_stat_D	3.1	3.4	9.3	25.8	41.7	3.0	19.9	14.8	37.7	0.2	3.6	0.3	4.1	0.32	b 0.86	9.0	3.6	0.19	bdl	bdl	bdl	bdl	2.6

bdl, below detection limit

NM, not measured

a, S 2p near 169 eV

b, S 2p near 162 eV

c, N 1s component in range of 397 to 398 eV

4.6.4 Nature of the adlayer formed by conditioning

Table S6 presents the scheme of the procedure used for converting the concentrations of markers (mole %) into concentrations of relevant chemical moieties (mass %), which provide a more practical presentation of the surface composition. The moieties considered were amide [HC-NH-(C=O)] quantified by N_{org} as a marker, CH_2 quantified by $C_{284.8}$ component, additional carbon C_{add} quantified by [$C_{ox} - 2*N_{org}$] and additional organic oxygen O_{add} quantified by [$O_{org} - N_{org} = C_{ox} - 2*N_{org}$].

Multiplying the molar concentration of marker (X, mol/100 mol) by the molar mass (MM) of the relevant model constituent provides its concentration W, in g/100 mol. Dividing W of each compound by the sum of W for all compounds (Tot) and multiplying by 100 finally gives the mass concentration in % of the constituent in the volume probed by XPS.

Table S6. Computation scheme used for converting marker concentrations (molar percentage of relevant element) into mass concentration (%) of model compounds.

Model constituents			W = X*MM (c)	W*100/Tot constituent concentration [mass%]
Nature	MM (a)	Name and concentration X (b)		
HC-NH-C=O	56.02	N_{org}	●●●	●●●
CH_2	14.01	$C_{284.8}$	●●●	●●●
additional C_{ox}	12.01	C_{ox} - 2N_{org}	●●●	●●●
additional O_{org}	16.00	C_{ox} - 2N_{org}	●●●	●●●
Total	–	–	Tot = ●●●	100

(a) Molar mass of constituent

(b) Name of marker, concentration X deduced from XPS spectra (mole / 100 moles excluding hydrogen)

(c) In gram of constituent / 100 moles of elements other than hydrogen

●●● From measurements

The results of the XPS analysis converted into weight % of amide, as defined above, CH_2, additional carbon C_{add} and additional organic oxygen O_{add} are given in Tables S7 and S8. They reflect the proportion of the model entities in the adlayer, except for PS samples.

In order to figure out the amounts of organic matter concerned, and to compare them between different modes of conditioning of the same subtrate, Tables S7 and S8 give also the sum of mole fractions of carbon, oxygen and nitrogen in the form of organic compounds, computed with respect to the sum all elements. For that purpose, the concentration of oxygen present in the adlayer formed on glass and stainless steel could be included by using the following relationship justified in the paper

$$C + O_{org} + N_{org} \cong C + C_{ox}$$

Table S7. Global presentation of the results of the XPS analysis of residues of evaporation (EVAP) of the solutions indicated and of glass conditioned by the solutions: sum of the mole fractions (% with respect to the sum of all elements except hydrogen) of carbon, organic oxygen and organic nitrogen evaluated by C + C_{ox}, and mass proportion of model moieties amide [HC-NH-(C=O)], CH_2, additional carbon C_{add} and additional organic oxygen O_{add} in the organic adlayer.

Sample		C + C_{ox}	Proportion in adlayer (weight %)			
		Mole fraction (%)	Amide	CH_2	C_{add}	O_{add}
EVAP	DA_LB_0.06_D	99.4	51.3	27.4	9.1	12.2
	DA_LB_0.6_D	94.2	43.5	36.0	8.8	11.7
	DA_TB_0.06_D	109.9	54.7	21.1	10.4	13.8
	DA_TB_0.6_D	97.7	57.1	33.0	4.3	5.7
	MB_D	86.4	47.0	32.4	8.8	11.8
	MB_D	90.6	48.1	32.2	8.4	11.2
	Sup_expo_D	99.5	48.6	27.5	10.3	13.7
	Sup_expo_D	101.6	54.9	21.0	10.3	13.7
	Sup_stat_D	101.1	50.6	27.8	9.3	12.3
	Sup_stat_D	91.8	47.3	27.1	11.0	14.6
Glass	Cleaned	16.0	8.4	53.1	16.5	22.0
	LPS	17.0	20.5	55.9	10.1	13.5
	DA_LB_0.06_D	25.0	27.6	57.9	6.2	8.3
	DA_LB_0.6_D	18.6	33.6	50.8	6.7	8.9
	DA_TB_0.06_D	42.5	49.4	43.8	2.9	3.8
	DA_TB_0.6_D	36.2	62.1	33.2	2.0	2.7
	DD_LB_SO_4_D	17.6	21.6	50.2	12.1	16.1
	DD_LB_NO_3_D	17.9	29.0	48.3	9.7	12.9
	MB_ND	20.6	34.4	47.5	7.8	10.4
	MB_ND	35.0	41.5	44.7	5.9	7.9
	MB_D	21.6	27.7	50.1	9.5	12.7
	Sup_expo_ND	28.4	32.4	47.7	8.5	11.4
	Sup_expo_ND	52.4	35.1	42.9	9.4	12.5
	Sup_expo_D	22.2	30.9	47.5	9.3	12.3
	Sup_stat_ND	39.8	24.6	42.6	14.0	18.7
	Sup_stat_ND	30.4	25.4	50.3	10.4	13.9
	Sup_stat_D	19.4	23.6	49.7	11.5	15.3

Table S8. Global presentation of the results of the XPS analysis of polystyrene and stainless steel treated by UV-Ozone or just cleaned with acetone, and conditioned by the indicated solutions: sum of the mole fractions (% with respect to the sum of all elements except hydrogen) of carbon, organic oxygen and organic nitrogen evaluated by $C + C_{ox}$, and mass proportion of model moieties amide [HC-NH-(C=O)], CH_2, additional carbon C_{add} and additional organic oxygen O_{add} in the organic adlayer.

Sample		$C + C_{ox}$	Proportion in adlayer (weight %)			
		Mole fraction (%)	Amide	CH_2	C_{add}	O_{add}
PS	Cleaned		0.0	100.0	0.0	0.0
	LPS		7.9	94.0	-0.8	-1.0
	DA_LB_0.06_D		11.8	84.4	1.6	2.1
	DA_LB_0.6_D		10.0	87.0	1.3	1.7
	DA_TB_0.06_D		16.9	80.3	1.2	1.6
	DA_TB_0.6_D		23.5	75.6	0.4	0.5
	DD_LB_SO_4_D		6.3	92.0	0.8	1.0
	DD_LB_NO_3_D		10.6	85.9	1.5	2.0
	MB_ND		15.9	82.5	0.7	0.9
	MB_ND		16.6	75.8	3.3	4.3
	MB_D		13.7	82.7	1.6	2.1
	Sup_expo_ND		12.9	83.6	1.5	2.0
	Sup_expo_ND		15.4	72.8	5.1	6.7
	Sup_expo_D		11.7	84.7	1.6	2.1
	Sup_stat_ND		12.7	80.9	2.8	3.7
	Sup_stat-ND		12.2	81.8	2.6	3.4
	Sup_stat_D		9.3	88.8	0.8	1.1
SS-UVO		44.7	2.4	74.8	9.8	13.0
	LPS	50.1	23.7	50.3	11.2	14.9
	DD_LB_SO_4_D	48.5	16.4	56.9	11.4	15.2
	DD_LB_NO_3_D	51.7	19.6	52.5	11.9	15.9
	MB_ND	49.3	16.5	48.1	15.2	20.2
	MB_ND	48.8	15.3	46.4	16.4	21.9
	MB_D	53.3	28.1	43.9	12.0	16.0
	Sup_expo_ND	58.3	30.6	38.8	13.1	17.5
	Sup_expo	60.7	24.2	40.1	15.3	20.3
	Sup_expo_D	57.5	33.7	37.0	12.6	16.8
	Sup_stat	68.4	20.4	42.8	15.8	21.0
	Sup_stat	64.9	21.2	32.5	19.9	26.5
	Sup_stat_D	57.7	31.3	39.2	12.6	16.8
SS-cl	DD_LB_SO_4_D	59.2	14.1	58.3	11.8	15.8
	DD_LB_NO_3_D	64.7	18.7	55.8	10.9	14.6
	MB_ND	61.6	24.6	46.1	12.6	16.7
	MB_ND	61.1	21.4	48.9	12.7	16.9
	MB_D	61.7	24.9	45.2	12.8	17.1
	Sup_expo_ND	67.1	23.6	46.1	13.0	17.3
	Sup_expo_ND	70.4	23.7	43.8	13.9	18.6
	Sup_expo_D	64.9	25.4	46.8	12.0	15.9
	Sup_stat_ND	75.9	20.2	47.1	14.0	18.7
	Sup_stat_ND	71.7	20.5	40.4	16.8	22.4
	Sup_stat_D	57.5	26.5	44.9	12.3	16.4

4.6.5 References

[1] Feio MJ, Zinkevich V, Beech IB, Llobet-Brossa E, Eaton P, Schmitt J and Guezennec J, 2004, *Desulfovibrio alaskensis sp. nov.*, a sulphate-reducing bacterium from a soured oil reservoir, Int. J. Syst. Evol. Microbiol., 54, 1747-1752.

[2] Zinkevich V and Beech IB, 2000, Screening of sulfate-reducing bacteria in colonoscopy samples from healthy and colitic human gut mucosa, FEMS Microbiol. Ecol., 34, 147-155.

[3] Frølund B, Palmgren R, Keiding K and Nielsen PH, 1996, Extraction of extracellular polymers from activated sludge using a cation exchange resin, Water Res., 30, 1749-1758.

[4] Burton K, 1956, A study of the conditions and mechanism of the diphenylamine reaction for the colorimetric estimation of deoxyribonucleic acid, Biochem. J., 62, 315-323.

[5] Caillou S, Boonaert CJP, Dewez J-L and Rouxhet PG, 2008, Oxidation of proteins adsorbed on hemodialysis membranes and model materials, J. Biomed. Mater. Res. B Appl. Biomater., 84B, 240-248.

[6] Landoulsi J, Genet MJ, Richard C, El Kirat K, Pulvin S and Rouxhet PG, 2008, Evolution of the passive film and organic constituents at the surface of stainless steel immersed in fresh water, J. Colloid Interface Sci., 318, 278-289.

[7] Genet MJ, Dupont-Gillain CC and Rouxhet PG, 2008, XPS Analysis of Biosystems and Biomaterials, in: Matijevic E (Ed.) Medical Applications of Colloids, Springer, New York, 177-307.

[8] Rouxhet PG and Genet MJ, 2011, XPS analysis of bio-organic systems, Surf. Interface Anal., 43, 1453-1470.

[9] Dupont-Gillain CC, Adriaensen Y, Derclaye S and Rouxhet PG, 2000, Plasma-Oxidized Polystyrene: Wetting Properties and Surface Reconstruction, Langmuir, 16, 8194-8200.

[10] Rouxhet PG, Misselyn-Bauduin AM, Ahimou F, Genet MJ, Adriaensen Y, Desille T, Bodson P and Deroanne C, 2008, XPS analysis of food products: toward chemical functions and molecular compounds, Surf. Interface Anal., 40, 718-724.

[11] Dufrêne YF, Vermeiren H, Vanderleyden J and Rouxhet PG, 1996, Direct evidence for the involvement of extracellular proteins in the adhesion of *Azospirillum brasilense*, Microbiology, 142, 855-865.

Chapter 5

Conclusions

5.1 General conclusion

The strategy used in this thesis to prevent biofouling is illustrated in Figure 1. In general, both molecular fouling and microfouling were prevented or reduced significantly on OPA-conditioned Ti and stainless steel (SS) with pre-adsorption of Pluronic F68 (Plu) copolymer in comparison to native metal oxides or to metal oxides solely conditioned with OPA or Plu. The reduction of biofouling is attributed to the brush structure (as illustrated in Figure 1) adopted by Plu on hydrophobized Ti and SS, at the origin of repelling properties.

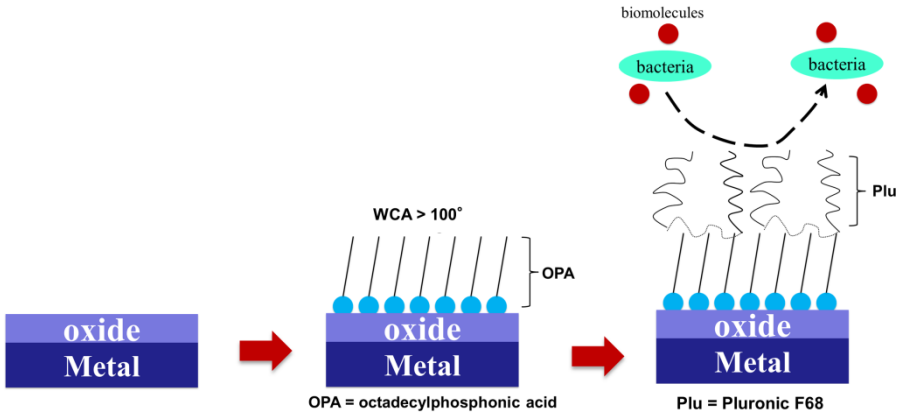

Figure 1. Schematic representation of the surface modification strategy used in this thesis to prevent biofouling.

5.1.1 Modification of metal oxide surface to prevent molecular and microfouling

Self-assembly of OPA was successfully applied to obtain a hydrophobic coating on Ti and SS. This process also replaced the organic contaminants on native Ti and SS, which imposed a standardized surface layer on Ti and SS for further copolymer coating. The sole OPA coating is however not sufficient to prevent molecular and microfouling.

Plu adsorption on OPA-conditioned Ti and SS was confirmed by the QCM results. The PEO chain density obtained here (0.34 – 0.54 PEO

chain·nm^{-2}) is comparable to the value obtained by adsorption of PLL-g-PEG, a well-known antifouling compound, on metal oxide surfaces. The subsequent adsorption of tested proteins (BSA, fibrinogen and cytochrome C) and polysaccharides (dextran) was prevented by adsorbed Plu on OPA-conditioned Ti and SS. On the contrary, all proteins and dextran adsorbed on native and Plu-conditioned Ti and SS surfaces, with varying level.

The results of competitive adsorption, analyzed by ToF-SIMS and XPS, agree with each other, showing the reduction of BSA adsorption on OPA-conditioned Ti and SS in the presence of Plu. This might be attributed to the higher adsorption affinity between Plu and hydrophobic OPA-conditioned surfaces in comparison to BSA. However, the reduction of BSA adsorption in the presence of Plu is not observed on native Ti and SS, demonstrating that making the surface hydrophobic using OPA assembly is a necessary step to increase Plu affinity for the surface and anchor Plu in the adequate conformation on metal oxide surfaces.

Pseudomonas 2021 was chosen as a model bacterium for microfouling tests. The bacterial adhesion was performed in a flow chamber, with the great advantage of allowing the effect of different surface treatments on bacterial adhesion to be compared in a single experiment. The fluorescence images showed that pre-adsorption of Plu on OPA-conditioned SS reduces the adhesion of *Pseudomonas* 2021 by a factor of 10 compared to the control experiments, for bacteria harvested both in exponential and stationary phase.

It is believed that the conformation more than the amount of adsorbed Plu plays an important role in reducing adhesion of *Pseudomonas* 2021, and this conformation strongly depends on the hydrophobicity of the underlying substrate.

In another approach, it was shown that adhered bacteria were partially removed on OPA-conditioned SS using Plu-containing solution for rinsing, but not on native SS. This might be attributed to the high affinity of

Plu for OPA-conditioned hydrophobic surface. This result is related to the above mentioned competitive adsorption results, and demonstrate that Plu could be used to clean installed fouling by bringing the copolymer in solution.

Taken together the results from Chapters 2 and 3 demonstrate the development of a successful strategy to deposit a PEO-based copolymer in adequate conformation on Ti and SS surfaces, in such a way that molecular fouling is prevented and microfouling is reduced.

5.1.2 Characterization of fouling from solutions containing molecules of bacterial origin

This work gives an overview and comparison of fouling layers formed by compounds of bacterial origin. It especially focuses on so-called extracellular polymeric substances (EPS) which may accumulate at interfaces. Firstly, biochemical and physico-chemical analyses show that proteins are the main (surface) active molecules present in the fouling solutions, and that these solutions cover a wide range of protein concentrations and molar masses. Furthermore, it was shown that loosely bound (LB) EPS, supernatants of bacterial culture and culture medium form conditioning layers with similar compositions, with 30 to 50% of proteins, although the concentration, constituents and origin of the solutions used were different. The conditioning layers formed by tightly bound (TB) EPS and dried residues of these different solutions are richer in proteins. The results obtained here thus highlight the importance of proteins in the conditioning layers formed at interfaces. These proteins might potentially play an important role to anchor further approaching bacteria (e.g. by providing specific recognition sites on the surface). This confirms the importance and relevance to design antifouling surfaces which are resistant to protein adsorption, with a view to reduce biofouling and biocorrosion.

5.2 Perspectives

This thesis proposes a straightforward method to reduce molecular fouling and microfouling on Ti and SS surfaces using a PEO-PPO-PEO triblock copolymer. This strategy can also be applied on other metal oxide surfaces with varying Pluronics. Other methods, such as competitive adsorption and rinsing using Plu-containing solution, providing alternative and complementary ways to reduce biofouling are also included, which could be explored further.

5.2.1 Pluronic adsorption on metal oxide surfaces to reduce biofouling

As seen in this thesis, the conformation of Plu plays an important role to reduce biofouling, and it strongly depends on the hydrophobicity of the underlying substrate. Therefore, self-assembly of OPA was a requisite to anchor PEO-PPO-PEO triblock copolymer in a brush structure on Ti and SS. On the one hand, self-assembly of OPA can also be performed on other metals which have an oxide layer, such as copper oxide. Since both OPA and Pluronic are non-toxic, the strategy developed here to design protein resistant coatings on metal oxides could also be used in implanted metal biomaterials, such as Ti, or other relevant field. On the other hand, other methods to achieve a hydrophobic surface on metal oxide could also be implemented including the introduction of nano or micro-topography.

The effect of varying PPO and PEO chain length ratio and molecular weight of Pluronic on preventing biofouling was not studied in this thesis. According to the literature, the higher PPO/PEO ratio and higher molecular weight of Pluronic are more effective to reduce protein adsorption, therefore other Pluronics, such as F127, could be compared to F68 used here.

The protein resistance property of Plu was observed in a short period of time (2 h). Long term experiments should be performed according to the

foreseen applications. The stability of Plu and/or OPA-conditioned surface should thus be investigated over days or weeks. The drying and rehydration steps after Plu adsorption might also affect the efficiency to reduce biofouling, which should be tested and/or avoided depending on the application.

The results of competitive adsorption indicate a relative higher affinity between Plu and OPA-conditioning layer, in comparison to BSA. The underlying mechanism might be that adsorbed BSA is replaced by Plu molecules on OPA-conditioned surfaces. This can be further studied over varying time periods, to check the replacement kinetics. Other proteins, such as fibrinogen and cytochrome C, could also be examined.

5.2.2 Modified flow chamber for bacterial adhesion

The modified flow chamber developed here is suitable to study the effect of different surface treatments on bacterial adhesion in a single experiment. For example, we could study coupons with self-assembled monolayers bearing different surface chemistries (-CH_3, -OH, NH_2, COOH etc). The bacterial adhesion kinetics and biofilm formation process on metal materials could be monitored *in-situ* and on line in this system, providing fluorescent bacteria are studied.

The modified flow chamber is also suitable for studying the influence (promotion or inhibition) of biomolecule (e.g. EPS) conditioning layer on bacterial adhesion, similarly as Plu conditioning studied in this thesis. The biomolecules can be brought in contact with substrates to form a conditioning layer. Bacterial adhesion can be performed following conditioning layer formation, without dehydrating this layer.

5.2.3 Influence of Pluronic on bacterial adhesion

In the thesis, it was shown that both pre-adsorption and post-adsorption of Pluronic significantly reduce *Pseudomonas* 2021 adhesion.

The adhesion experiment can be expanded with different bacterial species, different types of Pluronic, different adhesion times, and different rinsing times with Pluronic-containing solution.

Here, a single aerobic bacterial species (*Pseudomonas* 2021) was studied. The adhesion of more corrosive SRB species can also be studied providing the whole setup can be placed in an anaerobic glove box. Adhesion of mixed bacterial species is also feasible, however, to distinguish between different bacterial species after adhesion is more challenging.

Longer adhesion time will lead to form more mature adhered bacteria or biofilm. The stability of adsorbed Pluronic needs to be tested with longer adhesion time. Pluronic with different PPO and/or PEO chain length and molecular weight might have different efficiency to reduce bacterial adhesion, which could be tested in further to find the most effective one.

As shown in this thesis, rinsing with Plu-containing solution can "clean" already adhered bacteria on OPA-conditioned SS surface. The efficiency of Pluronic to remove bacteria after a long adhesion time, more firmly adhered bacteria or even entire biofilm should be tested.

The bacteria for adhesion test here were harvested at exponential or stationary phase, in absence of broth medium. However, adhesion can also be tested in presence of broth medium, to check whether the bacterial adhesion is promoted or hindered in presence of nutrients and in growth state.

5.2.4 EPS Conditioning layer

The substrate surface properties changes due to the EPS conditioning layer were not investigated in this thesis. Complementary information could be obtained by other techniques. Surface topography and wettability information can be obtained by using atomic force microscopy (AFM) and water contact angle measurement, respectively. The quantity of adsorbed EPS and its adsorption kinetics can be evaluated using QCM. The

distribution of EPS on surface can also be observed using molecular probes coupled with confocal laser scanning microscopy (CLSM).

5.2.5 Field experiment

The antifouling coating was tested on Ti and Al brass exposed to seawater, and the results are presented in the Appendix of this thesis. There is no clear effect of antifouling coating applied in real conditions according to visual observation and XPS analysis. There is a large gap to close between laboratory experiments and application in the field.

However, other information could be gained on samples fouled in the field by complementary analyses. Environmental scanning electron microscope (ESEM) can be used to qualitatively observe the biofilm on the surface, and energy-dispersive x-ray spectroscopy (EDX) can be used to quantify the inorganic elements on the surface. Depending on the thickness of fouling layer, the quantification of fouling organic substances is still a challenge. Measurement of total organic carbon (TOC) might be a direct method to determine the amount of organic fouling.

Appendix

Analysis of treated metal tubes exposed to seawater – a field experiment

6.1 Background and aim

Al brass and titanium (Ti) are used as cooling condenser materials fed with seawater in power plants due to their high corrosion resistance. However, biofouling is still the most undesired problem for condensers and heat exchangers cooled with fresh- or seawater. Currently, chlorination is the most common treatment to control microbial growth and biofouling in power plants. Due to the toxic by-products produced after chlorination, other strategies are wanted, including the use of antifouling coatings.

In our previous work, it was shown that the pre-adsorption of PEO-PPO-PEO triblock copolymer on octadecylphosphonic (OPA)-conditioned stainless steel (SS) is effective to reduce molecular fouling (biomolecule adsorption) and micro-fouling (bacterial adhesion) in simplified lab experiments. The same methodology should be applied on other materials and tested in field to prove the versatility and applicability of this approach.

In BIOCOR project, Al brass and Ti tubes are targeted materials used in cooling condensers fed with seawater in seashore power plants. This part of the work aims at testing the designed antifouling coatings in real conditions, in line with the global approach developed in BIOCOR project, bringing laboratory achievements to the field.

The aim of the present work is to implement PEO-PPO-PEO triblock copolymer-based antifouling coating on Al brass and Ti tubes, and to submit such samples to seawater in a bypass of a cooling circuit fed with seawater in a power plant (Piombino, Italy). The effect of a protein layer (albumin) on biofouling and biocorrosion was examined as well. The tubes were treated using different approaches in the lab and tested in field. They were retrieved after different periods, and were then analyzed by x-ray photoelectron spectroscopy (XPS) to highlight attention of the surface chemical composition after exposure to seawater.

6.2 Materials and methods

Al brass (elemental composition in mass/mass: 76% Cu, 22% Zn, 2% Al and 0.04% As) and Ti (elemental composition in mass/mass: 0.10% C, 0.30% Fe, 0.03% N, 0.25% O, 0.015% H, balanced Ti) tubes were provided by RSE SpA, Milan, Italy. The inside of the tubes was hand polished with emery paper 600, then 1200. After that, the samples were cleaned 3 times with acetone in ultrasonic bath for 15 min, and then submitted to UV/ozone cleaning for 15 min. The tubes are named Ref at this stage. The procedure used to prepare a self-assembled octadecylphosphonic acid (OPA) layer on Al brass and Ti was the same as on stainless steel, as described in Chapter 3. Briefly, Al brass and Ti tubes were immersed for 24 h into OPA (Sigma 715166) solution, prepared in tetrahydrofuran (THF, Sigma 33709) at a concentration of 10^{-2} M. After that, the tubes were rinsed with pure THF and dried in room conditions. The tubes submitted to this self-assembling procedure are named OPA. OPA-conditioned Al brass and Ti tubes were coated with Pluronic F68 (PEO_{76}-PPO_{30}-PEO_{76}, in short Plu, Sigma P1300) by immersion into a 2 mg/mL solution for 2 h, and rinsed with ultrapure water then dried with N_2 flow. These samples are named OPA+Plu. Additionally, the Ref and OPA-conditioned Al brass tubes were coated with bovine serum albumin (BSA, Sigma A4919) by immersion in BSA solution (0.2 mg/mL) for 2 h. After 2 h, the coupons were rinsed with ultrapure water to remove weakly adsorbed BSA and dried with N_2 flow. These samples are named BSA and OPA+BSA, respectively.

Al brass tubes were exposed to seawater for 30 h and 30 days, starting from 1st April 2011 (Piombino, Italy). Ti tubes were exposed to seawater for 6 months from October 2011 to March 2012. Seawater was not treated by chlorination here. After exposure, the tubes were cut using saw while the surface to be analyzed was carefully protected with an aluminum foil. The obtained coupons were submitted to XPS analysis. On Ti tubes, the particles deposited during exposure to seawater were scraped off using a

clean blade and collected as powder samples for XPS analysis, for comparison with the tubes.

The detailed procedure of XPS analysis and data treatment can be found in Chapter 4.

6.3 Results and discussion

6.3.1 Macroscopic observation

The Ref and OPA-conditioned Al brass tubes were examined before exposure by depositing a drop of pure water, as illustrated in Figure 1. The shape of these water drops revealed the much more hydrophobic character of the tube surface after OPA coating (Figure 1a). Further analysis of the wettability of tubes treated with BSA or Plu was not performed.

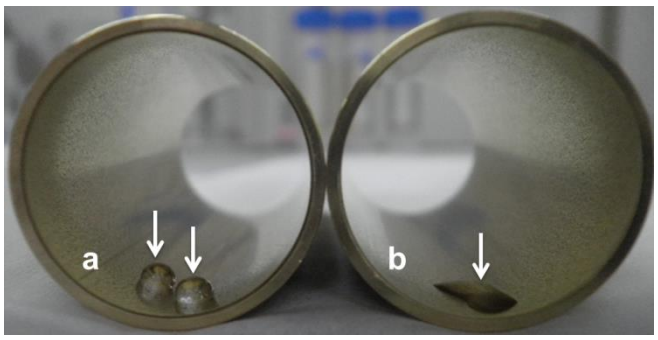

Figure 1. Picture of Al brass tubes: (a) OPA-conditioned; (b) Ref (just cleaned). Water droplets were deposited inside the tubes to illustrate their very different wettabilities.

There was no macroscopic difference between unexposed Al brass tubes with different surface treatments. They all looked shiny and smooth, similar to the one in Figure 2b. The pictures of the Al brass tubes retrieved after exposure to seawater are shown in Figures 2 (30 h), 3 (30 days). As seen in Figure 2, the surfaces of Al brass after 30 hours exposure in seawater were heterogeneous, showing dark and shiny zones, except for BSA-conditioned tube. It should be noted that samples were dried in ambient conditions, which may lead to some artefacts. As seen in Figure 3, Al brass tubes retrieved after 30 days of exposure in seawater were more

homogeneous. The surface of all these coupons had a greenish color. No difference could be observed by naked eyes between these different coupons.

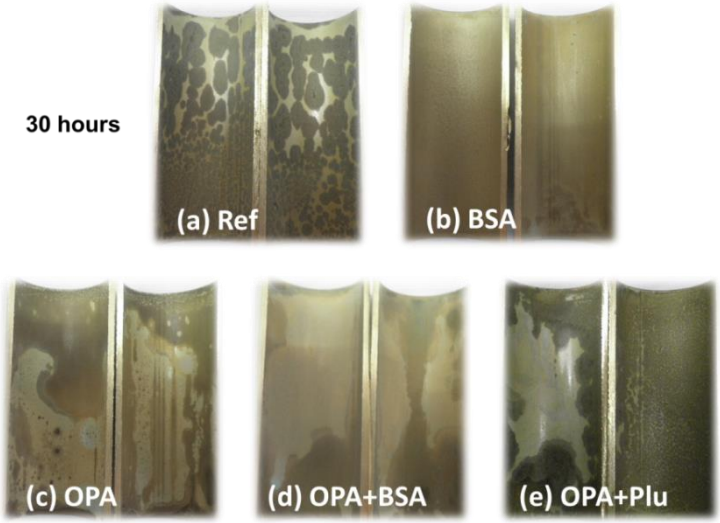

Figure 2. Pictures of Al brass after exposure to seawater for 30 hours: (a) Ref; (b) BSA; (c) OPA; (d) OPA+BSA; (e) OPA+Plu (coupons about 6 cm × 2.5 cm).

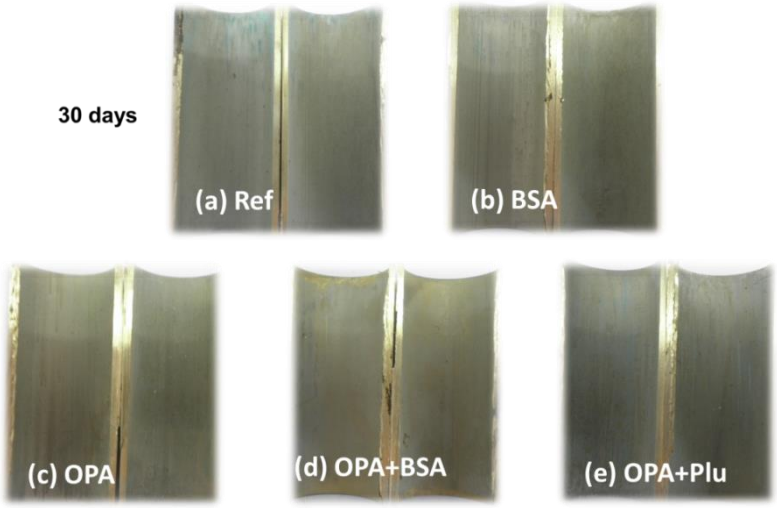

Figure 3. Pictures of Al brass after exposure to seawater for 30 days: (a) Ref; (b) BSA; (c) OPA; (d) OPA+BSA; (e) OPA+Plu (coupons about 6 cm × 2.5 cm).

These exposed (30 h and 30 days) Al brass samples were also submitted to scanning electron microscope (SEM) and energy dispersive X-

ray spectroscopy (EDX) analysis (results not shown). This did not reveal any clear biofilm on the examined samples, which might be due to the toxic effect of copper to microorganisms. There was also no difference recorded by EDX between different areas taken along the surface plane. Therefore, XPS is more useful to gain information related to accumulated organic matter on the sample surface exposed to seawater.

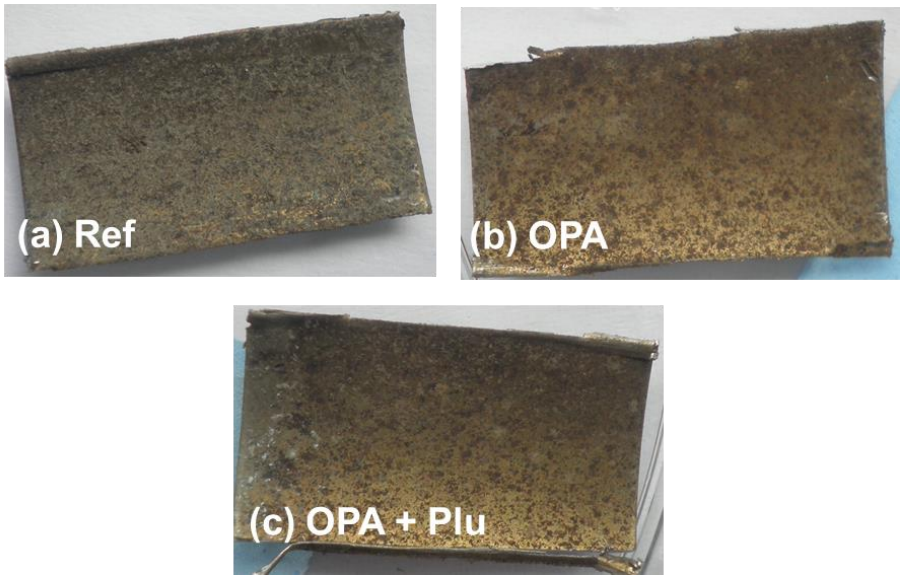

Figure 4. Pictures of Ti samples after exposure to seawater for 6 months: (a) Ref; (b) OPA; (c) OPA+Plu (coupons about 1 cm × 2 cm).

The Ti surface was shiny and smooth before exposure. As seen in Figure 4, after 6 months of exposure in seawater, all Ti tubes looked similar, irrespective of initial surface treatments. They were rougher than the initial Ti surface and heterogeneous at the millimeter scale, with zones more yellowish and other zones more brownish.

6.3.2 XPS analysis

An overview of samples analyzed by XPS is given in Table 1. Figures S1 and S2 (in Supplementary information) show the position of spots used for analysis of the Al brass coupons. The analysis was duplicated

for some spots. For each Ti tube, two coupons were analyzed, at two spots, one more yellowish and one more brownish.

Table 1. Overview of samples analyzed by XPS.

Materials	**Surface condition**					**Season**
Al brass	Ref	BSA	OPA	OPA+BSA	OPA+Plu	
unexposed	×	×	×	×	×	
30 h	×	×	×	×	×	2011 April
30 days	×	×	×	×	×	2011 April
Ti 6 months						
coupon	×		×		×	2011 Oct – 2012 Mar
powder	×		×		×	

The elemental compositions and concentration associated with peak components (molar fractions with respect to all elements except hydrogen) determined by XPS are listed in Supplementary Information (Tables S1 and S2).

Al, Zn and Cu are the main elements in the Al brass samples, and constitute about 20% of the molar composition of unexposed Al brass/Ref. These elements, from the substrate, were attenuated after different surface treatments. The concentration of organic compounds should be quantified by the sum of concentrations C + O_{org} + N_{org}, neglecting hydrogen. Since it is difficult to evaluate O_{org} (because oxygen from metal hydroxides is not easily distinguished from O_{org}), it was evaluated by the sum of C + C_{ox} (where the concentration of the oxidized forms of carbon $C_{ox} = C_{tot} - C_{284.8} \approx O_{org} + N_{org}$). The results are presented in Tables S3 and S4. The molar fraction of the elements due to organic compounds was 48% on unexposed Al brass/Ref coupon, and increased to the range of 60% − 96% following different surface treatments (Table S3). After exposure to seawater for 30 h, the molar fraction of organic elements on all Al brass coupons was close to the same level, from 52% to 61%, and the concentration of metals was close

to 11%, irrespective of surface pretreatments. After exposure to seawater for 30 days, the molar fraction of organic elements varied between 56% and 93%. The nitrogen molar fraction (Table S1) mainly due to amide functions increased significantly between 30 h and 30 days of exposure to seawater.

The concentration of Ti was below the detection limit on all Ti coupons after exposure to seawater for 6 months. Table S4 gives an evaluation of the fraction of organic compounds ($C + C_{ox}$) on analyzed Ti coupons and powders. The molar fraction of organic elements (see Table S4) was in the range of 54% – 58% on Ti/Ref coupon while it was about 63% – 74% on Ti/OPA and Ti/OPA+Plu coupons. It was slightly lower for the powder scraped off from Ti/OPA and Ti/OPA+Plu tubes, compared to the coupons. This shows that organic elements were dominant on analyzed Ti coupons and powders. Interestingly, Si and Al were detected (molar fraction of about 5 – 10% and 4 – 9%, respectively; Table S2) on these samples, which may be attributed to the deposition of clays. Other trace elements were also found (Mg, Fe, Mn).

6.3.3 Correlations between spectral data

Given the focus made in the present thesis on the role of biomolecules in the conditioning layers of metal oxide surfaces, further analysis of the XPS data will only involve signals originating from the organic adlayer found at the sample surface.

Correlations between spectral data were used to evaluate the significance of peak decomposition and assignment, and to generate new information. Figure 5 presents the plot of the concentration of carbon in oxidized form, $C_{ox} = C_{tot} - C_{284.8}$, of C_{288} and of $C_{286.2}$ as a function of N_{org}. Relations (2:1, 1:1 and 1:1, respectively) are expected for amide function [HC-NH-(C=O)]. The C_{ox}/N_{org} ratio of all analyzed samples are higher than 2 (Figure 5a). The C_{288}/N_{org} ratios of all samples are closer to 1, which is a typical ratio for amide groups, indicating that most of nitrogen is in the form

of amide (Figure 5b). The distance from this ratio of 1 might be due to the presence of carbon making two single bonds with oxygen in acetal [O-C-O, one per hexose unit in polysaccharides]. Figure 5c shows that the ratios of $C_{286.2}/N_{org}$ for all samples are much higher than 1, indicating the presence of carbon singly bound to oxygen, thus the presence of sugars or other oxygen-containing organic compounds.

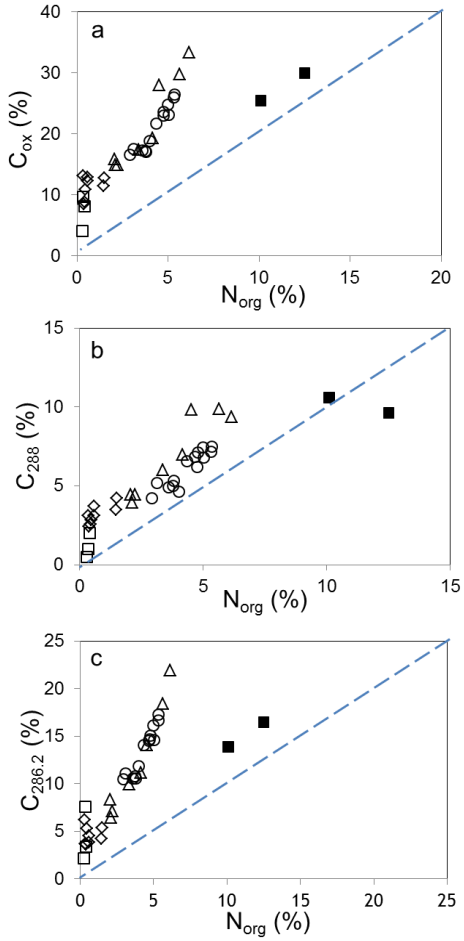

Figure 5. Plot of the molar concentrations associated to different C 1s components, versus the organic nitrogen concentration (N_{org}) determined by XPS: Al brass – unexposed (□), unexposed conditioned with BSA or OPA+BSA (■), exposed for 30 h (◇), 30 days (△) and Ti – exposed for 6 months (○). The broken lines show the relations expected if all N_{org} is in the form of amide.

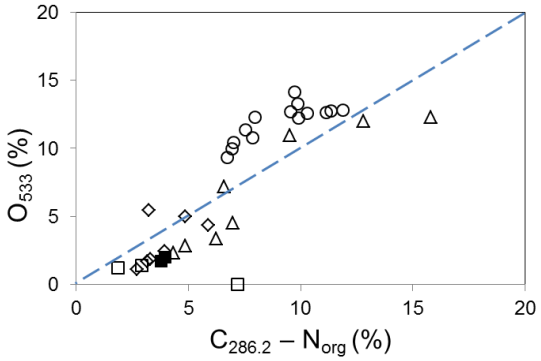

Figure 6. Plot of molar concentration of O_{533} vs ($C_{286.2}$ − N_{org}) determined by XPS: Al brass – unexposed (□), unexposed conditioned with BSA or OPA+BSA (■), exposed for 30 h (◇), 30 days (△) and Ti – exposed for 6 months (○). Broken line, 1:1 relation expected for alcohol, ester and polysaccharide.

The correlation between O_{533} and $C_{286.2}$ was also tested, as the former is attributed to oxygen simply bound to carbon, and the latter is due to carbon singly bound to O or N. Figure 6 shows that a rather good correlation is observed, provided the carbon bound to nitrogen is subtracted from $C_{286.2}$. A 1:1 relation is expected for alcohol and polysaccharides (C-OH, C-O-C; C-C-O), or ester (C-O-C=O). The slope shown in Figure 6 is close to unity.

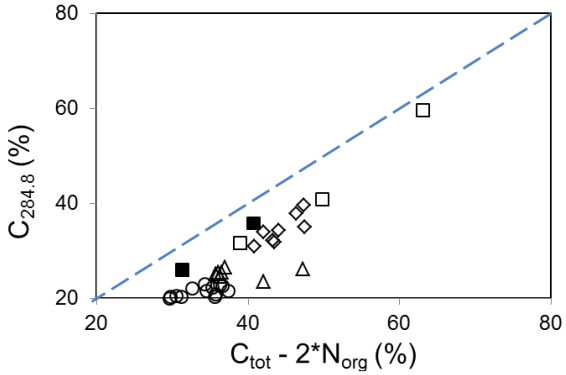

Figure 7. Plot of the molar concentrations of $C_{284.8}$ vs (C_{tot} – 2*N) determined by XPS: Al brass – unexposed (□), unexposed conditioned with BSA or OPA+BSA (■), exposed for 30 h (◇), 30 days (△) and Ti – exposed for 6 months (○). Broken line: unit slope.

Figure 7 presents the plot of $C_{284.8}$ vs (C_{tot} – 2*N_{org}) based on the hypothesis that N_{org} is in the form of amide structure [HC-NH-(C=O)], either

from proteins or N-acetylated aminosugars (see Figure 5b). $C_{284.8}$ and $C_{tot} - 2*N_{org}$ represent the concentration of carbon only bound to carbon and hydrogen (hydrocarbon function) and total carbon which is not in the form of amide, respectively. All the data are below the unit slope (1:1). The displacement with respect to the straight line reflects the importance of oxidized carbon other than that present in amides. The samples of unexposed Al brass are separated according to their surface treatment. After exposure in seawater, the samples are clustered according to the tube nature and to exposure time, showing no difference between different surface treatments.

6.3.4 Nature of the adlayer

The chemical nature of the organic adlayer on exposed tubes was investigated by converting molar concentrations of elements and chemical functions into contents in amide [HC-NH-(C=O)], hydrocarbon CH_2 and additional C+O (C_{add} + O_{add}) using the same hypothesis as in Chapter 4 (Tables S3 and S4). These may be related to the presence of proteins, lipids and polysaccharides.

The relative mass concentration corresponding to the three model compounds, in total 100%, is presented in Figure 8 for Al brass. In Figure 8a, the relative mass concentration of amide [HC-NH-(C=O)], CH_2 and (C_{add} + O_{add}) on Al brass/Ref was 3.4 wt%, 66.2 wt% and 30.4 wt%, respectively. The mass concentration of amide was about 52% for BSA and OPA+BSA conditioned coupons, while its concentration was lower than 3.5% for other conditions, as expected given the fact that the peptidic link of proteins is all amide. The CH_2 concentration of OPA-conditioned tubes was about 88% which is attributed to the aliphatic chain of OPA molecules. Its CH_2 concentration was decreased to 68% after further Plu conditioning, and (C_{add} + O_{add}) was increased to 30%, attributed to the presence of ether function in Plu.

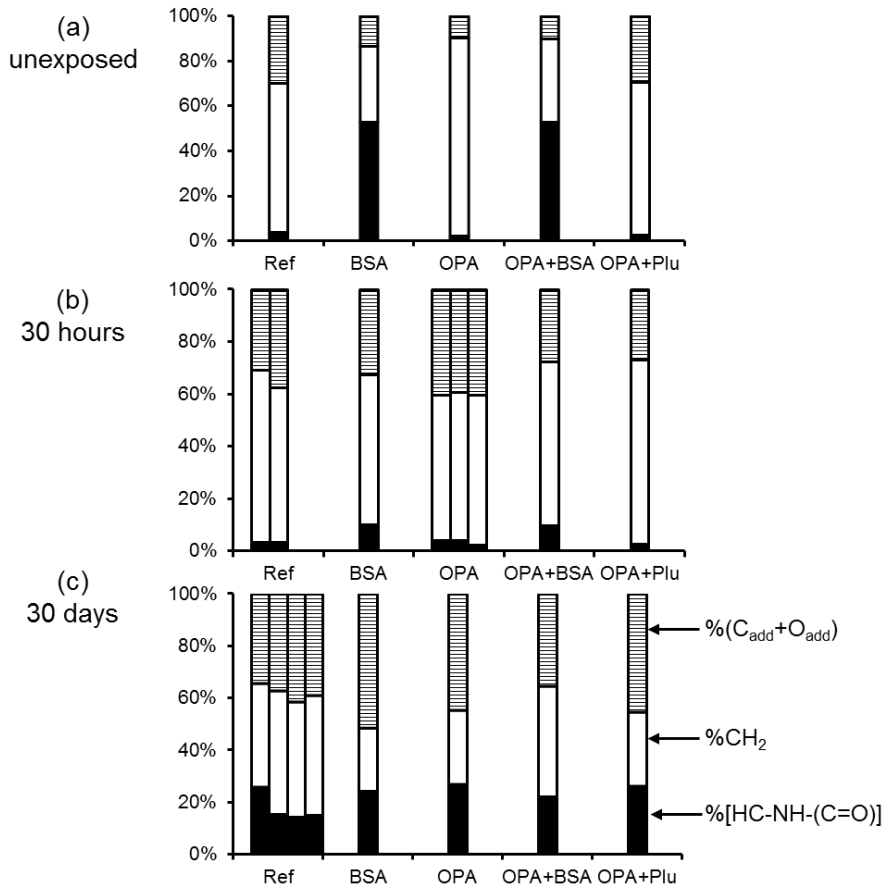

Figure 8. Relative mass concentration of amide [HC-NH-(C=O)], hydrocarbon CH_2 and the sum of C_{add} and O_{add} of Al brass surface with different treatments (a) as prepared or (b) after 30 h and (c) 30 days of exposure to seawater.

The relative mass concentration of the three model compounds formed on Al brass after 30 h of exposure to seawater is shown in Figure 8b. The difference between different surface conditions was smaller. The amide concentration is still about 10% on BSA and OPA+BSA conditioned samples, which was higher than for samples with other conditions. There is no significant difference of constituents between analyzed areas with different colors (see Figure S1).

As seen in Figure 8c, the amide proportion was increased on all Al brass samples after 30 days of exposure to seawater compared to 30 h,

indicating the accumulation of amide-containing molecules on Al brass surfaces. This might be attributed to proteins and/or N-acetylated amino-sugars. There is no marked difference between samples submitted to different surface treatments prior to exposure to seawater.

Table 2. Relative average mass concentration of amide [HC-NH-(C=O)], hydrocarbon CH_2 and sum of C_{add} + O_{add} on Ti with different surface conditions after 6 months of exposure in seawater, and on Al brass exposed for 30 h (Figure 8b) and 30 days (Figure 8c). The results of Chapter 4 for glass and stainless steel (SS) conditioned with various solutions are also given for comparison. Standard deviation is shown between brackets.

	%[HC-NH-(C=O)]	%CH_2	%(C_{add} + O_{add})	C + C_{ox}
Ti/Ref (6 months)	27.3 [0.7]	36.7 [0.9]	36.0 [1.1]	55.4 [1.8]
Ti/OPA (6 months)	26.9 [3.1]	32.5 [4.5]	40.5 [1.6]	68.6 [6.3]
Ti/OPA+Plu (6 months)	27.0 [3.2]	33.1 [4.0]	39.9 [1.7]	64.6 [6.1]
Ti_6 months (all)	27.1 [2.6]	33.9 [3.9]	39.0 [2.4]	63.4 [7.4]
Al brass_30 h (all)	4.9 [3.1]	60.5 [5.2]	34.6 [5.6]	57.1 [3.5]
Al brass_30 days (all)	21.6 [5.4]	37.5 [9.1]	41.0 [5.8]	67.7 [14.2]
glass_conditioning (all)	32.4 [10.9]	47.7 [5.7]	19.8 [7.4]	27.8 [10.6]
SS_conditioning (all)	22.8 [5.1]	45.7 [6.4]	31.5 [5.1]	60.2 [7.7]

Table 2 shows the results of the same modeling approach applied to Ti samples with three different surface conditions, after 6 months of exposure in seawater. The average XPS results of each condition shown here were based on the four analyzed spots on the same type of coupons and one analyzed powder scraped off from the same type of coupon. There is no difference between coupons and powder (see Table S4). Also, it is seen here that there is no significant difference between samples with different modes of conditioning after 6 months. Therefore the average values of all Ti samples were computed with their standard deviations. Table 2 presents their comparison with values computed for Al brass exposed during 30 h and 30 days. The mole fraction of the elements due to organic compounds, C + C_{ox}, is also given. Table 2 also provides a comparison with glass and stainless steel conditioned with different solutions, as presented in Chapter 4.

A great similarity is found between the different systems compared in Table 2, with two exceptions:

- All metal (oxide) surfaces are characterized by mole fractions C + C_{ox} which are around 60%. Glass conditioned with EPS and related solutions give a lower average value, but this is characterized by a great variability (variation coefficient about 30%). Its interpretation would require an evaluation of the adlayer thickness, which requires modeling with questionable assumptions, particularly regarding the uniformity of the adlayer thickness.
- Another exception is the lower amide concentration, revealing a lower protein concentration, found in the adlayer developed on Al brass exposed to seawater during 30 h. This may be attributed to the slow protein adsorption kinetics, due to the low protein concentration in seawater.

6.4 Conclusions

No marked difference was observed here between samples with different surface treatments. The PEO-PPO-PEO triblock copolymer-based coating does not seem to have any particular effect on the surface composition of samples exposed to real conditions. This might be due to the lack of stability of the coating under real conditions. The results obtained in Chapters 2 and 3 show the possibility to repeat Plu treatment from time to time in order to remove adsorbed biomolecules and adhering bacteria. The feasibility of this type of treatment in power plants or other facilities needs to be clarified. It is worth to point out that there is a big gap between lab experiments and real conditions in field, which should be considered in further studies.

From the XPS analysis of unexposed and exposed samples, it is shown that an accumulation of amide-containing molecules occurs in seawater. The similarity with glass and stainless steel conditioned with EPS

and related solutions, and the detailed analysis presented in Chapter 4 indicates these molecules are mainly proteins. Protein adsorption is much slower in seawater compared to EPS and related solutions, presumably due to the lower protein concentration in the aqueous phase.

Certain data must be considered with caution owing to limitations inherent to XPS analysis. It is striking that all metal surfaces, as analyzed, show a similar mole fraction of the elements due to organic compounds. However the physically meaningful quantity is the adlayer thickness and structure, and not its apparent contribution to the XPS spectrum. While the adsorption of protein occurs from the seawater or the conditioning solution, the contribution of other compounds containing oxidized forms of oxygen and of hydrocarbons is difficult to interpret, owing to the possible contribution of different compounds (substances from material processing and surface pretreatment, contaminants adsorbed from the ambient atmosphere or the spectrometer chambers), in addition to compounds adsorbed from seawater of conditioning solutions.

6.5 Supplementary information

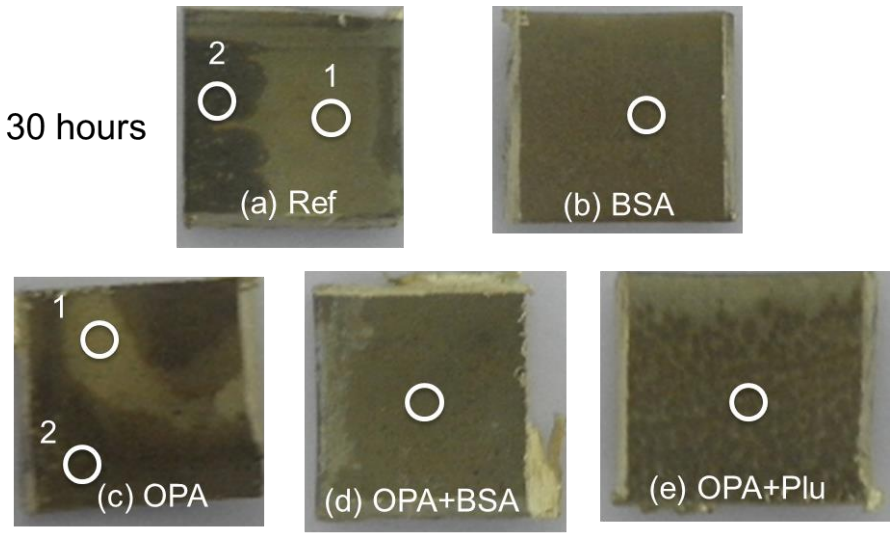

Figure S1. Spots of Al brass tube surfaces (30 h exposure in seawater) analyzed by XPS (coupons about 1 cm × 1 cm).

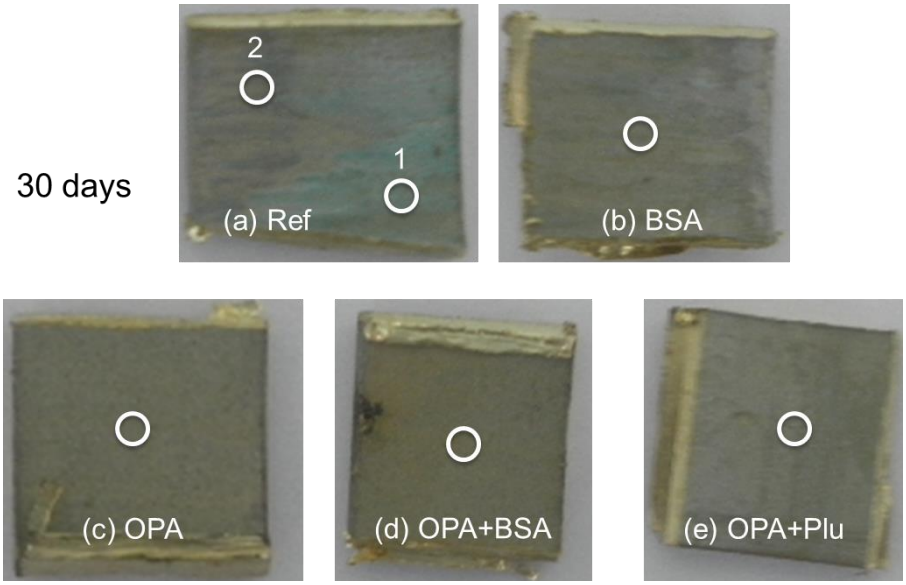

Figure S2. Spots of Al brass tube surfaces (30 days exposure in seawater) analyzed by XPS (coupons about 1 cm × 1 cm).

Table S1. XPS analysis of coupons cut from Al brass tubes with different surface pretreatments, after exposure to seawater for 0 (unexposed), 30 h and 30 days: surface concentration (mole fraction with respect to all elements except hydrogen, %) of elements and functions defined by the indicated binding energy (E_b, eV).

Al brass	C 1s					O 1s				N 1s				Na 1s	$Zn\ 2p_{3/2}$	$Cu\ 2p_{3/2}$	Ca 2p	K 2p	Cl 2p	S 2p	P 2p	Al 2s	Si 2p	Mg 2p
E_b (eV)	289.3	288.1	286.2	284.8	Total	533.0	531.4	529.6	Total	402.1	399.9	398.4	Total	1071.3	1021.7	934.1		293.5	198.8	168.1		119.1	102.5	50.3
Unexposed																								
Ref	2.75	2.02	3.34	31.69	39.79	1.42	22.71	10.30	34.43		0.41		0.41	0.08	2.29	16.91	bdl	bdl	1.47	0.26	3.76	0.60	bdl	NM
BSA	1.00	10.58	13.87	26.03	51.48	1.72	18.16	5.82	25.70		10.09	0.48	10.57	0.19	2.97	4.72	bdl	bdl	0.92	0.94	0.23	0.68	1.61	NM
OPA	1.41	0.48	2.13	59.61	63.63	1.23	17.45	3.95	22.64		0.28		0.28	0.17	1.34	6.64	bdl	bdl	0.19	bdl	4.70	0.42	bdl	NM
OPA+BSA	3.87	9.62	16.47	35.78	65.74	2.00	14.43		16.43		12.50	0.40	12.90	0.19	0.39	1.67	0.09	bdl	0.49	0.84	0.75	0.07	0.45	NM
OPA+Plu	1.05	1.02	7.55	40.86	50.48		30.82		30.82		0.34		0.34	0.10	2.98	7.44	0.24	bdl	1.41	1.03	2.04	1.28	1.86	NM
30 h																								
Ref_1	2.68	2.57	3.61	34.04	42.89	1.70	28.22	0.59	30.51		0.42		0.42	1.62	1.08	10.63	0.25	bdl	7.76	0.18	3.65	0.23	bdl	0.77
Ref_2	2.68	2.82	5.32	30.94	41.76	4.98	31.63	0.63	37.24		0.46		0.46	1.33	3.37	9.75	0.09	bdl	1.85	bdl	2.61	0.93	bdl	0.63
BSA	3.14	4.20	5.39	34.31	47.03	1.84	27.09	0.94	29.86		1.50	0.52	2.02	1.50	2.44	7.30	0.15	bdl	4.77	0.50	1.83	0.78	0.52	1.31
OPA_1	4.62	3.72	4.53	31.77	44.64	2.43	30.06	0.59	33.08	0.59			0.59	1.30	1.92	9.72	bdl	bdl	4.50	bdl	3.16	0.26	bdl	0.84
OPA_1R	5.39	3.10	3.82	32.12	44.43	5.43	27.60	1.17	34.20		0.58		0.58	1.87	2.92	8.52	0.74	bdl	3.09	bdl	2.41	0.27	bdl	0.96
OPA_2	3.73	3.13	6.23	35.09	48.18	4.35	28.00	1.63	33.97		0.33		0.33	2.21	5.31	4.64	0.23	bdl	1.15	bdl	1.22	1.37	bdl	1.39
OPA+BSA	3.74	3.48	4.20	37.92	49.33	1.10	28.90	1.23	31.23		1.47	0.56	2.03	2.49	2.76	6.67	0.60	bdl	0.92	bdl	2.34	0.81	bdl	0.82
OPA+Plu	2.33	2.43	3.68	39.67	48.11	1.86	29.03	1.07	31.97		0.37		0.37	1.63	2.42	8.06	0.37	bdl	2.31	0.15	2.96	0.92	bdl	0.73
30 days																								
Ref_1	1.15	6.97	11.15	25.51	44.78	4.54	27.09		31.64		4.16	0.28	4.44	0.96	0.92	8.17	0.21	bdl	5.97	0.83	bdl	bdl	1.06	1.04
Ref_1R	3.30	4.44	7.10	26.57	41.41	2.88	29.42	1.31	33.61		2.22	0.48	2.70	1.03	1.40	9.34	0.46	bdl	3.49	1.33	1.65	1.42	0.83	1.34
Ref_2	3.08	4.42	8.31	24.64	40.45	3.35	32.41	0.58	36.34		2.07	0.37	2.43	1.41	1.42	9.12	0.38	bdl	2.62	0.79	1.93	1.52	0.72	0.88
Ref_2R	4.45	3.96	6.44	25.06	39.92	2.33	32.18	2.07	36.58	0.36	1.75	0.52	2.64	1.29	1.78	10.31	0.38	bdl	2.68	0.70	1.57	0.48	0.64	1.03
BSA	4.16	9.82	14.04	17.90	45.92	10.96	24.21		35.17		4.52		4.52	2.14	0.38	4.09	0.11	bdl	0.55	0.14	1.28	1.73	2.94	bdl
OPA	1.47	9.87	18.43	23.59	53.35	11.97	16.01		27.98	0.24	5.41	0.32	5.97	1.42	0.24	1.73	0.16	0.13	1.18	1.00	0.65	1.56	3.46	bdl
OPA+BSA	1.34	6.02	9.98	25.44	42.78	7.20	23.81		31.01		3.37	0.44	3.81	2.68	0.52	4.84	0.22	0.30	4.28	0.55	1.68	1.62	4.46	1.25
OPA+Plu	2.07	9.36	21.94	26.18	59.55	12.29	13.27		25.57	0.19	5.95	0.29	6.44	1.15	0.51	1.29	0.08	bdl	1.27	1.08	0.56	0.58	1.12	0.83

bdl, below detection limit
NM, not measured
R, replicate

Table S2. XPS analysis of coupons cut from Ti tubes with different surface pretreatments, and powder scraped off from each type of tube, after exposure to seawater for 6 months: surface concentration (mole fraction with respect to all elements except hydrogen, %) of elements and functions defined by the indicated binding energy (E_b, eV).

Ti	C 1s					O 1s				N 1s			Na 1s	Cu $2p_{3/2}$	Fe $2p_{3/2}$	Mn $2p_{1/2}$	Ca 2p	K 2p	Cl 2p	S 2p	Si 2p	Mg 2s	Al 2p
E_b (eV)	289.0	288.0	286.2	284.8	Total	533.0	531.5	529.5	Total	402.0	399.9	Total	1071.9	932.9	711.2	653.1		293.3	199.2	168.8	102.7	88.9	74.5
Ref_powder*					44.38				31.09			3.19	1.46	0.31	0.67	0.84	0.48	0.70	3.34	NM	7.05	NM	6.50
Ref_1a	1.80	4.90	10.54	20.46	37.70	9.94	21.66	0.48	32.08	0.12	3.47	3.59	2.25	0.37	0.53	0.15	0.41	0.84	2.91	NM	10.22	NM	8.96
Ref_1b	2.40	4.61	11.86	20.37	39.24	10.81	18.30	0.55	29.66	0.11	3.90	4.01	1.77	0.37	0.55	0.23	0.35	0.72	4.17	NM	8.75	1.76	8.44
Ref_2a	1.39	5.01	10.77	20.04	37.22	10.46	21.26	0.50	32.22	0.16	3.61	3.76	2.12	0.37	0.59	0.11	0.30	0.92	3.12	0.37	9.43	1.65	7.84
Ref_2b	1.18	5.30	10.51	20.32	37.31	9.36	22.58	0.50	32.43	0.15	3.64	3.80	1.48	0.33	0.55	0.23	0.35	0.96	2.15	0.44	10.06	1.70	8.23
OPA_powder	1.24	5.16	11.09	23.05	40.54	12.29	20.81	1.72	34.82	0.18	2.94	3.11	0.94	bdl	0.85	0.58	0.45	0.88	1.99	0.49	8.84	NM	6.51
OPA_1a	2.15	6.22	14.66	22.80	45.82	12.24	16.11	1.75	30.11	0.11	4.64	4.75	1.40	0.09	1.33	0.31	0.35	0.48	2.78	0.63	5.75	1.57	4.65
OPA_1b	1.39	7.10	15.06	22.65	46.19	12.58	14.89	1.38	28.85	0.10	4.67	4.77	1.57	0.09	1.05	0.32	0.24	0.44	4.18	0.51	5.63	1.84	4.32
OPA_2a	2.06	7.17	16.67	20.39	46.29	12.75	14.81	1.94	29.50	0.10	5.23	5.33	1.78	0.11	0.92	0.46	0.37	0.46	3.19	0.84	4.85	1.75	4.16
OPA_2b	1.66	7.50	17.24	21.65	48.05	12.79	14.06	2.28	29.12	0.13	5.21	5.35	1.18	0.08	1.35	0.40	0.18	0.40	3.04	0.51	4.31	2.09	3.95
OPA+Plu_powder	1.81	4.22	10.48	22.02	38.52	11.34	23.44	1.81	36.59	0.15	2.78	2.93	1.08	bdl	0.99	0.46	0.46	0.75	1.86	NM	8.98	NM	7.39
OPA+Plu_1a	1.19	7.44	16.15	20.92	45.70	12.64	16.65	1.07	30.36	0.17	4.83	5.00	1.20	0.10	0.92	0.16	0.31	0.58	2.67	0.39	6.30	1.51	4.82
OPA+Plu_1b	1.77	6.80	14.58	22.24	45.38	12.70	15.92	1.69	30.31	0.06	4.97	5.02	1.24	0.11	1.08	0.32	0.41	0.59	2.74	0.70	5.85	1.49	4.77
OPA+Plu_2a	1.05	6.55	14.05	19.42	41.07	14.15	17.13	1.58	32.86	0.13	4.20	4.33	1.31	0.09	1.09	0.26	0.35	0.68	2.18	0.46	7.96	1.37	5.99
OPA+Plu_2b	0.93	6.85	14.54	21.51	43.83	13.29	16.68	2.22	32.18	0.07	4.60	4.67	1.30	0.09	1.31	0.31	0.36	0.45	2.20	0.50	6.43	1.34	5.05
bdl, below detection limit																							
NM, not measured																							
*charging effect																							

Table S3. Global presentation of the results of the XPS analysis of Al brass with different surface pretreatments, after exposure to seawater for 0 (unexposed), 30 h and 30 days: sum of the mole fraction (% with respect to the sum of all elements except hydrogen) of carbon, O_{org} and N_{org} evaluated by C + C_{ox}, and mass proportion of model moieties: amide [HC-NH-(C=O)], CH_2, additional carbon C_{add} and additional oxygen O_{add}.

Al brass	C + C_{ox}	Proportion in adlayer (weight%)			
	Mole fraction (%)	Amide	CH_2	C_{add}	O_{add}
Unexposed					
Ref	47.9	3.4	66.2	13.0	17.4
BSA	76.9	52.4	33.8	5.9	7.8
OPA	67.7	1.6	88.1	4.4	5.9
OPA+BSA	95.7	52.2	37.4	4.4	5.9
OPA+Plu	60.1	2.3	68.0	12.7	17.0
30 h					
Ref_1	51.7	3.3	65.8	13.3	17.7
Ref_2	52.6	3.5	58.9	16.2	21.5
BSA	59.8	10.0	57.4	14.0	18.6
OPA_1	57.5	4.1	55.3	17.4	23.2
OPA_1R	56.7	4.1	56.6	16.8	22.4
OPA_2	61.3	2.2	57.3	17.4	23.2
OPA+BSA	60.7	9.7	62.4	12.0	15.9
OPA+Plu	56.5	2.6	70.2	11.7	15.5
30 days					
Ref_1	64.0	26.0	39.8	14.7	19.5
Ref_1R	56.3	15.8	47.2	15.8	21.1
Ref_2	56.3	14.7	43.8	17.8	23.7
Ref_2R	54.8	15.4	45.8	16.6	22.2
BSA	73.9	24.5	24.2	22.0	29.3
OPA	83.1	27.2	28.4	19.1	25.4
OPA+BSA	60.1	22.4	42.3	15.1	20.1
OPA+Plu	92.9	26.5	28.2	19.4	25.9

R: replicate

Table S4. Global presentation of the results of the XPS analysis of Ti coupons with different surface pretreatments and powder scraped off from each type of coupon, after exposure to seawater for 6 months: sum of the mole fraction (% with respect to the sum of all elements except hydrogen) of carbon, O_{org} and N_{org} evaluated by C + C_{ox}, and mass proportion of model moieties: amide [HC-NH-(C=O)], CH_2, additional carbon C_{add} and additional oxygen O_{add}.

Ti	C + C_{ox}	Proportion in adlayer (weight %)			
	Mole fraction (%)	Amide	CH_2	C_{add}	O_{add}
Ref_1a	54.9	26.1	37.3	15.7	20.9
Ref_1b	58.1	27.6	35.1	16.0	21.3
Ref_2a	54.4	27.7	36.9	15.2	20.3
Ref_2b	54.3	28.0	37.4	14.8	19.8
OPA_powder	58.0	21.5	39.7	16.6	22.2
OPA_1a	68.8	27.6	33.1	16.8	22.4
OPA_1b	69.7	27.4	32.5	17.2	22.9
OPA_2a	72.2	29.5	28.3	18.1	24.1
OPA_2b	74.4	28.7	29.1	18.1	24.1
OPA+Plu_powder	55.0	21.3	40.0	16.6	22.1
OPA+Plu_1a	70.5	28.4	29.7	18.0	24.0
OPA+Plu_1b	68.5	29.3	32.5	16.4	21.8
OPA+Plu_2a	62.7	27.6	31.0	17.8	23.6
OPA+Plu_2b	66.1	28.3	32.5	16.8	22.4